CRYSTALLISATION AND

X-RAY FIBRE STUDIES OF HYALURONATES

by

J. K. P. SHEEHAN, M. Sc.

Being a dissertation submitted in support of an application to the degree of Doctor of Philosophy at the University of Bristol

August, 1973

MEMORANDUM

This dissertation contains an account of some of my investigations under the supervision of Dr. E.D.T. Atkins, during the period from November 1970 to June 1973. Due acknowledgment is made to work undertaken by other researchers.

No part of this work has been used previously in a degree thesis submitted to this or any other university.

J. Sheehan.

Bristol

August, 1973.

SYNOPSIS

A method has been developed for the crystallisation of hyaluronates in the form of films and fibres which has also been applicable to all the mucopolysaccharides. A survey of crystallisation of hyaluronates from different sources under various conditions has shown that a number of backbone conformations and packing schemes are attainable in the solid state and that there is considerable mobility between them. Trial conformations have been proposed for the various conformations discovered and preliminary structure factor computations have been performed for one of the conformations. The significance of these various conformations has been discussed and ideas about their interaction with water and biological function have been put forward.

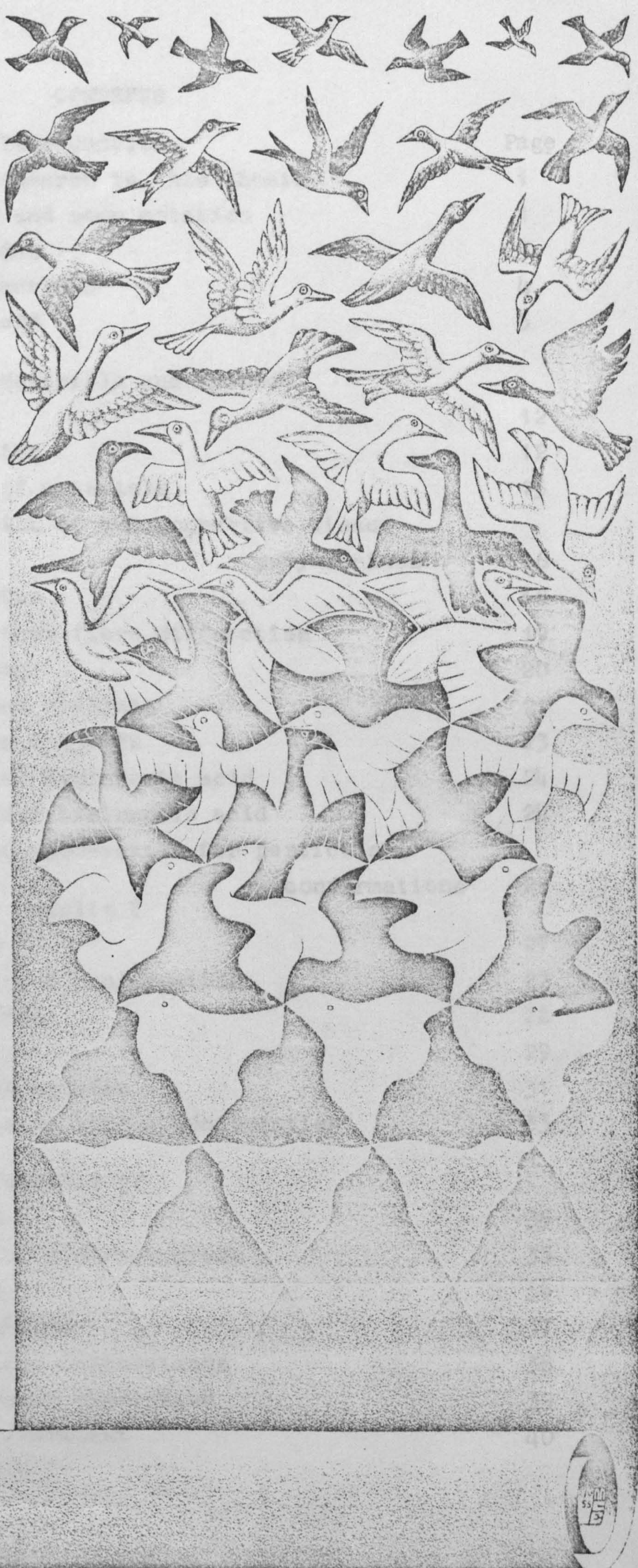

CONTENTS

CHAPTER I

I.1 Context of research in this thesis.

Nucleic acids, globular and fibrous proteins and, to a lesser extent, polysaccharides are three groups of macromolecules that have been the subject of much research in structural biophysics since the 1950's. The primary research method has been the application of X-ray diffraction techniques to crystalline or paracrystalline aggregates of these molecules.

Of the groups named above, structural studies on the first two have made important contributions to the understanding on a molecular level, of such phenomena as heredity, the biochemical action of enzymes and the structure and mode of action of muscle. On the other hand, X-ray diffraction studies on polysaccharides have remained centred on the structural polymers of plants and lower life forms such as cellulose and hemi celluloses, chitin, carrageenan, alginates etc.

There is, however, another group of polysaccharides, usually called mucopolysaccharides, which together with certain proteins form the ground substance in which the cells and fibres of the higher animals are embedded. This ground substance is usually "jelly like" and simultaneously acts as an adhesive, shock absorber, lubricant and extra cellular transport controller. Until recently much chemistry had been performed on these molecules but very little was known about their molecular shape, the conformation they can adopt and their changes of shape as a function of environment. It was this complete lack of conformational information that stimulated the research presently being carried out in this laboratory.

I.2 Basic Sugars and some Notation.

The building blocks of all polysaccharides are the simple carbohydrate sugars. Ref. 1. Carbohydrates may be defined as polyhydroxyaldehydes or ketones or as substances that yield one of these components on hydrolysis. Carbohydrate is a misnomer.

Originally it meant compounds that could be represented as hydrates of carbon i.e. $C_x(H_2O)_y$, but it soon became obvious that this definition was inadequate as many sugars were found to have a hydrogen oxygen ratio different from 2:1 and, sometimes, to contain other atoms such as nitrogen and sulphur.

Let us consider the sugar glucose, $C_6H_{12}O_6$. The atoms can arrange themselves in several ways to allow the molecule to adopt a number of different shapes. These various shapes are called isomers of glucose. Fig. I.1 shows the various configurations that the atoms may take in forming a glucose molecule.

In a solution of glucose under various thermodynamic and chemical conditions there will be a distribution of these isomers, but by far the most stable configuration under ordinary conditions is β-D glucose. Fig. I.2(a) shows the convention for naming the ring atoms while Fig. I.2(b) shows the convention for naming the direction of bonds connecting atoms or groups to the ring. Bond directions lying approximately parallel to the plane of the ring are called equatorial while those approximately perpendicular to the plane are called axial. These two conventions are useful in describing the linkage of one sugar to another e.g. a 1e → 4e glycosidic linkage is a bridge between the C(1) atom and C(4) atom of two adjacent sugars where both bonds are equatorial. The puckered pyranose ring can adopt a number of conformations as shown in Fig. I.3. It can be seen that for glucose the C1 chair conformation distributes the side groups equatorially while the 1C chair conformation distributes them axially so bringing them into close proximity and inducing unfavourable Van der Waal interactions. In general, the C1 chair appears to be the most stable form especially in the solid state, though this depends on the substituent groups on the ring.

It can be seen by examination of Fig. I.3 that changing from a C1 to a 1C chair changes the linkage group on the 1 and 4 positions

Fig. 1.1 Isomers of glucose ($C_6H_{12}O_6$).

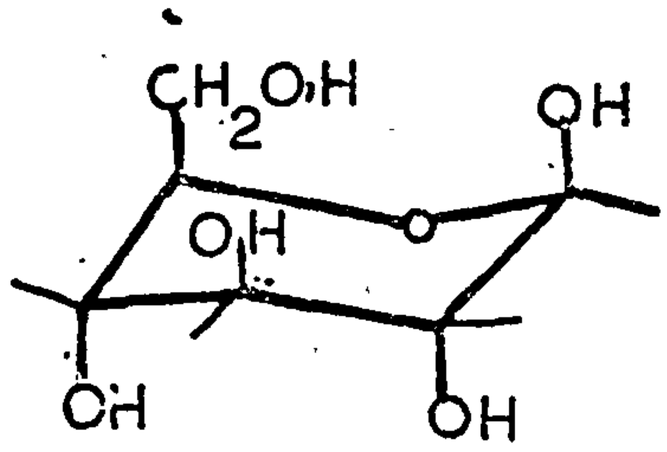

β-D-Glucopyranose

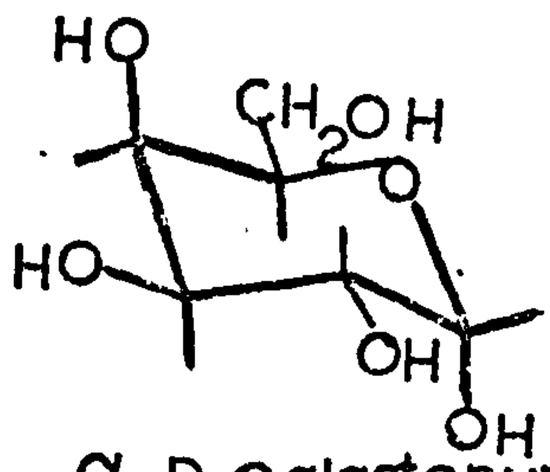

α-D-Galactopyranose

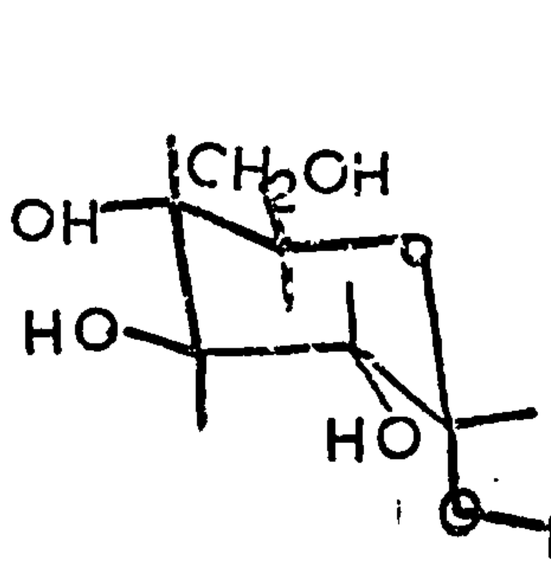

α-D-Glucopyranose

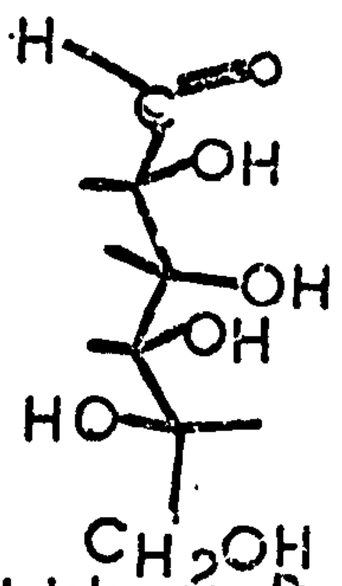

aldehydo-D-glucose

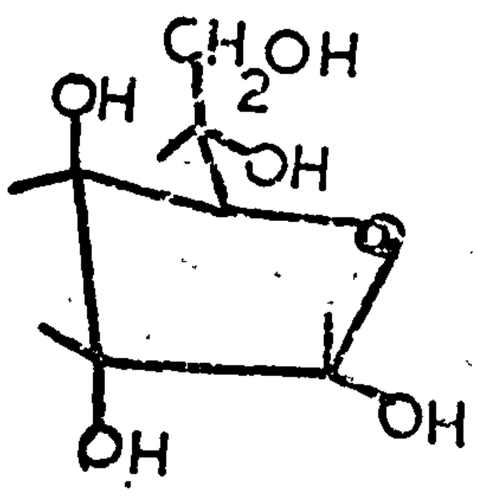

α-D-Glucofuranose

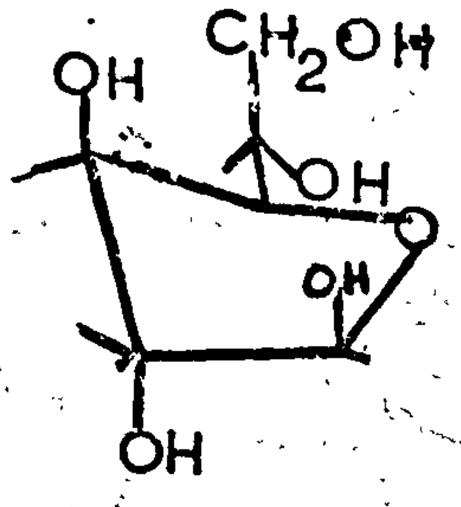

β-D-Glucofuranose

Fig. 1.2 (a) Convention for naming the atoms in the ring and
(b) Notation for defining the direction of bonds.

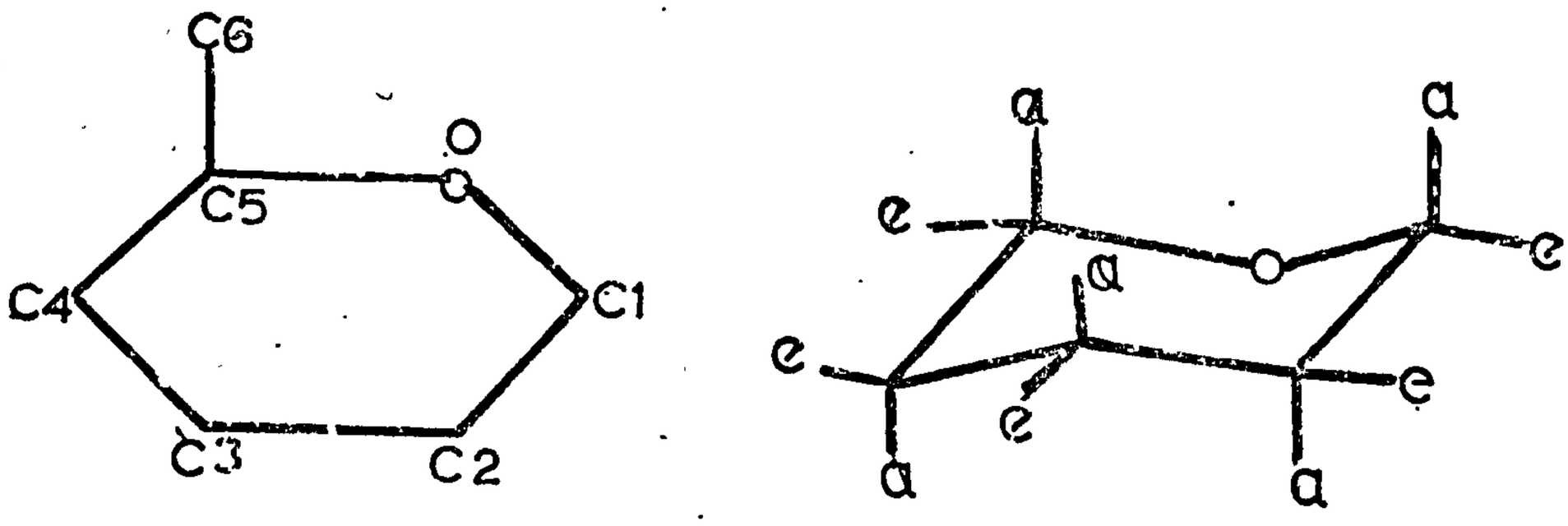

Fig. 1.3 Conformations of β-D-glucose.

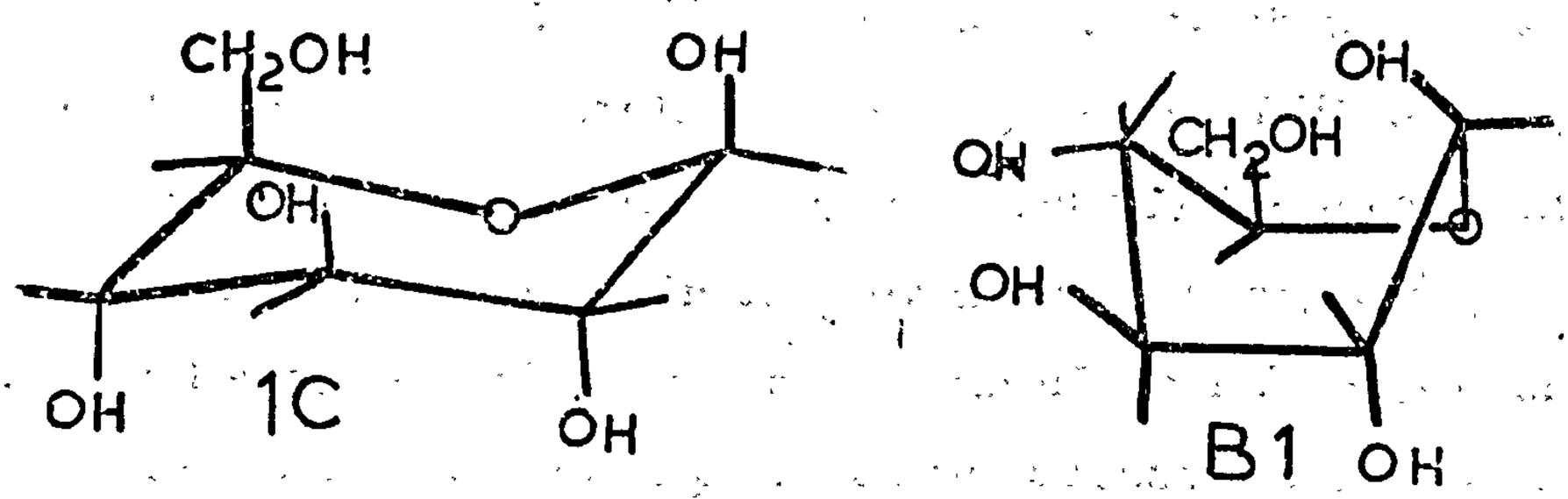

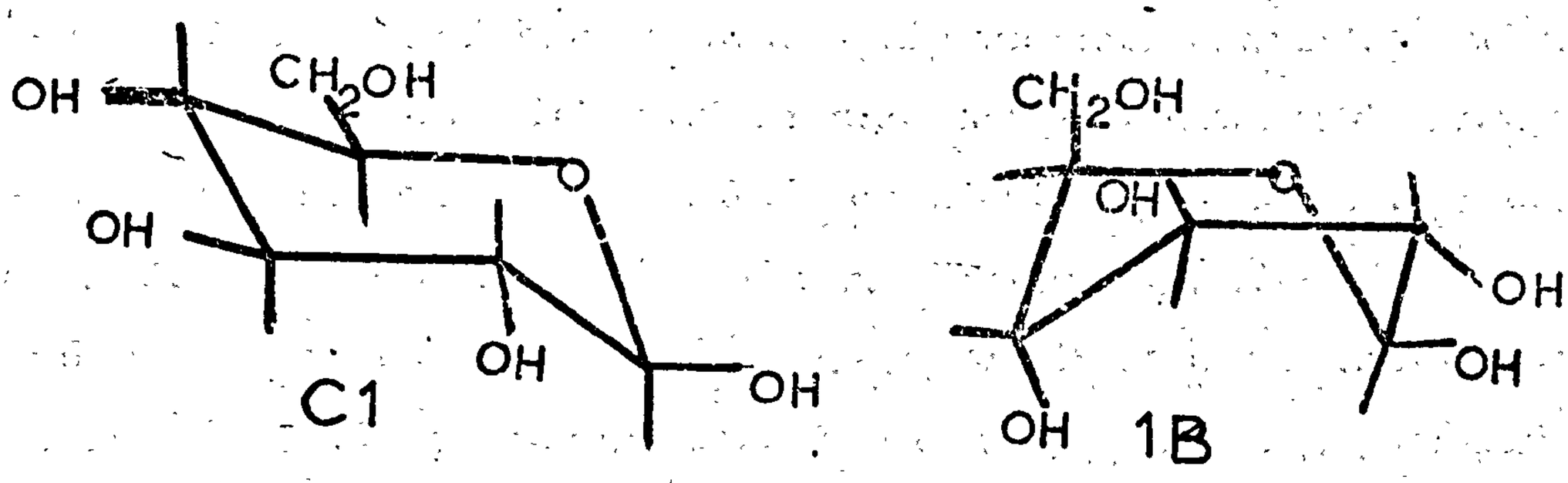

from equatorial to axial. Such a change in the polymer state could bring about a drastic change of shape and have important consequences on the biological function and properties of the substance.

I.3 Polysaccharides

There are a large range of polysaccharides in nature and their function, in general, is closely related to the constituent sugar residues and the control they exercise on the shape of the molecule. The polymer is formed by a bridge oxygen atom between two carbons on separate sugar rings as seen in Fig. I.4.

The shape that a polysaccharide may adopt is a function of four factors:

(i) The shape of the individual sugar residues

(ii) The sequence of sugar units if there is more than one type of sugar residue involved.

(iii) The mode of linkage between the sugar units.

(iv) The degree of freedom of rotation about the carbon to oxygen bridging bonds.

Interplay between these factors defines the possibilities of molecular shape and also, to a large extent, molecular interaction with the environment. Providing the sugar chair shape remains constant the shape is controlled mainly by factors (iii) and (iv). The steric conditions limiting the rotation about linking sugar units will be discussed in more detail in chapter II but here are examples of the general shape of polymers arising out of conditions (iii) and (iv). Fig. I.4(a) shows three examples of polysaccharides made up from units joining 1e → 4e. They are cellulose ref. 2, xylan ref. 3 and chitin ref. 4. All of these show a highly extended character, cellulose and chitin being flat, ribbon-like molecules with a two fold screw axis while β1 → 4 xylan has a three fold screw axis. β1 → 3 xylan is an example of a 1e → 3e linked polymer. This linkage gives the molecule an arced shape see Fig. I.4(b) and in nature it is found to interact with two similar molecules to form a spiralling, parallel

Fig. 1.4 Some examples of shapes for polysaccharide molecules.

(a)

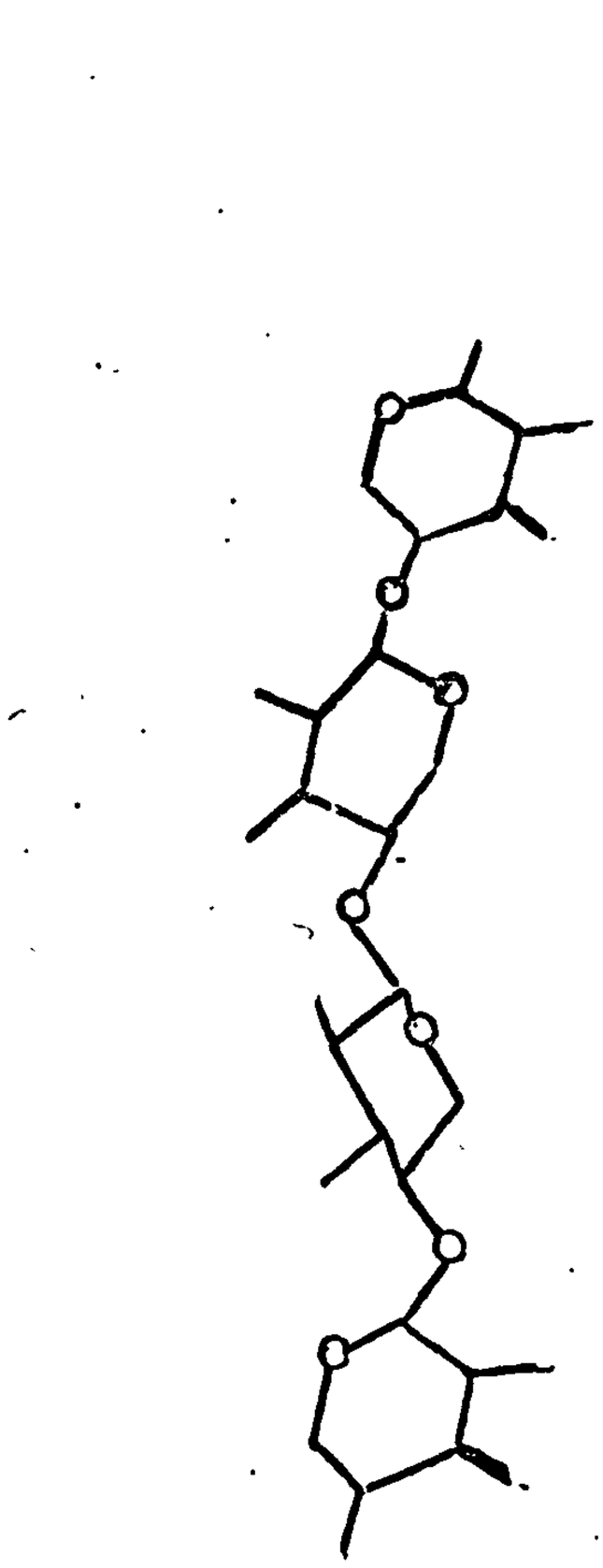

β 1–4 Xylan

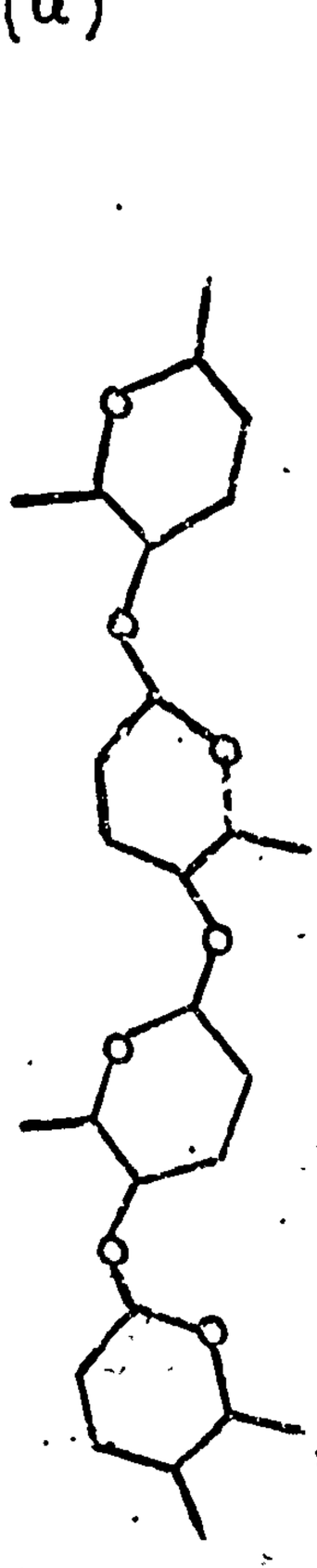

Cellulose

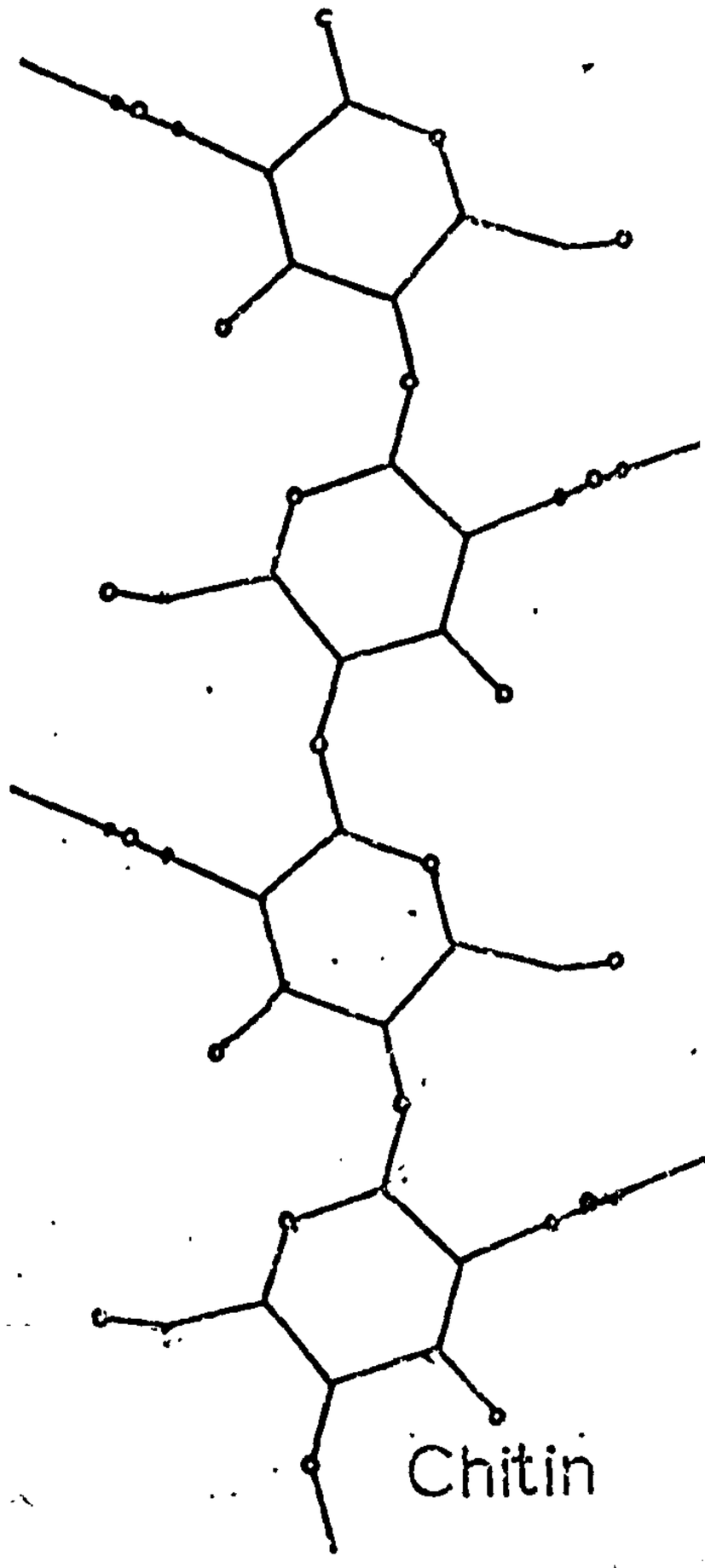

Chitin

(b)

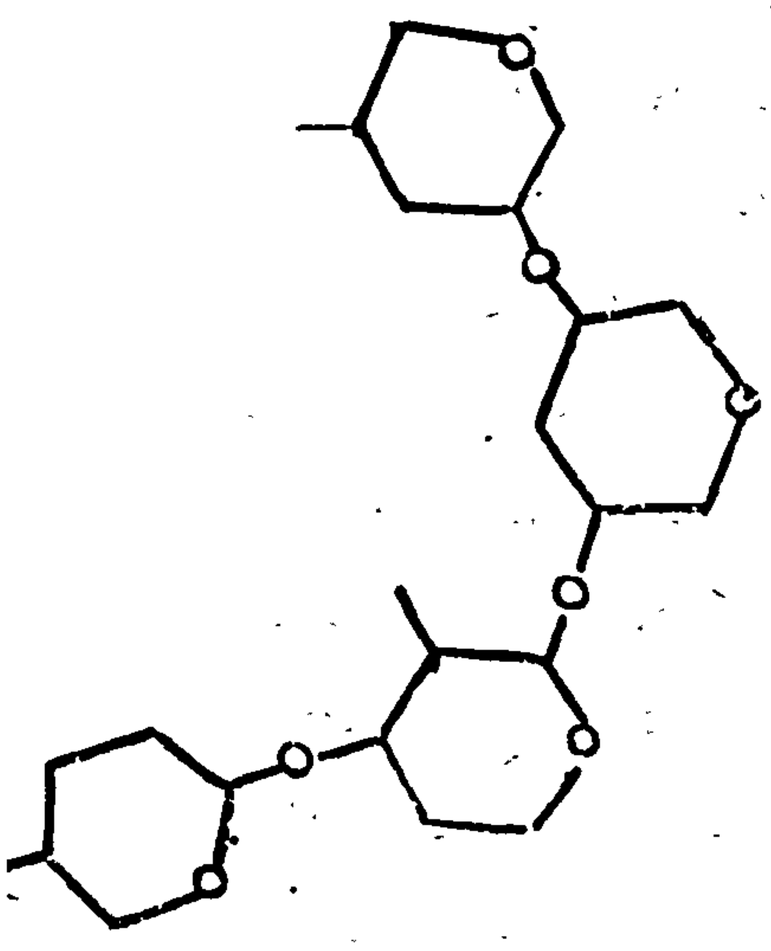

β 1–3 Xylan

(c)

Guluronic Acid

(d)

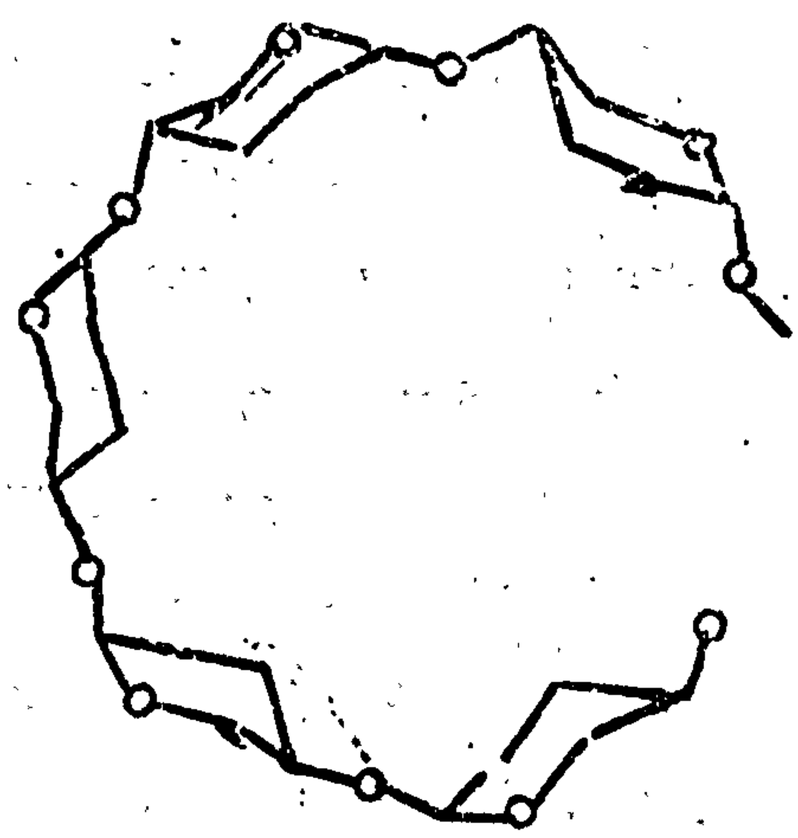

Amylose

three strand helix, Ref. 5.

Fig. I.4(c) shows a polymer linked 1a → 4a. This is glucuronic acid, Ref. 6, and the sugar ring has the 1C chair form. The molecule has a clefted, cylindrical shape, the clefts possibly being able to accommodate ions. Finally there is an example involving another form of glucose i.e. poly α - D glucopyranose (also known as amylose), Fig. I.4(d). Here the linkage is 1a → 4e and the nature of this linkage is such that there is a very small axial rise per residue and six residues almost form a closed loop. The open spiral structure that is formed as a result appears to be used in nature for complexing iodine atoms. Ref. 7.

So far the basic shape of polymers made out of one sugar and employing only one type of linkage has been discussed. There are, however, a number of important polysaccharides employing two or more different sugar residues and connected by a variety of linkages. The carageenan polymers are examples, also the connective tissue polyurinides. This incorporation of different sugars and linkages can increase the versatility of the molecule in terms of its shape and chemical interaction with the environment.

I.4 Mucopolysaccharides

The term mucopolysaccharide was coined by Meyer and includes all polysaccharides containing substances extracted from the vitreous and intercellular matrix of mammals. Many of these polysaccharides are covalently bound to protein and can also be described as glycoproteins or proteoglycosaminoglycans. The research interest in Bristol has concentrated on the polysaccharide component which in nearly every case has a uronic acid moiety hence the alternative name, connective tissue polyurinides. Table I.1 gives a list of the names of these polymers, their chemical structure where known or a possible structure based on the evidence to date, Ref. 8,9. It can be seen that keratin sulphate is the only one of the four which does not contain a uronic acid moiety. The chondroitin

Table 1.1

The Mucopolysaccharides

Hyaluronic Acid

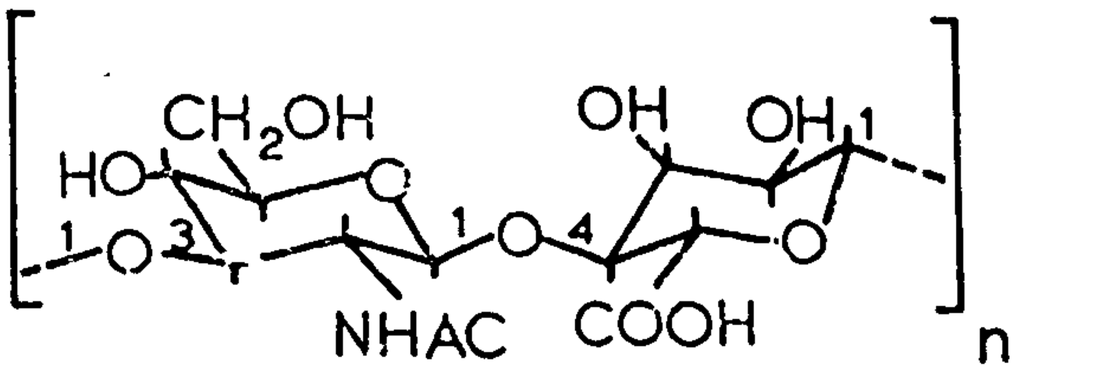

n-acetylglucosamine glucuronic acid

Chondroitin Sulphate A
(4-Sulphate)

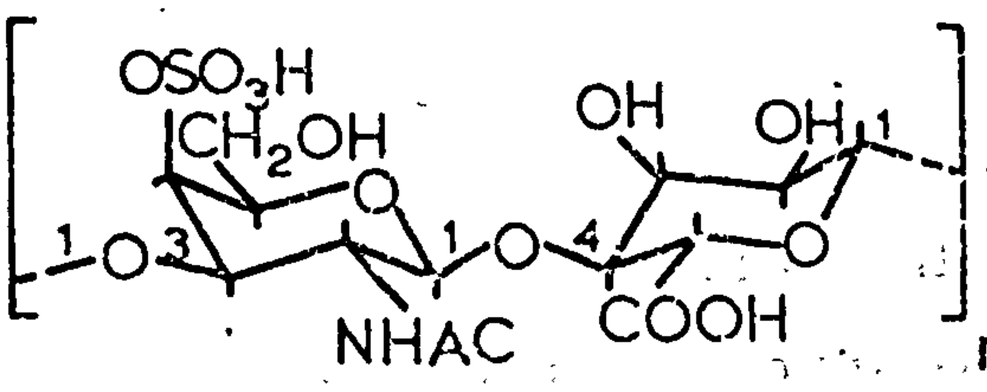

n-acetylgalactosamine glucuronic acid
4-Sulphate

Chondroitin Sulphate C
(6-Sulphate)

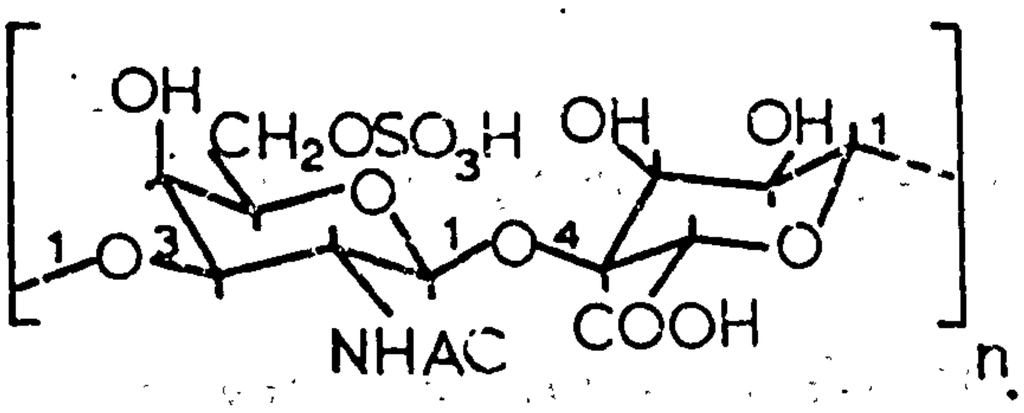

n-acetylgalactosamine glucuronic acid
6-Sulphate

Keratan Sulphate

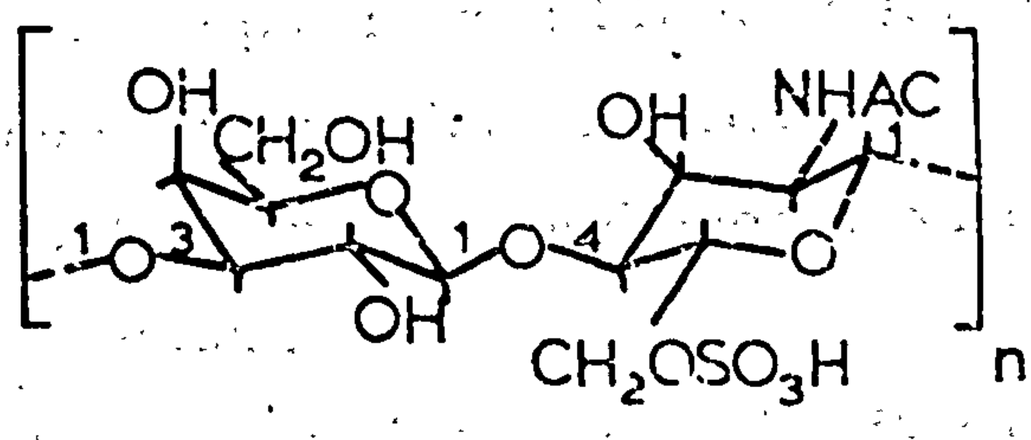

galactose n-acetylglucosamine
6-Sulphate

Chondroitin Sulphate B
(Dermatan Sulphate)

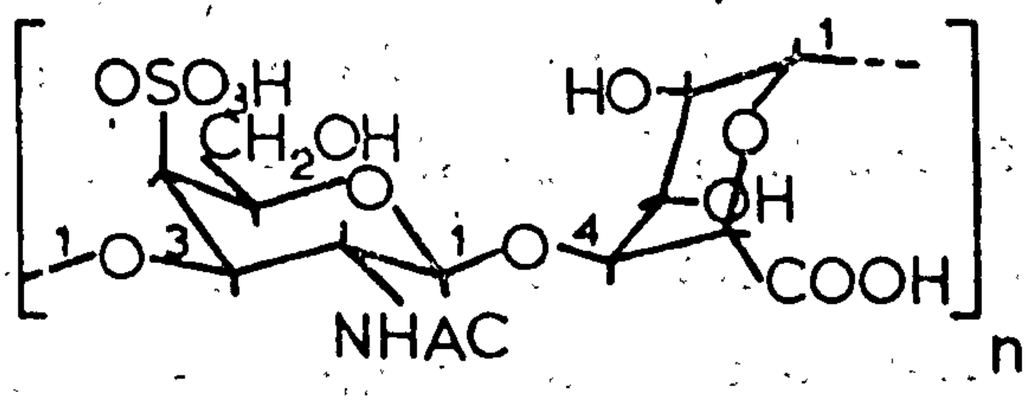

n-acetylgalactosamine L-iduronic acid
4-Sulphate

series of compounds mainly occur covalently bound to proteins. Their polydispersity seems to depend on the source, some sources being fairly monodisperse with molecular weights ranging from 20,000 to 50,000. The compounds heparin and heparan sulphate are the least well characterised. Their chemical structure is still in doubt and heparin appears to have a very low molecular weight, about 10,000-20,000. Their occurrence and function is also very different from the others. They occur in liver, aorta, blood and, not so abundantly, in the intercellular matrix. Their role is not structural but chemical in that heparin is a blood anticoagulant. Heparin is the most highly charged of all the polyurinides having approximately seven charged groups either carboxyle or sulphate to a tetrasaccharide repeat. At the other end of the scale of charge and physical size is hyaluronic acid. This occurs ubiquitously in animal tissue and is even synthesised by certain bacteria. It is the subject of this thesis and some of its chemistry and the properties it conveys to the solutions in which it is present will be discussed in more detail.

I. 5 Hyaluronic Acid

Hyaluronic acid is an odd man out in the group of polyurinides for the following reasons:

a) It is highly polydisperse, occurring with molecular weight distributions in some cases bordering on $(10 - 20) \times 10^6$.

b) There are no sulphate groups on the polymer and it has a low charge density, with only one ionisable group per disaccharide.

c) It does not appear to be covalently bound to proteins or to other polysaccharides to a significant extent.

Table I. 2 is a list (Ref. 10) of some of the tissues in which it occurs and to what percentage, showing how widely it is used in the animal body. The chemical structure for hyaluronic acid is shown in Fig. 1.5 and consists of two sugar moieties, glucuronic acid and N-acetyle glucosamine joined alternately through linkages $1e \rightarrow 3e$, $1e \rightarrow 4e$. A survey of the methods used in the determination of its chemical

Table 1.2

Occurrence of Hyaluronates in some Tissues

Source	Percent of Net. Wt.
Human Vitreous	0.02
Human adult skin	0.03 - 0.09
Human synovial fluid	0.14 - 0.36
Human umbilical cord	0.3
Rooster comb	0.75
Bovine brain	0.015
Normal urine	0.002
Tumours	
Rous Sarcoma	0.1
Mesothelioma	0.2 - 0.7
Streptococcal cultures	0.01 - 0.1

Fig. 1.5 Chemical structure of hyaluronic acid.

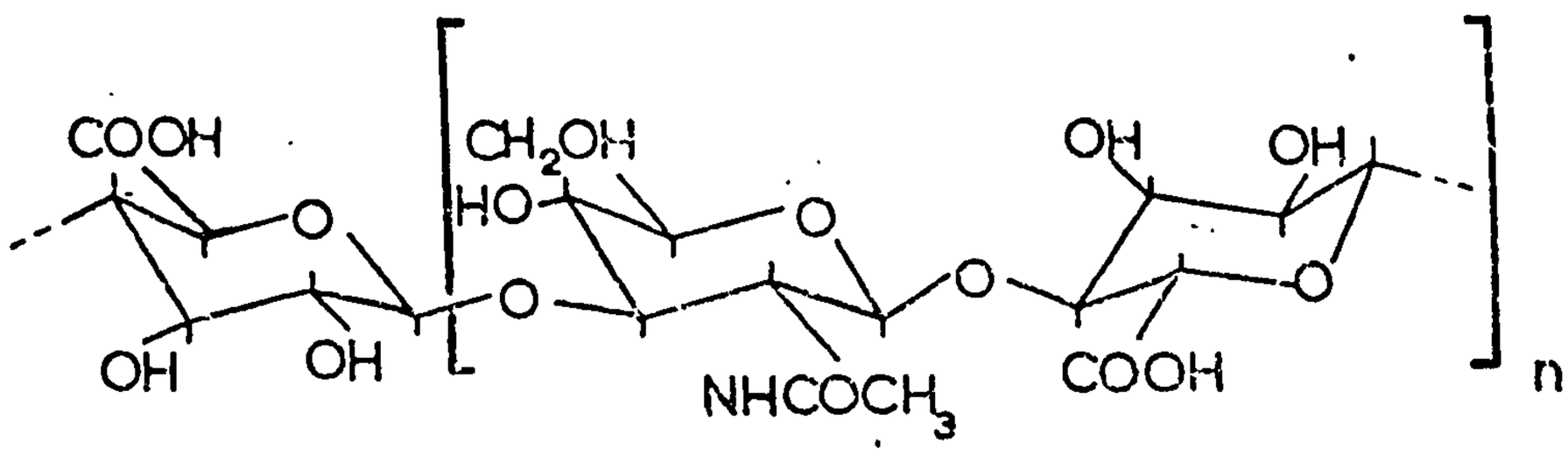

N G

structure is given in a review by Brimacombe and Webber Ref. 11. The main techniques for deciding on the linkages were acid hydrolysis and enzyme degradation using testicular hyaluronidase, bacterial hyaluronate lyase and leech hyaluronate hydrolase. These enzymes break up hyaluronate into oligosaccharides by attacking specific linkages. By examination of the terminal sugars of these various oligosaccharides the mode of linkage can be determined.

Hyaluronic acid in connective tissue occurs together with proteins and proteoglycans. It has been found that hyaluronate can be recovered from the complex almost totally free of proteins using gentle chemical techniques and this is the basis for suggesting that it is not covalently bound with other constituents of the intercellular matrix.

Most of the hyaluronate can be recovered from tissue by soaking it in salt solution. The solution recovered in this way contains about 20% protein present and some other proteoglycans. A number of techniques have been used to separate these components from the hyaluronate. The other polysaccharide components may be removed by selective precipitation techniques using cetylpyridinium chloride. This separates the components on the basis of charge, the most highly charged molecules being precipitated at lower concentrations of non solvent. Ref. 12.

Methods of separating the soluble proteins present with the hyaluronate are numerous but here are three important techniques:

1) Enzyme degradation of the protein using a substance such as papain. Ref. 13.
2) Separation by ultra centrifuge in a CsCl gradient. Ref. 14.
3) Gell techniques - using electrophoresis or gell chromatography. Ref. 15.

A protein content of 3% or less of the dry weight of recovered material is common after these procedures. The molecular weight of hyaluronates

recovered from various tissues has been measured and Table I.3 shows a selection of these values. Ref. 9. However the values quoted must be regarded as lower limits for the molecular weights on these tissues as degradation and sometimes appreciable degradation takes place with all extraction and purification procedures.

The ability of a small concentration of high molecular weight hyaluronate in water to create a very viscous solution and in some circumstances a paste or gell, has given rise to a large number of experiments investigating the hyaluronate molecule and the solutions in which it occurs. Data on molecular shape has come from electron microscopy, Ref. 16, where Fessler and Fessler's experiments showed it to have an extended, linear, unbranched structure. The work of Ogston and his collaborators, Ref. 17,18, using sedimentation, light scattering, streaming birefringence, viscosity and various hydrodynamic techniques gave considerable information about the hyaluronate molecule's size, shape and interaction. Light scattering and hydrodynamic volume experiments could best be interpreted on an extended random coil model with a hydrodynamic volume for a chain in the region of a hundred to a thousand times greater than the unhydrated chain. The Non Newtonian behaviour of polymer solutions was demonstrated by the dependance of viscosity on the velocity gradient. This behaviour decreased with decreasing polymer concentration and it was suggested that some cooperative process between chains was taking place, though no specific interaction could be postulated.

The role of hyaluronate as a polyelectrolyte has been closely examined. Laurant published titration curves of hyaluronic acid, Ref. 19, which suggested a p.K. for the carboxyle group of 2.95-3.3 depending on the concentration of counterion. Aldrich, Ref. 20, studied the distribution of counterion, and anion in hyaluronate solutions using equilibrium dialysis techniques. One important conclusion he reached was that Ca^{++} ions remain bound to a hyaluronate complex even on repeated washings with sodium chloride solutions.

Table 1.3

Some Molecular Weights of Hyaluronates from Different Tissues

(Compiled by Laurant)

Tissue	Molecular Weight	Technique
Human umbilical cord	3.4×10^6	Light-scattering
Bovine vitreous body	7.7×10^4	Light-scattering
	1.7×10^6	Sedimentation and Diffusion
Bovine Synovial Fluid	14×10^6	Light-scattering
Human Synovial Fluid		
Normal	6×10^6	Light-scattering
Rheumatoid	$(2.7\text{-}4.5) \times 10^6$	Light-scattering
Rooster comb	1.2×10^6	Ultracentrifugation
Streptoccal cultures	0.115×10^6	Sedimentation and
	0.93×10^6	Viscosity

On the basis of this finding he states "It would therefore be expected that hyaluronic acid in physiological solutions would be largely associated with Ca^{++} ions and that little residual charge would remain to interact with other ions and to influence their distributions."

The effect of ionic strength on the size and shape has been measured by a number of workers including Balazs and Laurant, Preston, Cleland and others. Techniques used were mainly viscosity measurements and light scattering and the main results are indicated by Cleland's results Table I.4. The differences in the radius of gyration correspond to a three fold difference in molecular volume between the most expanded and most contracted state.

Early experiments by Ogston, Laurant and others, Ref. 21, using the ultracentrifuge showed that for solutions containing a fairly high concentration of polymer i.e. approx. 0.5 → 1% all molecules sedimented together rather than sedimenting according to molecular weight. The system was likened to a porous plug which moved slowly through the liquid, the calculated permeability coefficient for a 1cm thick layer of 1% hyaluronate solution being 3×10^{11} g x cm^3/sec.

The existence of such a network and its effect on transport properties of other large molecules has been studied extensively. What has been called the sieve effect was first investigated by Laurant et al. Ref. 22. They looked at the sedimentation of particles of different sizes through hyaluronate solutions of varying concentrations Fig. I.6. shows their results. The effect is largely an exclusion effect by the polysaccharide molecules reducing the space available for other macromolecules in the solution. Ogston derived an equation giving the space available to a spherical particle of radius r_s in a random distribution of rigid rods of radius r_r with a total length L in a given volume being considered. The equation was

$$K_{AV} = \exp - (\pi . L . (r_s + r_r)^2)$$

and was found to be a useful first approximation in interpreting many

Table 1.4

Molecular Parameters of a Hyaluronic Acid Preparation in Different Electrolyte Solutions (Clelland, 1968)

Polymer	Electrolyte Conc.	Intrinsic Viscosity (ml/g)	Radius of Gyration (Å)
Hyaluronic Acid			
Solvent: aqueous HCl	0.01	508	588
	0.10	584	564
	1.00	450	522
Sodium Hyaluronate			
Solvent: aqueous NaCl	0.01	1400	758
	0.10	810	613; 649
	0.50	591	618
	2.0	453	625

Fig. 1.6 Sedimentation of some molecules through hyaluronate gell as a function of gell concentration.

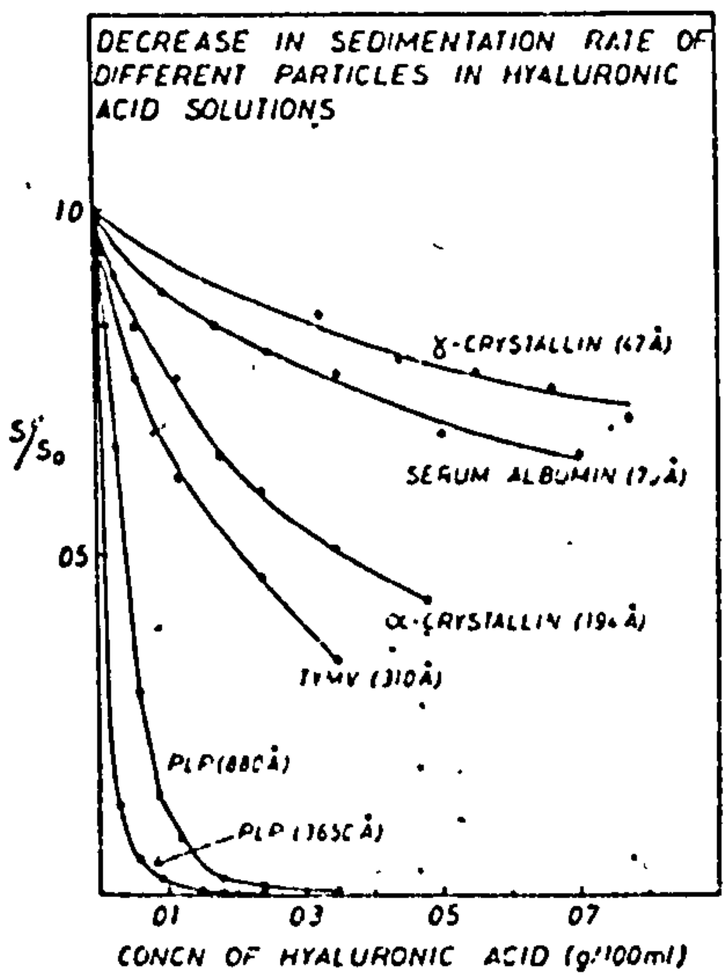

The relative decrease in sedimentation rate of molecules and particles with different diameters in the presence of hyaluronic acid. S/S_o = the sedimentation constant in the presence of hyaluronic acid/the sedimentation constant in free solution. (Data from Laurent and Pietruszkiewicz, 1961, and Laurent et al., 1963).

of the results, Ref. 23. Other techniques investigating this exclusion phenomena are sedimentation of the network in solutions of the excluded substance, equilibrium dialysis, gell chromatography and osmometry. The effort applied to the study of this phenomena may be justified by its biological significance. Certainly the transport properties of the intercellular medium are dependent on exclusion effects and thus such things as the spread of certain infections, the cell metabolism and the passage of macromolecules synthesised in the cell, out into the intercellular medium could be affected.

The rheological properties of these networks has been looked at in some detail by Merril, Gibbs and Balazs Ref. 24 as a function of p.H, ion concentration and polymer concentration using an oscillating Couette rheometer operating over a range of frequencies from .01 sec to a few secounds. They found as a general feature that at low frequencies the solutions were primarily viscous while at high frequencies the response had more of an elastic nature. Balazs and his collaborators made a special note of the fact that at p.H 2.5 this elastic behaviour at high frequencies was particularly pronounced.

Studies on synovial fluid taken from young and old knee joints both normal and osteoarthritic were carried out. It was found that for the normal donors the physical properties as measured by the hyaluronate concentration, and limiting viscosity number were the same for fluids taken from young and old and both fluids showed the changeover from viscous to elastic behaviour at higher frequencies. However there was a distinct difference at higher frequencies, where the value of the loss modulus was found to be much lower for fluid from young persons than old persons. Therefore the ratio of energy stored to energy dissipated at higher frequencies appears to decrease with ageing. Also they found an extreme dependence of the rigidity of synovial fluid on the concentration and size of the hyaluronate molecule.

On studies made of hyaluronate from osteoarthiritic patients

a number of chemical changes were found in the synovial fluid. They exhibited lower concentrations, and limiting viscosity numbers and higher protein concentrations. These chemical changes in the synovial solutions resulted in a much lower rigidity and a changeover from viscous to elastic behaviour at much higher frequencies than for normal fluid.

From a range of experiments on solutions of varying concentration, pH, ionic strength and temperature Gibbs et al. reached the conclusions that 1) there was no variation in the basic relaxation processes with these variables, and 2) that the relaxation mechanism was one of a breakdown of a highly elastic hydrogen bonded network followed by viscous flow due to normal long range cooperative motions of the hyaluronate chain segments. They did not postulate any specific interaction between chains but as will be shown later Chapter VI a possible interaction has been postulated on the basis of X-ray results.

It can be seen that though many aspects of hyaluronate molecule and its solutions have been studied no real effort to visualise the molecule in terms of model building had been made up till 1970. The interpretation of results of every kind was based on the extended random coil in solution i.e. a kind of molecular cotton wool.

PAGE MISSING
IN ORIGINAL

CHAPTER II

2.1 Introduction

It was pointed out in Chapter I that almost all the information on the molecular structure, biosynthesis and properties of solutions of connective tissue polyurinides has come from the application of various chemical and biochemical techniques. In general, chemical experiments are done in such a way as to measure some average property of a collection of molecules and therefore detailed knowledge about molecular conformation is not directly accessible. To obtain such knowledge about conformation and intra and inter molecular interactions a technique such as X-ray diffraction must be used, which, when applied to crystalline or paracrystalline samples, can yield this detailed information.

However, because the materials under consideration are long chain polymers the information that can be obtained from an X-ray diagram is largely dependent on a knowledge of the chemical building units and their connection. Where this knowledge is uncertain the X-ray diffraction pattern can only indicate those chemical structures not possible.

2.2 Crystallisation

Attempts to crystallise the connective tissue polyamides were made in the early and middle 1950's, Ref. 1,2, but with very little success. It is possible that the main difficulties were extraction and purification but this does not seem altogether likely considering the success achieved with impure samples of material in this laboratory. Perhaps the barrier was a psychological one in that the connective tissue polyurinides, compared with other polysaccharides, were 'amorphous' in occurrence, only being found in a dilute aqueous environment mixed with many other substances.

In 1959 Bethelheim, Ref. 3, reported obtaining poor fibre

diagrams of hyaluronic acid and other mucopolysaccharides. On the basis of measurements taken from these diagrams he proposed an extended model for hyaluronic acid with an axial projection per dissaccharide of 11.98Å. This value must be considerably in error because model building trials have shown that an axial projection of not more than 10.2Å can be achieved (even assuming quite unreasonable values for the bridge oxygen angle between residues).

Crystallisation of high polymer molecules presents problems and has certain phenomena associated with it. A simple linear polymer is a regularly repeating sequence of some molecular unit. In the special situation where these units are disposed in a regular manner with respect to some axis one molecule can be regarded as a one dimensional crystal. Because of their long length and polydisperse nature, so-called single crystals of a size useful for X-ray diffraction cannot be formed. In general the best one can do is to prepare specimens composed of a distribution of crystallites having the chain axis in common but otherwise randomly distributed about this axis. The diffraction pattern obtained from such a system is equivalent to a single crystal rotation photograph.

In 1958 Keller and others, Ref. 4,5, discovered that some high polymers can be induced to crystallise on precipitation from dilute solution. The crystals formed during this procedure are very small i.e. about one to ten microns in diameter and one hundred angstroms in thickness and Keller has shown that these crystals consist of a few molecules folding back and forth upon themselves as shown in Fig. 2.1. Though electron diffraction can be used in the study of these crystals, and X-ray diffraction on precipitated mats of them, they do not offer the best means of studying structural details.

Many high polymers crystallise spontaneously when cooling from the melt or on evaporation of solvent and, unless some preferred direction is imposed on the crystals while the process is taking place, a random distribution of crystallites will be obtained. Other polymers

Fig. 2.1 Schematic Diagram of Chain Folded Crystal

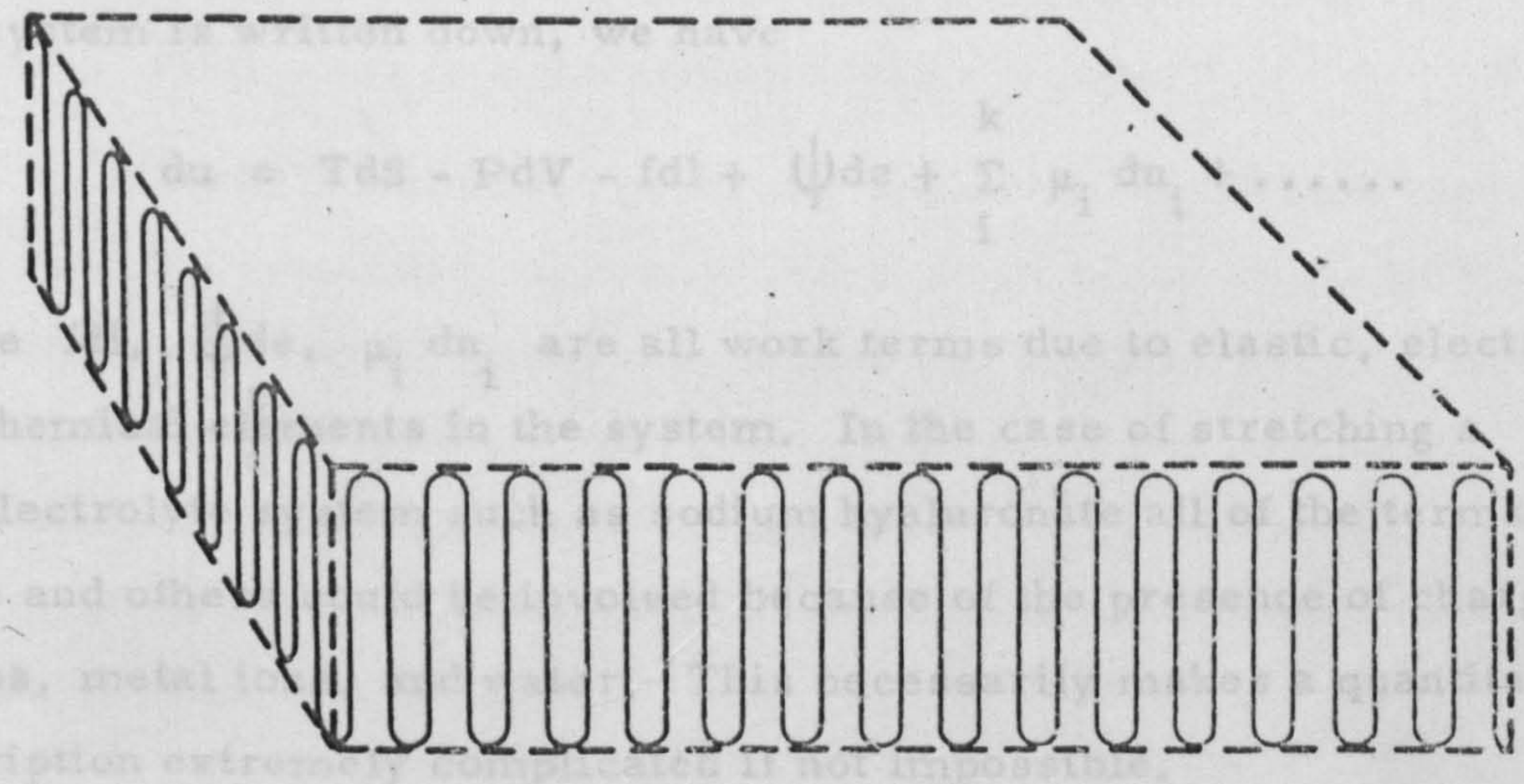

Fig. 2.2 Diffraction from potassium hyaluronate immediately after 300% extension

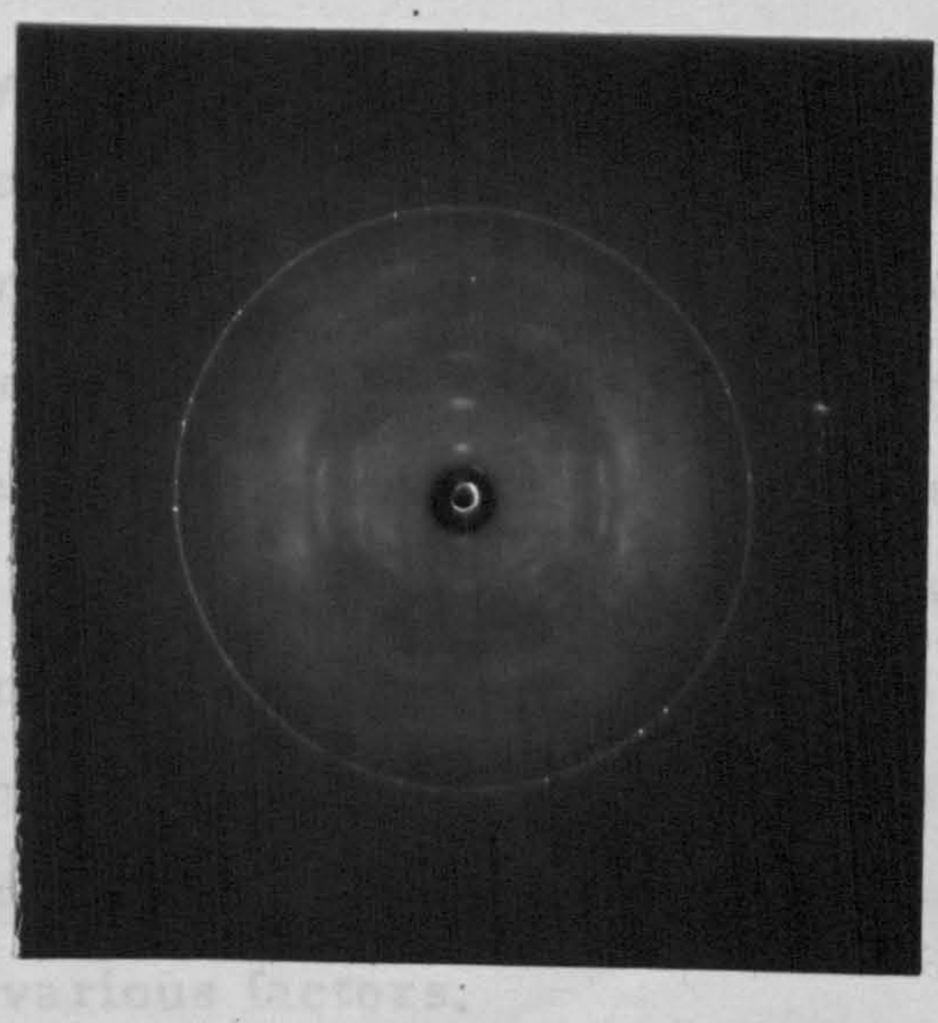

do not crystallise spontaneously on going from solution to the solid state and it is to this class of polymers that hyaluronic acid belongs. In many cases these polymers can be induced to crystallise by orientating the molecules under the correct conditions. These conditions and the understanding of the processes involved can be complicated in certain situations.

If the equation of J.W. Gibbs for the change of internal energy of a system is written down, we have

$$du = TdS - PdV - fdl + \psi de + \sum_{i}^{k} \mu_i \, dn_i + \ldots\ldots$$

Where fdl, ψde, $\mu_i \, dn_i$ are all work terms due to elastic, electrical and chemical elements in the system. In the case of stretching a polyelectrolyte system such as sodium hyaluronate all of the terms above and others could be involved because of the presence of charged groups, metal ions, and water. This necessarily makes a quantitative description extremely complicated if not impossible.

Writing the equation for the change of free energy at constant pressure and temperature as

$$\Delta G = \Delta H - T \Delta S$$

then for stable crystallisation of a long chain polymer to take place after orientation we need a decreasing free energy. Because the orientation of a chain polymer leads to a considerable decrease in the entropy, a large reduction of the enthalpy is required to bring about this decrease of free energy. This drop in enthalpy is caused by favourable Van der Waal and hydrogen bonding reactions between the aligned molecules. Depending on the complication of the system, the sorting out required in crystallisation relies on factors such as time, temperature, stress, humidity and the term annealing is often used to describe these various factors.

The process of annealing has been widely used in metallurgy

and the study of synthetic polymers. In these fields it is often used to describe various heat treatments performed on materials after subjecting them to deformation. In the case of metals heat treatment, can be used to reduce dislocation density, increase grain size, or effect the formation of precipitates in certain alloys. In the synthetic polymer field it is used in a similar way to increase the degree of perfection of an already crystalline sample. One interesting case of annealing is that described in Ref. 6 where annealing of single polymer crystal leads to a thickening of the crystals.

The term has not been generally applied in the field of biopolymers and indeed the application of heat to increase or speed up the process of crystallisation is rare. However, Atkins and Mackie, Ref. 7, used the technique successfully in the crystallisation of the alginates, where temperatures of up to 70°C have been used for 24 hours to to bring about a crystallinity which would otherwise take months to achieve at room temperature.

In this study on hyaluronic acid the conditions under which specimens have been crystallised often involve stress, humidity and elevated temperature simultaneously so that the use of the term 'annealing' is applied when any mixture of these is used for a stated period of time.

2.3 Preparation of Materials

Hyaluronates from a variety of sources have been used. The first batches of material were kindly prepared and purified by Dr. Charles Phelps and his colleagues in the Biochemistry Department of the University of Bristol. The sources are listed in Table 2.1 together with their approximate molecular weight in purified form. The purification procedure was to remove the protein present and the principal technique was degradation of the protein by papain digest. The details are given in Ref. 8. The raw vitreous humour listed in Table 2.1 was simply centrifuged to remove certain proteins and then

Table 2.1

Hyaluronates Used in Experimental Studies

Type	Source	Comments	Molecular Wt.
Na	Mesathelioma fluid	High Protein content	$(10-20) \times 10^6$
K, Na	Mesathelioma fluid	Purified (Papain)	$(1-5) \times 10^6$
Na	Bovine vitreous	Dialysed only	$(.5-1) \times 10^6$
Na	Bovine vitreous	Purified (Papain)	$(10-50) \times 10^3$
K	Human umbilical cord	Grade I (commercial)	$(1-5) \times 10^6$
K	Human umbilical cord	Grade II	1×10^6

dialysed. Human umbilical cord hyaluronate was supplied by Miles Seravac Ltd. in two Grades. Grade I had up to 15% chondroitin sulphate and 3% protein present while Grade II had only 3% chondroitin sulphate and 3% protein present.

2.4 Crystallisation of the Connective Tissue Polyurinides

The techniques described here were employed on chondroitin-6-sulphate and hyaluronic acid but essentially the same techniques have been used to crystallise all the connective tissue polyurinides. Two techniques have been used, one a film and the other a fibre technique.

Hyaluronate films were made by drying down aqueous polymer solutions on various substrates chiefly glass. The concentrations of solution used depended on the molecular weight (M) and the thickness of the film (t) required. Films of various thicknesses could be cast by knowing the volume of solution of known concentration that covered a certain area (A). The thickness is thus

$$t = \frac{M}{\rho A}$$

where ρ is the density.

For many experiments solutions of one percent by weight were prepared and cast on clean glass slides. The films were formed by slow evaporation in air, the slides being partially covered to prevent dust or dirt settling in the solutions. Specimens were cut in the form of strips approximately 2mm wide by 0.5 to 1cm long from these films; and specimens of various thicknesses were made by stacking strips to the required thickness. Films made of pure sodium hyaluronate have a transparent appearance and, if the molecular weight is greater than half a million, a tough resilient texture which makes them easy to handle when dry even when the films are very thin. However if the molecular weight is 50,000 or below, dry films become difficult to handle having a tendency to crack while being cut with a razor blade and also to fracture easily on handling.

Dry hyaluronate films with a molecular weight in the region of one million, will only stretch a few percent under tension and break by brittle fracture, without necking. However, the films were highly hygroscopic at relative humidities greater than 70% and their behaviour under stress was quite different. When films are loaded, under conditions where the relative humidity is held between 75 and 85%, with loads typically of a 1gm to 10gm, depending on the film thickness there is a gradual uptake of water. After 5 to 10 minutes at a relative humidity of 80% the film begins to stretch and over a period of an hour stretches up to a 100 to 400% depending on the molecular weight. During this deformation the sample necks and no significant proportion of the deformation can be recovered on removing the load. On increasing the humidity above 85% specimens of sodium and potassium salts will break under load without flowing significantly past their point of maximum deformation. A diffraction pattern taken after this initial deformation is shown in Fig. 2.2 showing evidence of orientation.

The experimental arrangement is simple. Film specimens are suspended by and loaded from miniature 'Bulldog' clips. Contact between polymer and the metal clips is prevented using a soft covering such as filter paper over the ends of the specimen. Alternatively the ends of the specimen may be glued to paper or light card which is gripped by the clips.

The humidity control was carried out using saturated salt solutions enclosed in a container with the suspended polymer. Fig. 2.3 shows the arrangement commonly used. The relative humidity in the container was controlled by using saturated solutions of various salts. Table 2.2 shows a list of the common salt solutions employed and the relative humidity of their saturated solutions at various temperatures.

Techniques described above were the basic ones used in crystallisation and clearly the process is rather uncontrolled. It has been found that a large number of conformations and packing

Fig. 2.3 Experimental arrangement for the crystallisation of the hyaluronates

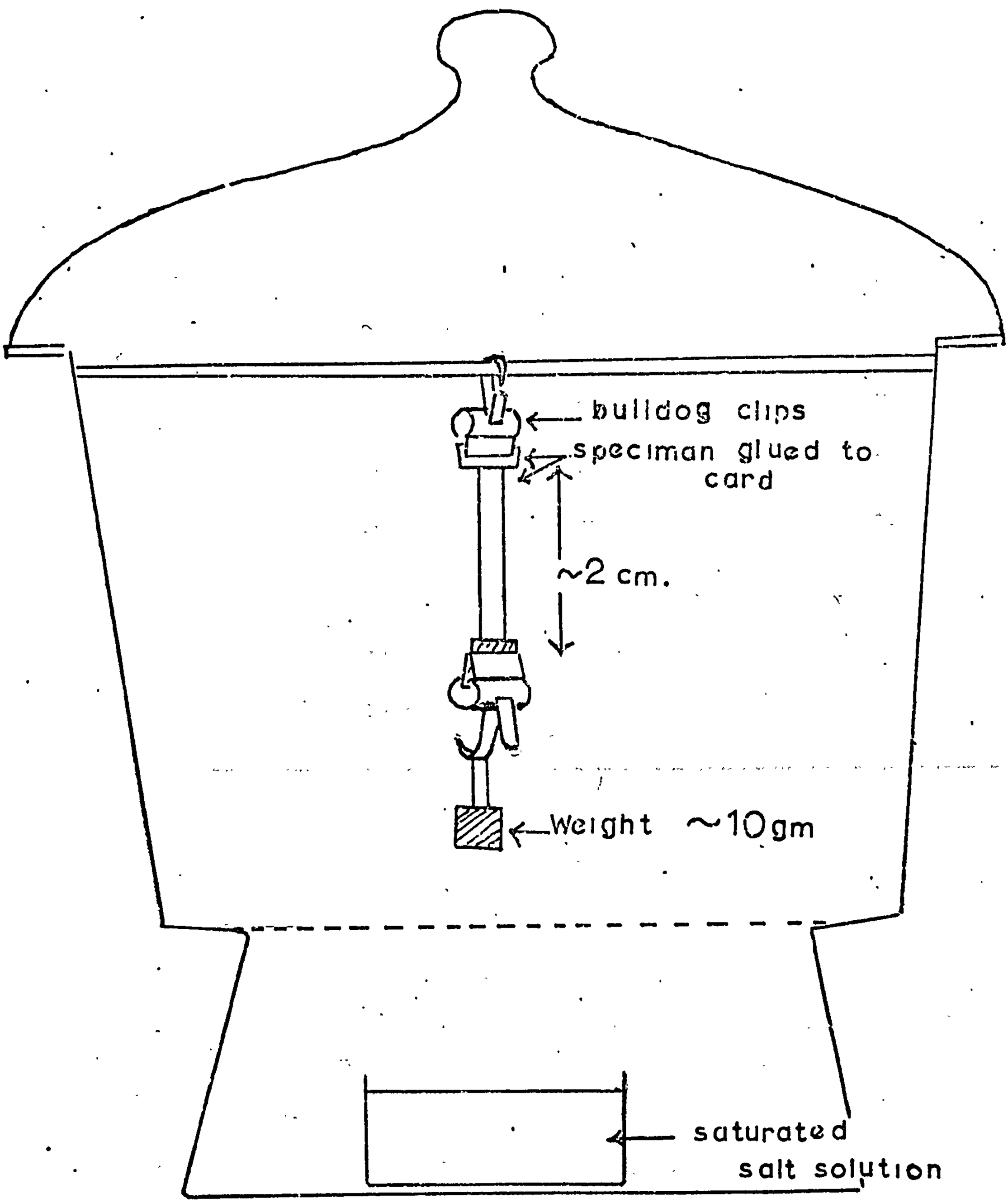

Table 2.2

Saturated Salt Solutions used for Humidity Control

Temp. = 20°C		Temp. = 40°C	
Salt	Percent Rel. Humidity	Salt	Percentage R.H.
K_2SO_4	98	K_2SO_4	97
KNO_3	93	KNO_3	89
$ZnSO_4.7H_2O$	90	$ZnSO_4.7H_2O$	84
KCl	86	$(NH_4)_2SO_4$	79
$NaNO_3$	78	NaCl	75.5
NaCl	76	$NaNO_3$	70.5
NH_4NO_3	67		
$NaNO_2$	66		
KNO_2	45		

arrangements exist for the hyaluronates and all the conditions such as source of material, means of preparation, and purification, as well as the conditions under which it is crystallised have not been systematically investigated. It has been found that specimens of the acid form do not yield to the same treatment as salt forms. Acid films will only stretch about 20% at 95% R.H., and do not show signs of orientation. Experiments using crystallised specimens in the solid state show conformational and packing changes with change of temperature and chemical environment. Some of these effects and the diffraction patterns obtained will be discussed later in Chapters III, IV and V.

Specimens were also made by wet spinning fibres. It was found that solutions of hyaluronate containing calcium ions precipitate rapidly in the presence of some non solvent such as acetone or ethanol. Solutions of 1% concentration were syringed through jets of diameter 0.5 - 1mm into solutions of 90% acetone 10% $CaCl_2$ solution. On emerging from the jet the solution immediately congealed into a highly hydrated fibre. These fibres were harvested and stretched under constant load in the manner described previously. A number of fibres were bundled together to form a specimen.

2.5 X-Ray Apparatus

For monitoring the state of crystallisation of the specimens an ordinary flat plate, Astbury type, camera was commonly used. This was employed in conjunction with a Phillips fine focus tube and a 500μ collimator. Exposures were of the order two to five hours depending on the collimator employed and the thickness of the specimen. Diffraction patterns obtained in this way could not be used for making accurate measurements due to air scatter surrounding the beam stop. To overcome the problem of air scatter specimens were X-rayed either in vacuum or in hydrogen using a camera especially constructed for this purpose. Fig. 2.4 shows this camera, which can give a specimen to film distance of four to six centimetres, set up on an

Fig. 2.4 Vacuum and hydrogen camera on Elliot Rotating Anode X-ray machine

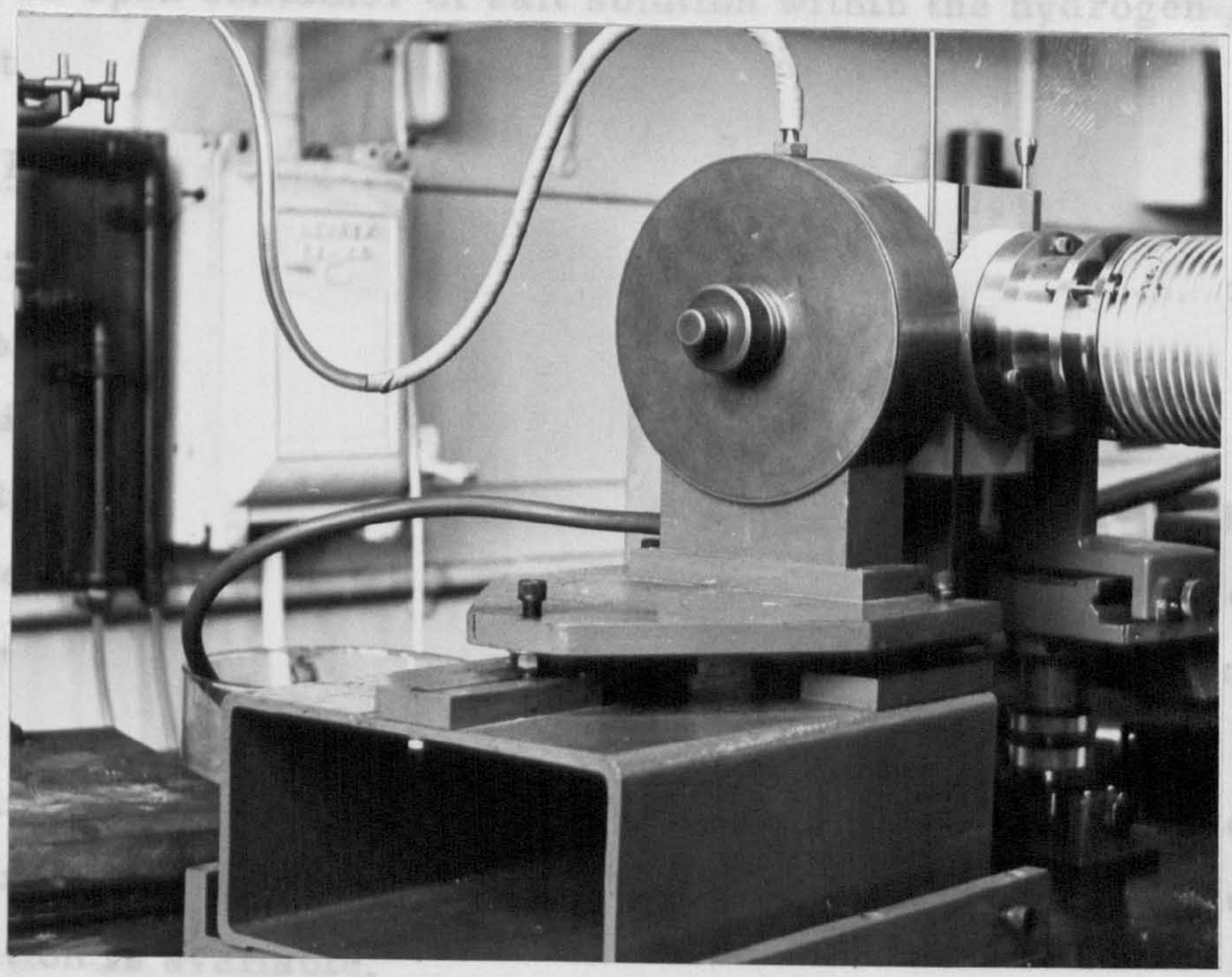

Elliot type rotating anode X-ray machine. This powerful machine allowed clean X-ray diagrams to be obtained from very thin films within twenty four hours and of ordinary thickness specimens i.e. about 100μ, in two to six hours, using a 250μ collimator.

Humidity was controlled by either enclosing the specimen in a thin walled silica glass tube with the appropriate salt solution or by placing an open container of salt solution within the hydrogen camera restricting the hydrogen flow to almost zero.

2.6 Information from Fibre Diffraction

The examination of a fibre diffraction diagram can be divided into two stages.

Stage I is a preliminary examination of the diagram noting the degree of crystallinity, and any particular disorder effects, such as layer line streaking. Also at this stage lateral and axial periodicities are measured and a visual estimate of the intensities on the equator is made. Stage II involves detailed structure factor calculations using all the intensity data, and this can in principle yield the position of all non hydrogen atoms in the unit cell providing certain stereochemical information is available.

The amount of information obtained at stage I may be quite considerable. Determination of axial periodicity from layer line spacing and of the fundamental repeating unit from the meridional reflections often make it possible to distinguish between a number of configurational models which are suggested by the chemical evidence. Combining this data with information about the other dimensions of the unit cell and the density of the material it is possible to get details about the number, size, shape and approximate environment of the molecules in the unit cell. In certain cases it is possible to say whether single or multi-strand helices form the basic unit. X-ray diffraction used at this level can monitor changes of metal ions, humidity and temperature and so give more information about polymer interaction.

The feasibility of a stage II investigation depends on a number of factors and as the process is time consuming and expensive in computer time it is sometimes difficult to decide whether it is worthwhile. Due to the limited data obtained even from a high quality fibre diagram it is not possible to make a direct attack on a molecular structure using direct methods such as those applied in the crystallography of globular proteins. Therefore the method of trial and error has to be used in which the Fourier transform of a trial model is computed and compared with the observed data. The model is then adjusted to reduce the difference between the calculated and observed data. This adjustment in its most sophisticated form is made by a process of least squares refinement, Ref. 9, where the derivatives of the variables involved are used to give the direction of shifts in successive cycles of refinements. The final test of the structure is then made using Fourier synthesis and Fourier difference synthesis. There are many pitfalls in the process and the number of variables one can realistically consider is limited by the quality of the fibre diagram.

An important limitation of these variables depends on precise structural information about the chemical groups e.g. the planar amide in protein structure and the sugar ring in polysaccharides. In general the asymmetric unit is formed from one or more chemical groups joined by single bonds allowing freedom of rotation which can be investigated using the techniques of model building, computer model simulation and conformational analysis.

Fig. 2.5 shows a block diagram of the procedure for solving a fibre structure. Certain difficulties not mentioned in Fig. 2.5 may arise when there are appreciable numbers of water molecules and anions such as sodium or potassium present. Fourier difference techniques may find the position of ions but the presence of a number of water molecules in the unit cell is a difficult problem to treat.

2.7 Model Building

Model building has played a vital role in the development of

Fig. 2.5 Block diagram for the method of solving a fibre structure

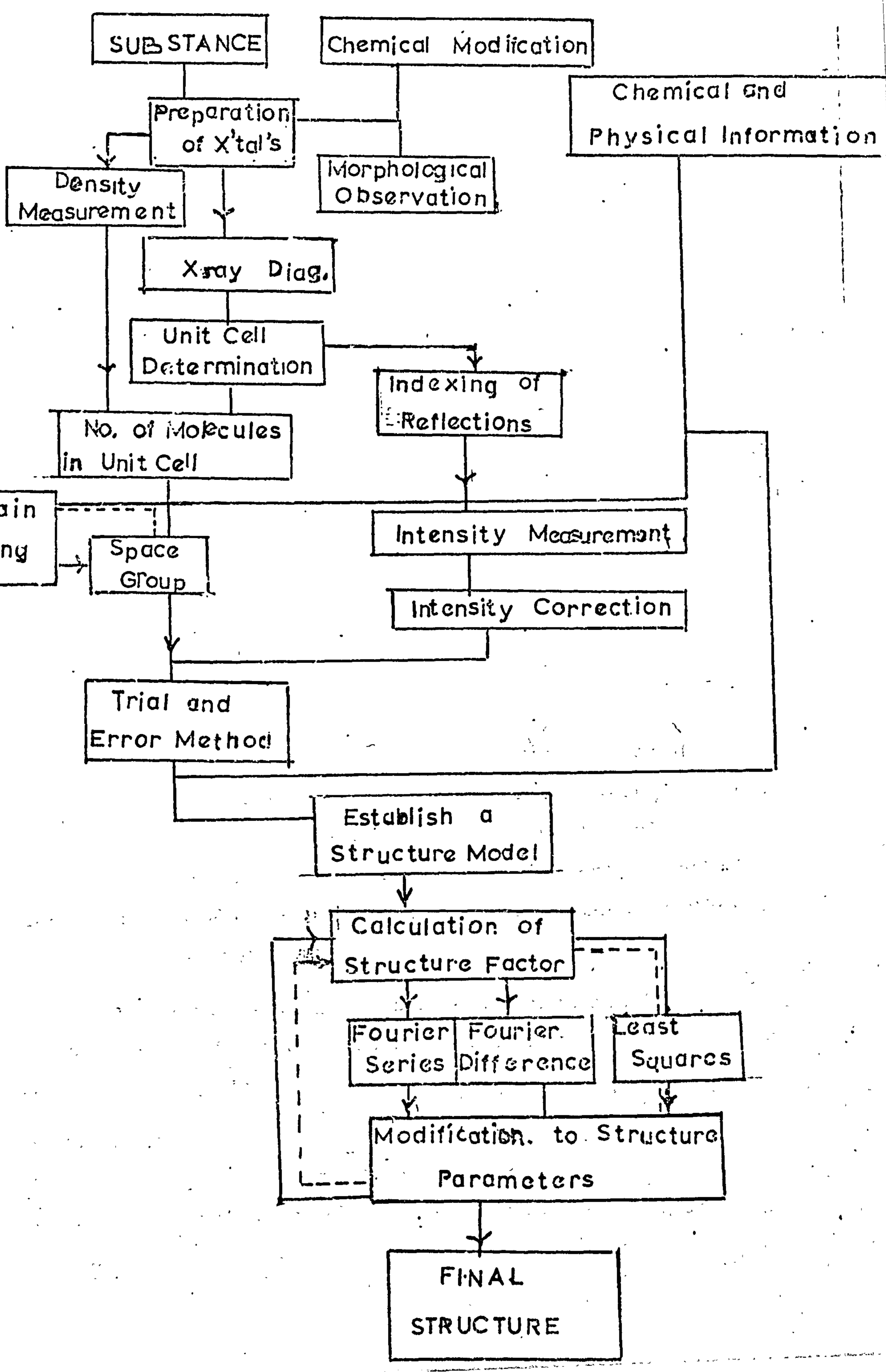

molecular biology and although many of the roles once performed by the examination of accurate models are now replaced by sophisticated computer methods, they are still invaluable for conveying a "feel" for the molecule. There are three basic types of model, they are

1) Stick, or skeletal models
2) Space filling models
3) Ball and stick models.

Fig. 2.6 shows the basic building unit of hyaluronic acid in the three systems.

Computer model simulation is developing at a considerable rate and in its most advanced form offers an almost complete alternative to solid model building. The latest advances in real time computing coupled with visual soft ware devices allow problems of conformation, chain packing and molecular interaction to be examined quickly. The facilities required for this kind of approach are expensive and therefore rare. The more usual approach is a mixture of the two techniques of model building and standard computer procedures of conformational and chain packing analysis.

2.8 Conformational Analysis

Conformational analysis is the prediction of allowed conformations (based on certain stereochemical criteria) of two or more stereoregular units joined by single bonds about which there is freedom of rotation. It was first applied by the Indian school of biophysicists under Ramachandran, Ref. 10, and subsequently extended by them and others Ref. 11, 12.

The method consists in the examination of a molecule taken in vacuo using certain approximations for the internal forces involved. The main energy terms are

1) Van der Waal repulsion between atoms.
2) Van der Waal attraction between atoms.
3) Tortional energy about single bonds between the chemical units being considered.

Fig. 2.6 Model building systems used in this research

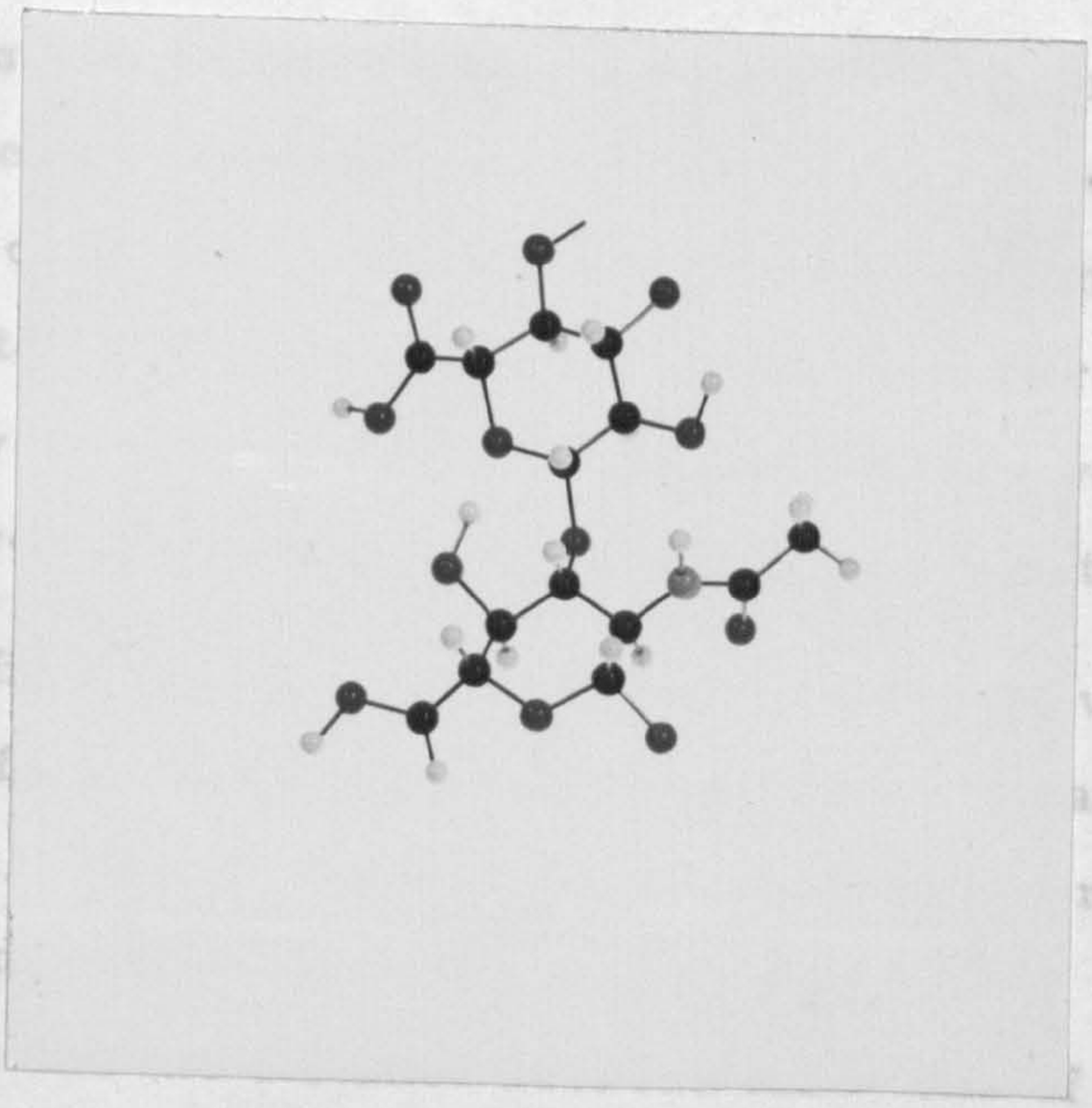

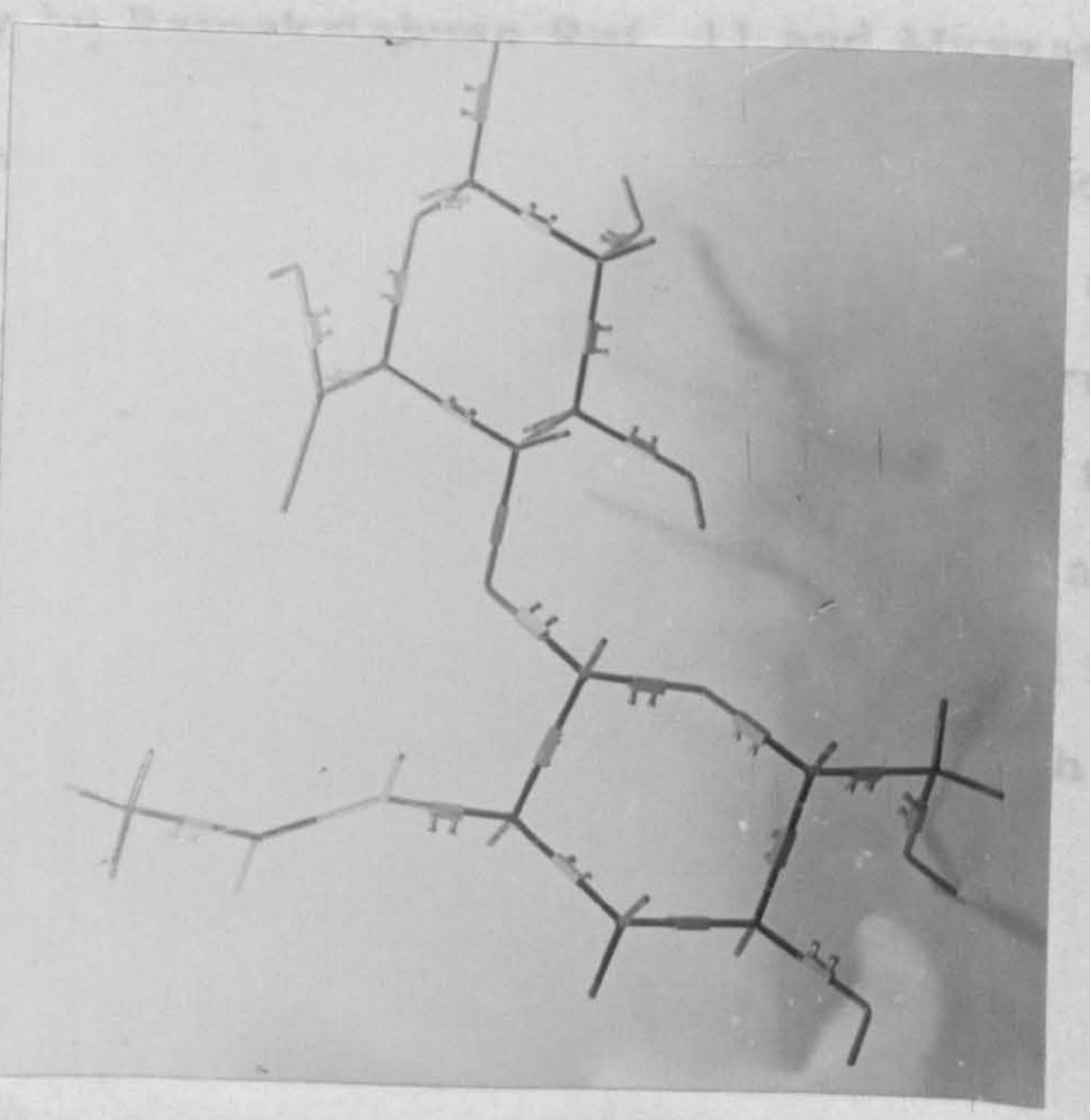

4) Possible intra molecular hydrogen bonds.

An internal equilibrium, for the molecule in vacuo, will be reached based on these forces. However, for the real situation in the solid state, or in solution, there are other important interactions which operate, and which make the application of results from any simple analysis very uncertain. The results are very useful when applied to problems concerning simple fibrous proteins and polysaccharides.

The first calculations used only the repulsive term (1) which meant, in effect, that a particular Van der Waal radius was assigned to each atom. Fig. 2.7 shows the presentation of results for two glucose residues Ref. 10. The angles ϕ_1 and ϕ_2 were stepped at 10^{o} intervals and the distance between all atoms of the two residues was measured. The conformation was accepted or rejected on the grounds of the Van der Waal radii of two or more atoms overlapping to an unacceptable degree. The type of representation used is called a conformational map and the area within the boxes denotes the sterically allowed regions. On adding further energy terms it is possible to draw in potential energy contours indicating the most favourable conformation within the box.

When these methods are applied to molecules having a helical conformation the condition of a regular helix puts further constraints on the rotational parameters between units. The application of the mathematics for determining the helical parameters of a chain molecule as a function of its internal rotational angles was carried out independently by Ramakrishnan Ref. 11 and Myszawa et al.. Ref. 13.

The two methods differ in an important aspect. In the Ramakrishnan method the helical parameters i.e. axial repeat (h) and rotation (ω) are calculated for each set of internal angles considered but the equations are not formulated in such a way that the tortional angles required can be calculated when h and ω are known. In the Myszawa et al. approach the polymer is described in very general terms as an arbitrary number of linked atoms each having its own

Fig. 2.7 Conformational Map for Cellobiose

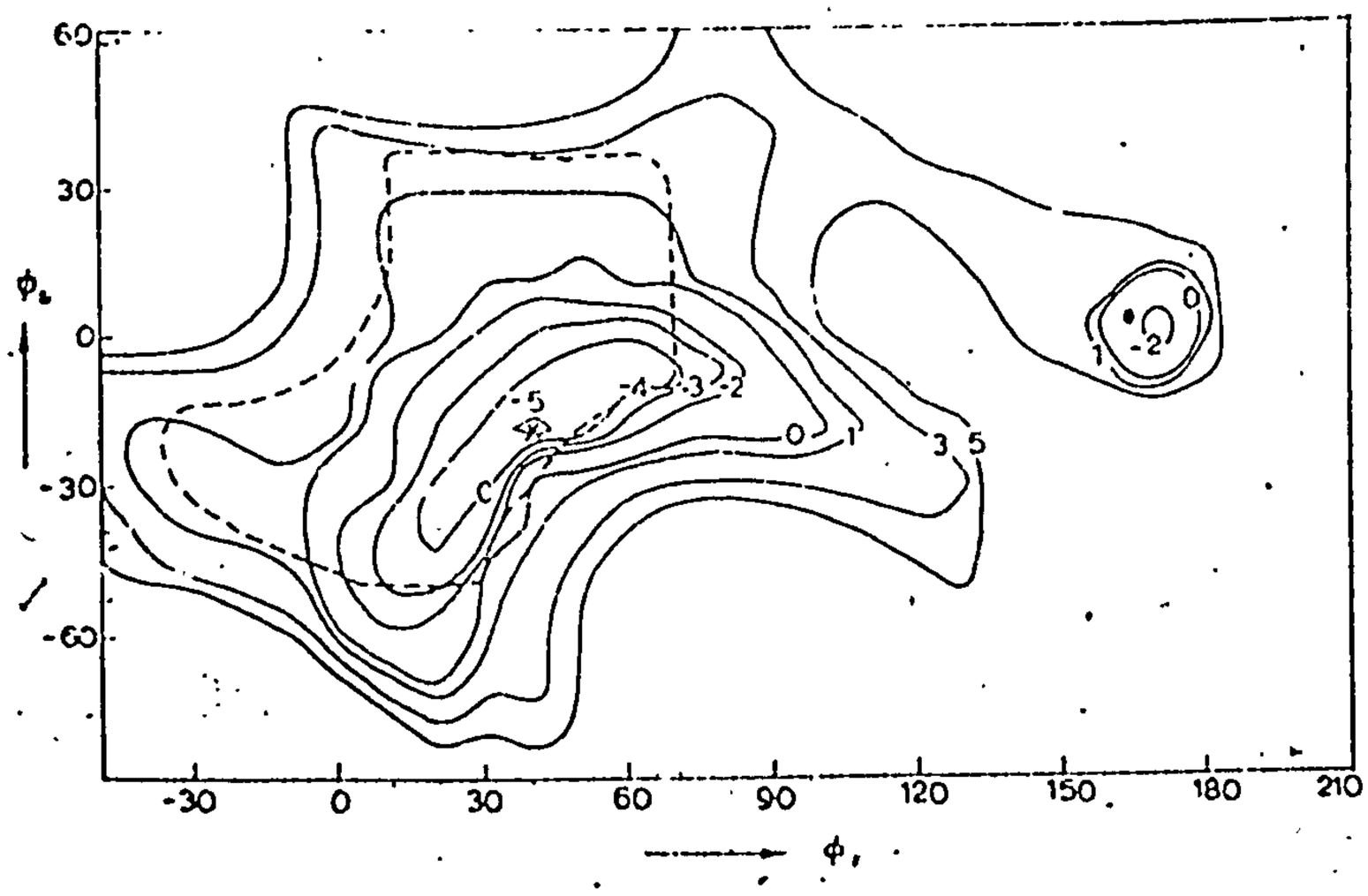

Energy contour diagram (in kcals 'mole) obtained using the expression (1) for a pair of β-D-glucose residues joined through (1 → 4) linkage. The steric map is indicated (- - - -). © The position of occurrance of cellulose. ⊗ Position of occurrance of minimum energy

allowed range of values of internal rotation. The equations are implemented so that tortional angles may be calculated from given helical parameters. Thus the method is more powerful because the helical parameters are obtained directly from the X-ray diffraction pattern.

2.9 Chain Packing Analysis

Chain packing is a natural extension of conformational analysis and is used in conjunction with results obtained from X-ray fibre studies. It finds two applications when used in a simple way

(1) The exclusion or possibility of two or more chains forming a multistranded helix.

(2) The confirmation of the number of chains in a unit cell and the determination of the possible relative positions of the chains.

The main energy terms are precisely those employed in conformational analysis, i.e.

1) Van der Waal repulsive and attractive forces between chains.

2) Inter chain hydrogen bonding.

3) Electrostatic and possible dipole-dipole interactions between chains.

The work in this thesis only makes use of the repulsion term in (1) and is used as a means of testing postulated packing schemes for proposed conformations. Computer programmes for this purpose were developed by I. Nieduszynski Ref. 14 and have been used in a modified form. The method consists of tabulating all the ways the asymmetric element of one chain can see the same unit of the other chain. In the case of a two stranded helix both chains have the same axis and therefore the only variables are a translation and rotation of the two units. For the most general case where the two chains are not coaxial but are placed a specified distance apart and are not symmetry related there are three possible variables to consider. These are, a rotation for each unit, and a translation. Fig. 2.8 shows schematically the variables involved and the method used for

Fig. 2.8 Schematic diagram for the description of the variables employed in the chain-packing program

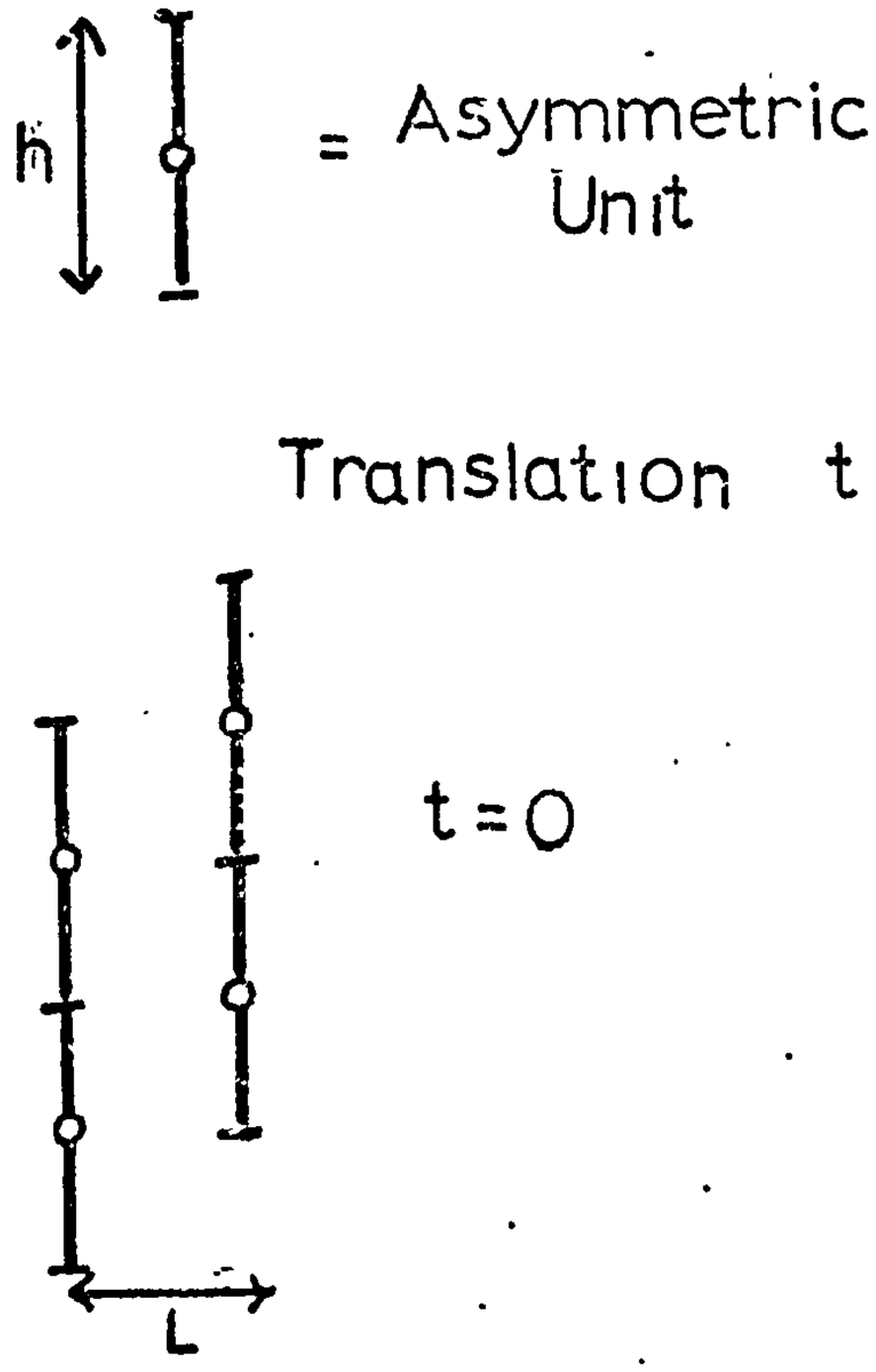

displaying the results. The number of close contacts are tabulated as a function of translation and rotational variables and the regions of no contacts denote the allowed packing regions. Assuming a symmetry relation between chains reduces the number of situations that have to be looked at.

2.10 Application to Hyaluronic Acid

There are two pieces of information available from the spacings measured on the meridian of an X-ray diagram, and they are the axial rise per residue (h) and the rotation per residue (ω). In the case of a disaccharide repeating unit with two different glycosidic linkages there are four conformational angles to be considered i.e. Φ_1, Ψ_1, Φ_2, Ψ_2. Fig. 2.9 shows the repeat unit of hyaluronic acid where N is the N-acetyl-glucosamine residue and G is glucuronic acid. Clearly no unique solution exists in terms of these angles for a specified helix. Rather is there a range of angles Φ_1, Ψ_1, for which an allowed PH12, PS12 exists giving the specified helical parameters. In view of this difficulty model building and conformational analysis were used together.

2.11 Coordinates for Hyaluronic Acid

For the basic description of the pyranose ring the coordinates compiled by Ramachandran Ref. 15 were used. As hyaluronic acid is built up from two such units, each with certain side groups attached, a 'pseudo monomer' was created consisting of the two sugar rings joined at the 1e - 4e linkage.

As a zero-zero convention has been agreed upon, Ref. 16, all values of the PHI's and PSI's in the trial models are in the following convention. Namely, that the zero position for the dihedral angles is taken to be where the five atoms H1(N), C1(N), 0, C4(G), H4(G) are all in the same plane (see fig. 2.9) with the C1(N) - H1(N) vector in the same sense as the C4(G) - H4(G) vector. A positive rotation of Φ_1 is then taken to be a rotation of the G residue in a clockwise

Fig. 2.9 Chemical structure of hyaluronic acid.

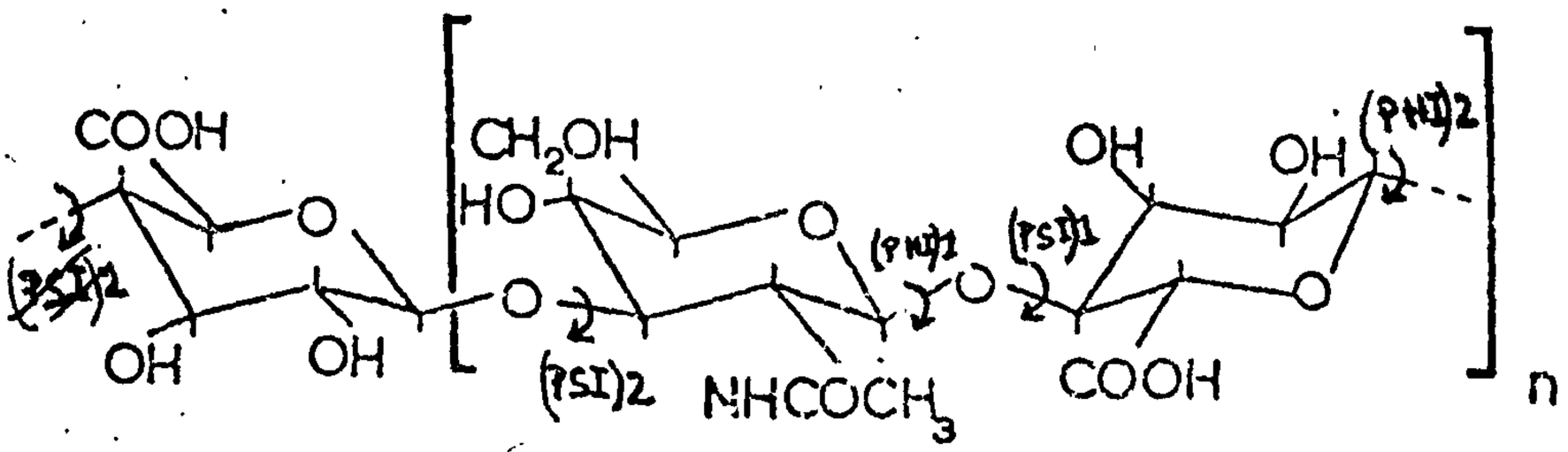

direction around the C1(N)-O bond while looking along direction C1(N)-O. A rotation of positive (PSI) is a rotation, again of the G residue, about the bond O - C4(G) in a clockwise direction looking along the O - C4(G) direction. The zero, zero position at the 1e - 3e linkage is precisely analogous.

Full coordinates for the disaccharide of hyaluronic acid were completed by putting in the coordinates of the groups $-CH_2OH$, -COOH and $-\overset{H}{\underset{|}{N}}-\overset{\overset{O}{\|}}{C}-CH_3$ in their respective positions. The coordinates of these groups were worked out relative to systems of axes fixed in the respective side groups and then transferred to the Ramachandran system. Fig. 2.10 shows the axes systems employed in the side groups and the initial positions in which the side groups were fixed.

Once a trial set of coordinates had been produced for the N residue and the G residue in the Ramachandran system, the two sets of coordinates were added together into the same system as shown in Fig. 2.11. The origin was moved to the bridge oxygen i.e. the O4(G), O1(N) atom and the coordinate system set up as indicated with the two residues in the zero-zero position. The pseudo momomer was then formed by choosing values for (PHI) and (PSI). Table 2.3 gives the full coordinates for the N and G residues in the Ramachandran system.

2.12 Generation of Coordinates for Particular Conformations

Sathyanarayana and Rao Ref. 17, and Rees Ref. 12, have published conformational maps and potential energy data for simple 1e → 3e and 1e → 4e linked glycans. These are reproduced in Fig. 2.12. Examination of these two linkages for hyaluronic acid using Courtauld space filling models indicated that the presence of the carboxyle and acetamido side groups did not restrict, to a significant extent, the range for the allowed regions shown in Fig. 2.12. This suggested that, although the potential energy curves could not be considered reliable

Fig. 2.10 Description of the side group coordinates

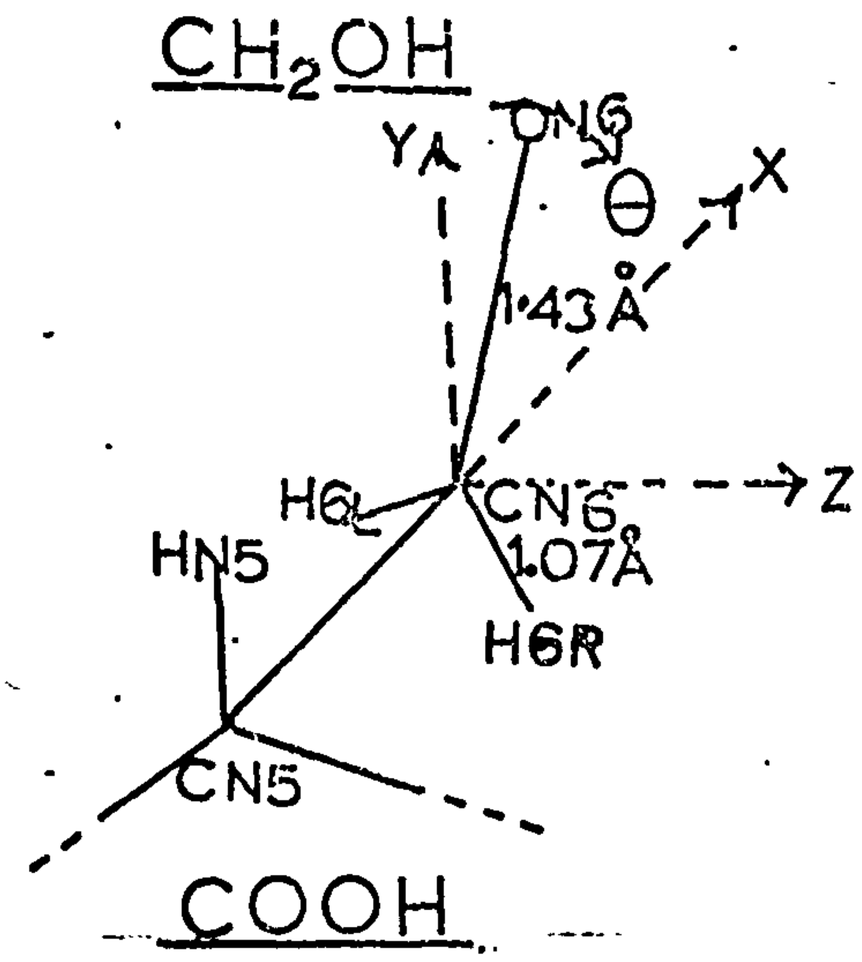

X(ONG) = 0.4767
Y(ONG) = 1.3482 cos θ
Z(ONG) = -1.3482 sin θ
X(HGL) = 0.3567
Y(HGL) = 1.01cos(120-θ)
Z(HGL) = -1.01sin(120-θ)
X(HGR) = 0.3567
Y(HGR) = 1.01cos(120+θ)
Z(HGR) = 1.01sin(120+θ)

X(OGD) = 0.5655
Y(OGD) = 1.1595cos θ
Z(OGD) = 1.1595sin θ
X(OGS) = 0.6571
Y(OGS) = -1.0515cos θ
Z(OGS) = -1.0515sin θ

X(HNA) = 1.876
Y(HNA) = 0.913 cos θ
Z(HNA) = 0.913sin θ
X(CNA) = 2.188
Y(CNA) = 1.105cos θ
Z(CNA) = 1.105sin θ
X(ONA) = 1.724
Y(ONA) = 2.255cos θ
Z(ONA) = 2.255sin θ
X(CNB) = 3.643
Y(CNB) = 0.866 cos θ
Z(CNB) = 0.866 sin θ

Fig. 2.11 Zero-Zero at the 1e→4e linkage of hyaluronic acid and the coordinate system to describe the disaccharide

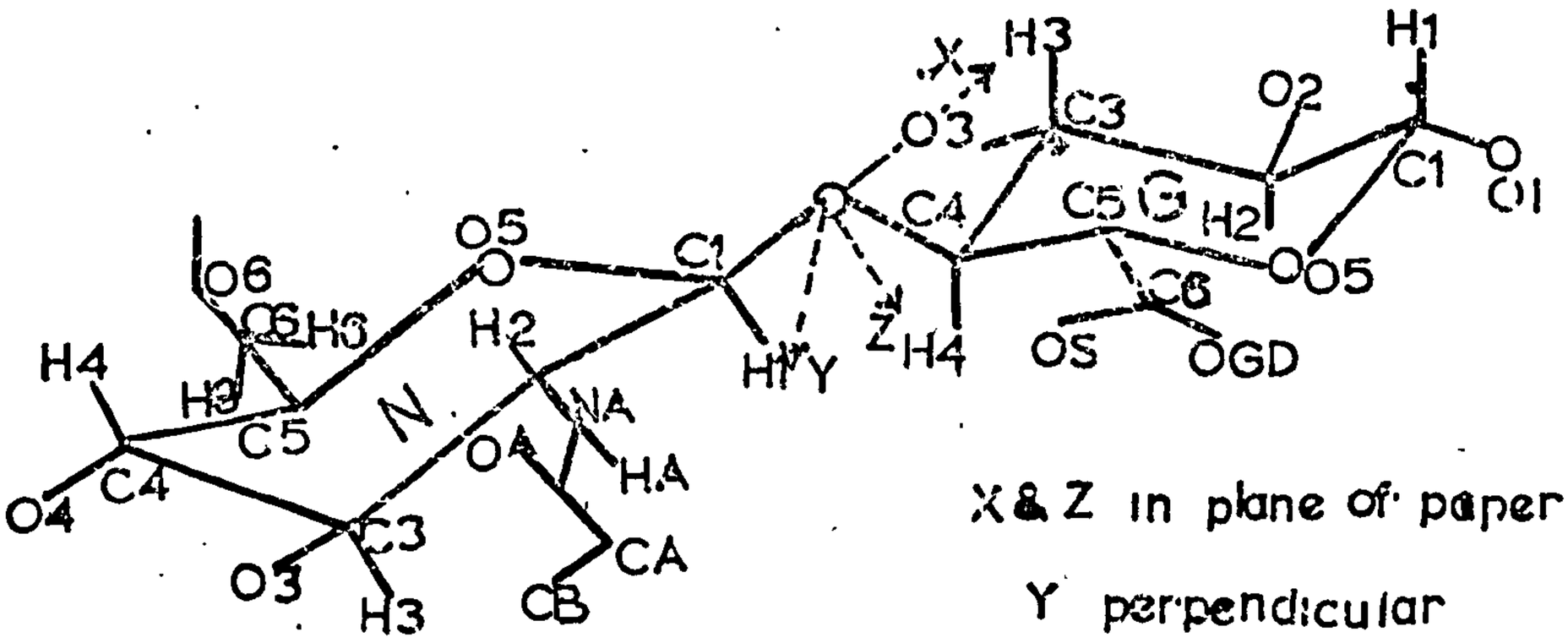

X & Z in plane of paper

Y perpendicular

Atoms in N res. are named

CN1, CN2 etc.

Atoms in G Res. are named

CG1, CG2 etc.

Table 2.3

Ramachandran Coordinates for Glucuronic Acid and N-acetyle-Glucosamine Residues

N.B. Zero has been shifted to OG4, ON1 atoms.

CG1	3.8625	0.1219	-1.4930
CG2	3.4654	-1.1729	-0.8145
CG3	1.9566	-1.2340	-0.6865
CG4	1.4115	0.0000	-0.0000
CG5	1.9388	1.2657	-0.6792
OG5	3.3510	1.2260	-0.7555
HG1	3.4457	0.1219	-2.4783
HG2	3.8823	-1.1729	0.1708
OG2	3.9625	-2.2772	-1.5350
OG3	1.5886	-2.3887	0.0122
HG3	1.5397	-1.2340	-1.6718
HG4	1.8284	0.0000	0.9853
OG4	0.0000	0.0000	0.0000
CG6	1.5708	2.5611	-0.0354
OG6	0.8721	3.4178	-0.5919
OG6	2.0040	2.7106	1.1714
HG5	1.5220	1.2657	-1.6646
OG1	5.2379	0.2216	-1.4994
CN3	-2.2782	-1.1896	-2.6349
CN4	-3.0609	0.1011	-2.7496
CN5	-2.1435	1.3042	-2.5204
ON5	-1.4470	1.1603	-1.2973
CN1	-0.6261	0.0000	-1.2288
ON1	0.0000	0.0000	0.0000
HN1	0.0674	0.0000	-2.0437
CN2	-1.4863	-1.2415	-1.3438
HN2	-2.1798	-1.2415	-0.5289
NNA	-0.6540	-2.4523	-1.2787
HNA	0.0123	-2.5058	-2.0117
CNA	-0.7863	-3.3605	-0.3409
ONA	-1.5871	-3.3431	0.5927
CNB	0.2124	-4.5328	-0.4363
HN3	-1.5843	-1.1896	-3.4498
ON3	-3.1352	-2.2929	-2.7077
ON4	-3.6914	0.2029	-4.0085
HN4	-3.7544	0.1011	-1.9348
CN6	-2.8057	2.6419	-2.4931
H6R	-3.5814	2.6349	-3.2189
H6L	-3.3063	2.8080	-1.5928
ON6	-1.8394	3.6888	-2.7900

G RESIDUE

N RESIDUE

Fig. 2.12 Conformational Maps of 1e→3e linkage and 1e→4e linkage for β glucans.

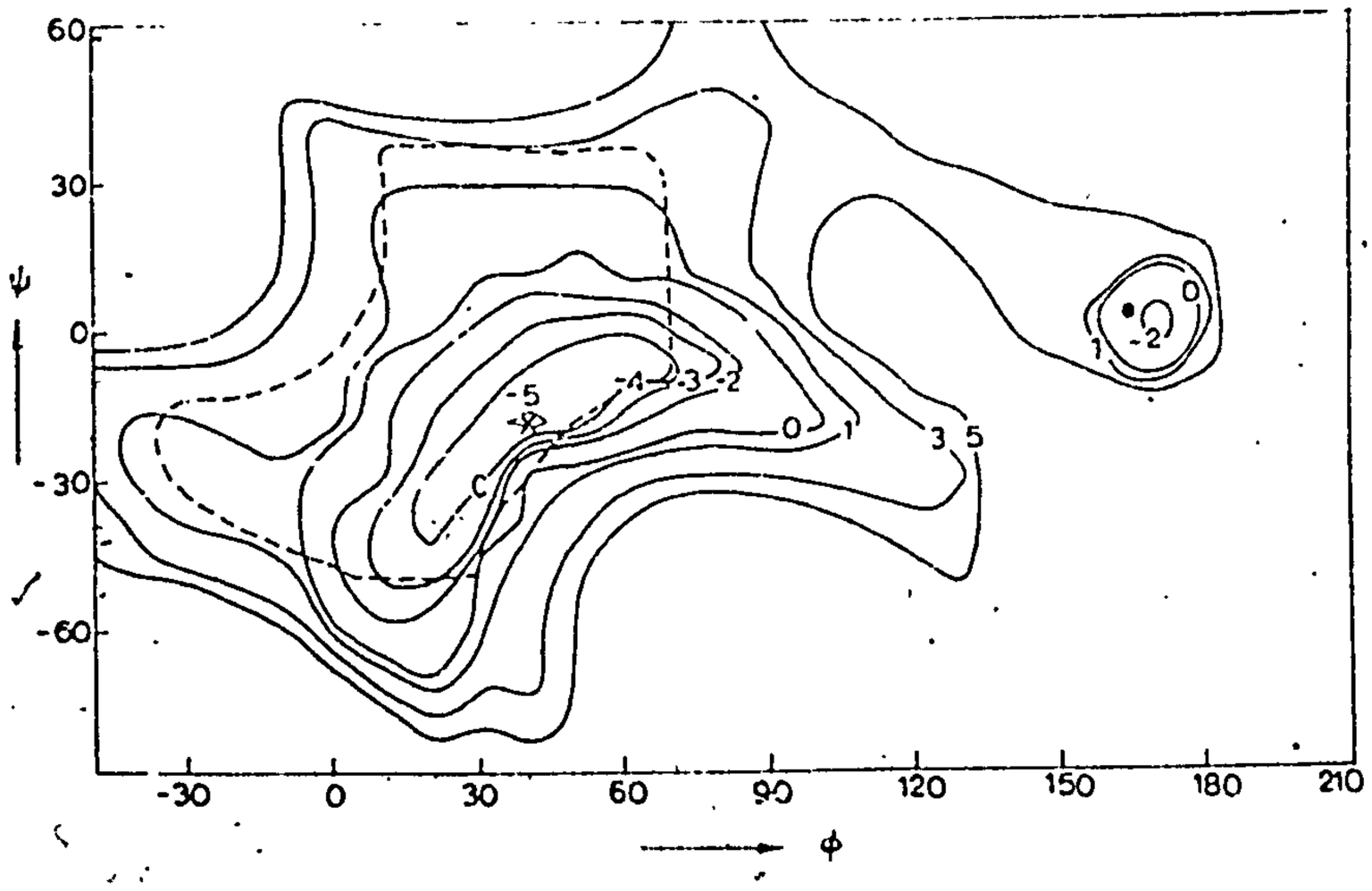

Energy contour diagram (in kcals 'mole) obtained using the expression (1) for a pair of β-D-glucose residues joined through (1 → 4) linkage. The steric map is indicated (- - - -). © The position of occurrance of cellulose. ⊗ Position of occurrance of minimum energy

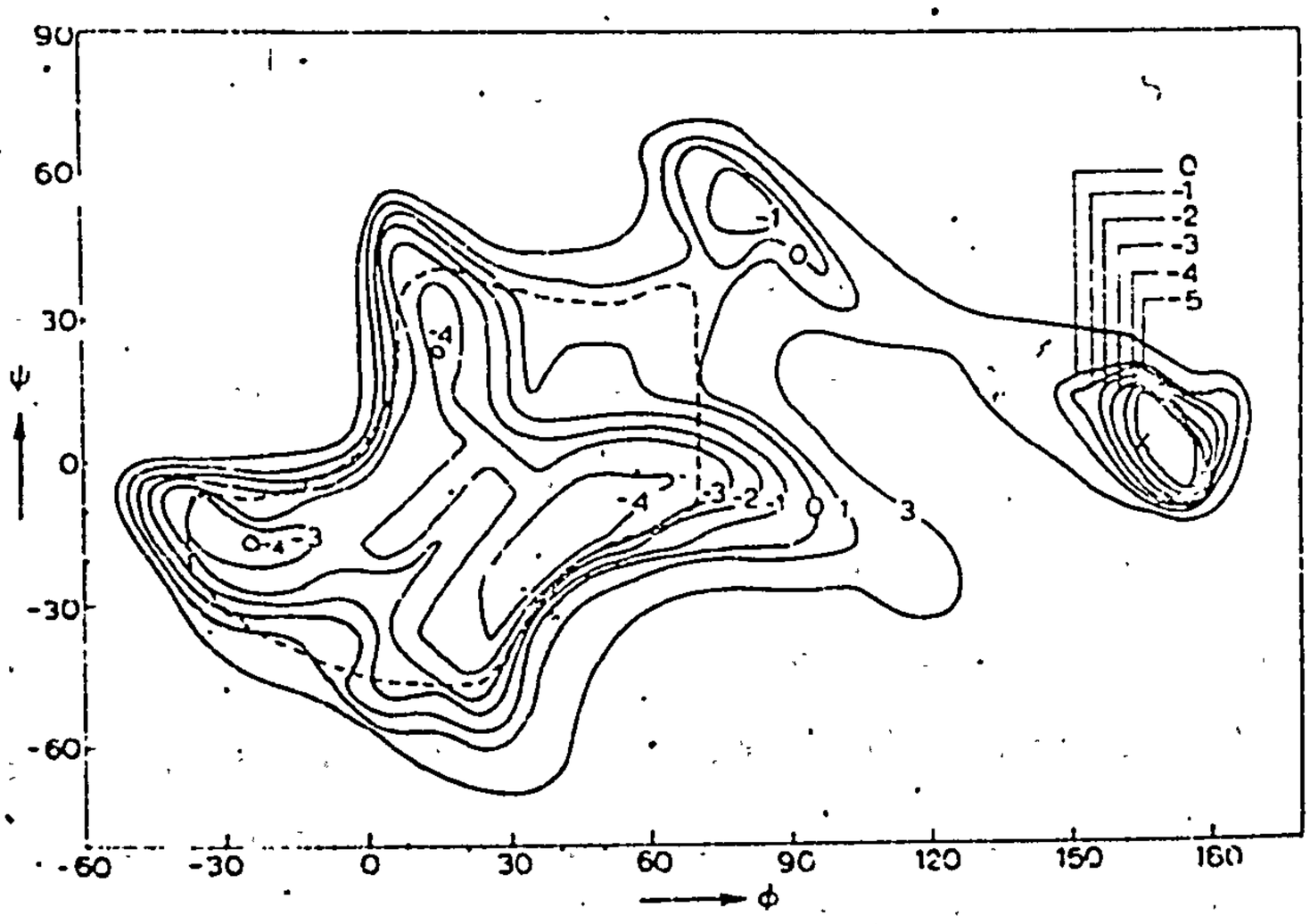

Energy contour diagram (in kcals mole) obtained using the expression (1) for a pair of β-D-glucose residues joined through (1 → 3) linkage. The steric map is indicated (- - - - -). © The position of occurrance of minimum energy.

for hyaluronic acid, the sterically allowed box was reasonable. It can be seen that the allowed regions centre around the zero-zero for both positions. The resulting equilibrium conformation is close to a two fold helix vis. Fig. 2.13(a) and distributes the carboxyle and acetamido groups on either side of the helix. A slight rotation about the linkages is thus sufficient to distribute the carboxyles uniformly over a cylindrical surface. As Atkins and Sheehan pointed out Ref. 18, the construction of the molecule with two 1e → 4e linkages would put all the carboxyle and acetomido groups on the same side of the molecule Fig. 2.13(b).

A further examination of the linkages using models reveals their very different nature as pointed out in Chapter I. Rotation of the angles $\langle PHI \rangle 1$, $\langle PSI \rangle 1$ at the 1e → 4e linkage leaves a virtual bond, drawn between the bridge oxygen atoms at extreme ends of the disaccharide, little affected. The effect, however, of rotation about the 1e → 3e linkage is to kink the disaccharide, thereby reducing the virtual bond length and changing the 'direction' of the molecule. These considerations indicate how a 1e → 3e, 1e → 4e knitting pattern allows the polymer a variety of shapes.

In deriving the conformations used in Chapters IV and V the conformational maps were used in the following way. Allowed values of $\langle PHI \rangle 1$, $\langle PSI \rangle 1$ at the 1e - 4e linkage were scanned at 20^{o} intervals and a pseudo monomer set up for each pair of values. A search was then made at the 1e - 3e linkage using the Ramakrishnan approach (see Appendix) for a helix with the desired parameters and values of $\langle PHI \rangle 2$, $\langle PSI \rangle 2$ within the allowed conformational area. An average conformation satisfying the conditions was then chosen, making use of intra molecular hydrogen bonds where possible. Fig. 2.14 is a simple flow diagram for the computing of these conformations.

Fig. 2.13 Illustrating the effect of (a) alternating linkage and (b) all 1e→4e linkage

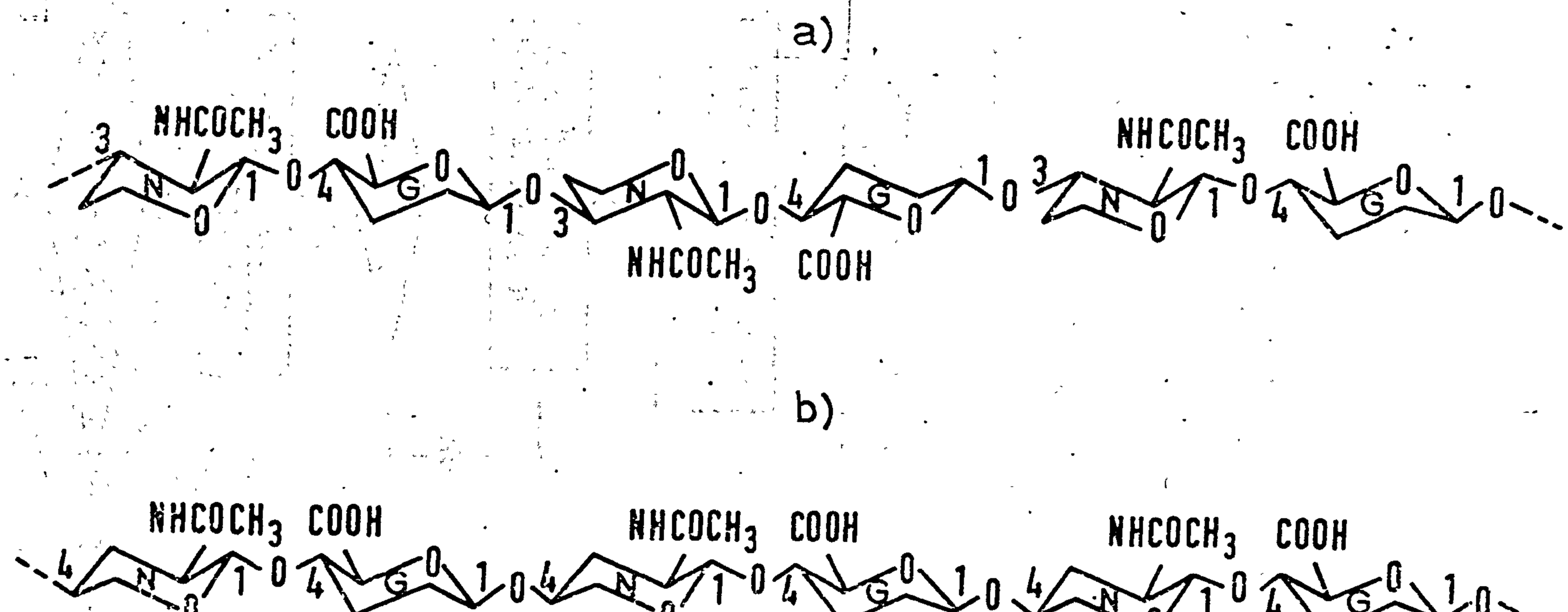

Fig. 2.14 Flow chart for computing trial conformations

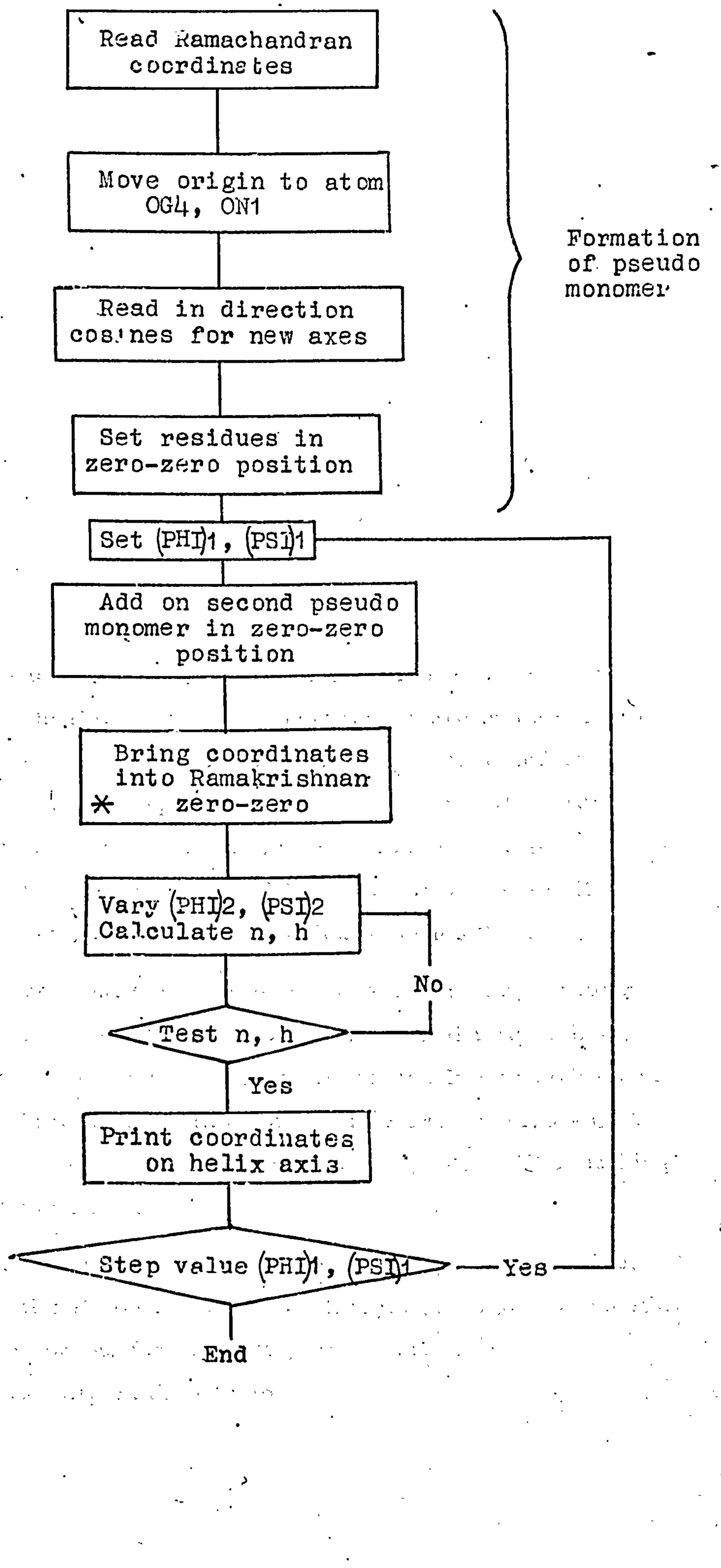

* See appendix

CHAPTER III

3.1 Introduction

Using the methods of crystallisation discussed in chapter II together with the computer and model building methods outlined in the same chapter, a survey of various conformations and packing of hyaluronate chains was undertaken. The X-ray diagrams exhibited in the next two chapters are not in a chronological order resulting from a systematic series of experiments; rather they have been obtained during a survey of different experimental approaches and conditions, and any relationship between them has been seen with hindsight. This survey may act as a foundation for a systematic approach to the study of the various conformations of hyaluronate found in solid state preparations.

3.2 Results Type I Conformation

Fig. 3.1 shows X-ray diagrams obtained from sodium and potassium salts of hyaluronate. The specimens were made using the film method and held under stress at room temperature and at 85% relative humidity. Though specimens X-rayed immediately after stretching showed this diagram it improved on being held in the above conditions over a number of weeks. The material was grade II, human umbilical cord, hyaluronate supplied by Miles Seravac.

It can be seen that the sodium and potassium samples form an isomorphous series and that the degree of crystallinity is high. Table 3.1 shows the measured spacings of the row lines which index on an orthorhombic unit cell with basal parameters $a = 11.0 \pm 0.2\text{Å}$ $b = 9.9\text{Å} \pm .02$ and a layer line spacing of $33.4\text{Å} \pm 0.4\text{Å}$. The striking features of the diagrams are

(a) the very strong meridionals on the 2nd, 4th and 6th layer lines

(b) that the meridionals on the 2nd and 4th layer lines have a peculiar shape, the one on the former being almost circular

(c) the lack of intensity on the equator.

Fig. 3.1 (a) Type 1 sodium hyaluronate

(b) Type 1 potassium hyaluronate

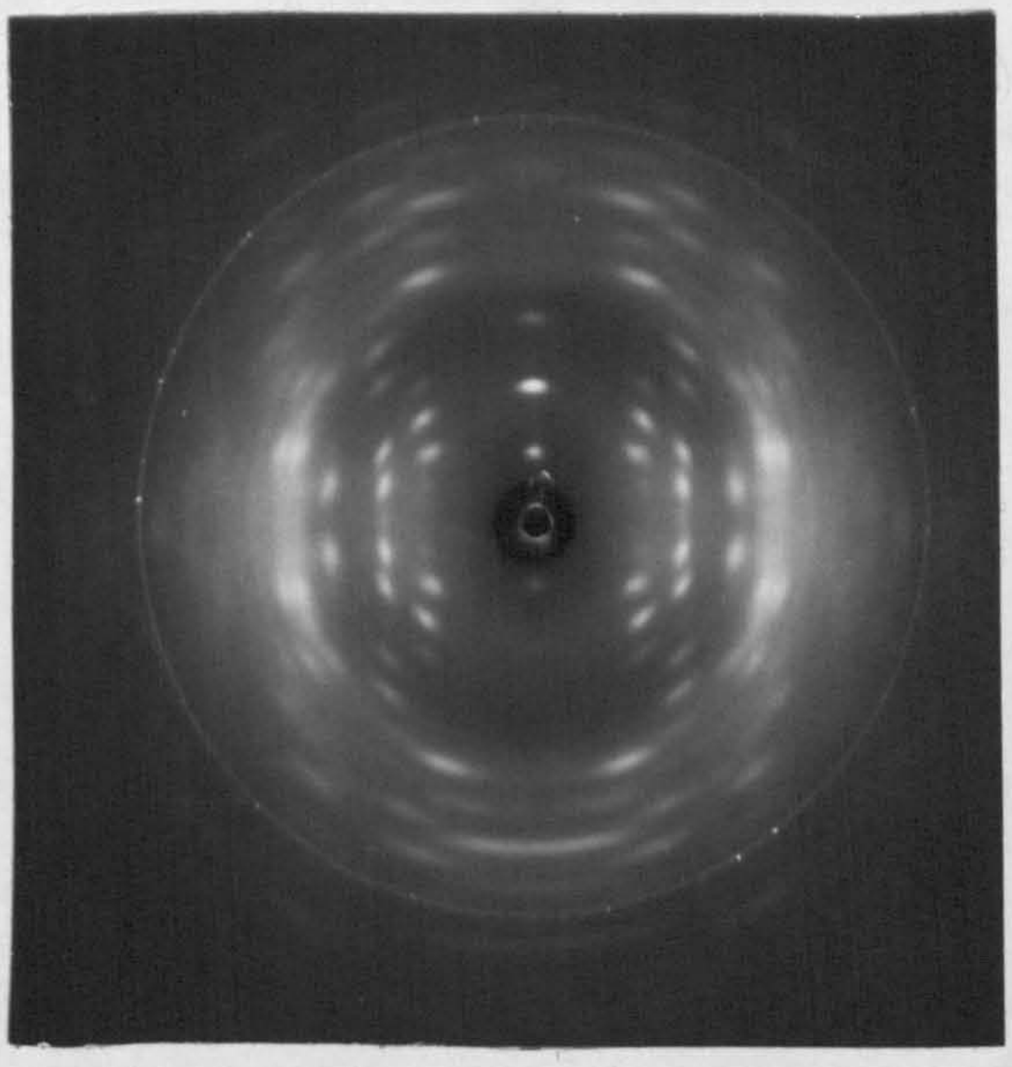

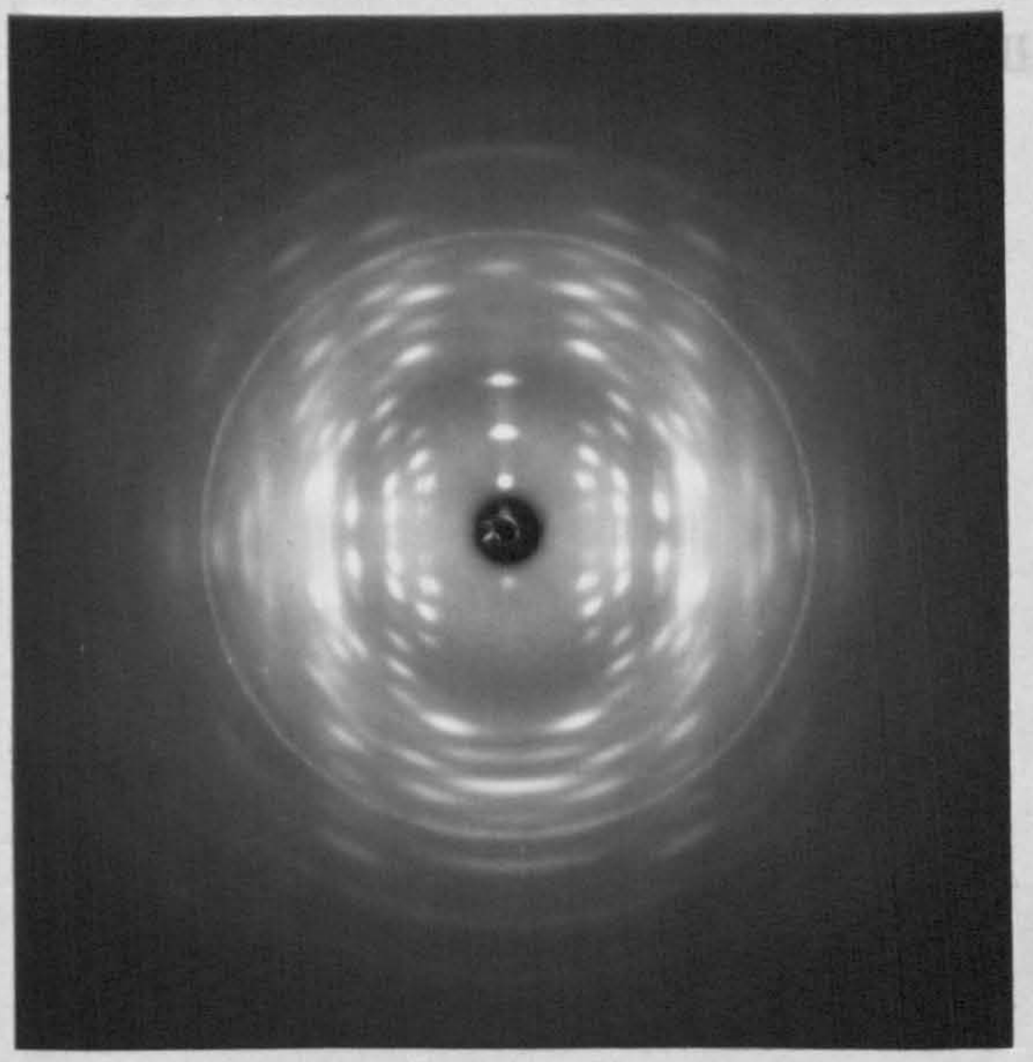

Table 3.1

Measured Spacings for Potassium Hyaluronate and Sodium Hyaluronate

Measured Spacing Å	Description	Index
11.0 ± 0.2	Absent	100
9.9 ± 0.2	Absent	010
7.3 ± 0.15	Weak	110
5.5 ± 0.1	Absent	200
4.8 ± 0.1	Medium	210
4.5 ± 0.1	Medium	120
3.6 ± 0.1	Medium-Weak	300
3.45 ± 0.1	Medium-Weak	220
3.2 ± 0.1	Medium	130
2.83 ± 0.1	Medium	

Measurement of layer line spacing using off-meridional reflections 33.4Å ± .5Å.

Row Lines index on orthorhombic lattice

a = 11.0Å b = 9.9Å.

Well crystallised specimens of sodium hyaluronate in type I conformation were washed in an ethanolic acid solution. The procedure adopted was to dip the specimen in a bath of 80% ethanol, 20% 0.2N HCl, for 10 minutes, repeating the process three times in fresh solutions. Finally it was washed in ethanol and hung up under stress at 85% relative humidity. Fig. 3.2 shows the diagram obtained from such a specimen and Table 3.2 gives measured row line spacings. The reflections index on an orthorhombic unit cell where $a = 10.4\text{A} \pm 0.2\text{A}$, $b = 9.9\text{A} \pm 0.2\text{A}$ and the layer line spacing is again 33.4A. The important features of the diagram are that

a) the unit cell is close to a tetragonal form

b) diffraction spots are resolvable out to 1.5A

c) some strong equatorial reflections have appeared

d) the meridional distribution and intensity is markedly different from Fig. 3.1.

Point d) is very interesting because the very strong meridional on the second layer line has disappeared and the meridionals on the fourth, sixth and tenth layer lines are much weaker than those in Fig. 3.1. This change of meridional intensity without any apparent change in backbone conformation indicates that the meridional intensity in the sodium and potassium salt forms arises from a curious distribution of these counterions. It is as if the counterions were clustered at two levels in the unit cell 16.7A apart.

3.3 Choice of Model

The number of chains in the unit cell can frequently be deduced from density and volume considerations. Densities measured by the flotation method gave a value of 1.46 ± 0.02 gms. per c.c. If the density is expressed in terms of the molecular weight of a disaccharide and Avogadro's Number (N) then

$$d = n \times \frac{\text{Molecular Weight}}{\text{Vol. of unit cell}} \times \frac{1}{N}$$

where n is the number of disaccharides in the unit cell. Substituting

Fig. 3.2 Type I specimen washed in dilute hydrochloric acid

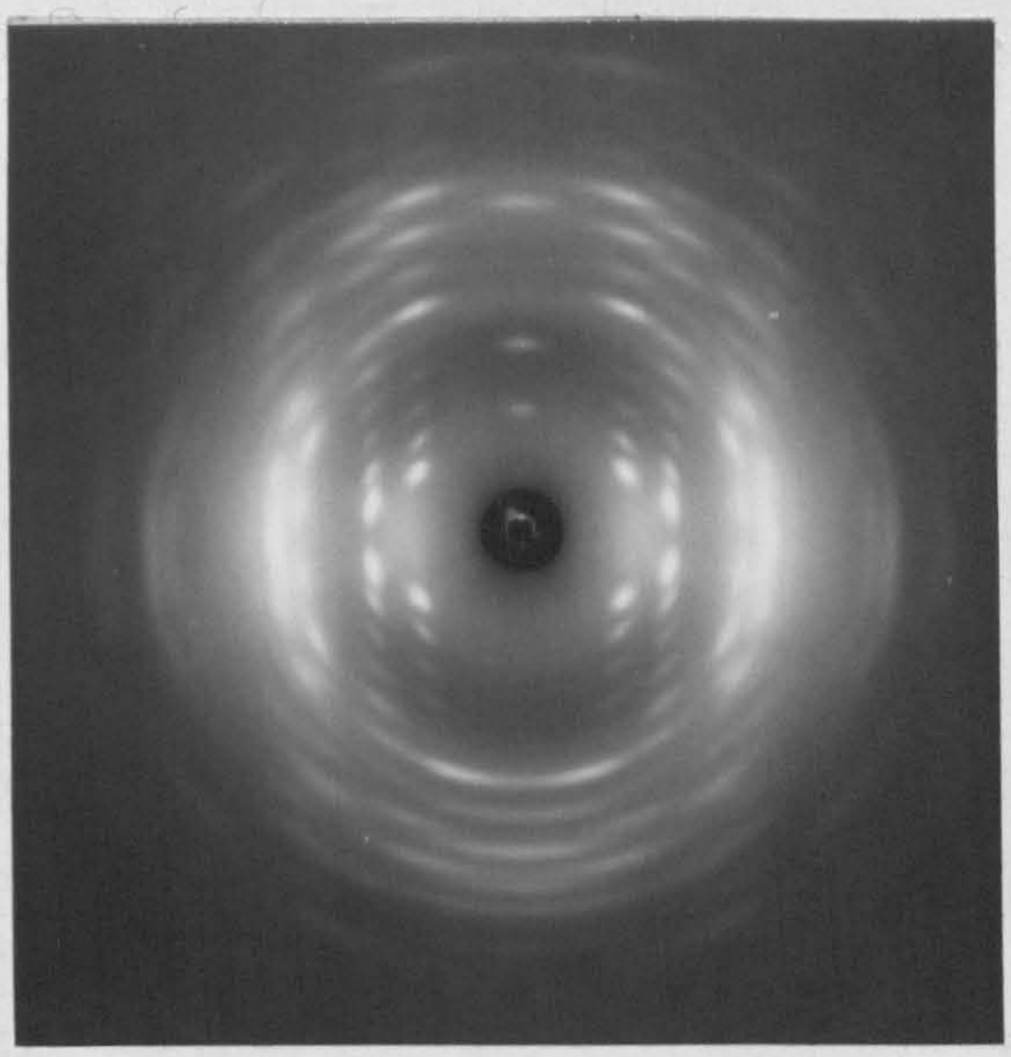

Table 3.2

Measured Spacings for 'Acid Washed' Type I Specimen

Measured Spacing Å	Description	Index Type
10.5 ± 0.2	V. Weak	100, and 010 not resolved
7.2 ± 0.2	V. Weak	110
5.20 ± 0.1	Absent	200
5.96 ± "	V. Weak	020
4.54 "	Strong	210
4.46 "	Strong	120
3.3 "	Medium	030
3.14 "	Medium Strong	$3\bar{3}0$)
2.82 "	Medium	320 ?) Indices
2.52 "	Medium	410 ?) cannot
2.4 "	Possibly strong (with correction)	420 ?) be
2.015 "	" " " "	) separated

Row lines index on an orthorhombic lattice

$$a = 10.5\text{Å} \pm 0.2\text{Å}, \quad b = 9.9\text{Å} \pm 0.2\text{Å},$$

$$c = 33.4\text{Å} \pm 0.4\text{Å}.$$

the values in the above formula gives a value of n = 7.7 which implies that there are eight disaccharides in the unit cell. The presence of eight disaccharides suggests that there are two chains each having four disaccharides in one repeat of the helix.

It was pointed out in Chapter II that an intelligent guess at the backbone conformation of the molecule is made on the basis of measurements taken from the meridian of the X-ray diagram together with a knowledge of the structural units making up the chain. The interpretation of the diffraction data in this case presents some difficulties because the fundamental repeating unit appears to have an axial rise of $16.7\text{Å} \pm 0.3\text{Å}$. This must represent at least a tetrasaccharide unit in the known hyaluronic acid chemical structure. The most general case of a tetrasaccharide repeat would require eight variables to describe the backbone alone and this is a formidable number when testing possible structures with model building methods.

If it is assumed that the backbone conformation has not a tetrasaccharide nature but rather a disaccharide repeating unit then the number of variables is reduced to four. The model thus adopted is a regular four fold helix and the tetrasaccharide nature is assumed to arise out of (1) Different dispositions of the side groups on alternate disaccharides

or (2) Some irregular distribution of the counterions present. Either or both of these effects are possible and some support for viewing the problem in this manner comes from the comparison of Figs. 3.1 and 3.2.

3.4 Chain Packing

The presence of two chains in the unit cell is strongly suggested by the density measurements but the problem then arises as to the positions of the chains in the unit cell. The simplest possibilities are

(a) Two single chains parallel or antiparallel with one at the corners and one at the centre.

(b) A two stranded unit placed at the corners of the unit cell.

The assumption of a four fold helix as a backbone conformation with an axial rise of 8.35Å was made by Dea et al. Ref. 1., and a packing analysis on a trial four fold conformation was carried out. Their conclusions from this packing analysis and conformational analysis were that

(1) Left handed four fold helices are highly favoured over right handed helices.
(2) A trial four fold conformation could not be packed with a similar chain in a two stranded parallel system.
(3) Two chains could not be packed as separate chains with one at the corners and one in the middle of the unit cell.

This led them to propose the model for hyaluronic acid, of two antiparallel strands intertwining in a double helix, which they showed could be packed with only one or two short contacts between chains.

Using the same assumption as Dea et al. Ref. 1 about the backbone helix, a packing analysis was carried out using the principles outlined in Chapter II. Model building quickly showed that only left handed helices were really feasible and that the choice of four fold helices of axial repeat 8.4Å was limited.

A trial model was chosen with the dihedral angles at the $1_e \rightarrow 4_e$, $(PHI)1 = 50$, $(PSI)1 = 0^\circ$ and at the $1_e \rightarrow 3_e$, $(PHI)2 = 78^\circ$, $(PSI)2 = 20.5^\circ$. The coordinates for the conformation are given in Table 3.3. and the two projections are shown in Fig. 3.3.

The packing possibilities attempted were

(a) Antiparallel packing about the same axis
(b) Antiparallel packing of two chains in space group $P2_12_12_1$ i.e. one chain at the corners and an antiparallel one in the middle.
(c) Parallel packing of single chains with one in the middle.

The possibility of packing two chains in a parallel double helix was not considered, because of the following arguments. In general when two strands pack together around a single axis they are constrained by space filling considerations to be 180°, or close to 180°, out of phase.

Table 3.3

Trial Coordinates for Type I Conformation

1e→4e $(PHI)1 = 50.$, $(PSI)1 = 50$; 1e→3e $(PHI)2 = 78^{\circ}$, $(PSI)2 = 20.5^{\circ}$

	X	Y	Z
CG1	0.1548	-3.2079	5.4363
CG2	1.2360	-4.1487	4.9461
CG3	2.1399	-3.4169	3.9743
CG4	1.3441	-2.7763	2.8574
CG5	0.2092	-1.9240	3.4307
OG5	-0.5716	-2.6926	4.3266
HG1	0.6270	-2.4049	5.9626
HG2	0.7639	-4.9516	4.4197
OG2	1.9672	-4.6657	6.0340
OG3	3.0906	-4.3024	3.4558
HG3	2.6120	-2.6140	4.5007
HG4	0.8720	-3.5792	2.3511
OG4	2.1730	-1.9884	2.0300
CG6	-0.7283	-1.3221	2.4377
OGD	-0.3542	-0.1005	2.2828
OGS	-1.3770	-2.1732	1.7164
HG5	0.6814	-1.1220	3.9571
OG1	-0.7237	-3.9125	6.2265
CN3	3.1903	-1.7007	-1.4757
CN4	3.8350	-3.0440	-1.5609
CN5	3.1565	-4.0651	-0.6344
ON5	3.0030	-3.5597	0.6281
CN1	2.2571	-2.3502	0.7913
ON1	2.1730	-1.9884	2.0300
HN1	1.2963	-2.4907	0.2523
CN2	2.9781	-1.2585	-0.0617
HN2	3.9388	-1.1180	0.3678
NNA	2.2195	0.0000	0.0000
HNA	1.3154	-0.0711	-0.4020
CNA	2.6988	1.0972	0.5368
ONA	3.8056	1.2409	1.0540
CNB	1.7243	2.2336	0.5318
HN3	2.2296	-1.8412	-1.9453
ON3	3.9276	-0.7315	-2.1843
ON4	3.9630	-3.5119	-2.3904
HN4	4.8457	-2.9035	-1.1114
CN6	3.7981	-5.4078	-0.5650
H6R	4.2198	-5.6511	-1.5192
H6L	4.6182	-5.3590	0.0788
ON6	2.8586	-6.4093	-0.1946

Fig. 3.3 (a) Projection perpendicular to axis of the proposed type I conformation
(b) Projection down the axis

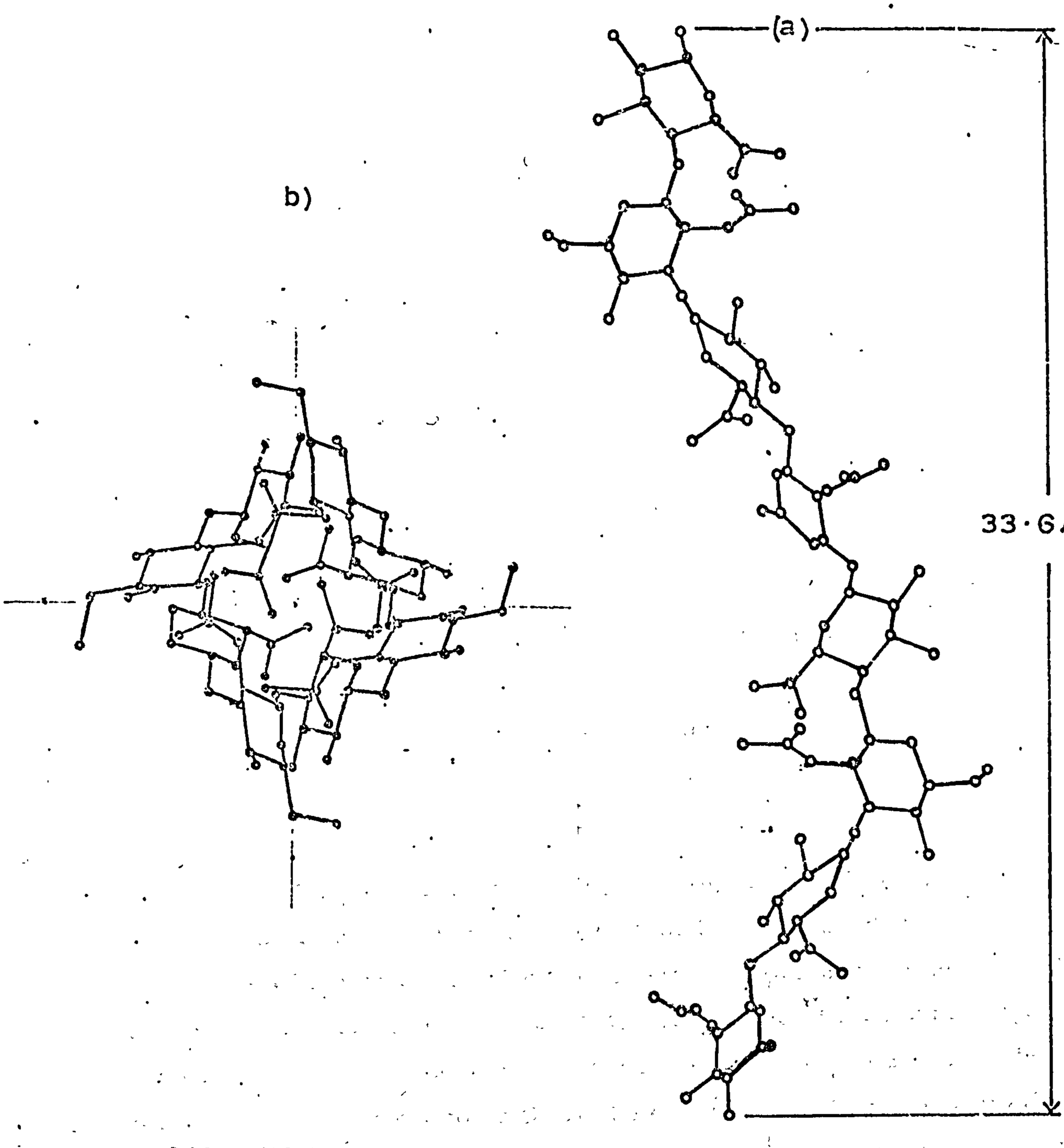

For the case of two parallel strands exactly 180° out of phase all odd layer lines would be absent i.e. there would be a halving of the X-ray diffraction pattern. The true repeat would thus be 33.4Å x 2 = 66.8Å and the appropriate model would certainly not be a simple four fold helix as proposed. In the case where the helices are almost 180° out of phase there should be a weakening of odd order layer lines and this does not appear to be the case for Figs. 3.1 and 3.2. In the case of antiparallel two stranded helices there is no simple symmetry relationship between the chains and therefore the transform that is sampled is basically that of a single chain.

3.5 Chain Packing Results

The chain packing results for the possibilities cited above are presented in Fig. 3.4. In the case of the double helix only one allowed region is found and this still has two close contacts. On closer examination these contacts are found to be between the most extreme carbon atoms on the acetamido side groups of the two chains. The position of this atom, being far from the axis of the helix, is sensitive to both slight change in the backbone conformation of the chain and also to rotation of the side group. It might therefore be expected that short contacts due to this atom may be eliminated by refinement of the conformation.

The packing result maps of Fig. 3.4 (b) and (c) show clearly that the chains can be packed as single strands when one chain is put at the centre of the unit cell. The conclusions of Dea et al. thus seem to be premature, if not incorrect. Only detailed structure factor calculations will yield a conclusive result. It might be thought that the difference in conclusions could lie in the difference of trial conformations but comparison with their published diagrams shows the trial conformations to be very similar. It was hoped that the intensity distribution on the equator of Fig. 3.1 and 3.2 would resolve the dilemma. The lack of intensity on the equator suggests that a view down the fibre axis shows no strong scattering planes but only a fairly uniform distribution of electron density over the unit cell.

Fig. 3.4 Chain packing results for the proposed type I conformation
(a) Antiparallel Double Helix
(b) Antiparallel Single Helices, space group $P2_12_12_1$
(c) Parallel Single Helices

(a) (detail of allowed region)

	275	277	279	281	283	285	287	289	291
-55	9	7	7	7	3	3	3	3	5
-53	11	11	11	11	11	11	3	1	3
-51	9	9	9	9	9	9	9	9	5
-49	9	9	9	9	9	9	9	9	9
-47	13	13	13	13	13	13	13	13	13
-45	17	13	13	13	13	13	13	13	13

(b)

	0	45	90	135	180	225	270	315	360
-50	98	23	2	0	0	1	37	99	98
-30	76	7	2	0	0	3	56	99	76
-10	60	3	3	0	0	3	80	99	60
10	58	9	1	1	1	16	99	99	58
30	59	13	1	1	1	25	99	99	59
50	55	9	0	0	2	37	99	99	55

(c)

	0	45	90	135	180	225	270	315	360
-50	57	92	99	75	14	5	2	8	57
-30	37	79	95	89	27	8	0	1	37
-10	27	60	84	81	27	3	0	4	27
10	16	31	66	70	27	2	0	5	16
30	8	26	60	62	27	0	0	2	8
50	1	10	42	53	14	1	0	0	1

Table 3.4 gives the coordinates of the possible double helix as suggested by the packing results and Fig. 3.5 shows the two projections of the double helix plotted by computer. Fig. 3.6 shows the projection down the c axis of unit cell with (a) The double helical units placed at the corners and

(b) Single chains placed in the unit cell with one in the middle. The rotation of the units in case (a) is a guess using only the constraints of the unit cell. In (b) the rotation of the chains has been obtained from the packing programme. It can be seen that for both systems the electron density distribution is uniformly spread over the area of the unit cell and that a conclusive answer is not provided by this approach. The suggested symmetry of the hyaluronate molecule for the double helix is $P4_22$ while the symmetry assumed for packing the single helices was $P2_12_12_1$.

A model of the proposed antiparallel double stranded packing arrangement is shown in Fig. 3.7 and it illustrates an interesting feature. The carboxyle groups stick in towards the axis of the double helix. This means that the charged groups are shielded from the environment to a large extent which in turn implies a considerable modification to its role as a polyelectrolyte. A comparison with the double helix of carrageenan Ref. 2 shows that the sulphate groups of the carrageenan are on the outside of the double helix so that the role of the charged groups appears to be very different for the two polymers.

The position of the carboxyles suggests that the proposed double helix would be sensitive to p.H and ionic concentration. The p.K. of the carboxyles in the double helix might well be different from carboxyles in a random coil part of the molecule but the ionisation of these carboxyles would almost certainly lead to disruption of the double helix due to electrostatic repulsion. Some further aspects of this proposed structure and its possible effects on solution properties will be discussed in Chapter VI.

Table 3.4

Coordinates for Double Helix from Chain Packing

	Two Residues of Chain I			Two Residues of Chain 2		
	X	Y	Z	X	Y	Z
CG1	2.7296	1.6922	-7.6296	0.7113	3.1313	3.1629
CG2	4.1178	1.3355	-7.1304	-3.1313	.7113	-5.2479
CG3	4.0770	0.1766	-6.1526	-3.0779	4.3263	2.6727
CG4	3.0488	-.4679	-5. 417	-4.3263	-0.0770	-5.7331
CG5	1.7039	0.9196	-5.6150	-1.1449	3.8057	1.7099
CG6	0.6756	1.3408	-4.6220	-3.3657	-1.1449	-6.7099
CN3	3.2103	-1.6626	-1. 6686	-0.5502	3.0350	0.5640
CN4	4.7197	-1.4727	-0.6234	-3.0350	-0.5502	-7.3268
CN5	5.1583	-0.2935	-1.4999	0.3148	1.9105	1.1573
CN1	3.2158	-0.5256	-2.8861	-1.9105	0.3148	-7.2535
CN2	2.7258	-1.7387	-2.1226	1.0563	1.0782	0.1543
CNA	0.6273	-2.0450	-2.7211	-1.0782	1.0563	-8.2465
CNB	-0.9108	-2.7211	-2.7172	-2.6172	2.4941	-3.7691
CN6	0.6081	-0.0602	-1.6193	-2.4941	-2.6172	-12.1799
OG5	1.8933	1.9981	-6.5109	-2.9261	3.0746	-3.8343
OG2	4.9583	1.0267	-6.2183	-3.0746	-2.9261	-12.2451
OG3	5.2964	-0.1046	-5.6461	-1.0504	4.7628	-2.0578
OG4	2.8702	-0.6616	-4.2143	-4.7623	-1.0504	-11.3486
OGD	-0.4013	0.7665	-4.4072	-1.5439	2.8695	-1.5716
OGS	1.0086	2.3668	-3.9607	-2.8695	-1.5439	-9.5324
OG1	-2.8087	2.8195	-6.4108	-2.5314	2.0112	-2.3351
ON5	4.6351	-0.4538	-2.8124	-2.0112	-2.5314	-10.7459
ON1	2.8702	-0.6616	-4.2143	-2.8942	-0.3331	-1.7366
NNA	1.2590	-1.8278	-2.1643	0.3331	-2.8942	-10.1474
ONA	1.1368	-3.8380	-3.2383	-2.2765	-1.7471	-1.7415
ON3	2.8394	-2.8195	-0.4108	1.7471	-2.2765	-10.1523
ON4	5.1402	-1.2715	0.7061	-2.2033	6.2285	-2.6384
ON6	0.8995	1.2820	-1.9897	-6.2285	-2.2033	-11.2492
CG1	1.6922	-2.7296	0.7902	1.2723	2.4407	2.0532
CG2	1.3355	-4.1173	1.2864	-2.4407	1.2723	-6.3576
CG3	0.1766	-4.1278	2.2522	-0.6435	5.0224	3.7606
CG4	0.4679	-3. 436	3.3091	-5.0224	-0.6435	-4.6562
CG5	0.9196	-1.7039	2.7956	-1.3232	4.9733	1.1324
CG6	1.3408	-0.6756	3.7926	-4.9733	-1.3232	-7.2284
CN3	-1.6626	-3.2103	1.7222	-1.5604	2.6984	-0.2434
CN4	-1.4727	-4.7197	1.7074	-2.4984	-1.5604	-8.6542
CN5	-0.2935	-5.1583	0.9109	0.8499	-1.1323	0.8995
CN1	-0.5256	-3.2158	1.5247	0.1323	0.8499	-8.4013
CN2	-1.7387	-2.7258	0.2862	1.8995	1.7242	-0.5570
CNA	-2.0450	-0.6273	1.6397	-1.7242	1.8995	-8.9678
CNB	-2.7211	0.9108	1.6946	1.7515	3.5736	3.9531
CN6	-0.0602	-0.6081	0.7915	-3.5736	1.7515	-4.4577
OG5	1.9981	-1.8933	1.8999	-1.9331	4.2348	-1.6453
OG2	1.0267	-4.9583	0.1925	-4.2348	-1.9331	-10.0561
OG3	-0.1046	-5.2964	2.2727	-1.5604	2.4984	-0.2434
OG4	-0.6616	-2. 702	4.1965	-2.4984	-1.5604	-8.6542
OGD	0.7665	0.4013	3.0436	-2.1331	0.5953	-2.2734
OGS	2.3668	-1. 186	4.5121	-0.5953	-2.1331	-10.6642
OG1	2.8195	-2.8087	0.2000	-3.9990	-0.1747	-1.2194
ON5	0.4538	-0.4351	3.5074	0.1747	-3.9990	-9.6392
ON1	-0.6616	-2.8702	4.1965	-3.5374	1.7583	-4.4577
NNA	-1.8278	-1.2590	0.2265	-1.7583	-3.5674	-12.8665
ONA	-3.8380	-1.1368	3.1725	-2.8757	4.4462	-5.1633
ON3	-2.8195	-2.8394	0.4108	-4.4462	-2.8757	-13.3746
ON4	-1.2715	-5.1402	0.1169	-1.0341	0.9419	-2.4000
ON6	1.2820	-0.8995	0.4211	-0.9419	-1.0341	-10.8788

Fig. 3.5 Projection of double helix predicted from chain packing results

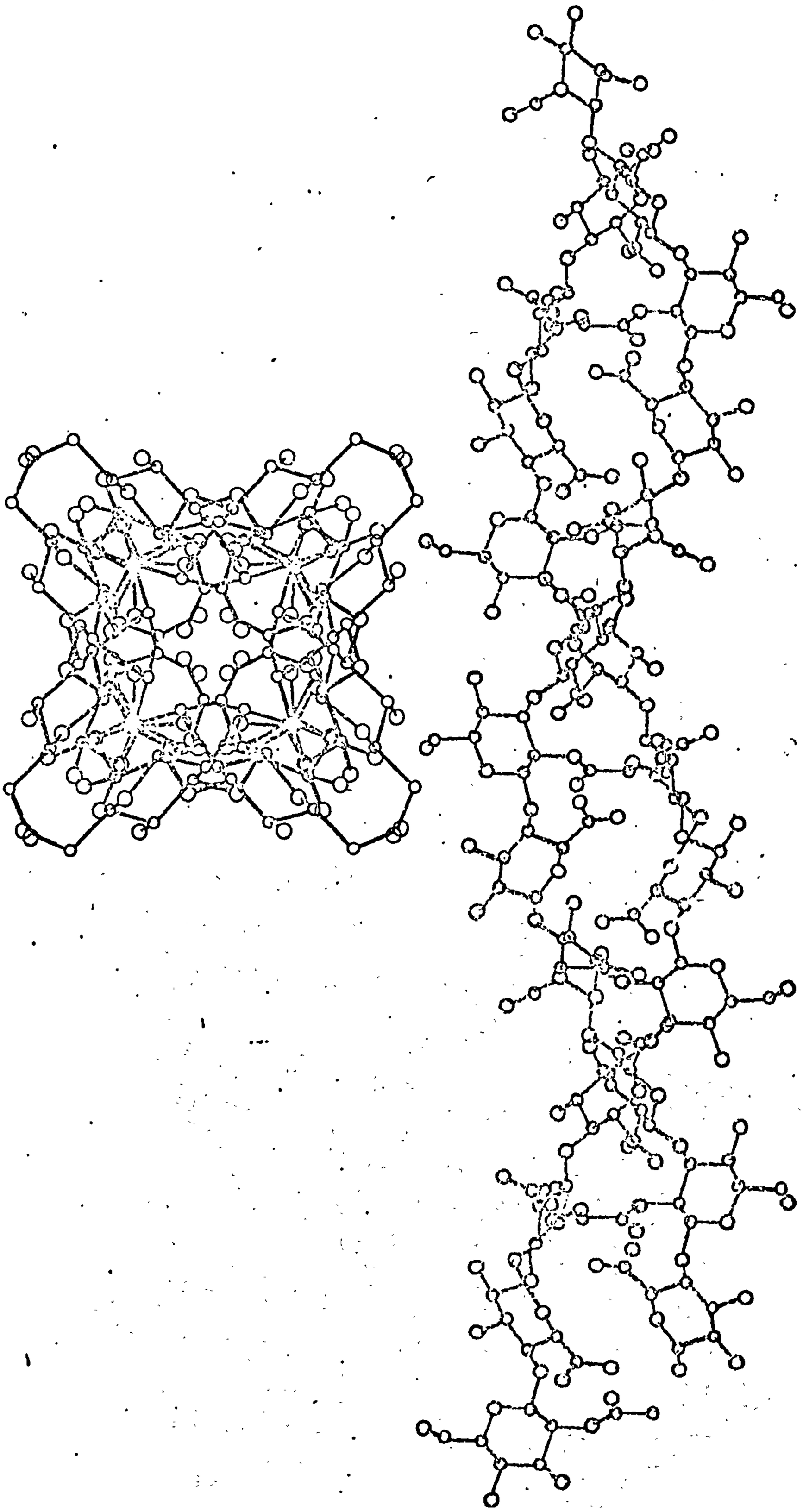

Fig. 3.6 Projection down 'c' axis of Type I lattice
(a) Double helix
(b) Single helix with space group $P4_2 2_1 2_1$

(a)

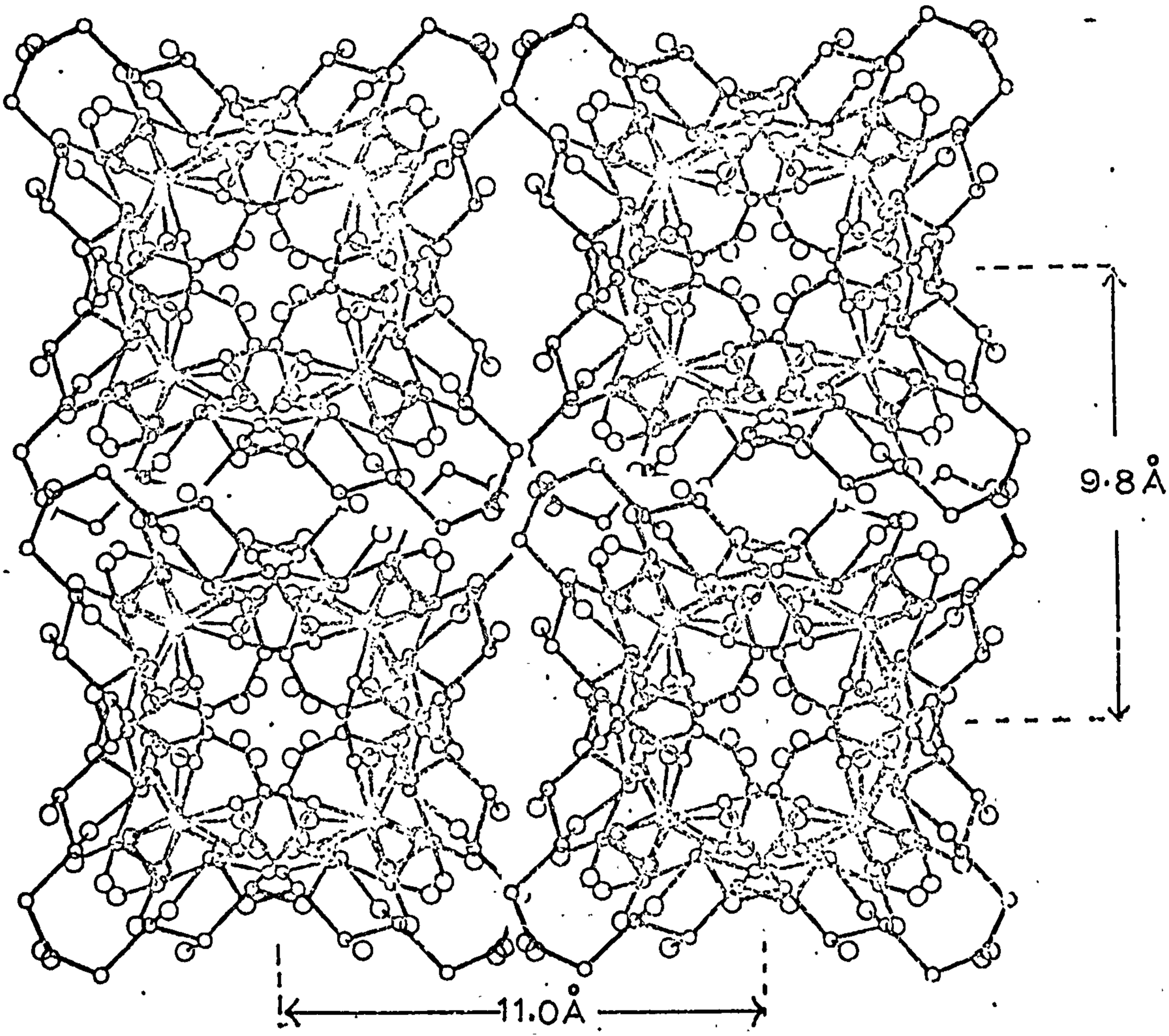

(b)

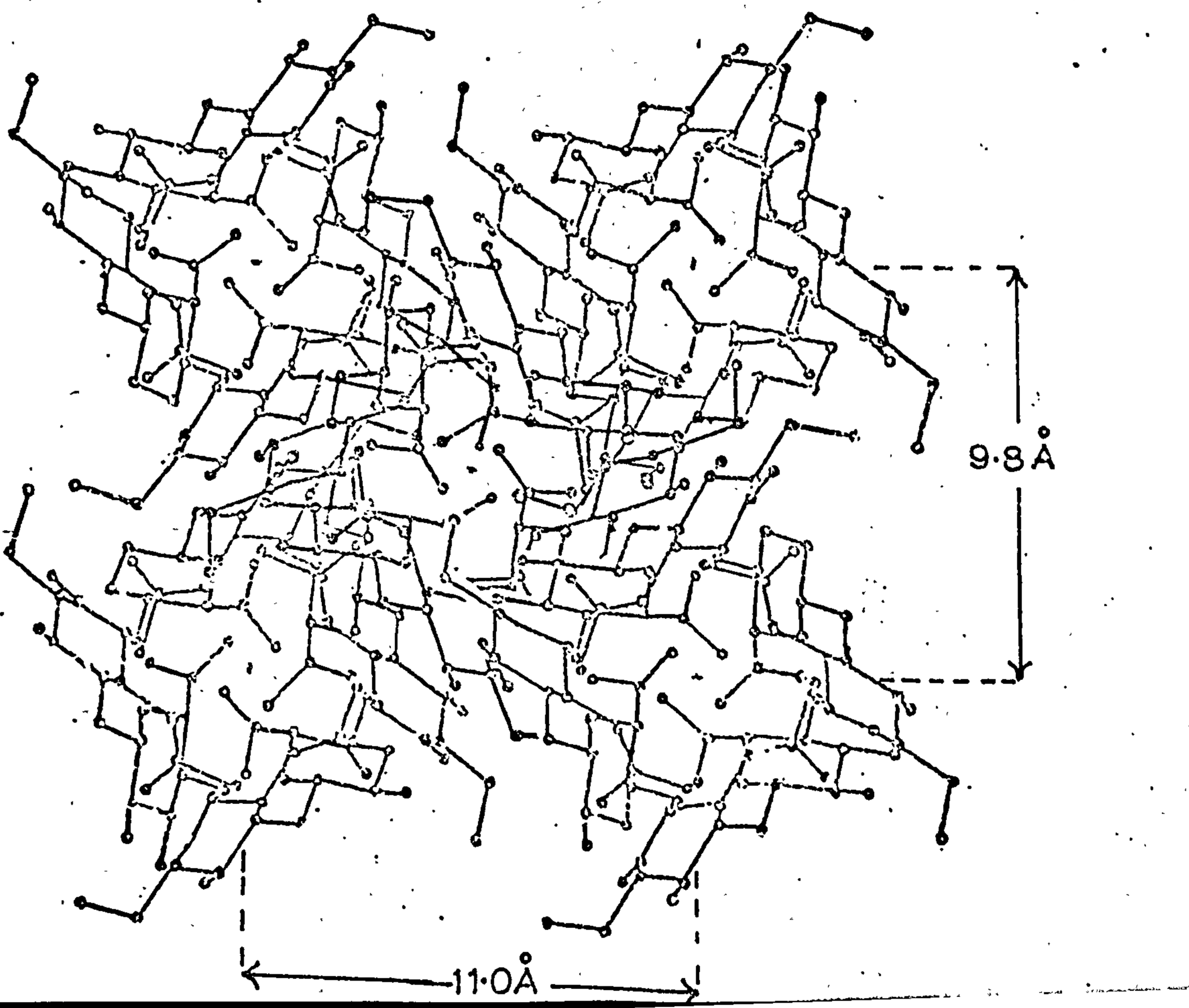

Fig. 3.7 Courtauld space filling model of the proposed double helix

3.6 Perturbations on Type I Conformation

A number of experiments were carried out to perturb the type I conformation. One such experiment was to perform the crystallisation procedure at 60° - 70°C. Gradually, over the period of one to two weeks, the stretched films underwent a phase change. Fig. 3.8(a) shows a diffraction diagram of potassium hyaluronate containing two phases. Table 3.5 gives the measurement and assigned indices of the two dimensional unit cell. It can be seen that, in addition to the unit cell with $a = 11.0\text{Å} \pm 0.2\text{Å}$ and $b = 9.9\text{Å} \pm 0.2\text{Å}$, there is another unit cell present in which $a = 11.0\text{Å} \pm .2\text{Å}$ and $b = 9.0\text{Å} \pm 0.2$; the change in the fibre period is not easily measured however. A further annealing of some specimens under the same conditions of stress at 70°C and 80% relative humidity yielded a diagram of the second phase alone which from now on will be referred to as a type II conformation. The X-ray diagram is shown in Fig. 3.8(b) and has a number of features in common with the diagrams of type I conformations. The general intensity distribution is very similar with a weak equator but the meridionals are very different and there is a change of layer line spacing. Fig. 3.8(b) indexes on a unit cell where $a = 11.0 \pm 0.2\text{Å}$, $b = 9.0\text{Å} \pm 0.2\text{Å}$ and $c = 37.2\text{Å} \pm 0.4\text{Å}$, where c is the fibre axis. The strong meridionals on the second, fourth and sixth layer lines of the type I X-ray diagram, have now gone and there is only a medium strong meridional on the 8th layer line with another very weak one on the fourth. An interesting feature of the diagram is that the third, fifth and sixth layer lines are exceedingly weak.

The volume of the unit cell for type II is 3680Å^3, i.e. close to that for type I at 3640Å^3. This suggests that the number of chains in the unit cell is still two. The meridional distribution now favours a regular four fold helix with an axial repeat increased from 33.4Å to 37.2Å. The axial rise per disaccharide in this conformation is 9.3Å which raises the interesting question of whether a conformation as extended as this can pack as a double helix. A trial conformation comprised of a left handed, four fold helix was selected, using model

Fig. 3.8 (a) X-ray diagram of type I and type II phases
(b) X-ray diagram of type II

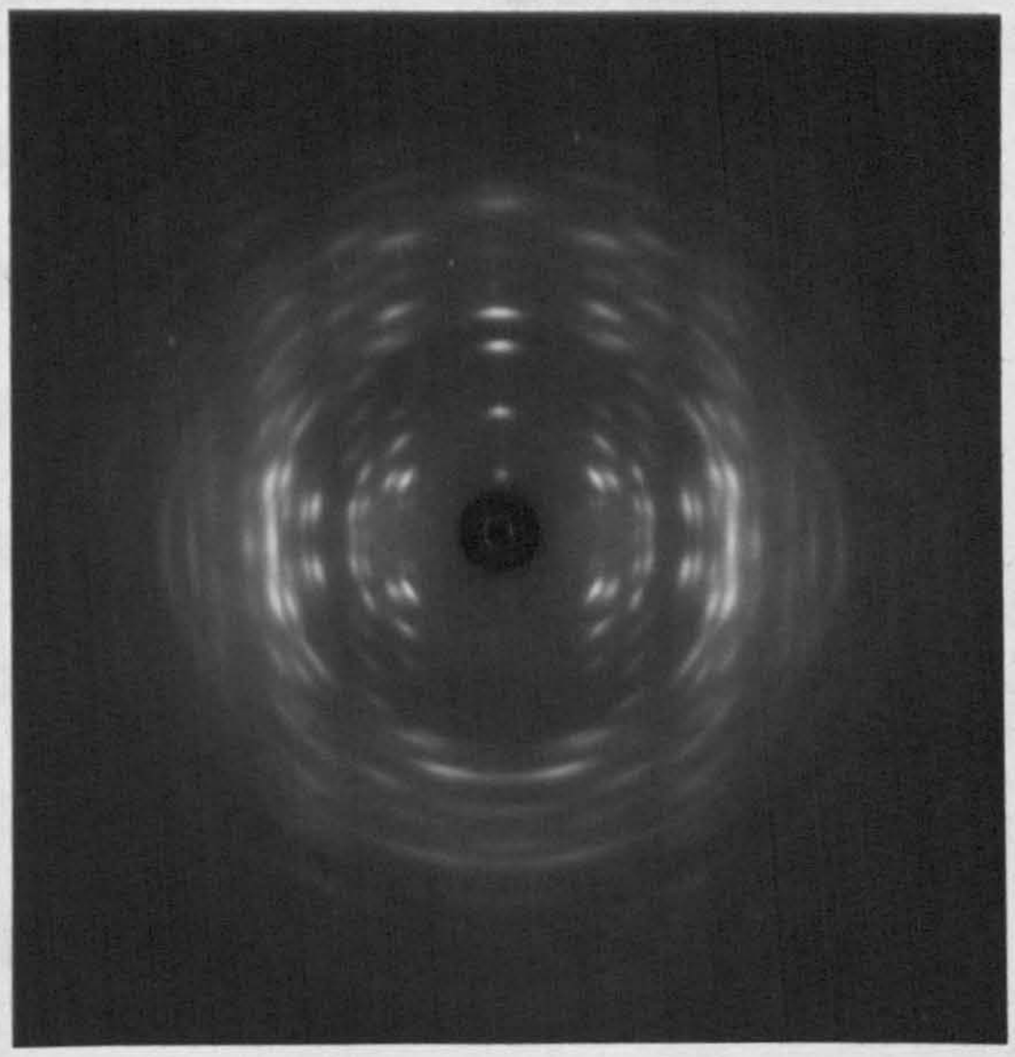

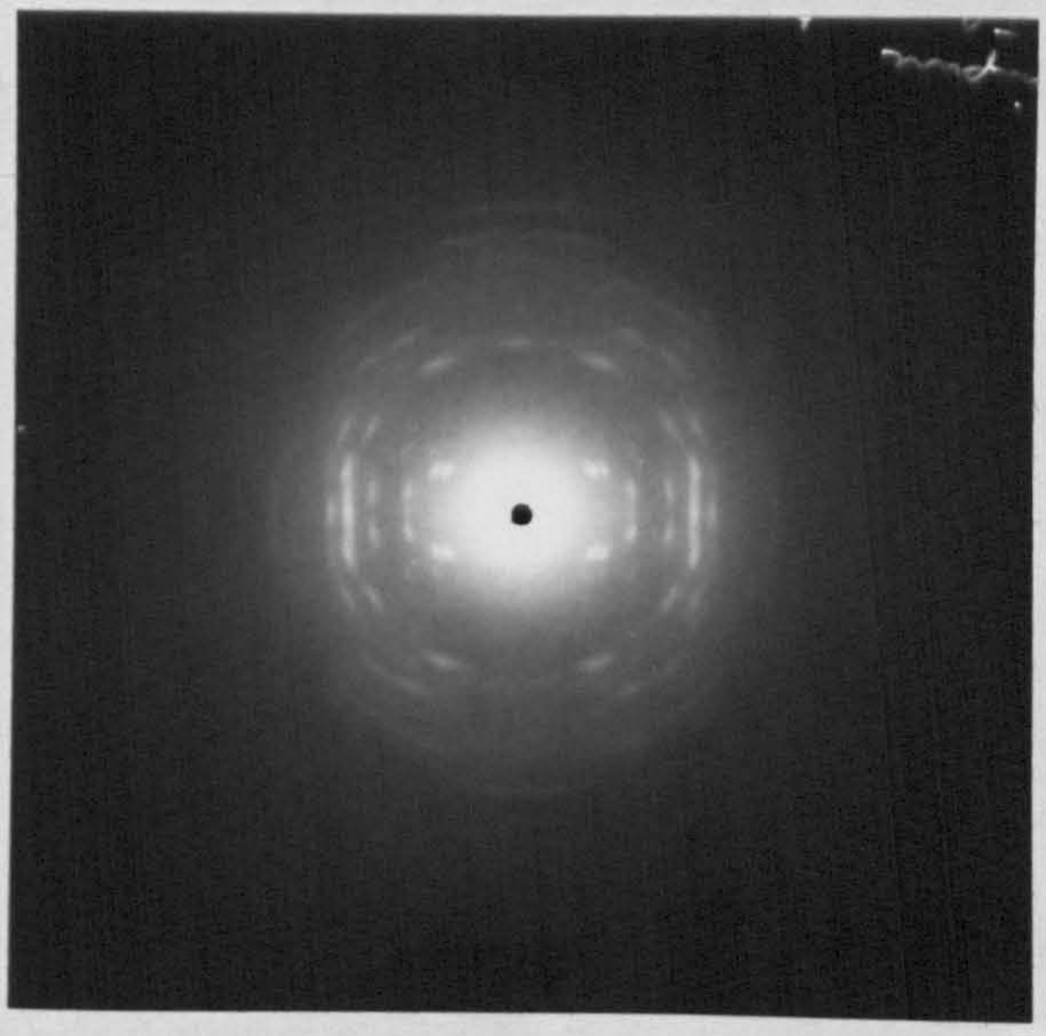

Table 3.5

Measured Spacings for Type II Diagram c.f. Fig. 3.8(b)

Measured Spacings Å		Description	Index
10.4	± 0.2	Absent	100
8.9	± 0.2	Absent	010
6.8	± 0.2	Weak	110
5.1	± 0.1	Absent	200
4.5	± 0.1	Strong	210,020
4.1	± 0.1	Medium	120
3.27	± 0.1	Medium Weak	310

Fow Lines Index on Orthorhombic Lattice

$a = 10.4\text{Å} \pm 0.2\text{Å}, \quad b = 8.9\text{Å} \pm 0.2\text{Å}.$

Layer line spacing measured on a number of general reflections is

$37.2\text{Å} \pm 0.4\text{Å}.$

building and stereochemical criteria. The coordinates are listed in Table 3.6. Two projections, perpendicular to and down the axis are shown in Fig. 3.9.

As for the type I conformation, two basic types of packing were considered

(a) Two chains packing in an antiparallel double helix

(b) Single chains packing in an antiparallel system with one at the corners and one in the middle of the unit cell.

Results from the two packing searches are seen in Fig. 3.10 and it is clearly shown that, for the conformation chosen, the molecules will not pack as a double helix but <u>will</u> pack with one chain at the centre of the unit cell. A view down the axis of the preferred packing scheme is shown in Fig. 3.11. If, as these results indicate, the type II conformation is not a double helix then the formation of type II from type I poses some interesting questions especially if type I is a double helix.

The two X-ray diagrams of Fig. 3.1 and Fig. 3.8(b) indicate that the transform of the molecule is very similar in both cases. Therefore the shape of the molecule is only slightly changed in going from an axial repeat of 8.4Å to one of 9.3Å. Clearly, if the type I conformation is a double helix, a melting process must take place in the transition between the two states. However, the transition X-ray diagram shown in Fig. 3.8(a) is highly crystalline and does not show much evidence of a melted, amorphous phase. Also the transition from double helix to single helix in the solid state raises interesting, topological problems.

The change of intensity as well as position of the meridionals between types I and II X-ray diagrams again suggests that in type I they are due to some kind of clustering effect of metal ions around the helix as put forward in Section 3.3. This, in some measure, supports the assumption of a four fold regular helix backbone for the type I conformation, the tetrasaccharide feature being caused by an interaction of carboxyle and metal ions on adjacent disaccharides of the same chain. Again detailed structure factor calculations hopefully will resolve the issues raised above, and these are now in progress.

Table 3.6

Trial Coordinates for Type II Conformation

1e→4e $(PHI)1 = 0^{o}$, $(PSI)1 = 60^{o}$; 1e→3e $(PHI)2 = 66^{o}$, $(PSI)2 = 0^{o}$

	X	Y	Z
CG1	-1.9038	-1.0400	5.2790
CG2	-2.0413	-2.3899	5.1670
CG3	-1.0731	-2.4418	4.3023
CG4	-1.2451	-1.2468	3.8693
CG5	-1.1966	0.0527	3.8958
OG5	-2.1287	0.0018	4.2539
HG1	-0.9102	-0.9940	6.9702
HG2	-3.0349	-2.4559	4.7758
OG2	-1.8183	-3.4527	6.0649
OG3	-1.2528	-3.6334	3.2929
HG3	-0.9795	-2.3758	4.3035
HG4	-2.2387	-1.3128	2.6980
OG4	-0.2571	-1.2309	2.9814
CG6	-1.4656	1.3096	3.1366
OGD	-0.6247	2.2071	2.9965
OGS	-2.6559	1.3788	2.5971
HG5	-0.2030	0.1107	4.2870
OG1	-2.3672	-0.9755	6.8629
CN3	0.0464	-1.4727	-1.5788
CN4	-0.7865	-2.7279	-1.7150
CN5	-1.9152	-2.7341	-0.6825
ON5	-1.3393	-2.5315	0.6153
CN1	-0.6040	-1.3003	0.7752
ON1	-0.2571	-1.2309	2.9814
HN1	-1.3368	-0.4861	0.5128
CN2	0.5061	-1.2681	-0.1485
HN2	1.1489	-2.0823	0.1139
NNA	1.2361	-0.0000	0.0000
HNA	0.6869	0.7937	-0.2266
CNA	2.4350	0.0628	0.3977
ONA	3.2097	-0.8842	0.7900
CNB	3.0484	1.4939	0.5222
HN3	-0.5943	-0.6586	-1.8412
ON3	1.1596	-1.5259	-2.4269
ON4	-1.3195	-2.3448	-3.0181
HN4	-0.1437	-3.5421	-1.4534
CN6	-2.7524	-3.9699	-0.6285
H6R	-2.0757	-4.3211	-1.6232
H6L	-2.2587	-4.7503	-0.1451
ON6	-4.0201	-3.7145	-0.0551

Fig. 3.9 Projections perpendicular to and down the axis for proposed model of type II conformation

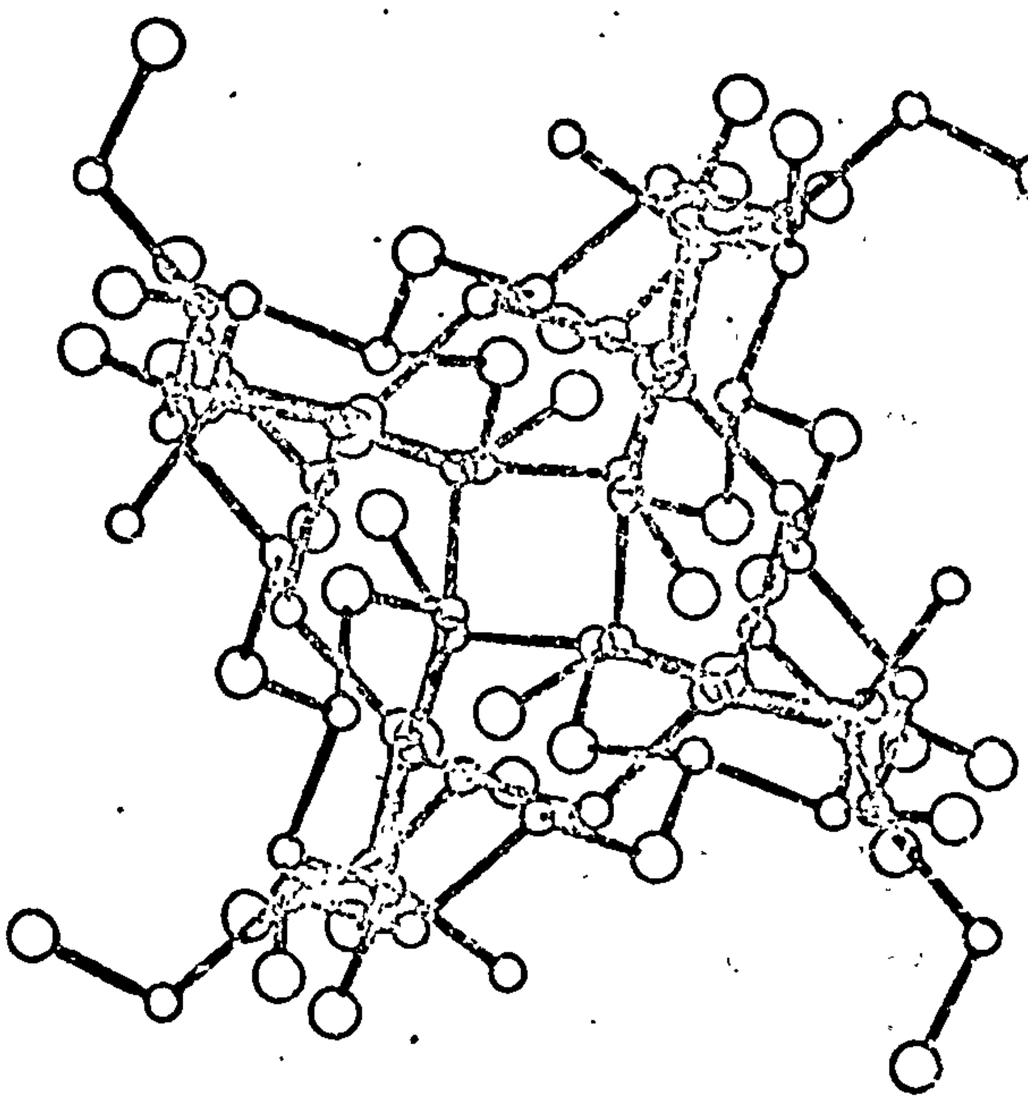

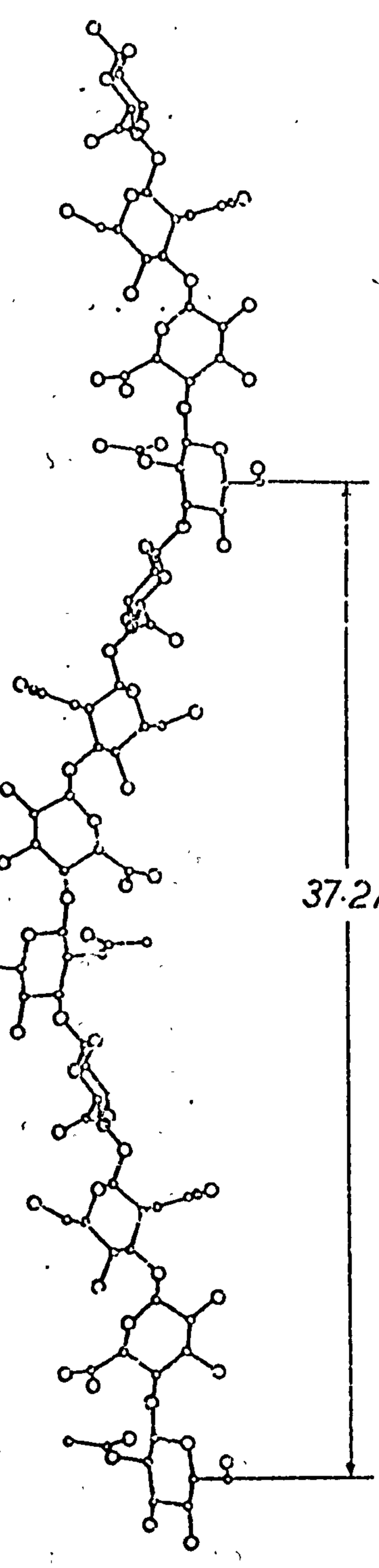

37·2Å

Fig. 3.10 Packing results of type II
(a) Antiparallel double helix
(b) Antiparallel single helices, space group $P2_12_12_1$

(a)

	0	45	90	135	180	225	270	315	360
-50	99	99	99	78	79	79	99	99	99
-30	99	99	86	99	99	99	99	99	99
-10	99	94	86	99	99	99	99	99	99
10	99	99	82	99	99	99	99	99	99
30	99	91	96	99	99	99	99	99	99
50	90	75	92	99	99	99	99	99	90

(b)

	0	45	90	135	180	225	270	315	360
-50	7	0	0	11	58	90	45	36	7
-30	6	3	4	10	71	99	39	27	6
-10	4	9	5	6	81	99	38	13	4
10	1	7	2	5	71	99	28	3	1
30	0	3	2	6	73	99	25	5	0
50	0	1	1	9	60	99	24	1	0

Fig. 3.11 View down the 'c' axis of type II lattice

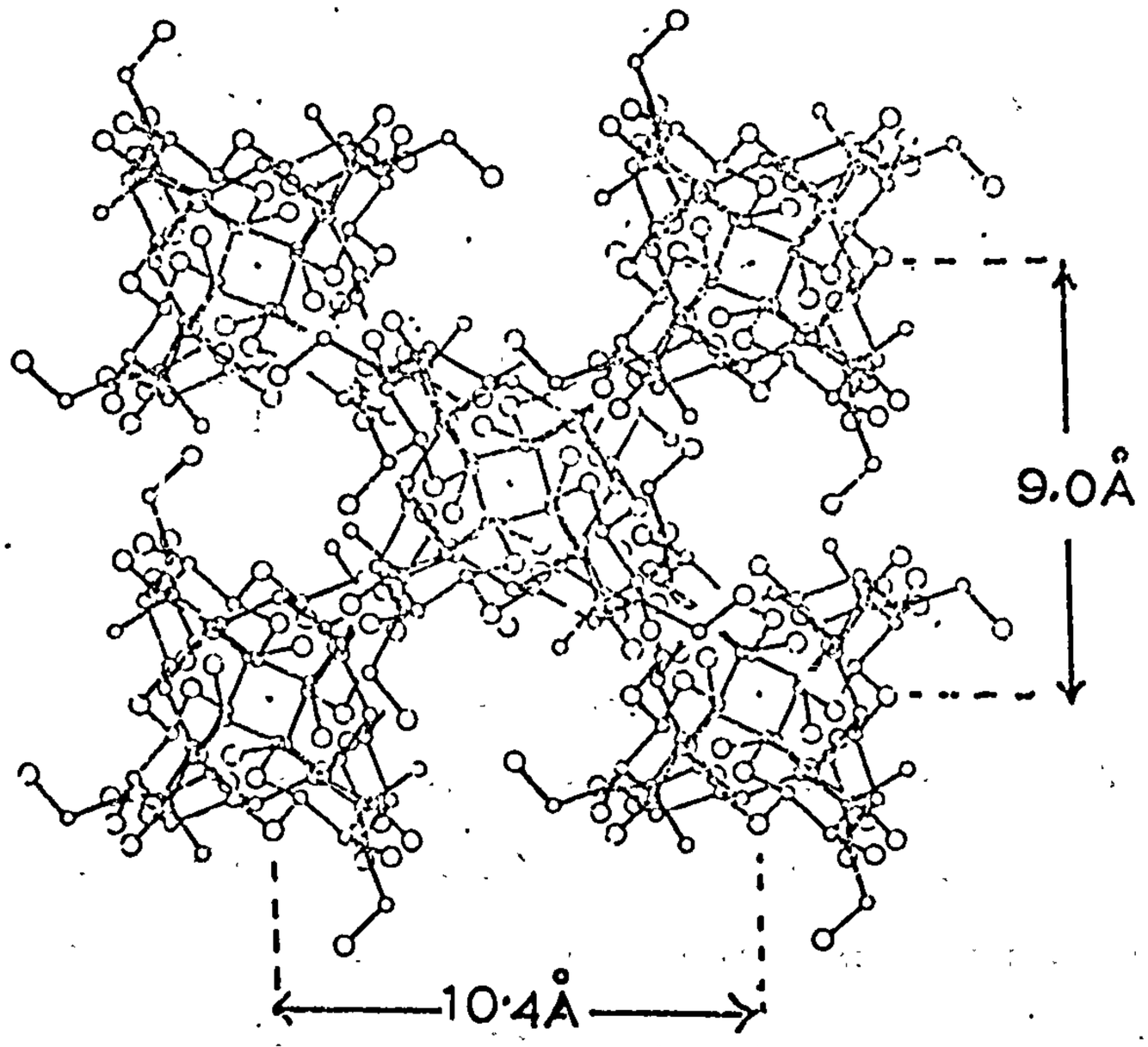

CHAPTER IV

4.1 Introduction

As pointed out at the start of Chapter III the X-ray diagram shown in Fig. 3.1 was not the first crystallised form of sodium hyaluronate. The original experiments were done with material obtained from human mesathelioma fluid which, in its unpurified form, had a molecular weight in the region of $10\text{-}20 \times 10^6$ and in its purified form about $1\text{-}2 \times 10^6$. The first diffraction patterns were obtained from the sodium and potassium salts of the purified form of this material.

4.2 Description of Diffractograms

The first diffraction pattern obtained is shown in Fig. 4.1. The technique previously described was used in crystallisation, but the specimen was maintained at 40-50°C during the preparation. The crystallinity of the sample as revealed by the number of reflections and the resolution attained is not very high. Table 4.1 gives the spacing of the row lines and it can be seen that they index on a hexagonal lattice of $a = b = 11.7 \pm 0.2$Å. The meridionals are on the 3rd, 6th and 9th layer lines with a layer line spacing of 28.5Å ± 0.4Å. However there are indications of another phase present with reflections on the first and higher layer lines that do not index on the above simple lattice. Layer line streaking, the size and shape of the reflections, and the low resolution of the diagram all indicate para crystalline defects.

When samples were annealed at 40-60°C in a relative humidity of about 80% they gradually underwent a transition until the diffractogram shown in Fig. 4.2 was obtained. The reflections have become more arced but are now much sharper and the resolution of the diagram is about 2.5Å. Table 4.2 shows the spacings of the row lines which index satisfactorily on a hexagonal lattice $a = b = 18.7$Å ± 0.3Å. The backbone conformation as indicated by layer line spacing and meridionals has remained the same indicating that only a packing rearrangement has occurred.

Fig. 4.1 Type III conformation of sodium hyaluronate with 11.7A unit cell

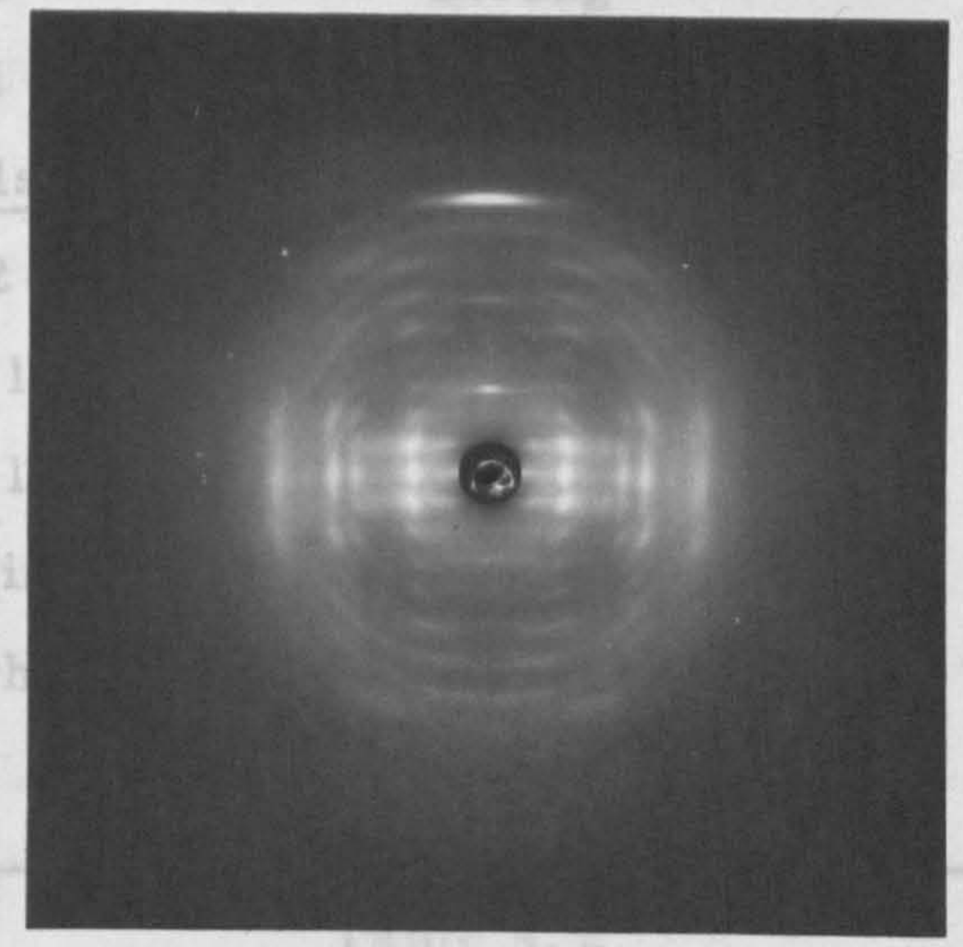

Fig. 4.2 Type III conformation of sodium hyaluronate with 18.7A unit cell

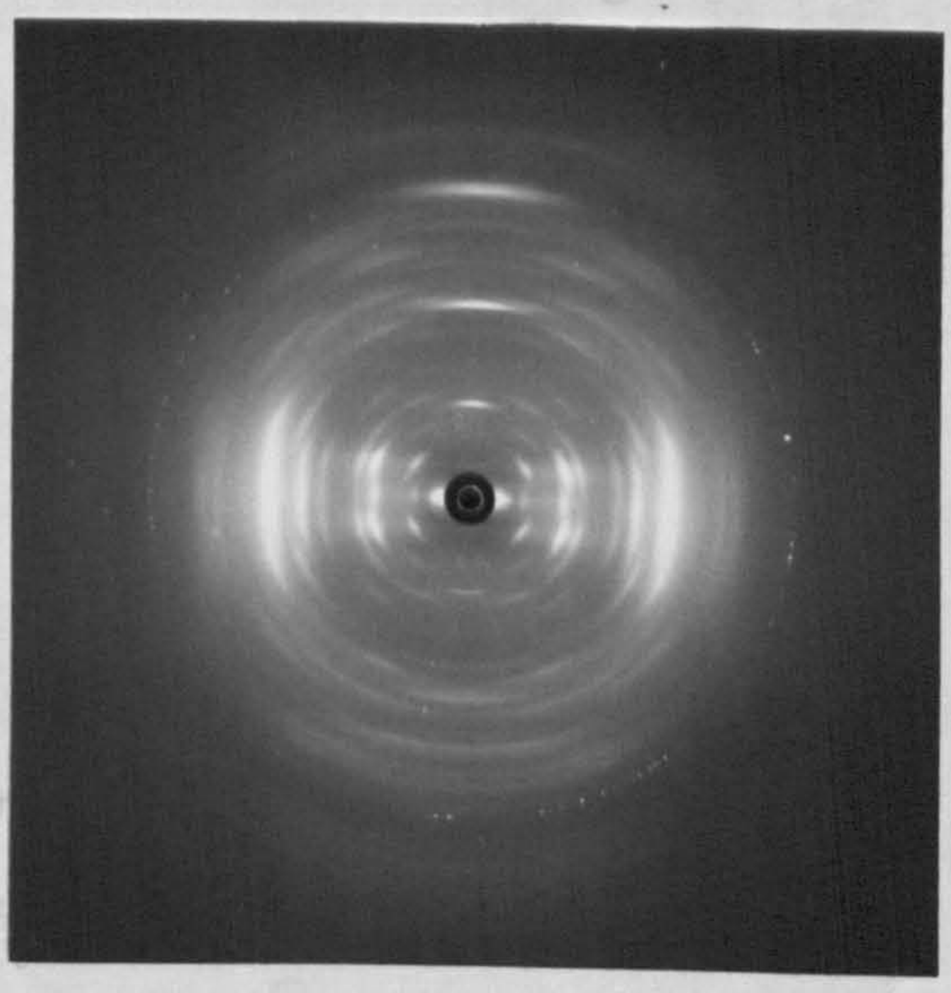

Table 4.1

Measured Spacings and Indices of Type III 11.7Å Hexagonal Unit Cell

Row lines	Description	Type
10.1 ± 0.2	Strong	100
5.81 ± 0.1	Medium	110
5.07 ± 0.1	Strong	200
3.84 ± 0.1	Strong	120
Meridionals		
9.5Å ± 0.2	Medium strong	003
4.75Å ± 0.1	Weak	006
3.16Å ± 0.1	Very strong	009

Row lines index on a hexagonal lattice

where $a = b = 11.7Å \pm 0.2Å$

Layer line spacing $= 28.5Å \pm 0.4Å$

Table 4.2

Measured Spacings and Indices of Type III 18.7Å Hexagonal

Measured Spacings Å Row lines	Intensity	Index Type
16.25 ± 0.3	Medium Weak	100
9.37 ± 0.2	Medium Strong	110
7.83 ± 0.2	Weak	200
6.11 ± 0.1	Medium	210
5.42 ± 0.1	Strong	300
4.68 ± 0.1	Very Strong	220
4.50 ± 0.1	Strong	310
3.75 ± 0.1	Medium Strong	320
3.58 ± 0.1	Medium Strong	410
Meridionals		
9.5 ± 0.2	Medium	003
4.75 ± 0.2	Medium Strong	006
3.16 ± 0.2	Very Strong	009

Row lines index on a hexagonal lattice

where $a = b = 18.7Å \pm 0.3Å$

Layer line spacing $= 28.5Å \pm 0.4Å$.

4.3 Conformation

The layer line spacing of 28.5Å with meridionals on every third layer line can be interpreted as a three fold helix with each disaccharide having an axial rise of 9.5Å. The maximum theoretical extension for a disaccharide is 10.2Å so that the above model represents an extended conformation. Model building trials with a conformation having these parameters rule out the possibility of an antiparallel double helix. A parallel double helix would raise the problem of a different conformation. Two stands 180° out of phase would mean that the X-ray spacings on the meridian are halved i.e. there are missing odd layer lines. The true repeat would be 57Å with meridionals on the 6th, 12th and 18th layer lines. The model for a single helix would thus be a six-fold helix with a repeat of 57Å and this appears stereochemically unfavourable, requiring dihedral angles at the 1e - 4e linkage outside the allowed region of Fig. 2.12.

In the case where the two strands are not 180° out of phase but close to it there should at least be a weakening of odd order layer lines and there is no evidence for this on Figs. 4.1 and 4.2.

As mentioned in Chapter II, the stereochemically allowed regions of both linkages are centred on the zero zero position. The equilibrium conformation is therefore close to a two-fold helix with an axial rise per disaccharide between 9.5Å and 10.2Å. A perturbation on this two-fold state gives rise to a three-fold helix and model building trials were made on both left handed and right handed conformations. It was found that although right handed helices could be constructed they were not so favoured as three-fold, left handed helices. This was due to the rotation at the 1e → 4e linkage, which for the left handed case cleared the acetamido and carboxyle groups but for the right handed helices brought these side groups into close contact (see Fig. 4.3(a) and (b)).

Since there are four variables, $(PHI)1$, $(PSI)1$, $(PHI)2$, $(PSI)2$ governing the backbone conformation and only two helix parameters, there is no unique solution for the PHI and PSI values. The left handed

Fig. 4.3 Courtauld space filling models of situation at the 1e→4e linkage

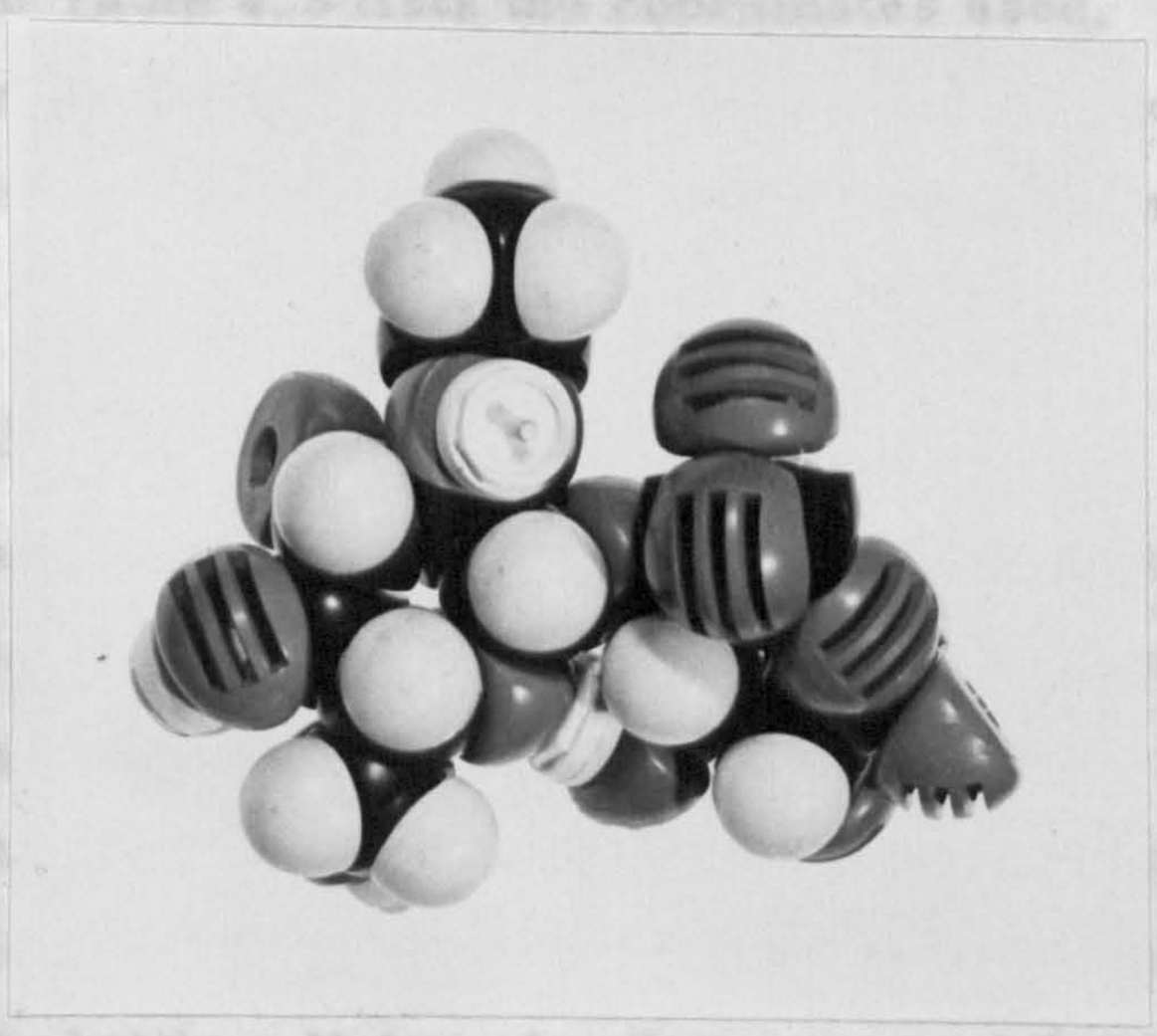

trial model was thus chosen on the basis of possible hydrogen bonds stabilising the conformation. These hydrogen bonds are between the O-H.. on the 4 position of the N residue and the ring oxygen of the G residue, and the O-H.. on the 3 position of the G residue with the ring oxygen of the N residue. Fig. 4.4 shows two projections of this conformation and Table 4.3 lists the coordinates used. This model is favoured conformationally but Fig. 4.5 shows two projections of the alternative model for the right handed conformation using coordinates in Table 4.3(b).

4.4 Packing of Chains

The density of a number of specimens which gave the X-ray diagrams in Figs. 4.1 and 4.2 was measured by the flotation method using the two liquids carbon tetrachloride and acetone. The mixture was adjusted until the specimen floated freely throughout the volume of the fluid. The specific gravity of the fluid was then measured using a specific gravity bottle. Values for the measured density were $1.47 \pm .02$ gm. per c.c. but an estimation of the errors in this kind of density determination is difficult due to the presence of impurities, air bubbles and also to slight specimen solubility in the liquids used. Using the formula

$$d = n \times \frac{\text{Molec. weight of 1 disaccharide}}{\text{Volume of unit cell}} \times \frac{1}{N}$$

where n is the number of disaccharides

d is the measured density

N is Avogadro's Number.

Table 4.4 shows a comparison of the measured and calculated densities for the hexagonal 11.7Å and 18.7Å unit cells. These calculations strongly suggest that the 11.7Å cell, on annealing, changes from a two chain cell to a larger six chain cell.

The positions of the two chains in the 11.7Å unit cell were deduced by packing simple model projections of the three-fold chains

Fig. 4.4 Two projections of the proposed left handed type III conformation

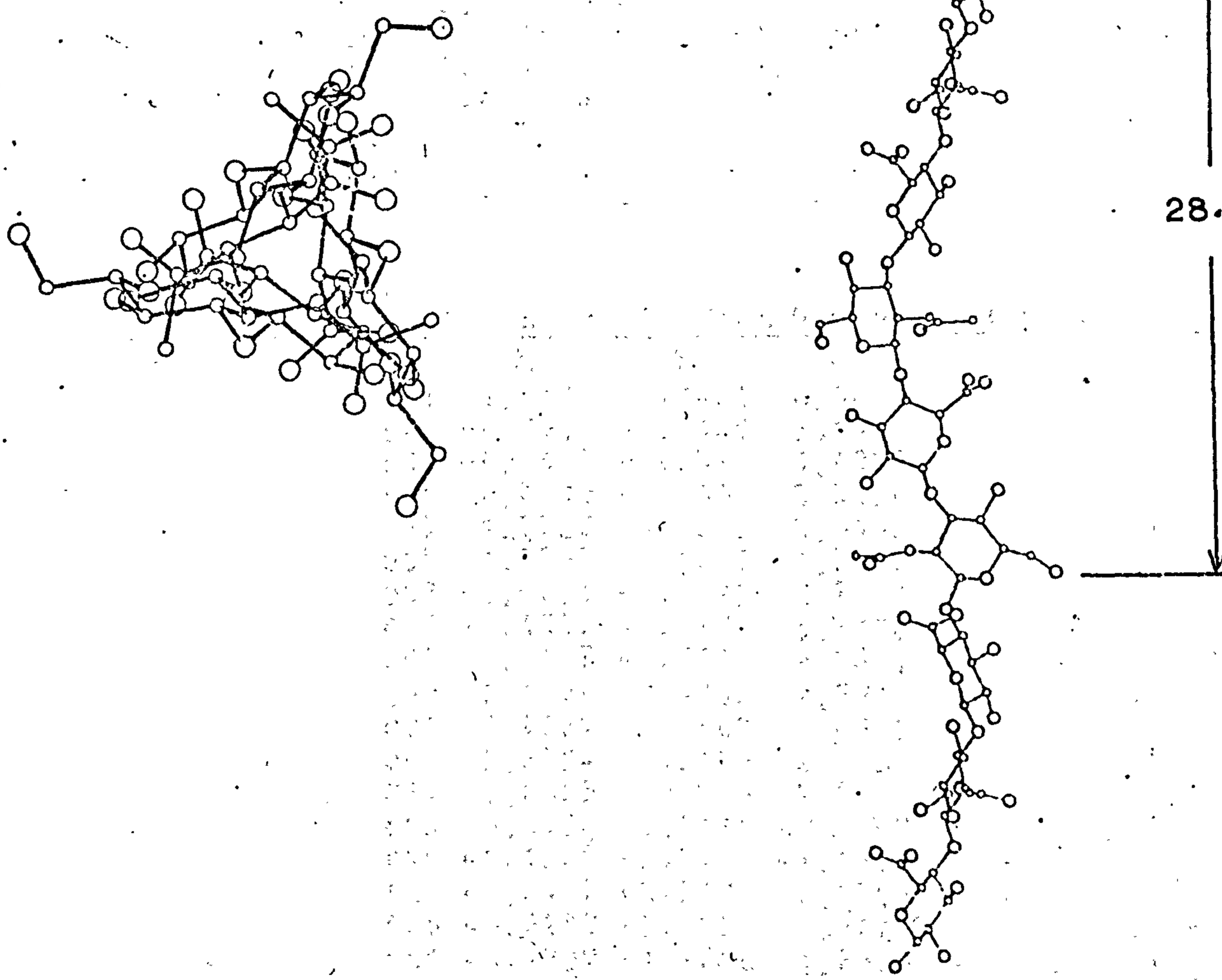

Table 4.3(a)

Coordinates for Trial Left Handed Helix for Type III Conformation

	X	Y	Z
CG1	-1.1387	-0.3978	6.1650
CG2	-1.5502	-1.7529	5.6277
CG3	-0.7156	-2.0872	4.4076
CG4	-0.7816	-0.9822	3.3751
CG5	-0.4537	0.3679	4.0166
OG5	-1.2785	0.5848	5.1454
OG2	-1.4145	-2.7385	6.6255
OG3	-1.1465	-3.2996	3.8583
OG4	0.0979	-1.2369	2.3011
CG6	-0.5909	1.5659	3.1366
OGD	0.3641	2.2906	2.8286
OGS	-1.7809	1.7731	2.6823
OG1	-1.9805	-0.0514	7.2009
CN3	0.0235	-1.6791	-1.3523
CN4	-0.6856	-3.0162	-1.3266
CN5	-1.6872	-3.0674	-0.1708
ON5	-1.0462	-2.7325	1.0452
CN1	-0.4701	-1.4314	1.0596
ON1	0.0979	-1.2369	2.3011
CN2	0.6115	-1.3404	0.0029
NNA	1.2168	0.0000	0.0000
CNA	2.4884	0.2099	0.2469
ONA	0.4895	2.0802	-0.3438
CNB	2.9094	1.6943	0.2310
ON3	1.0344	-1.6767	-2.5193
ON4	-1.3421	-3.2669	-2.5508
CN6	-2.3798	-4.3725	0.0436
ON6	-3.6055	-4.2085	0.7468

Table 4.3(b)

Coordinates for Trial Right Handed Helix for Type III Conformation

	X	Y	Z
CG1	1.1351	-0.2084	6.0699
CG2	-0.2512	-0.6469	5.6453
CG3	-0.1472	-1.5372	4.4233
CG4	0.6396	-0.8660	3.3180
CG5	1.9825	-0.3666	3.5496
OG5	1.7807	0.4539	4.9867
OG2	-0.9033	-1.3077	6.7052
OG3	-1.4265	-1.5736	3.9776
OG4	0.8457	-1.7464	2.2341
CG6	2.8170	0.4236	2.3920
OGD	3.9289	0.7469	2.4995
OGS	2.2754	1.5150	2.4667
OG1	1.0225	0.3926	7.1078
CN3	-0.5108	-1.5137	-1.1797
CN4	-1.1240	-2.9976	-1.1915
CN5	-1.6467	-3.2621	0.1998
ON5	-0.6252	-3.0934	1.1641
CN1	-0.1209	-1.7656	1.2506
ON1	0.8457	-1.7464	2.2341
CN2	0.5106	-1.3724	-0.0690
NNA	1.0349	0.0000	0.0000
CNA	2.3041	0.2858	-0.1656
ONA	0.1708	2.0232	0.3669
CNB	2.6472	1.7857	-0.0155
ON3	0.0891	-1.2398	-2.4114
ON4	-2.1655	-2.9840	-2.1404
CN6	-2.1782	-4.3477	0.3619
ON6	-3.0777	-4.7413	1.4600

Fig. 4.5 Two projections of a possible right handed type III helix

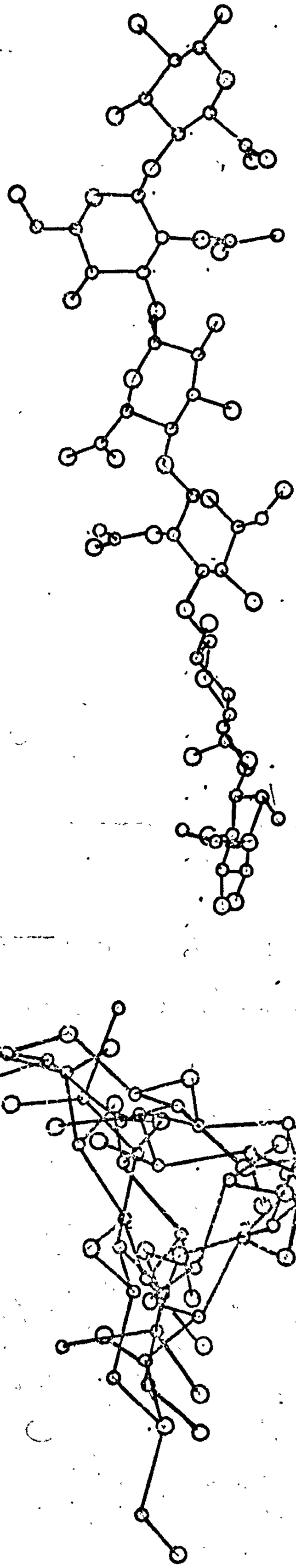

28.5 Å

Table 4.4

Calculated Densities for 11.7Å and 18.7Å, Type III Conformations

Equation $d = n \times \frac{\text{Molec. Wt. of 1 Disaccharide}}{\text{Volume of Unit Cell}} \times \frac{1}{N}$

N = Avogadro's number

n = Number of dissacharides

	Volume A^{o3}	Number of Chains	n	d
11.7Å	3380	1	3	0.64
	"	2	6	1.28
	"	3	9	1.93
18.7Å	8630	3	9	0.75
	"	4	12	1.0
	"	6	18	1.5
	"	8	24	2.0

Most favourable case for 11.7Å cell is 2 chains.

Most favourable case for 18.7Å cell is 6 chains.

and testing the results against the main equatorial reflections of Fig. 4.1. The preferred arrangement is shown in Fig. 4.6 where the chains are placed along the main diagonal of the unit cell and the corners of the cell are 'vacant' lattice sites. Nieduszynski and Morchessault Ref. 1 performed a packing analysis and subsequentiy a structure factor calculation Ref. 2 of $\beta 1 \rightarrow 4$ Xylan. This molecule also has a three-fold helix conformation and it was shown to pack in the manner indicated in Fig. 4.6. It was suggested Ref. 2 that the so-called 'vacant' site was occupied by water molecules having a three-fold screw symmetry and that the whole arrangement of polymer and water molecules fitted the space group $P3_221$.

The packing shown in Fig. 4.6(a) can be regarded as a honeycomb the chain positions being at the vertices of the comb. Viewed in this way the motif of six chains suggests itself see Fig. 4.6(b). If a unit cell is drawn using this motif as a basis the hexagonal lattice has a side of 20.25Å. The six chain 18.7Å unit cell was eventually evolved by repacking the six chain rings as indicated in Fig. 4.7(a), (b) and (c). If all the rings are rotated 30° in the same direction a situation arises as in Fig. 4.7(b) where the chain environment has been changed. This change allows the rings of six to pack closer together, Fig. 4.7(c), and to generate a hexagonal lattice of side 18.7Å in the process. This lattice has been formed while still maintaining the nearest neighbour distance but the number of nearest neighbours has increased from three to four and a 'vacant' site has been eliminated in the process. The proposed packing of the 18.7Å cell agrees satisfactorily with the equatorial intensity data of Fig. 4.2 and if the chains are represented as being up and down as in Fig. 4.7(c) the arrangement possibly has the same symmetry as the 11.7Å cell i.e. $P3_221$.

4.6 Structure Factor Calculations

To test some of the assumptions above structure factor calculations were carried out on the 11.7Å unit cell. To attack the problem in detail would be a formidable and perhaps impossible task.

Fig. 4.6 (a) Proposed hexagonal packing for 11.7Å cell with 'vacant site.
(b) Emphasising the ring-of-six motif in the unit cell.

(a)

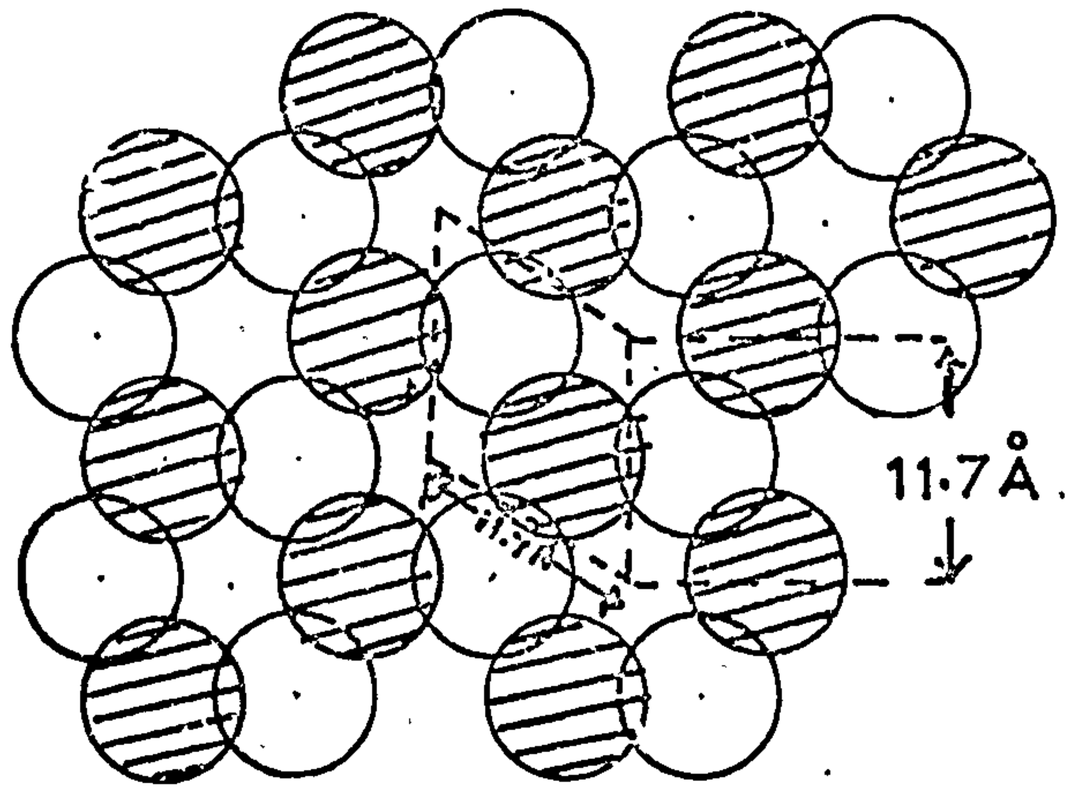

(b)

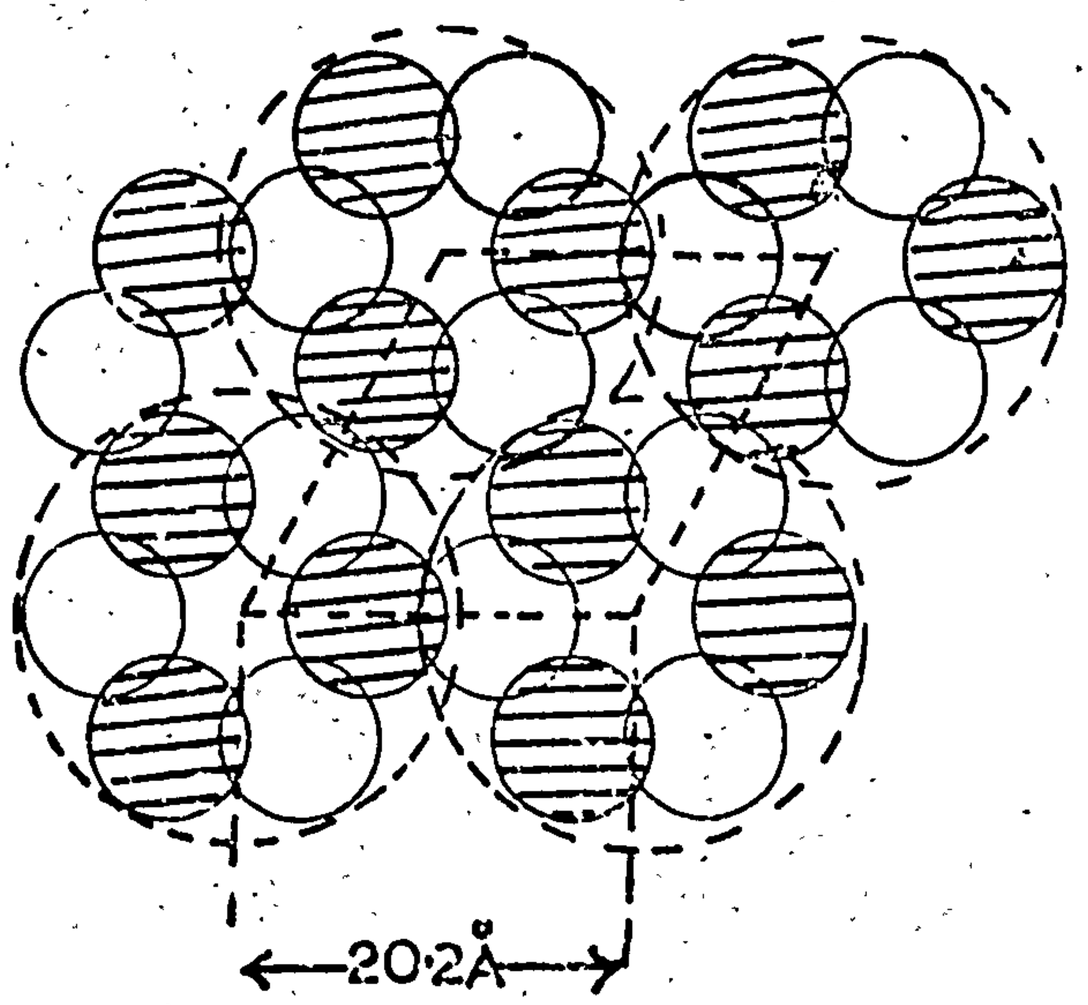

Fig. 4.7 Transition from 11.7Å to 18.7Å hexagonal unit cell.
(a) 11.7Å packing
(b) Rotation of ring-of-six by 30°
(c) Repacking of 'rings'

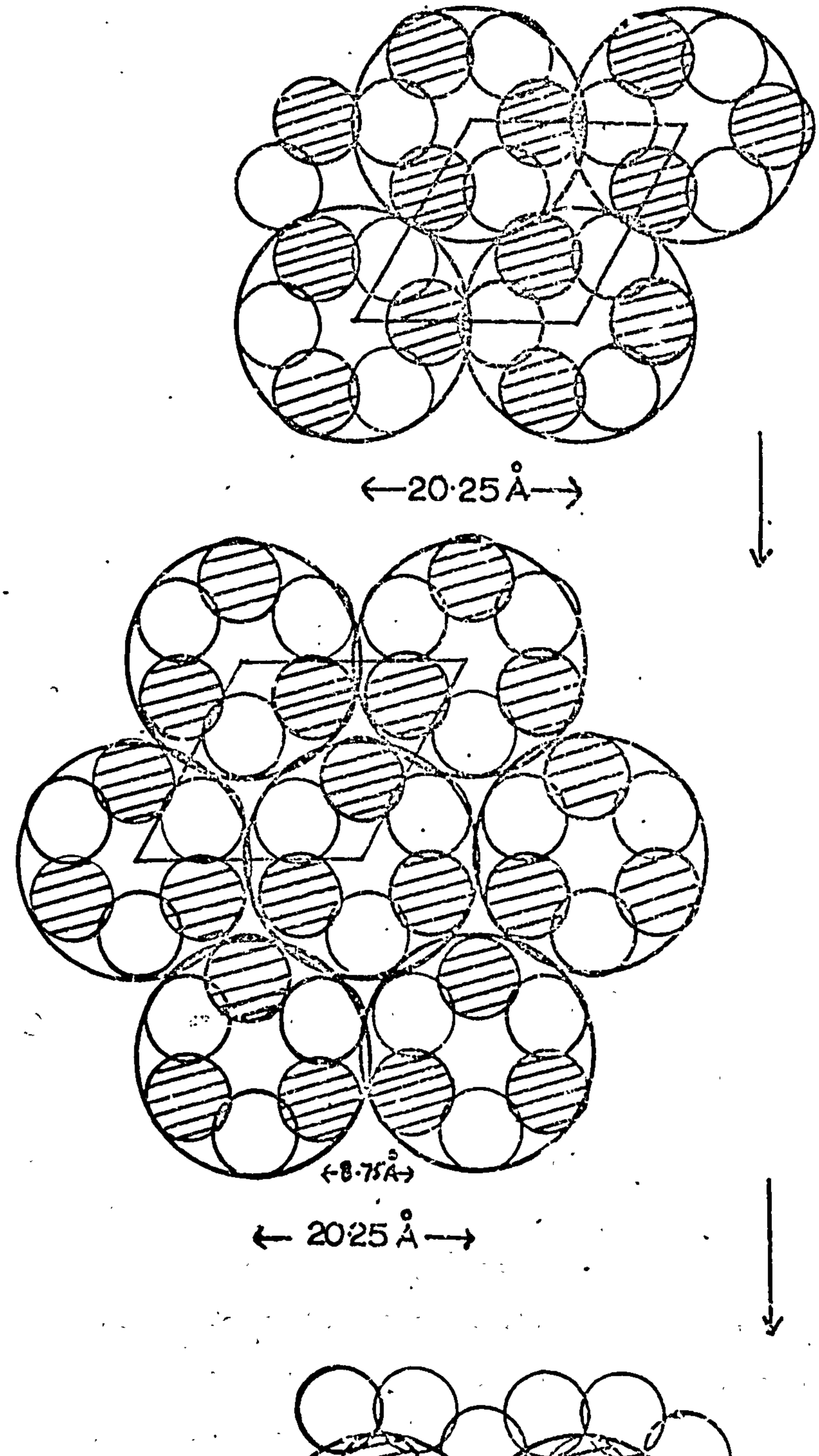

The system comprises polymer, metal ions and water, thus being a very complex problem involving many variables. Table 4.5 lists some of the variables, there being at least eleven before the missing metal and water atoms are considered. Even a constrained, least squares approach Ref. 3 would be of little use as the intensity data for this unit cell is rather poor.

The assumptions on which the structure factor calculations were based are

(a) The space group for the unit cell is either $P3_221$ or $P3_121$.

(b) The polymer chains dominate the scattering.

(c) The chosen 'average' right handed or left handed conformation is close to the true conformation.

It was hoped that the agreement between calculated and observed intensities would confirm or deny the choice of space group and possibly distinguish between the left handed and right handed conformations. The only variables considered were those of rotation and translation of the chains.

4.7 Structure Factor expression

The general expression for the scattering of X-rays from a crystal containing several species of atoms in the unit cell is

$$F(h,k\ell) = \sum_n f_j \exp \quad 2\pi i(hx + ky + \ell z)$$

where $F(h,k,\ell)$ is the scattering amplitude in direction h,k,ℓ.

x,y,z are the fractional coordinates of the atoms in the unit cell

f_j are the atomic scattering factors for the various atoms in the unit cell.

In the present computations the analytical approximations of Vand, Eiland and Pepinsky were used for the representation of the atomic scattering factors Ref. 4.

For the space group $P3_221$ the above expression reduces to, for the real part

Table 4.5

Variables in a Structure Determination for a Mucopolysaccharide

N.B. These are the variables required after assuming a correct trial model and the positions of the chains on a lattice.

Effect	No. of variables
Chain Rotation	1
Chain Translation	1
Chain Conformation	4
Side Group Rotation	3
Scale Factor	1
Temperature Factor	1
For 'missing' atoms that have to be placed per atom are required in principle.	3 variables

$$A = 2\ \cos\pi\ (h-k)(x-y) + 2\ell z \cdot \cos\pi i(x+y) + \cos\pi\ (k-i)(x-y) + 2\ell z -$$

$$\cos\pi\ (h(x+y)+2\tfrac{\ell}{3}\ + \cos\pi\ (i-h)(x-y)+2\ell z\ \cos\pi\ k(x+y)-2\tfrac{\ell}{3}$$

and for the imaginary part

$$B = 2\ \cos\pi\ (h-k)(x-y) + 2\ell z\ \sin\pi i(x+y)$$

$$+ \cos\pi\ (k-i)(x-y) + 2\ell z\ \sin\pi\ h(x+y) + 2\tfrac{\ell}{3}$$

$$+ \cos\pi\ (i-h)(x-y) + 2\ell z\ \sin\pi\ k(x+y) - 2\tfrac{\ell}{3}$$

Where $B = 0$ if $\ell = 3n$ and $h = -k$ (or $k = -i$ or $i = -h$)

and $A = B = 0$ if $\ell = 3n \pm 1$ $h = k = 0$.

The expression for $P3_121$ is identical except for the $\frac{2}{3}\ell$ term changes sign. Trial coordinates for the two models are given in Tables 4.3a and 4.3b and the intensity given by FF^* was calculated and compared with the measured intensities. Fig. 4.8 shows a diagram of space groups $P3_221$ and $P3_121$.

4.8 Intensity Measurement

The intensities of the X-ray diagram shown in Fig. 4.1 were measured using a Joyce Loeble densitometer; the trace obtained from the equator is shown in Fig. 4.9. The area under the peaks was estimated using the triangle approximation and all reflections were put on a scale where the(200) reflection was considered equal to 100.

The measured values were operated on with four correction factors which were

(a) Polarization Factor

(b) Lorentz Factor

(c) Cox and Shaw Factor

(d) Obliquity Factor

The polarization factor takes into account the effect whereby an initially unpolarised X-ray beam becomes partially polarised on being scattered. The resultant mean intensity after scattering is thus dependent on the scattering angle (2θ) and given by the equation

Fig. 4.8 Space groups $P3_221$ and $P3_121$ exployed in structure factor computations

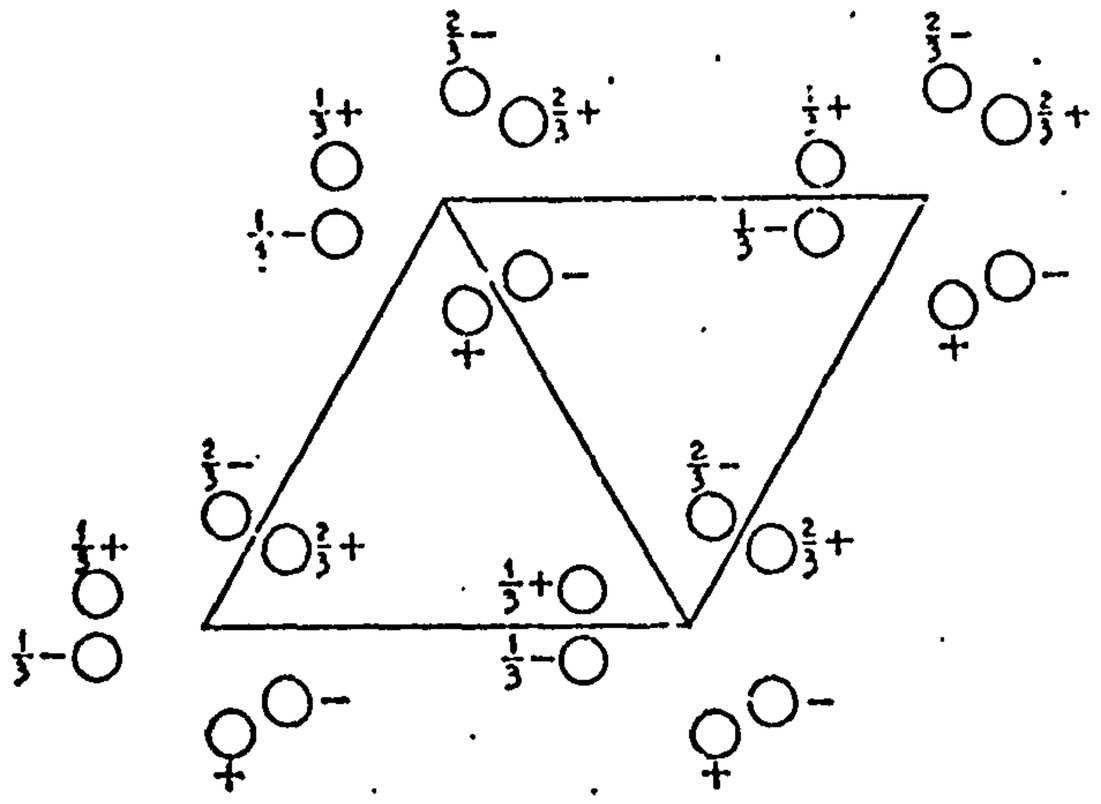

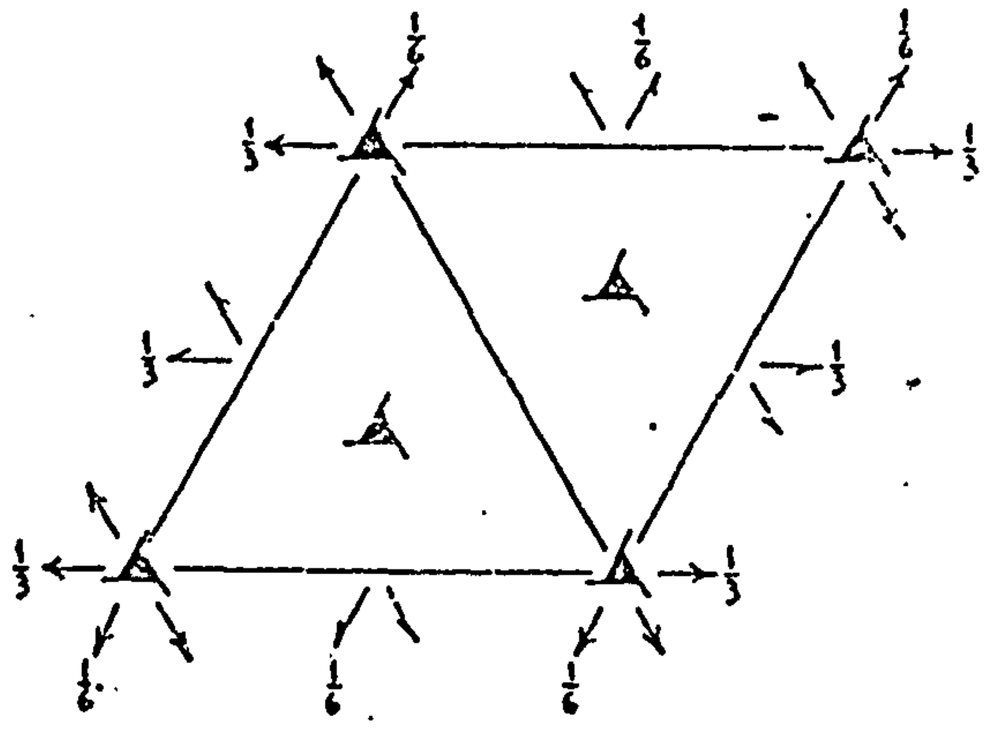

Origin at 3_221 [2-axis normal to $(11\bar{2}0)$]

Number of positions, Wyckoff notation, and point symmetry			Co-ordinates of equivalent positions			Conditions limiting possible reflections
						General:
6	*c*	1	x,y,z;	$\bar{y},x-y,\frac{2}{3}+z$;	$y-x,\bar{x},\frac{1}{3}+z$;	*hkil*: No conditions
			$y,x,\bar{z}$;	$\bar{x},y-x,\frac{2}{3}-z$;	$x-y,\bar{y},\frac{1}{3}-z$.	000*l*: $l=3n$
						Special: as above only
3	*b*	2	$x,0,\frac{1}{6}$;	$0,x,\frac{5}{6}$;	$\bar{x},\bar{x},\frac{1}{2}$.	
3	*a*	2	$x,0,\frac{2}{3}$;	$0,x,\frac{1}{3}$;	$\bar{x},\bar{x},0$.	

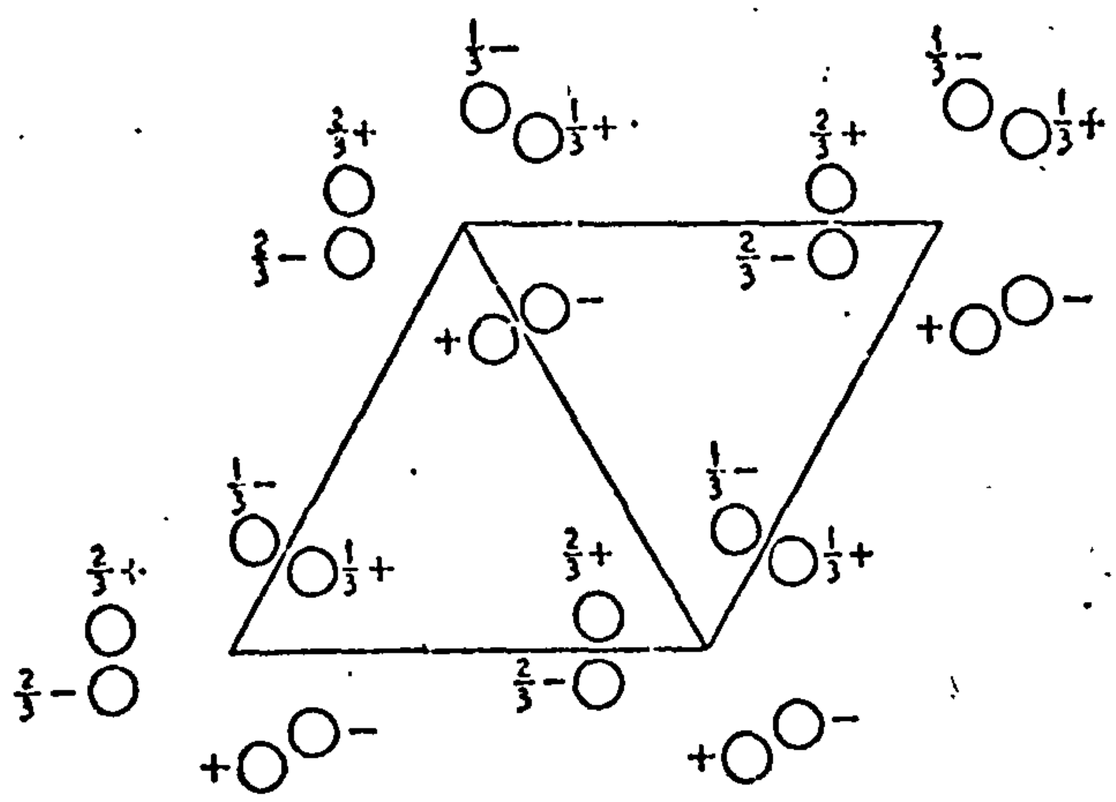

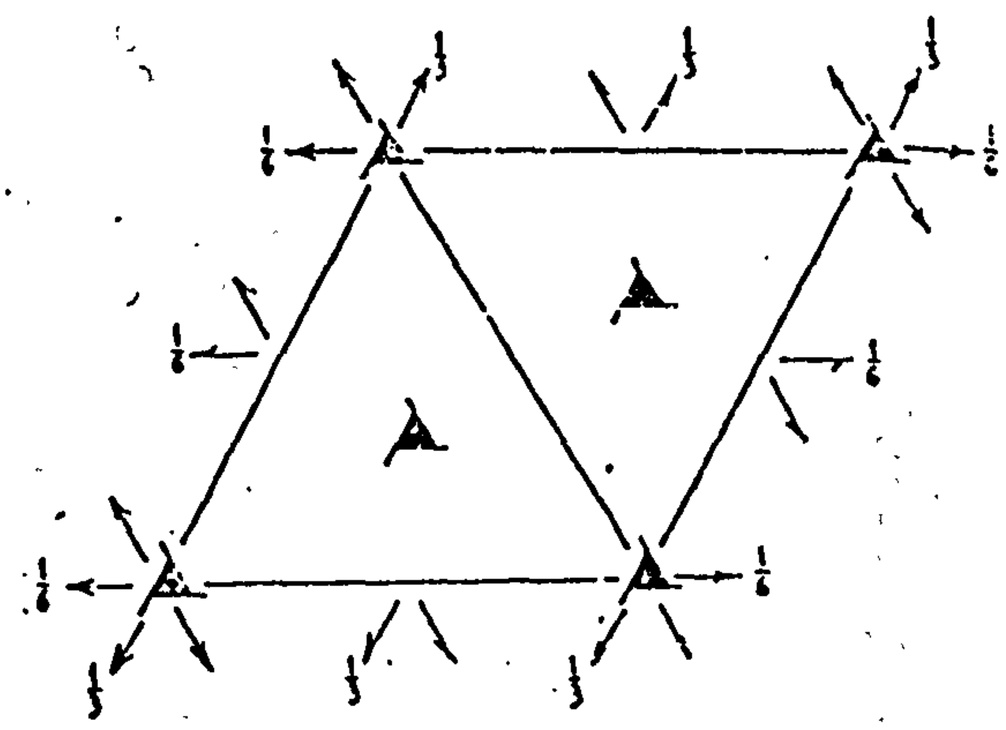

Origin at 3_121 [2-axis normal to $(11\bar{2}0)$]

Number of positions, Wyckoff notation, and point symmetry			Co-ordinates of equivalent positions			Conditions limiting possible reflections
						General:
6	*c*	1	x,y,z;	$\bar{y},x-y,\frac{1}{3}+z$;	$y-x,\bar{x},\frac{2}{3}+z$;	*hkil*: No conditions
			$y,x,\bar{z}$;	$\bar{x},y-x,\frac{1}{3}-z$;	$x-y,\bar{y},\frac{2}{3}-z$.	000*l*: $l=3n$
						Special: as above only
3	*b*	2	$x,0,\frac{5}{6}$;	$0,x,\frac{1}{6}$;	$\bar{x},\bar{x},\frac{1}{2}$.	
3	*a*	2	$x,0,\frac{1}{3}$;	$0,x,\frac{2}{3}$;	$\bar{x},\bar{x},0$.	

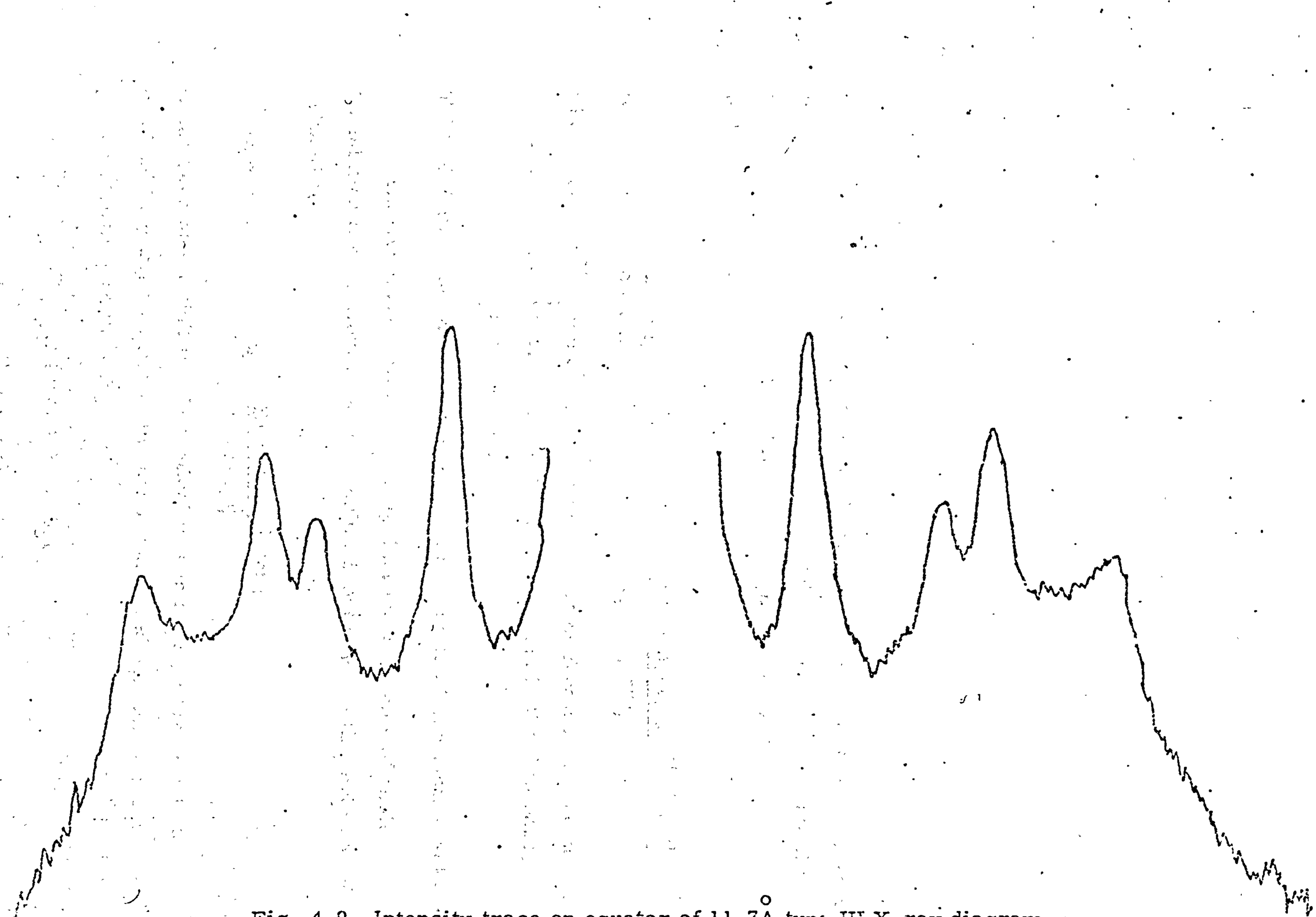

Fig. 4.9 Intensity trace on equator of 11.7Å type III X-ray diagram

$$P = \tfrac{1}{2}(1 + \cos^2\theta)$$

Factors (b) and (c) are geometrical correction factors taking into account the fact that the intensity of a reflection is proportional to the time a reciprocal lattice point spends in the Ewald sphere. For the equatorial reflections this correction is called the Lorentz factor and modifies the measured intensity according to the function $\underline{\sin 2\theta}$.
The general expression for any reflection is embodied in the Cox and Shaw factor Ref. 5 which is given by the formula

$$D = \frac{\sqrt{\sin^2 a - \sin^2\theta}}{\cos\theta}$$

where a is the angle shown in fig. 4.10.

Finally, the obiiquity factor arises because the interaction of the X-rays with the film depends on the angle χ at which the X-rays strike the film. For a dublitised film Whittaker Ref. 6 has derived the following expression

$$\left(\begin{array}{l}\text{Energy absorbed}\\ \text{(enhancement) at angle } \chi\end{array}\right) = \frac{(1-(1-c)^{\sec\chi})(1+(1-c)^{\sec\chi} e^{-\mu t\sec\chi})}{c(1+(1-c)e^{-\mu t})}$$

where $1-c = e^{-A}$ and e^{-A}, e^{-B} are absorption factors for the normal
and $B = \mu t$ beam in a single emulsion, and in the film base, respectively.

Table 4.6 lists the measured intensities and the total correction factor used.

The two models were tested against the variables of chain translation and rotation using the residual index R as the measure of reliability.

where $$R = \frac{\Sigma\,||Fo| - |Fc||}{\Sigma|Fo|}$$

It has been shown that the theoretical values for R, which would be obtained by using as a model the proper kind and number of atoms placed randomly in the cell, are

R_{rand}, (centric) = 0.83

R_{rand}, (acentric) = 0.59 Ref. 7.

Fig. 4.10 Diagram of the angles referred to in Cox and Shaw correction factor.

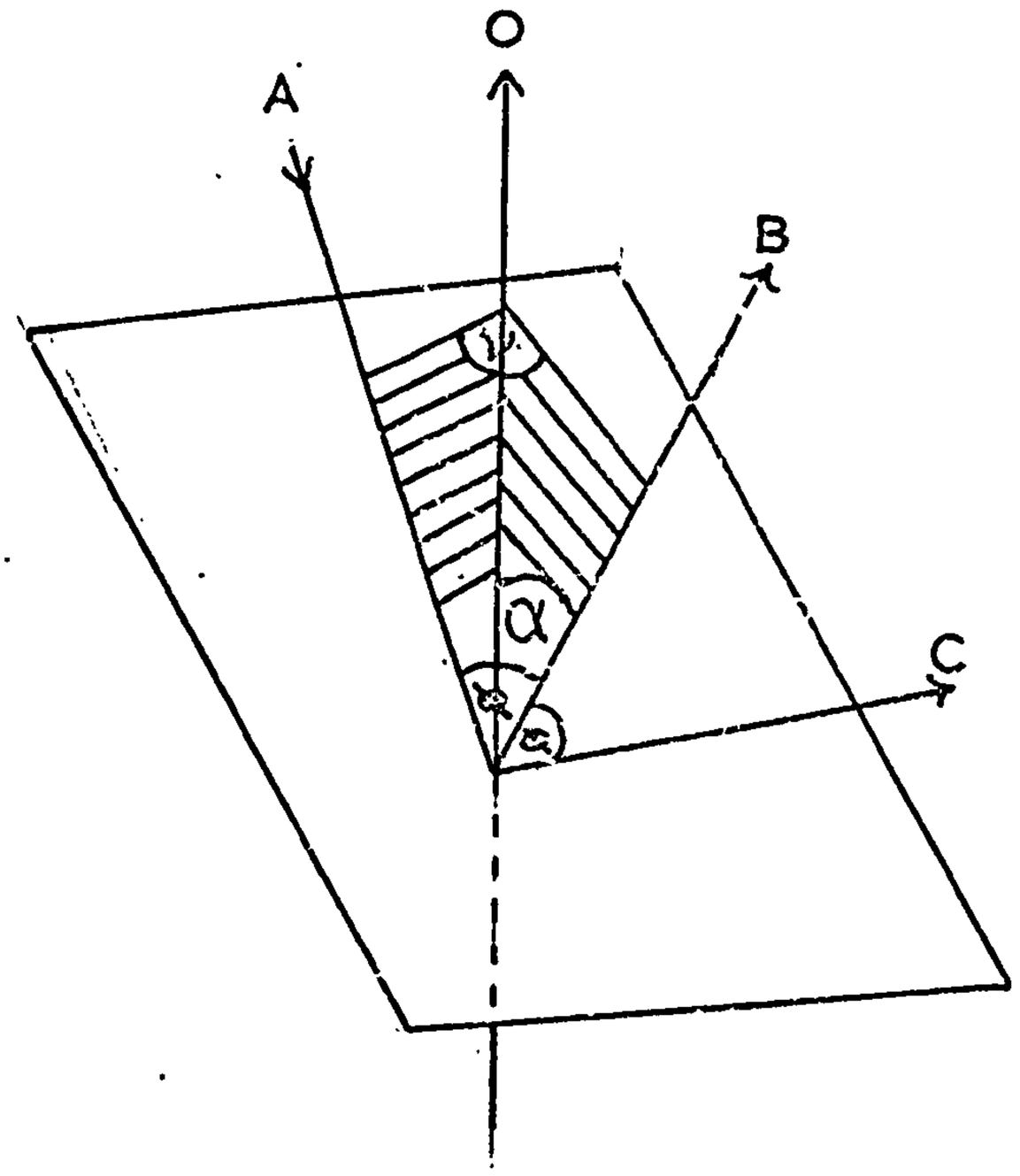

O is fibre axis

A is incident ray

B is normal to reflecting plane

C is reflected ray

Table 4.6

Intensities for Type III 11.7Å Hexagonal Cell

Reflection	Total Correction Factor	Multiplicity	Corrected Intens.
100	0.0039	3	12
110	0.016	3	24
200	0.038	3	100
210	0.029	3	29
101	0.004	3	12
102	0.0048	3	1.3
103	0.0057	3	0.7
104	0.0068	3	0.5
105	0.0079	3	3.5
106	0.0089	3	5.0
107	0.0096	3	6.0
108	0.0095	3	1.5
111	0.012	3	7.5
112	0.013	3	14.0
113			Absent
114			Absent
115	0.01739	3	14.5
116			Absent
117	0.02108	3	6.5
201	0.016	3	17.0
202	0.017	3	26.5
203			Absent
204	0.02	3	7.8
205	0.022	3	5.0
211	0.029	3	22.0
212	0.03	3	32.5

The above values serve as an upper limit to the region of interest, while a value of .35 is regarded as a hopeful structure that should yield to routine refinement. However, the above criterion must be used with care as it can be misleading. For fibre work the number of observed reflections and the accuracy to which intensities can be measured limit the possible value of R to about 0.2.

The values for the residual index as a function of translation and rotation are shown in Fig. 4.11 and it can be seen that the results are very similar, giving nearly the same region of rotation and translation for both models. They discriminate in favour of the left handed model although the difference in residual index is not sufficient to make a final decision. Fig. 4.12 shows a view down the fibre axis of the unit cell showing the rotation of the chains for the two unit cells and Table 4.7 gives the listing of observed and calculated intensities for the two models in the region of the most favourable residual index.

Fig. 4.12 shows that, in a search to minimise R, the rotation is such as to push as much scattering power as possible into the 'vacant' site. Because there is an important amount of scattering power absent from the hole in terms of water and anions this rotation is likely to be misleading. If the water molecules in the structure are localised around the centre of the hole there should be a discernible effect on the structure factors calculated for the reflections on the equator. See Table 4.8 below.

Table 4.8

Observed and Calculated Equatorial Reflections for three fold Left Handed Helix

Reflection	Calc.	Observ.	d spac.
100 type	54.2	12.4	10.13Å
110 "	42.1	24.2	5.85Å
200 "	55.8	100	5.06Å
210 "	14.4	28.9	3.83Å

Fig. 4.11 Residual index as a function of rotation and translation
(a) Right handed trial structure
(b) Left handed trial structure.

for Space Group $P3_121$

↓ rotation \ translation →	0	1	2	3	4	5	6	7	8	9	10	11	12	13
430	1·22	1·22	1·24	1·13	1·14	1·22	1·32	1·29	1·26	1·24	1·23	1·24	1·17	1·13
420	1·12	1·22	1·21	1·11	1·15	1·14	1·25	1·26	1·21	1·23	1·25	1·24	1·15	1·11
410	1·09	1·13	1·09	1·06	1·15	1·09	1·17	1·16	1·09	1·04	1·14	1·16	1·12	1·03
400	1·08	1·1	1·08	1·07	1·16	1·12	1·14	1·1	1·08	1·09	1·18	1·22	1·13	1·05
390	1·13	1·15	1·19	1·14	1·19	1·19	1·19	1·23	1·1	1·12	1·21	1·25	1·2	1·09
380	1·17	1·19	1·23	1·18	1·20	1·21	1·24	1·18	1·11	1·14	1·23	1·24	1·17	1·11
370	1·09	1·14	1·18	1·15	1·16	1·16	1·19	1·15	1·08	1·05	1·15	1·16	1·09	1·04
360	·86	·9	·96	·99	1·01	1·03	1·06	1·01	0·88	·92	·98	·98	·91	·84
350	·73	·75	·78	·80	·84	·85	·9	·82	·74	·76	·8	·83	·77	·71
340	·72	·73	·73	·75	·75	·79	·87	·8	·75	·76	·75	·79	·73	·71
330	·91	·98	·93	·94	·93	·96	1·05	1·03	·94	·93	·88	·98	·93	·9
320	1·16	1·28	1·23	1·17	1·15	1·13	1·23	1·2	1·14	1·13	1·12	1·17	1·14	1·07
310	1·2	1·3	1·33	1·24	1·25	1·22	1·25	1·18	1·12	1·19	1·22	1·23	1·18	1·13
300	1·12	1·22	1·23	1·2	1·23	1·23	1·26	1·15	1·11	1·15	1·23	1·19	1·16	1·12

for Space Group $P3_221$

↓ rotation \ translation →	0	1	2	3	4	5	6	7	8	9	10	11	12	13
420	1·09	1·13	1·09	1·06	1·11	1·15	1·17	1·21	1·1	1·07	1·09	1·08	1·1	1·1
410	·96	1·03	1·0	·96	1·02	1·0	1·0	1·06	1·02	1·0	1·04	1·06	1·02	·94
400	1·0	1·04	1·05	1·03	1·1	1·1	1·1	1·1	1·08	1·08	1·1	1·08	1·0	1·0
390	1·04	1·04	1·05	1·075	1·11	1·09	1·076	1·06	1·0	1·1	1·1	1·1	1·1	1·0
380	1·06	1·04	1·06	1·09	1·12	1·12	1·1	1·03	1·02	1·09	1·09	1·22	1·17	1·06
370	1·04	·98	1·05	1·04	1·08	1·12	1·09	1·01	1·07	1·11	1·1	1·25	1·19	1·06
360	·84	·81	·92	·9	·92	·96	·96	·94	·99	1·0	1·0	1·11	1·0	·88
350	·65	·78	·74	·72	·75	·74	·78	·82	·82	·85	·86	·72	·67	·66
340	·67	·79	·81	·7	·68	·7	·72	·83	·86	·79	·83	·76	·64	·67
330	·86	·98	·922	·79	·861	·8	·86	1·03	1·0	·93	·89	·85	·81	·83
320	1·1	1·12	1·01	·97	·98	·94	·061	1·15	1·08	1·02	1·04	1·05	1·05	1·02
310	1·17	1·15	1·07	1·11	1·13	1·11	1·21	1·17	1·07	1·1	1·2	1·23	1·24	1·16
300	1·04	1·06	1·06	1·08	1·04	1·08	1·14	1·05	1·05	1·11	1·13	1·12	1·2	1·07

Fig. 4.12 View down the fibre axis (c axis) of the 11.7Å unit cell for 'best' R value.
(a) Proposed left handed model
(b) Trial right handed model

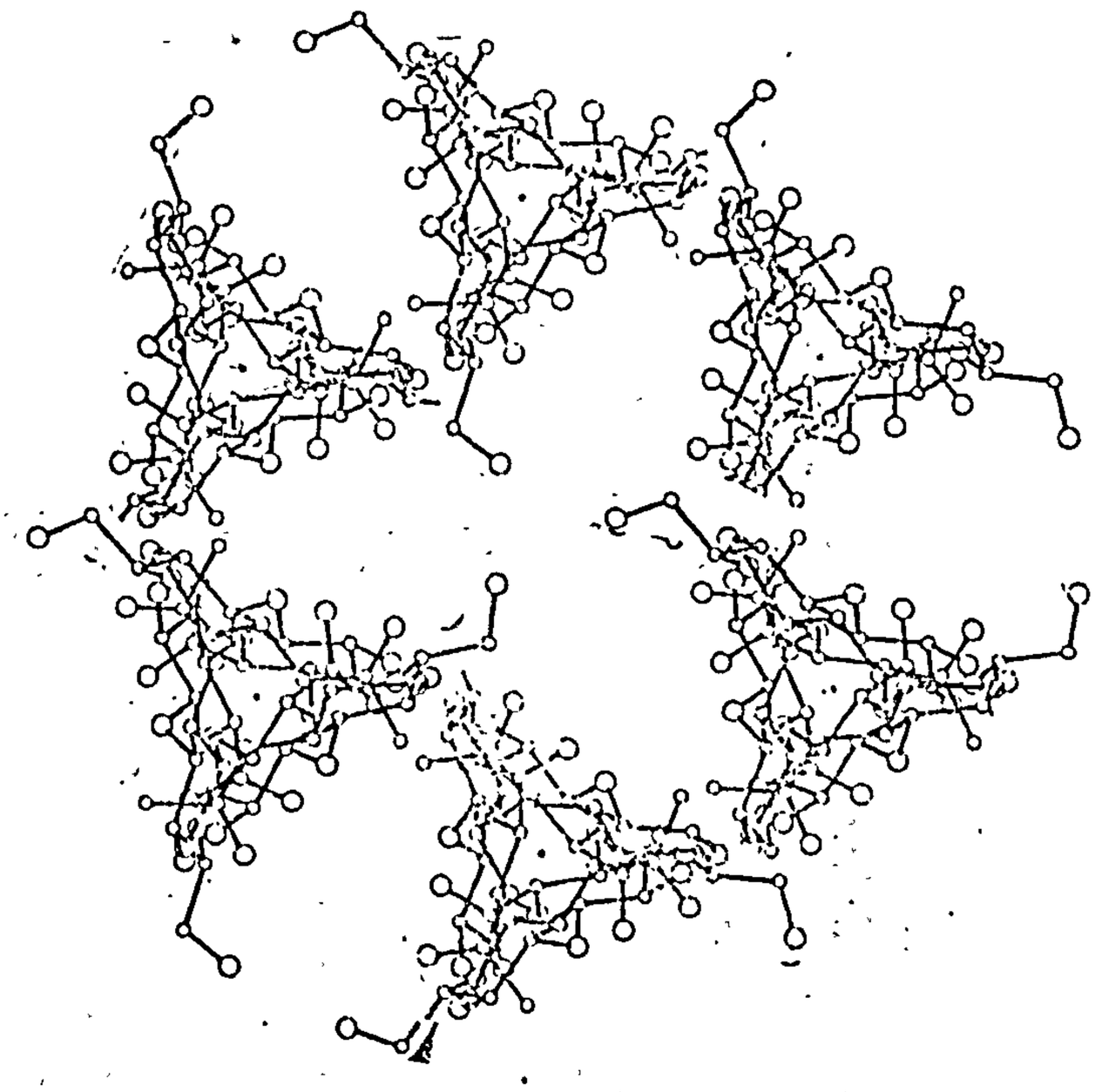

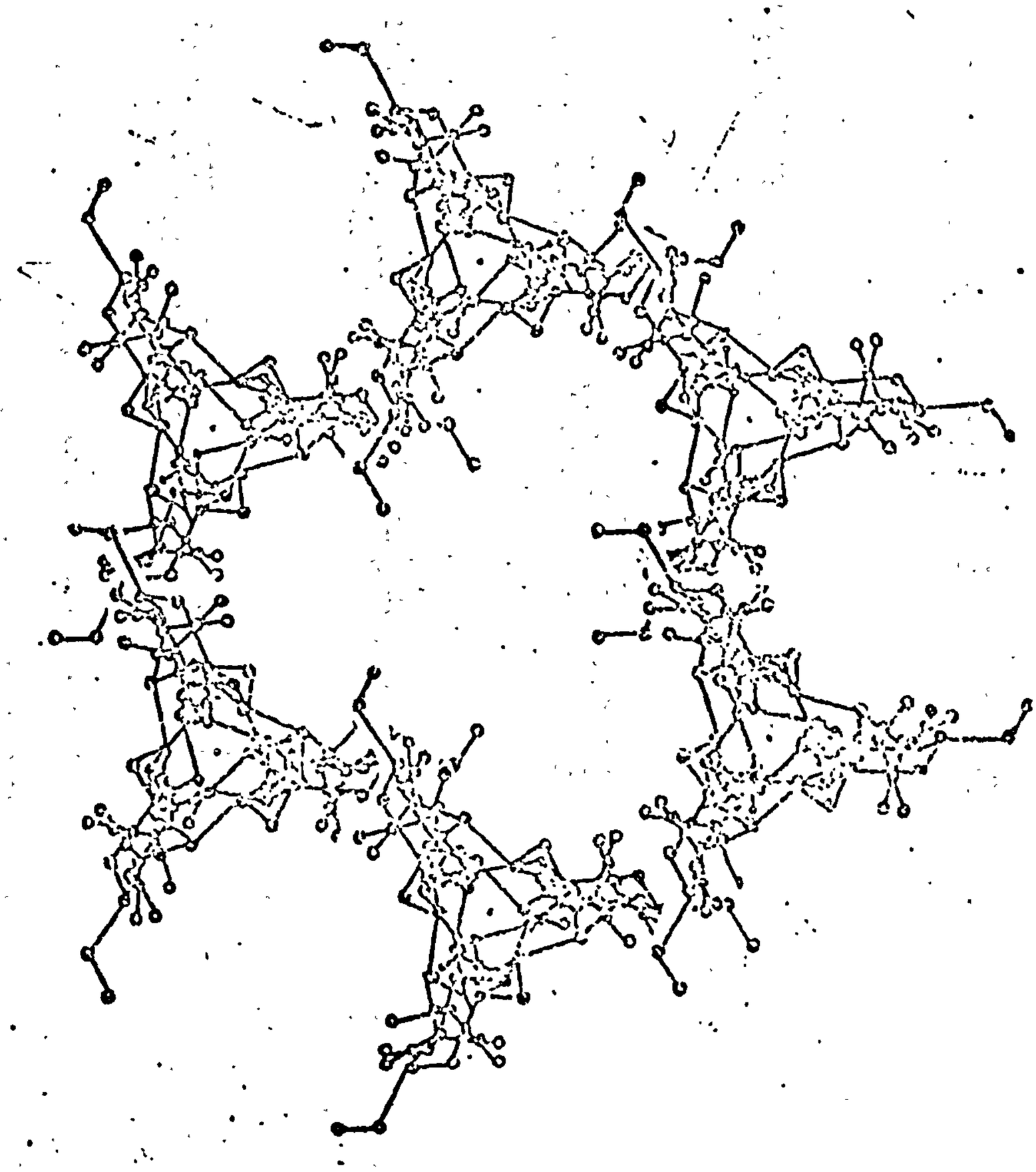

TABLE 4.7

TRANS.13
ROT. 350°

(b) Structure Factor Calculations for +3 Helix

h	k	l	d	A	B	Ical	Iob
-3	3	3	3.378	-56.1	-0.0	4.1	0.0
-3	3	1	3.354	19.3	-0.0	0.3	0.0
-3	3	2	3.237	-98.0	-0.0	7.7	0.0
-2	2	0	5.066	-218.7	-0.0	62.9	100.0
-2	2	1	4.988	156.5	-0.0	43.5	16.9
-2	2	2	4.775	-135.5	-0.0	12.7	26.4
-2	2	3	4.472	34.9	-0.0	0.8	0.0
-2	2	4	4.132	58.5	-0.0	5.2	7.7
-2	2	5	3.790	85.1	-0.0	4.8	3.1
-2	2	6	3.469	-26.3	-0.0	0.7	0.0
-2	3	0	3.830	71.7	-44.3	16.7	28.9
-2	3	1	3.796	40.6	68.9	31.2	22.3
-2	3	2	3.699	56.7	-8.0	4.9	32.6
-2	3	3	3.553	-47.8	68.6	13.7	0.0
-2	3	4	3.375	-21.2	-14.9	4.1	0.0
-1	1	0	10.133	-211.4	-0.0	38.8	12.4
-1	1	1	9.549	-112.4	-0.0	27.8	11.7
-1	1	2	8.264	64.7	-0.0	3.3	0.0
-1	1	3	6.938	-69.8	-0.0	4.7	0.0
-1	1	4	5.837	50.3	-0.0	2.1	0.0
-1	1	5	4.976	-14.2	-0.0	0.1	3.5
-1	1	6	4.308	5.7	-0.0	0.2	5.1
-1	1	7	3.755	104.2	-0.0	7.2	6.2
-1	1	8	3.367	48.4	-0.0	7.3	1.8
-1	2	0	5.850	132.1	-121.0	42.2	24.2
-1	2	1	5.731	-112.6	-41.1	18.9	7.6
-1	2	2	5.413	-24.3	76.9	2.6	13.8
-1	2	3	4.984	103.0	-11.4	14.1	0.0
-1	2	4	4.525	-8.4	14.6	0.4	0.0
-1	2	5	4.087	-33.6	-62.6	7.5	14.5
-1	2	6	3.692	26.0	33.1	2.3	0.0
-1	2	7	3.346	-29.4	56.8	4.3	6.5
-1	3	0	3.830	71.7	-44.3	0.0	0.0
-1	3	1	3.796	74.1	-93.1	0.0	0.0
-1	3	2	3.699	-12.1	-18.1	0.0	0.0
-1	3	3	3.553	25.8	52.7	0.0	0.0
-1	3	4	3.375	23.1	-43.9	0.0	0.0
0	0	1	28.560	-0.0	-0.0	0.0	0.0
0	0	2	14.280	-0.0	-0.0	0.0	0.0
0	0	3	9.520	-197.3	-0.0	25.6	19.9
0	0	4	7.140	0.0	-0.0	0.0	0.0
0	0	5	5.712	0.0	-0.0	0.0	0.0
0	0	6	4.760	50.2	-0.0	1.7	27.5
0	0	7	4.080	0.0	-0.0	0.0	0.0
0	0	8	3.570	0.0	-0.0	0.0	0.0
0	1	0	10.133	-211.4	-0.0	0.0	0.0
0	1	1	9.549	86.2	-149.3	0.0	0.0
0	1	2	8.264	-14.9	-25.9	0.0	0.0
0	1	3	6.938	-47.3	-0.0	0.0	0.0
0	1	4	5.837	12.7	-22.1	0.0	0.0
0	1	5	4.976	0.2	0.4	0.0	0.0
0	1	6	4.308	17.5	0.0	0.0	0.0
0	1	7	3.785	3.2	-5.5	0.0	0.0
0	1	8	3.367	47.0	81.3	0.0	0.0
0	2	0	5.066	-218.7	-0.0	0.0	0.0
0	2	1	4.988	-87.6	151.7	0.0	0.0
0	2	2	4.775	13.6	26.9	0.0	0.0
0	2	3	4.472	1.8	0.0	0.0	0.0
0	2	4	4.132	-33.6	58.5	0.0	0.0
0	2	5	3.790	5.6	5.7	0.0	0.0
0	2	6	3.469	-20.6	-0.0	0.0	0.0
0	3	0	3.378	-56.1	-0.0	0.0	0.0
0	3	1	3.354	-6.0	10.4	0.0	0.0
0	3	2	3.237	23.2	40.3	0.0	0.0
1	1	0	5.850	132.1	121.0	0.0	0.0
1	1	1	5.731	91.9	76.9	0.0	0.0
1	1	2	5.413	54.4	59.6	0.0	0.0
1	1	3	4.984	103.0	11.4	0.0	0.0
1	1	4	4.525	-8.5	14.6	0.0	0.0
1	1	5	4.087	-41.7	-62.9	0.0	0.0
1	1	6	3.692	26.0	-33.1	0.0	0.0
1	1	7	3.346	-27.3	49.9	0.0	0.0
1	2	0	3.830	71.7	44.3	0.0	0.0
1	2	1	3.796	43.6	-110.8	0.0	0.0
1	2	2	3.699	-9.6	-19.5	0.0	0.0
1	2	3	3.553	25.8	-32.7	0.0	0.0
1	2	4	3.375	26.4	-42.0	0.0	0.0
2	1	0	3.630	71.7	44.3	0.0	0.0
2	1	1	3.796	-77.4	9.1	0.0	0.0
2	1	2	3.699	-35.2	45.1	0.0	0.0
2	1	3	3.553	-47.8	-68.6	0.0	0.0
2	1	4	3.375	23.5	11.0	0.0	0.0

TABLE 4.7

Trans. 12
Rot .342°

(a) Structure Factor Calculations for −3 Helix

h	k	l	d Å	A	B	Ical	Iob
-3	3	0	3.379	-164.1	-0.0	37.5	3.0
-3	3	1	3.354	175.8	-0.0	22.7	3.0
-3	3	2	3.287	-2.1	-0.0	0.5	0.0
-2	2	0	5.066	-200.2	-0.0	55.8	100.0
-2	2	1	4.988	64.2	-0.0	20.3	16.9
-2	2	2	4.775	137.3	-0.0	23.3	26.4
-2	2	3	4.472	10.2	-0.0	5.3	0.0
-2	2	4	4.132	-98.8	-0.0	7.6	7.7
-2	2	5	3.790	35.2	-0.0	5.9	5.1
-2	2	6	3.469	-10.7	-0.0	0.3	0.0
-2	3	0	3.383	60.2	-39.4	14.4	28.9
-2	3	1	3.796	-93.9	64.8	24.3	22.3
-2	3	2	3.699	-32.7	-64.9	18.5	32.6
-2	3	3	3.553	34.6	-24.2	6.5	0.0
-2	3	4	3.375	75.3	38.2	17.7	0.0
-1	1	0	10.133	-197.4	-0.0	54.2	12.4
-1	1	1	9.549	-246.7	-0.0	49.3	11.7
-1	1	2	8.264	-12.7	-0.0	5.2	0.0
-1	1	3	6.938	25.1	-0.0	0.5	0.0
-1	1	4	5.837	5.8	-0.0	4.1	0.0
-1	1	5	4.976	-85.3	-0.0	12.0	3.3
-1	1	6	4.308	-40.2	-0.0	2.0	5.1
-1	1	7	3.785	-133.0	-0.0	14.3	6.2
-1	1	8	3.367	103.9	-0.0	7.5	1.5
-1	2	0	5.850	125.0	-41.4	24.1	24.2
-1	2	1	5.731	105.7	62.2	20.9	7.6
-1	2	2	5.415	-82.1	63.4	15.0	13.8
-1	2	3	4.984	-38.2	0.2	2.0	0.0
-1	2	4	4.525	10.4	16.3	0.5	0.0
-1	2	5	4.087	-3.3	75.9	8.0	14.3
-1	2	6	3.692	-12.6	-8.2	0.3	0.0
-1	2	7	3.346	36.2	41.4	6.8	4.3
-1	3	0	3.830	60.2	-39.4	0.0	0.0
-1	3	1	3.796	55.3	-36.8	0.0	0.0
-1	3	2	3.699	23.1	73.6	0.0	0.0
-1	3	3	3.553	-49.1	21.8	0.0	0.0
-1	3	4	3.375	-47.3	57.6	0.0	0.0
0	0	1	22.560	-0.0	-0.0	0.0	0.0
0	0	2	14.280	-0.0	-0.0	0.0	0.0
0	0	3	9.520	-122.1	-0.0	10.4	19.9
0	0	4	7.140	-0.0	-0.0	0.0	0.0
0	0	5	5.712	-0.0	-0.0	0.0	0.0
0	0	6	4.760	-17.4	-0.0	0.2	27.5
0	0	7	4.080	0.0	-0.0	0.0	0.0
0	0	8	3.570	0.0	-0.0	0.0	0.0
0	1	0	10.133	-197.4	-0.0	0.0	0.0
0	1	1	9.549	-50.2	-87.0	0.0	0.0
0	1	2	8.264	42.7	-74.0	0.0	0.0
0	1	3	6.938	-7.3	0.0	0.0	0.0
0	1	4	5.837	38.5	66.6	0.0	0.0
0	1	5	4.976	-30.9	88.2	0.0	0.0
0	1	6	4.309	34.8	-0.0	0.0	0.0
0	1	7	3.785	-26.8	-46.4	0.0	0.0
0	1	8	3.367	-3.7	6.5	0.0	0.0
0	2	0	5.066	-200.2	-0.0	0.0	0.0
0	2	1	4.988	-79.2	-137.1	0.0	0.0
0	2	2	4.775	60.6	-105.0	0.0	0.0
0	2	3	4.472	86.9	0.0	0.0	0.0
0	2	4	4.132	16.8	29.0	0.0	0.0
0	2	5	3.790	42.3	-73.5	0.0	0.0
0	2	6	3.469	18.4	-0.0	0.0	0.0
0	3	0	3.378	-164.1	-0.0	0.0	0.0
0	3	1	3.354	-22.0	-38.1	0.0	0.0
0	3	2	3.287	-13.3	23.0	0.0	0.0
1	1	0	5.850	125.0	41.4	0.0	0.0
1	1	1	5.731	1.0	122.7	0.0	0.0
1	1	2	5.415	-13.9	102.8	0.0	0.0
1	1	3	4.984	-38.2	-0.2	0.0	0.0
1	1	4	4.525	9.0	17.2	0.0	0.0
1	1	5	4.087	-64.1	40.8	0.0	0.0
1	1	6	3.692	-12.6	8.2	0.0	0.0
1	1	7	3.346	7.8	69.4	0.0	0.0
1	2	0	5.850	60.2	39.4	0.0	0.0
1	2	1	5.796	-39.5	29.4	0.0	0.0
1	2	2	5.699	-75.3	16.8	0.0	0.0
1	2	3	5.553	-49.1	-21.8	0.0	0.0
1	2	4	5.375	73.5	-12.2	0.0	0.0
2	1	0	5.830	60.2	39.4	0.0	0.0
2	1	1	5.796	-103.1	-49.0	0.0	0.0
2	1	2	5.699	82.5	13.2	0.0	0.0
2	1	3	5.553	34.6	24.2	0.0	0.0
2	1	4	5.375	-4.6	84.4	0.0	0.0

If an approximation for the presence of water molecules around the 'vacant' site is made by placing tubes of constant electron density on these sites it is possible to indicate the change of calculated structure factor on the equator owing to the presence of these molecules.

Fig. 4.13 shows the normalised intensities for a solid cylinder and a tube of constant electron density where the ratio of the internal to external radius of the tube is 0.5 and the external radius is taken to be 3.5Å (see Fig. 4.13(b)). The positions where the lattice samples this intensity distribution are shown in Fig. 4.13(c) and it can be seen that the correct modifications to the calculated equatorial intensities of Table 4.8 are predicted.

No important significance can be given to these considerations but taken together with the structure factor calculations they confirm the general packing arrangement and indicate that the space group chosen is a reasonable one. The results further suggest that the choice of a left handed, three-fold helix is preferred to a right handed conformation. No detailed extrapolation about interchain or intrachain hydrogen bonding can be made on the basis of present results owing to the missing electron density which gives rise to unreliable values of rotation and translation of chains. The quality of the 11.7Å diffraction diagram does not merit a deep fibre attack using least squares and Fourier difference methods but such an approach to the 18.7Å unit cell combined with chain packing methods will undoubtedly yield much more information.

Fig. 4.13 Normalised intensities for scattering from
(a) Cylinder of uniform electron density
(b) Tube of uniform electron density
(c) Points where 11.7Å net samples these intensity functions.

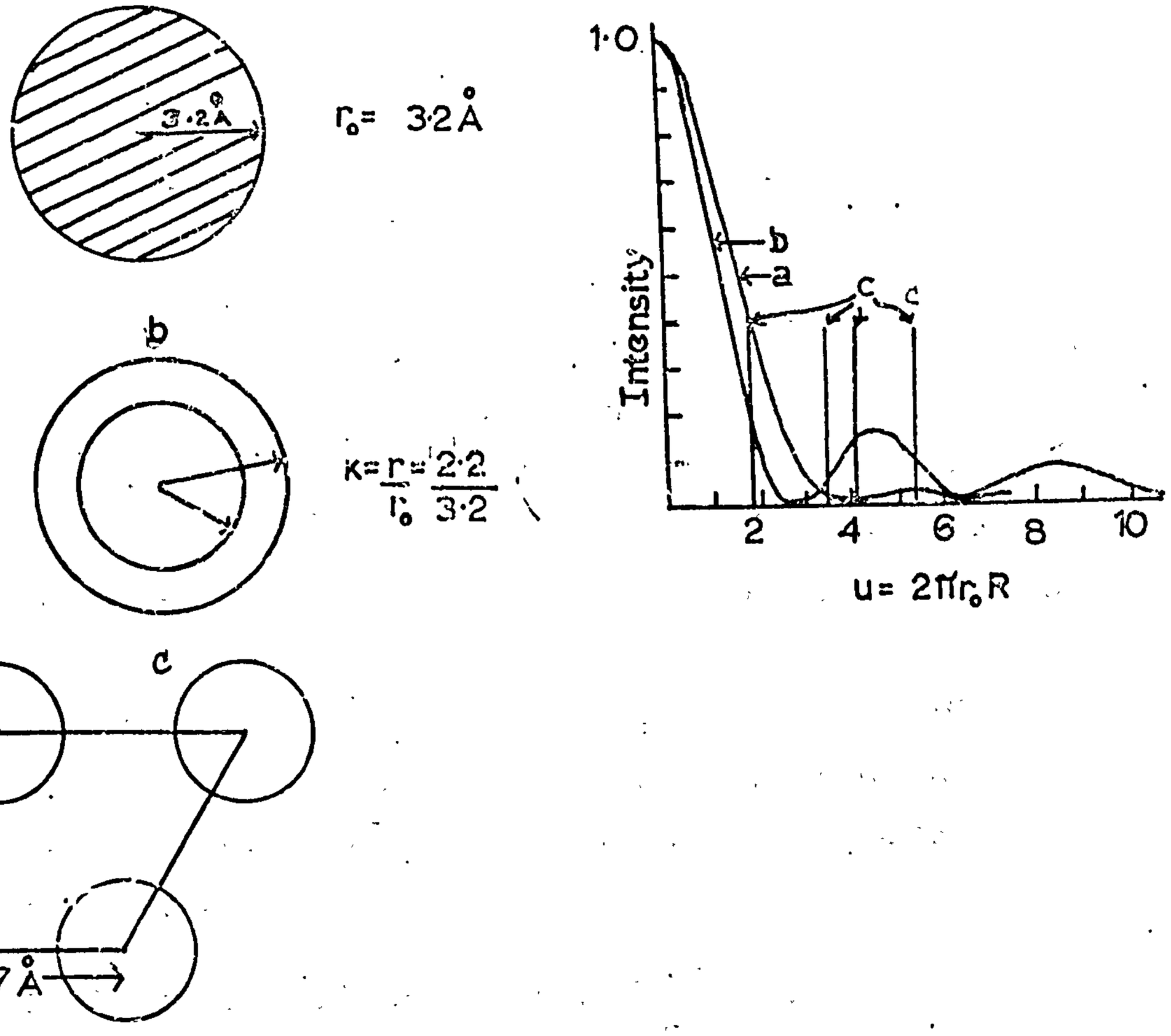

CHAPTER V

5.1 Introduction

In Chapters III and IV three essentially different backbone conformations have been introduced. The three-fold conformation, henceforth called type III, introduced in Chapter IV was found first in experiments using purified human mesathelioma fluid while type I and type II conformations were found later, using hyaluronate from human umbilical cord supplied by Miles Seravac Ltd. These three states, however, did not always exist separately and experiments showed transitions could be induced by physical and chemical means.

5.2 Transitions Between Type II and Type III (Humidity induced)

In Chapter III the method of going from Type I to II was described. It consisted of maintaining films under stress and humidity at temperatures of approximately 60°C. If films having the type II conformation were subsequently rehumidified at room temperature a second phase developed having meridional spacings characteristic of type III. Fig. 5.1 shows the diagram on which some type I, II and III meridionals are present. The quality of the diagram is not sufficient to index the phases on their various unit cells, in fact the development of the third phase appears to have stimulated a breakdown of the crystallinity of the sample.

5.3 Transformations During Chemical Processes, I

A 1% potassium hyaluronate solution from umbilical cord supplied by Miles Seravac was passed down a mixed monobed resin column to obtain the free acid form. A solution of this free acid was titrated back with sodium chloride to p.H. 7 to form the sodium salt. The solution was dialysed and freeze dried. Films of this material were stretched in the normal way at room temperature. The X-ray diagram obtained is shown in Fig. 5.2. The layer line spacing is 28.5Å and the meridionals on the third and ninth layer lines indicate that it is a type III conformation. The packing indicated by the row lines

Fig. 5.1 X-ray diagram of potassium hyaluronate containing a number of phases

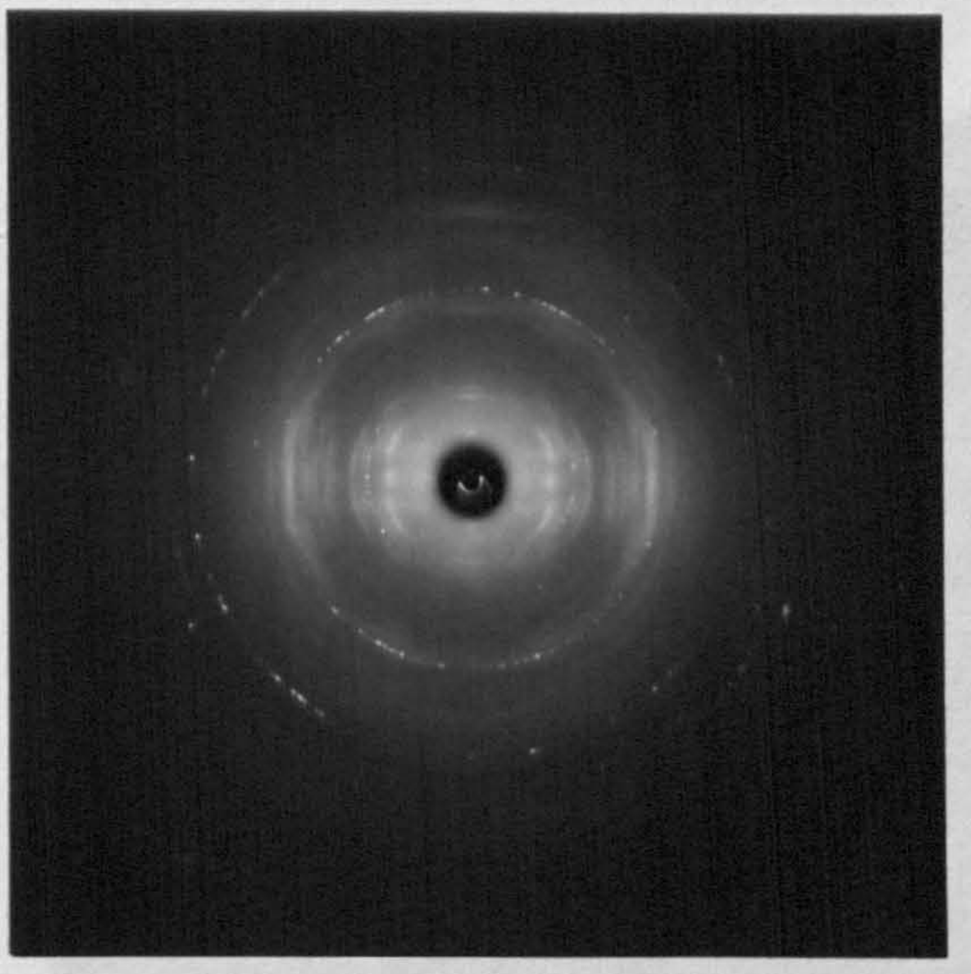

Fig. 5.2 X-ray diagram of sodium hyaluronate with a type III conformation but with orthorhombic packing

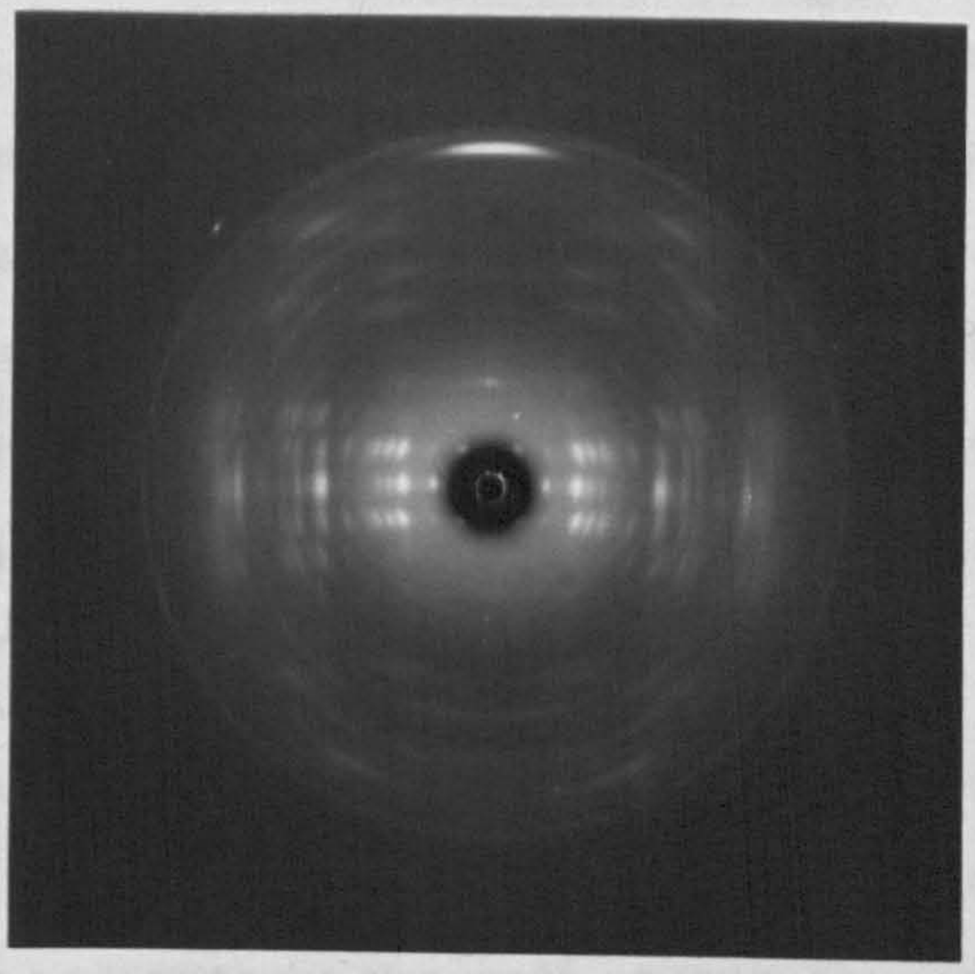

shows some extraordinary features. Table 5.1 lists all the row line spacings and shows that the unit cell may be indexed on an orthorhombic system where $a = 34.2\text{A} \pm 0.4\text{A}$, $b = 11.7\text{A} \pm 0.2\text{A}$, $c = 28.5\text{A} \pm 0.4\text{A}$ (c is the fibre axis).

Only two guiding principles were available for the placing of the chains in the unit cell.

(a) The ring-of-six motif present in the 11.7A and 18.7A unit cells of type III

(b) The 11.7A spacing is a familiar one.

Using these principles the most likely position for the chains is that shown in Fig. 5.3. When the chains are phased according to these positions, hand calculations show a satisfactory agreement with the equatorial intensities. Assuming an antiparallel distribution of chains, two space group types can be suggested both having a pair of chains as the asymmetric unit. Fig. 5.3(a) and (b) shows the two schemes, the one preferred being $P2_122$ which maintains the antiparallel ring-of-six motif.

The unit cell has many interesting aspects, being orthorhombic and yet containing units with trigonal symmetry. There are two different chain environments in the cell, some chains being surrounded by five near neighbours and one 'vacant' site and other chains having four near neighbours and two 'vacant' sites. From one point of view the cell may be regarded as a hybrid between the 11.7A hexagonal and 18.7A hexagonal cell but a completely different way of viewing it is as pairs of chains arranged in corrugated sheets with the two sheets in the unit cell being in antiphase.

This idea of pairing the chains is an interesting one because the starting material was in a type I conformation, i.e. possibly a double helix. The question arises as to whether this is a true intermediate between the single helix and double helix conformations. Specimens giving the above diagram, were annealed in a humid environment for a number of weeks at room temperature. A diagram shown in Fig. 5.4

Table 5. 1

Measured Spacings and Indices of Orthorhombic Type III

Measured Spacings Å	Intensity	Index Type
34.4 ± 0.4	Very Weak	100
17.2 ± 0.3	Medium Strong	200
11.68 ± 0.2	Medium	010
11.40 ± 0.2	Strong	300
11.0 ± 0.2	Strong	110
9.6 ± 0.2	Medium	210
8.63 ± 0.1	Medium	400
8.14 ± 0.1	Weak	210
6.8 ± 0.1	Very Weak	410
5.9 ± 0.1	Strong	510
5.8 ± 0.1	Strong	020, 600
5.55 ± 0.1	Weak	220
5.1 ± 0.1	Medium	320
4.82 ± 0.1	Weak	420
4.39 ± 0.1	Medium	
4.00 ± 0.1	Strong	
3.84 ± 0.1	Medium	
3.75 ± 0.1	Medium	
3.2 ± 0.1	Medium	

Row lines index on a rectangular lattice

$a = 34.2\text{Å} \pm 0.4\text{Å}$ $b = 11.7\text{Å} \pm 0.2\text{Å}$

Meridionals on the 3rd and 9th layer lines

and layer line spacing = $28.5\text{Å} \pm 0.4\text{Å}$.

Proposed unit cell is Orthorhombic $a = 34.2 \pm 0.4\text{Å}$, $b = 11.7 \pm 0.2\text{Å}$

c (Fibre axis) $= 28.5 \pm 0.4\text{Å}$.

Fig 5 3 Possible packing and space group schemes for the orthorhombic type III lattice

Space Group P2,22

2 chains in asymmetric unit

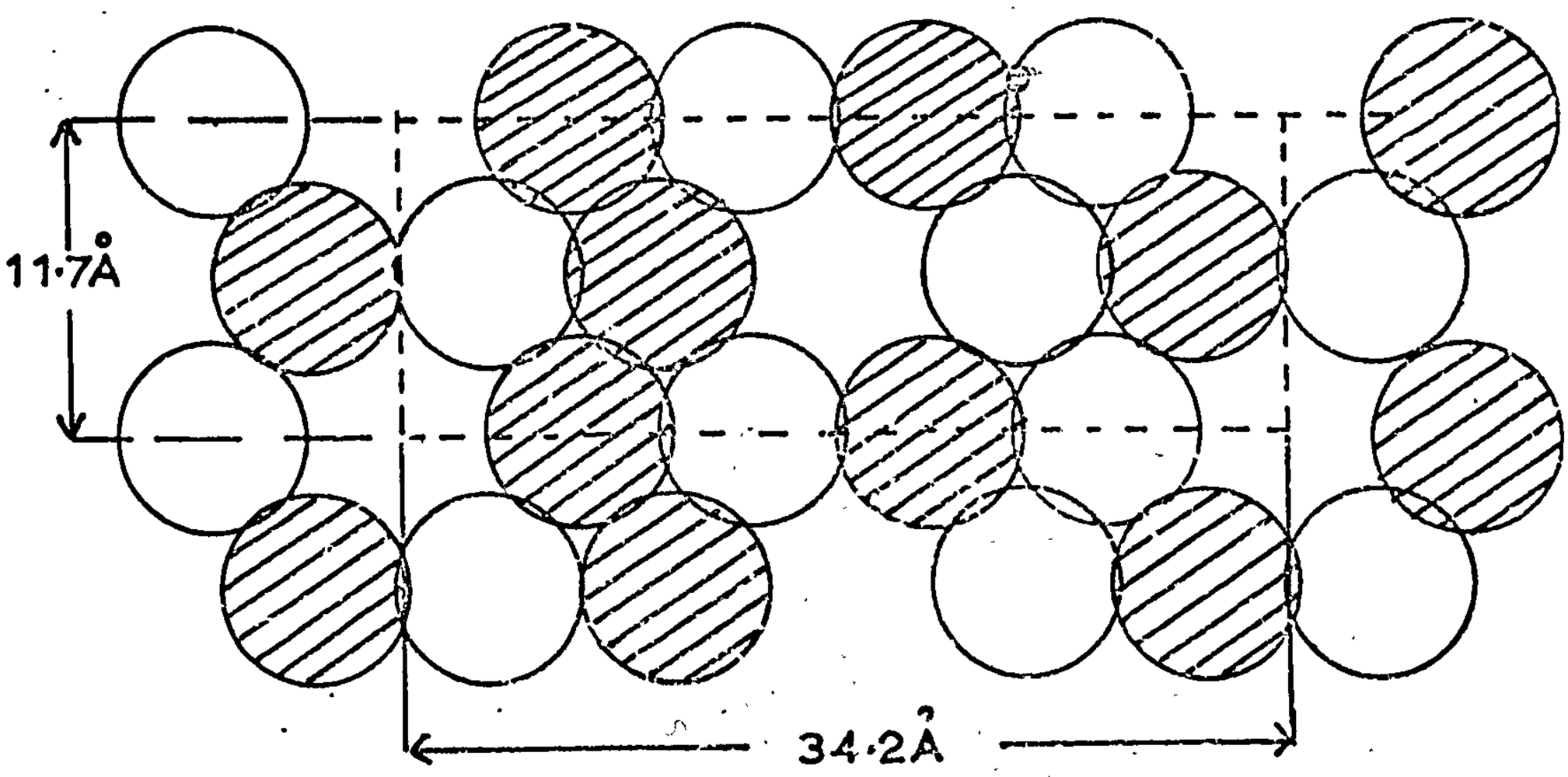

Space Group P2,2,2,

2 chains form asymmetric unit

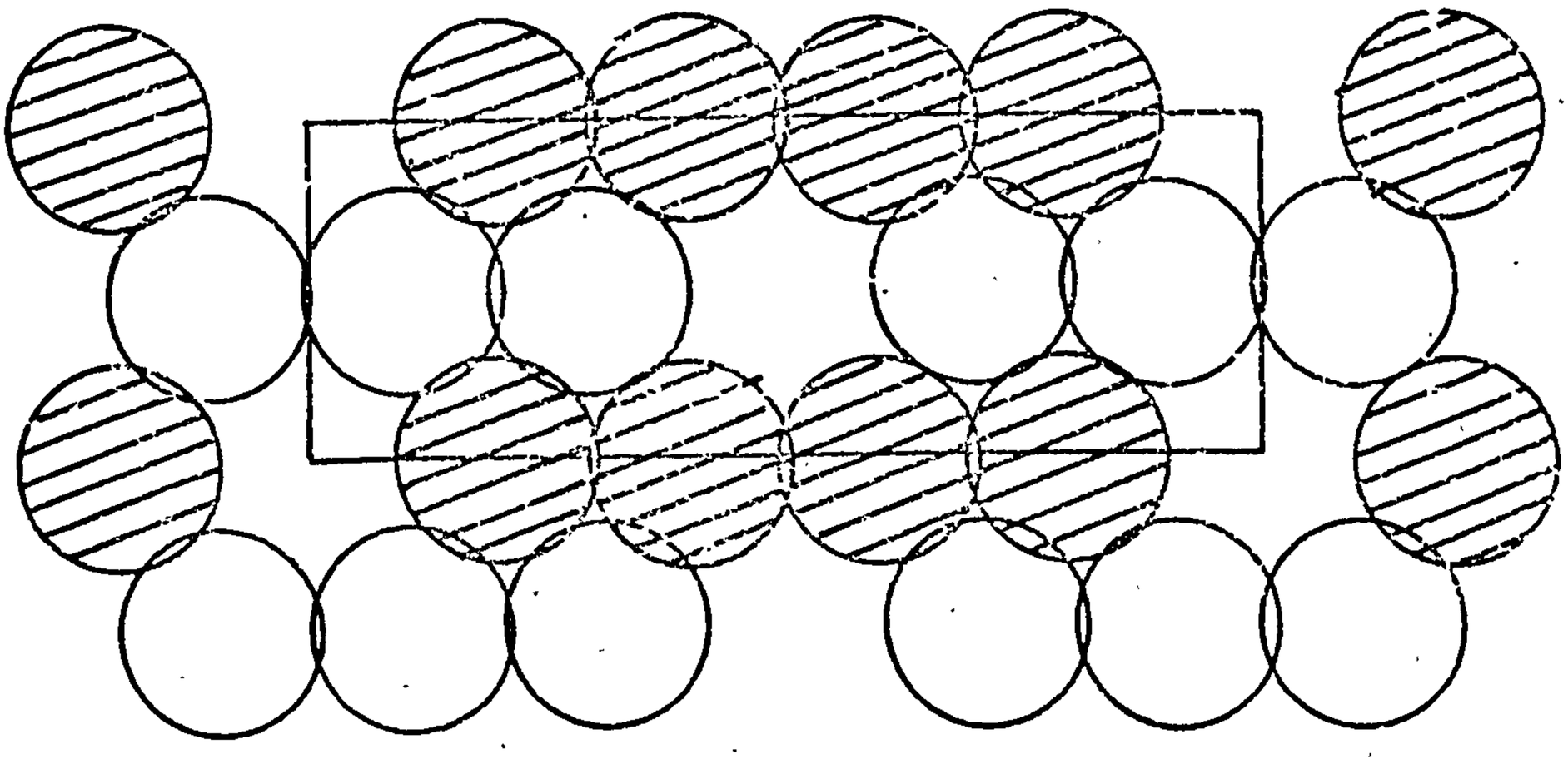

Fig. 5.4 X-ray diagram showing the developement of the type I conformation from the orthorhombic type III conformation

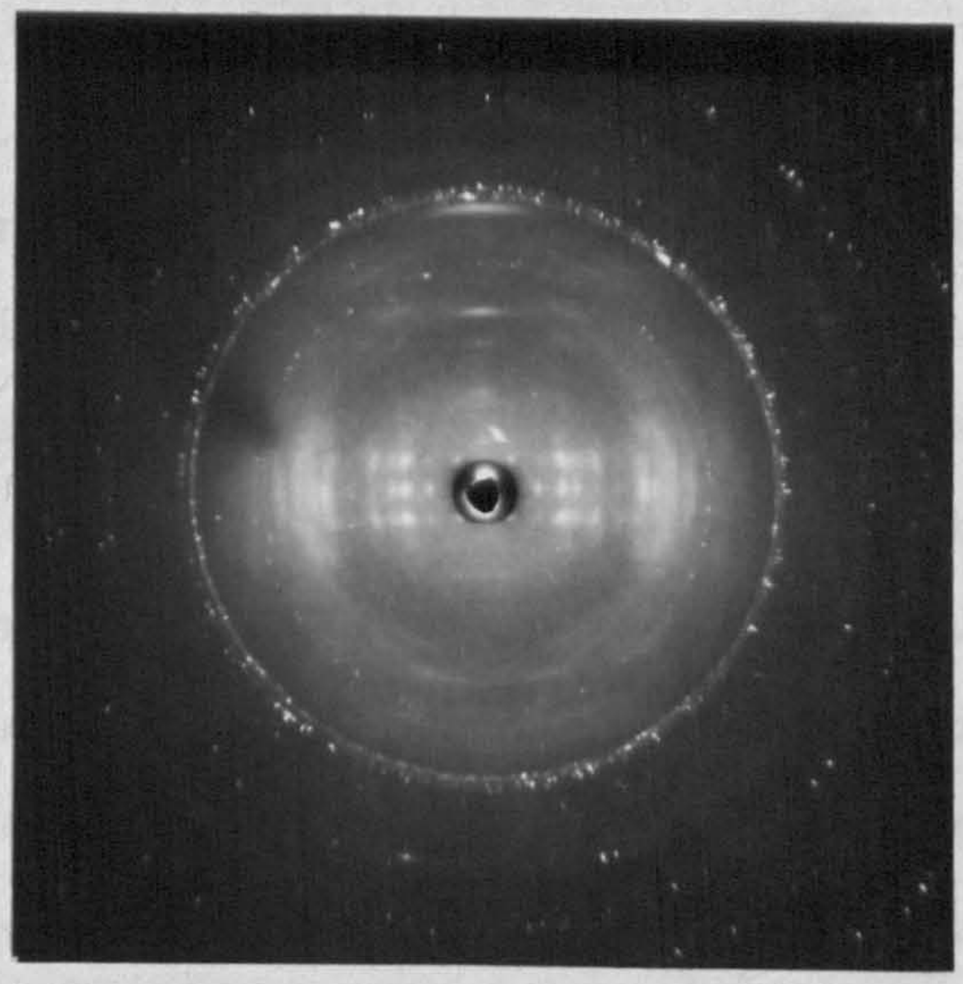

was subsequently obtained, which shows clearly the development of meridionals consistent with the type I conformation. The two phases appear to coexist in equilibrium. This is supported by Dea et al. who show the same diagram Ref. 1, though they were not aware of the orthorhonibic unit cell and refer to it wrongly as being hexagonal. If the type I conformation is truly a double helix then a detailed examination of the diagram shown in Fig. 5.2 should in time throw light on the interaction between antiparallel pairs of chains.

5.4 Transformations II Effect of Calcium

A 2% solution of potassium hyaluronate (the same source which gave type I and type II conformations discussed in Chapter III) was syringed through a 1m.m. hypodermic into a 90% solution of acetone or ethanol plus 10% concentrated calcium chloride solution. As described in Chapter II, a good fibre was formed which was subsequently bundled and stretched at 90% relative humidity. An X-ray diagram taken after a few days at 50% relative humidity is shown in Fig. 5.5(a). Again the conformation is recognised as type III but with the meridionals being uncharacteristically weak on the third and ninth layer lines and strong on the sixth layer line. The diagram is of generally poor quality and with the equatorial reflections becoming increasingly diffuse with decreasing 'd' spacing. Table 5.2 gives the measured spacings and shows that they may be indexed on a hexagonal unit cell where $a = b = 15.4 \pm 0.3$Å, $c = 28.5 \pm 0.4$Å (where c is the fibre axis). On X-raying a similar specimen at much higher humidity, approximately 85%, the diagram shown in Fig. 5.5(b) was obtained, which is similar in all respects except that the unit cell now indexes on a hexagonal system where $a = b = 16.3$Å ± 0.3Å and $c = 28.5 \pm 0.4$Å. The X-ray pattern was sensitive to humidity changes, exhibiting a range of values for the unit cell dimensions.

Specimens under stress at 90% R.H. for approximately two weeks gradually underwent a packing rearrangement indicated by the presence of two phases in Fig. 5.6(a). The transformation proceeded

Fig. 5.5 (a) Calcium fibre after initial stretching treatment, X-rayed at 50-60% R.H.

(b) Calcium fibre same as (a) but X-rayed at 80-90% R.H.

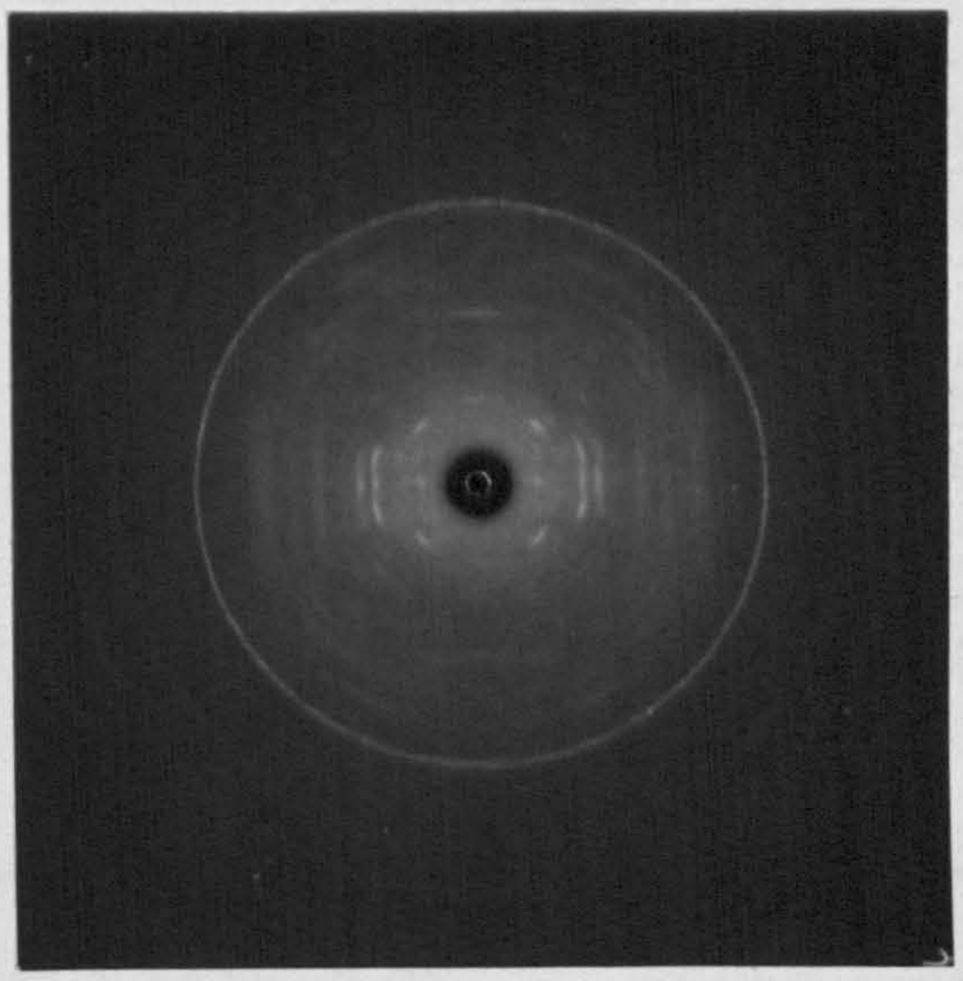

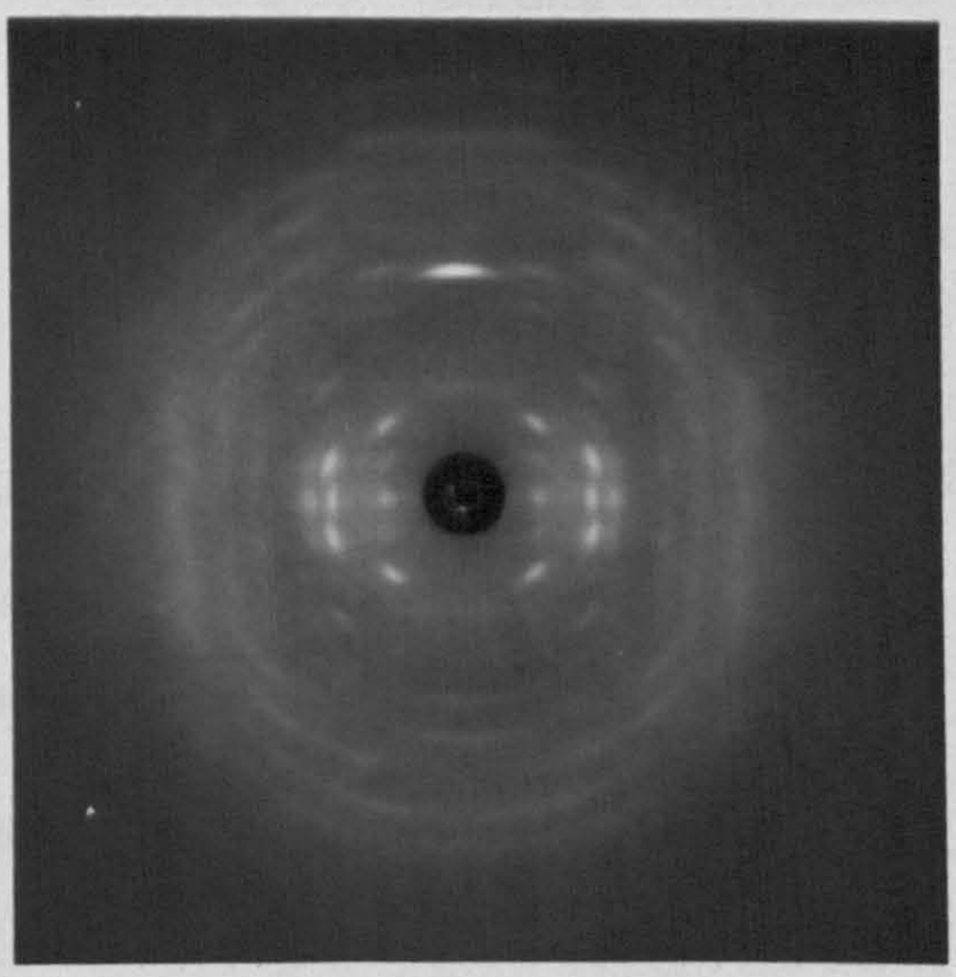

Table 5.2

(a) Spacings and Indices for Initial Calcium Hyaluronate Fibre Diagram at 50-60% R.H.

Measured Spacings Å	Intensity	Index Type
13.3 ± 0.3	Weak	100
7.7 ± 0.2	Strong	110
6.7 ± 0.1	Medium	200
5.0 ± 0.1	Weak	210
4.4 ± 0.1	Medium	300
3.8 ± 0.1	Medium Strong	220
Meridionals		
9.5 ± 0.2	Weak	003
4.75 ± 0.1	Very Strong	006
3.16 ± 0.1	Weak	009

(b) Same Specimen at 80-95% R.H.

Measured Spacings Å	Intensity	Index Type
14.2 ± 0.3	Medium	100
8.2 ± 0.2	Strong	110
6.9 ± 0.1	Medium	200
5.2 ± 0.1	Weak	210
4.6 ± 0.1	Medium	300
3.9 ± 0.1	Medium Strong	220

For (a) Row lines index on a hexagonal lattice

$$a = b = 15.4\text{Å} \pm 0.3\text{Å}.$$

For (b) Row lines index on a hexagonal lattice

$$a = b = 16.3 \pm 0.3\text{Å}.$$

Layer line spacing is the same for (a) and (b) i.e. 28.5 ± 0.4Å.

Fig. 5.6 (a) Calcium fibre annealed at room temperature for 1-2 weeks, X-rayed at 70-80- R.H.

(b) Calcium fibre annealed for 3-4 weeks at room temperature, X-rayed at 80-90% R.H.

(c) Calcium fibre, same as (b) but X-rayed at 50-60% R.H.

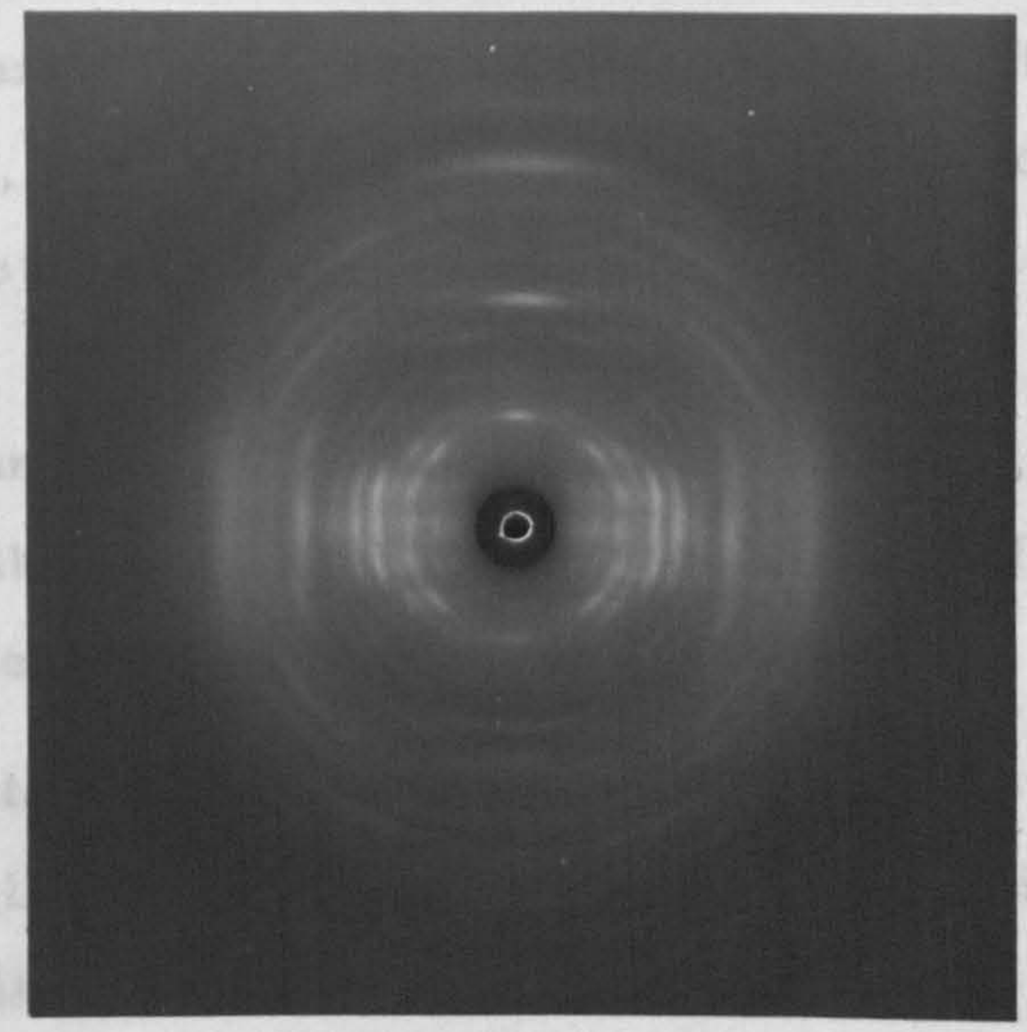

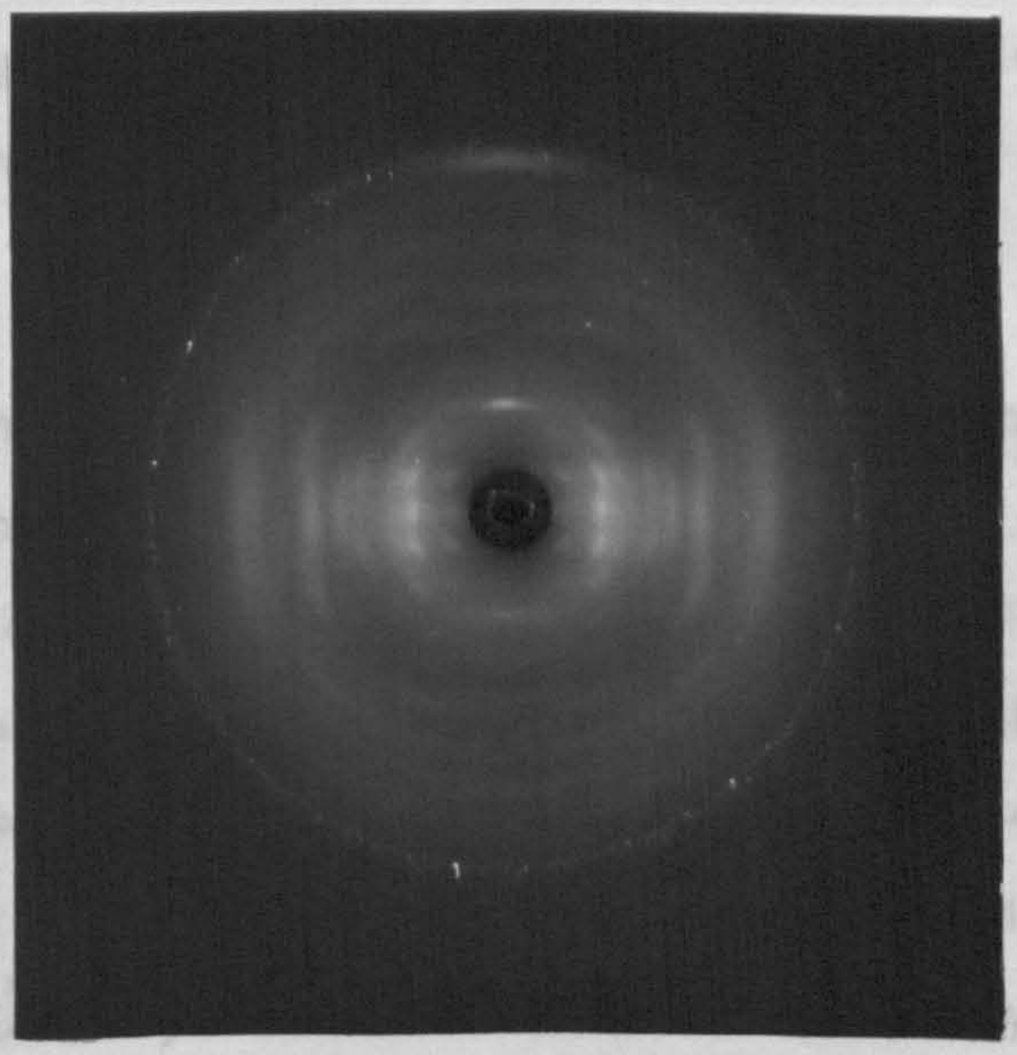

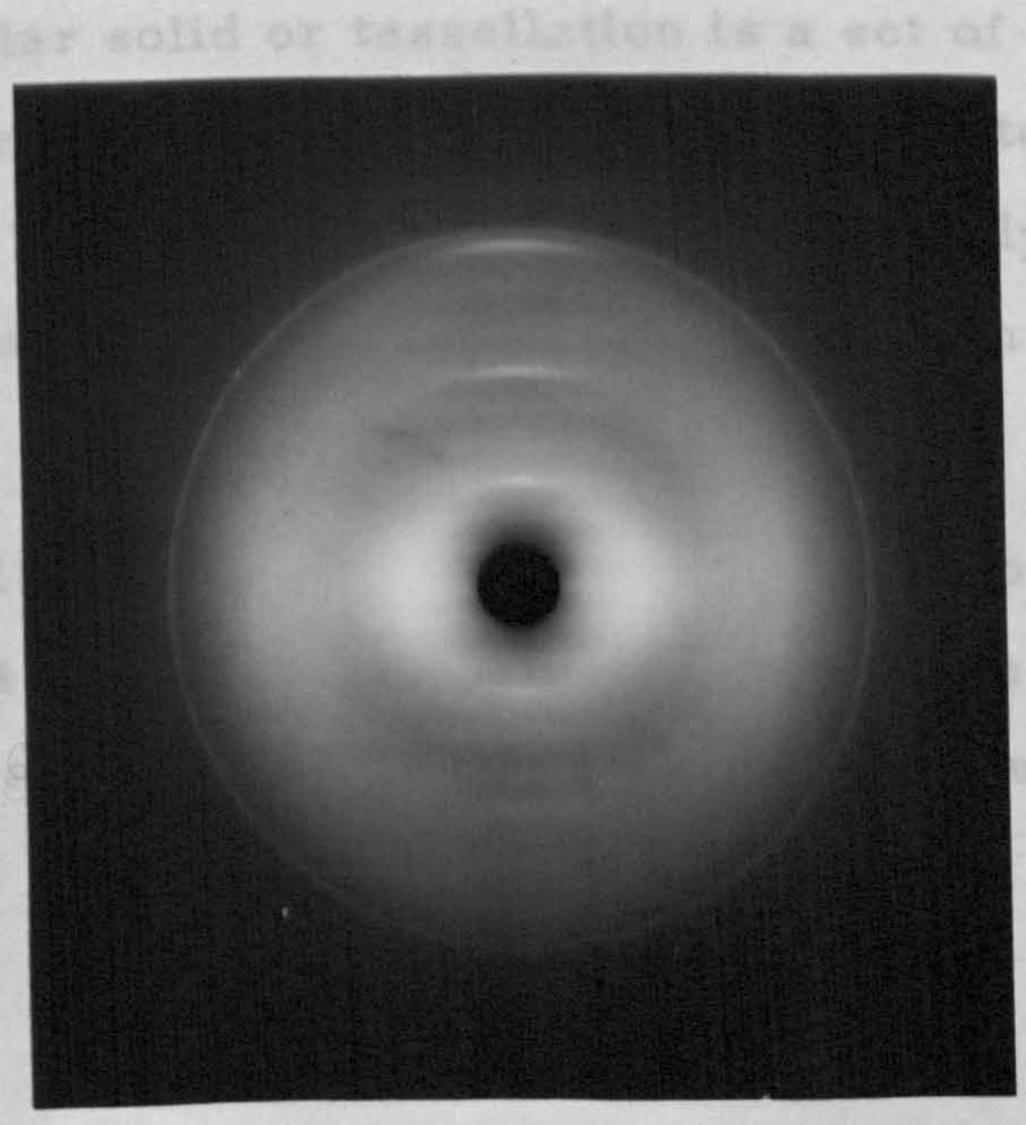

until a diagram shown in Fig. 5.6(b) was obtained. Table 5.3 lists the 'd' spacings of the diagram 5.6(b) and it can be seen that they index on a hexagonal unit cell, $a = b = 20.8\text{Å} \pm 0.4\text{Å}$, and $c = 28.5\text{Å} \pm 0.4\text{Å}$ (where c is the fibre axis). The meridional intensity distribution also indicates a change, with a weak sixth layer line meridional, and a very strong ninth layer line meridional. This diagram is interesting for two reasons.

(1) It is sensitive to humidity, the crystallinity collapsing below 50% R.H.

(2) The intensity distribution is almost identical to that of the six chain 18.7Å cell discussed in Chapter IV.

Point (2) supplies an interpretation of the diagram in Fig. 5.6(b), i.e. a six chain unit cell, but it does not answer the question why, unlike the 18.7Å cell, the unit cell is humidity sensitive. The question of the presence of water in all the packing systems will be dealt with in detail in the next chapter, but it is clear that in this calcium form water plays an important role.

5.5 Tessellations

Before discussing the interpretation of the diagram shown in Fig. 5.6 a useful scheme for considering two dimensional packing of regular objects will be introduced. It was pointed out by Professor Frank that the two packing schemes proposed for the type III conformation in Chapter IV were both cases of regular and semi-regular tessellations. These tessellations are shown in Fig. 5.7 and the notation for describing them is a modified Schläfli symbol. In the words of Cundy and Rollett Ref. 2 "A facially-regular solid or tessellation is a set of regular polygons of two or more kinds so arranged that every vertex is congruent to every other vertex. The whole figure is then completely specified by giving the polygons occurring at any vertex in the order in which they are found".

The 11.7Å and 18.7Å unit cells, discussed in Chapter III, are cases of 6^3 and 6.4.3.4 tessellations respectively. In the two tessellations the interchain distance as represented by the distance between vertices

Table 5.3

Spacings and Indices for Final Annealed State of a Calcium Fibre at 80-90% R.H.

Measured Spacings Å	Intensity	Index Type
Row Lines		
18.0 ± 0.3	Medium	100
10.45 ± 0.2	Strong	110
8.9 ± 0.2	Very Weak	200
6.66 ± 0.1	Medium	210
6.0 ± 0.1	Medium Strong	300
5.14 ± 0.1	Strong	220
4.5 ± 0.1	Weak	400
4.1 ± 0.1	Strong	320
3.9 ± 0.1	Strong	410
3.44 ± 0.1	Medium	420
Meridionals		
9.5 ± 0.2	Strong	003
4.75 ± 0.1	Weak	006
3.16 ± 0.1	Very Strong	009

Row lines index on a hexagonal lattice

$a = b = 20.8\text{Å} \pm 0.3\text{Å}$

and layer line spacing = $28.5 \pm 0.4\text{Å}$.

Fig. 5.7 Regular and Semi-Regular Tessellations.

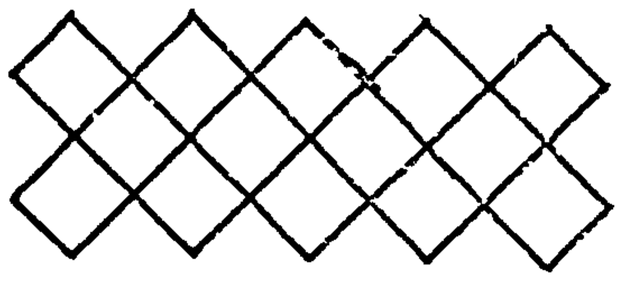

4^4

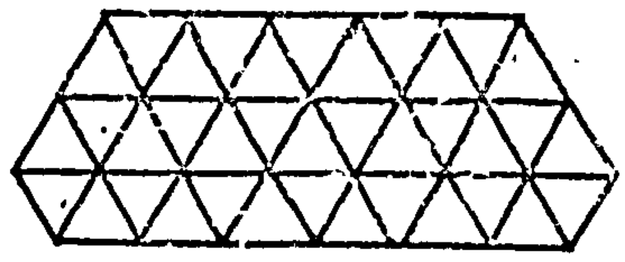

3^6

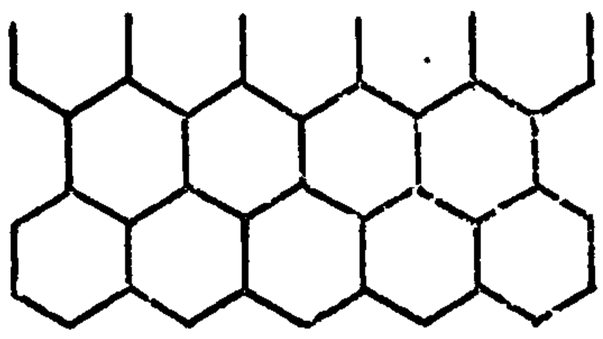

6^3

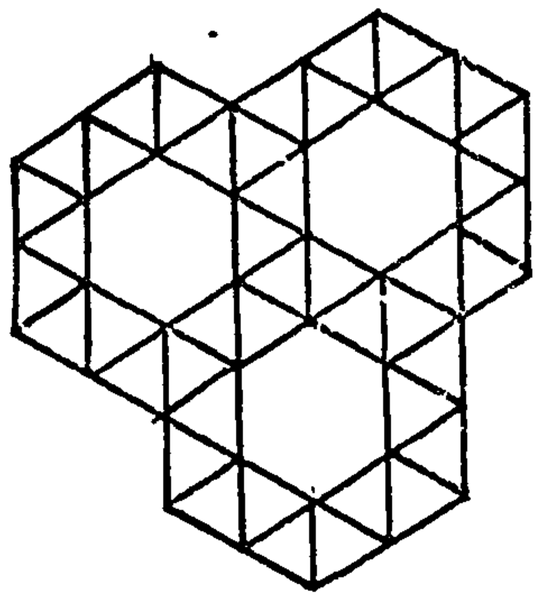

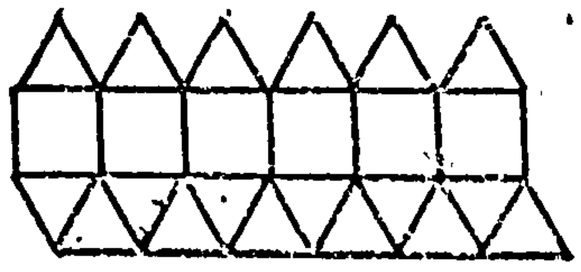

$3^3.4^2$

$3^4 6$

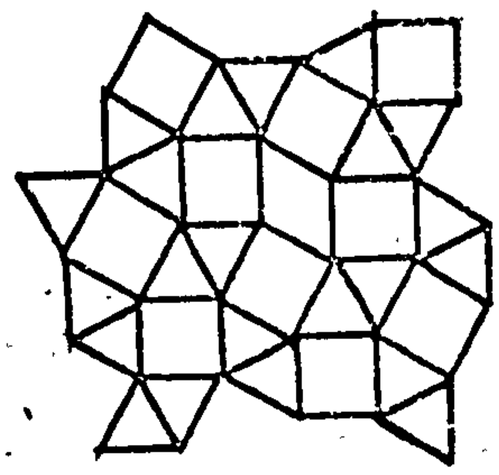

$3^2.4.3.4.$

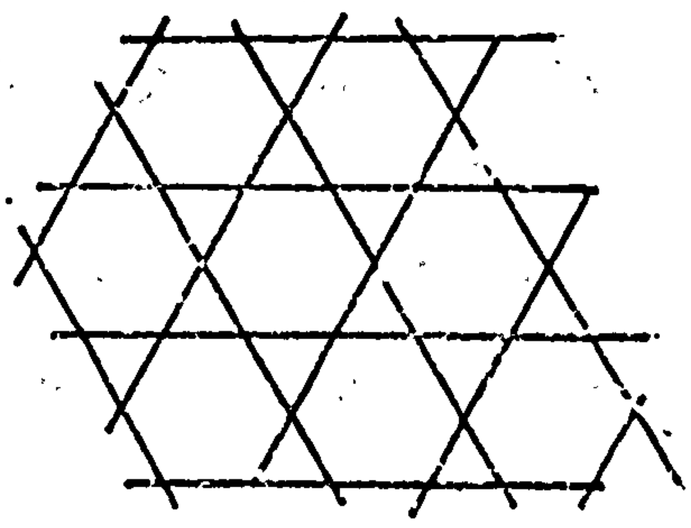

3.6.3.6

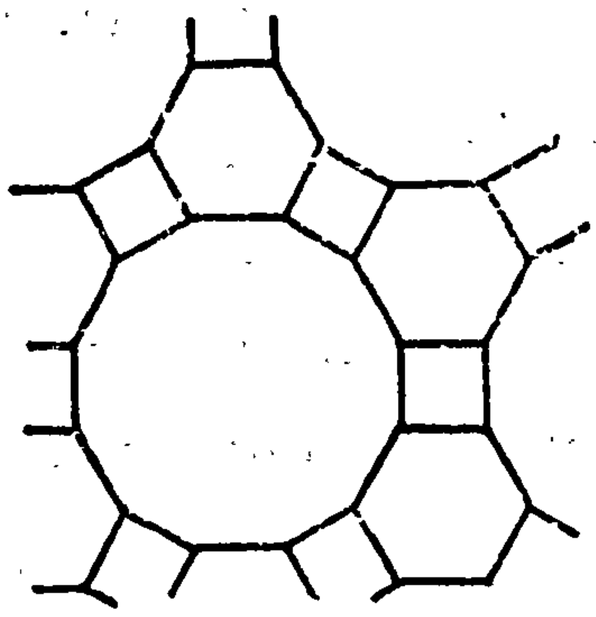

4.6.12.

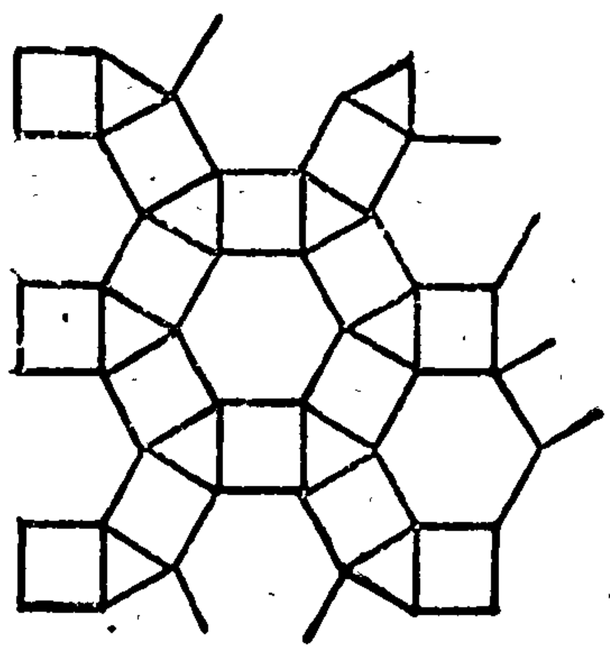

3.4.6.4.

remains almost constant while the unit cell side changes by a ratio $\frac{1+\sqrt{3}}{\sqrt{3}}$ so that $11.7 \times \frac{(1+\sqrt{3})}{\sqrt{3}} = 18.5\text{Å}$.

An interpretation of the 15.4Å - 16.3Å hexagonal unit cells indicated in Fig. 5.5(a) and (b) was attempted using the principles of (a) Regular or semi-regular tessellations plus (b) the 'ring of six' motif, was sought. The intensity distribution on the equator for the 15.4Å unit cell is very different from the 11.7Å unit cell and appears to rule out the possibility of a similar two chain unit cell with both chains on the main diagonal and a 'vacant' site at the corners. In fact no satisfactory two chain system could be devised to give the observed equatorial reflections. It was thought that, as the crystalline specimens were so sensitive to humidity and water content, density measurements might give misleading values. However, the calculated densities for a two, three and four chain model are 0.74, 1.11, and 1.48 gm/c.c. respectively and of the three values the three chain unit cell appears to give the most reasonable value without including any water when compared with similar calculations for the 11.7Å and 18.7Å unit cells. The density of a four chain cell, though not unreasonable, is very high and does not allow for any appreciable inclusion of water. When two water molecules per disaccharide are included in the density calculations a value of 1.6 gm/c.c. results, which is getting unreasonably large compared with other measured values of density for hyaluronates. Furthermore, an examination of the four chain possibilities for such a unit cell did not yield a satisfactory explanation of the equatorial intensity distribution.

The above considerations suggested a three chain unit cell as the most favourable model, though it appeared partly to contradict the conclusions reached about the polarity of chains for other structures. One piece of information that clarifies the situation is that the final equilibrium situation for the chains appears to be the 6.4.3.4. tessellation. Assuming this to be true, the distance between chains is $\ell = \frac{20.8}{(1+\sqrt{3})} = 7.6\text{Å}$. Using the tessellation concept, a search was

made for a semi-regular tessellation that would maintain this distance approximately, and also yield a 'six-chain' motif. Only one such tessellation could be found and this is the tessellation 6.3.6.3. shown in Fig. 5.7.

By placing chains at the vertices of this tessellation and drawing in the unit cell, a three chain cell is obtained, Fig. 5.8. The significance of this three chain unit cell is puzzling unless there is a possibility that Fig. 5.8 represents a statistical structure in which the chains are grouped in triads. If these assumptions are made Fig. 5.8(b) might represent a packing of the chains in which there is a random distribution of antiparallel triads of chains. As pointed out above, the diagram in Fig. 5.6(a),(b) shows paracrystalline defects, with good resolution of the meridional reflections but increasing diffuseness with decreasing d spacing on the equator, plus some layer line streaking. The diagram does not improve with time but rather changes into the 20.8Å unit cell which in turn may be regarded as a packing scheme for antiparallel triads of chains, see Fig. 5.8(c). The humidity behaviour of the two systems would require explanation in terms of these triads drifting apart, so that all distances between vertices in the Fig. 5.8(c) need not be the same i.e. the packing can be regarded in terms of triangles and rectangles as in Fig. 5.8(d).

All of the considerations above must be regarded as speculation since no structure factor or detailed chain packing calculations have yet been carried out. However, the scheme outlined for the experimental transitions observed is the only one found so far that correlates the various aspects and it suggests that the presence of calcium ions in the system may cause an interesting aggregation of three chains. One other aspect of the 20.8Å hexagonal cell is the number and position of the calcium ions present. The presence of six chains implies eighteen carboxyle groups requiring neutralisation. If a one to one ratio of anion charge to carboxyle charge is assumed there must be nine calcium ions present. A $P3_221$ space group for the six chain cell as shown in Fig. ~~5.9(a)~~ 4.8 requires the calcium ions to have special positions, as shown

Fig. 5.8 (a) 6.3.6.3 tessellation
(b) Packing system for triads of chains
(c) Transition of 6.3.6.3 to 6.4.3.4 tessellation
(d) Humidity behaviour of 6.4.3.4 packing

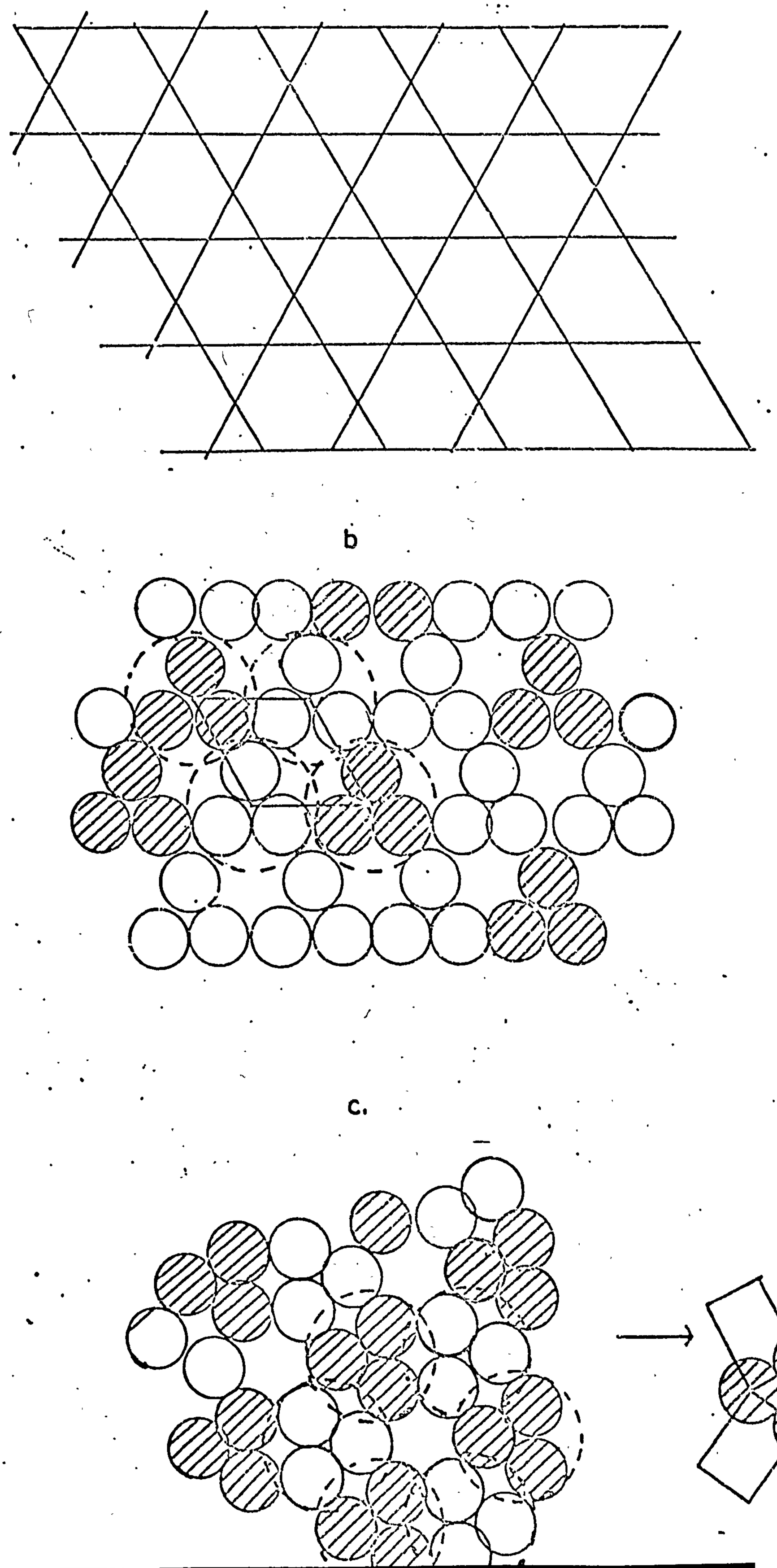

Fig. 5.9 Placing of Calcium ions in $P3_221$ space group.

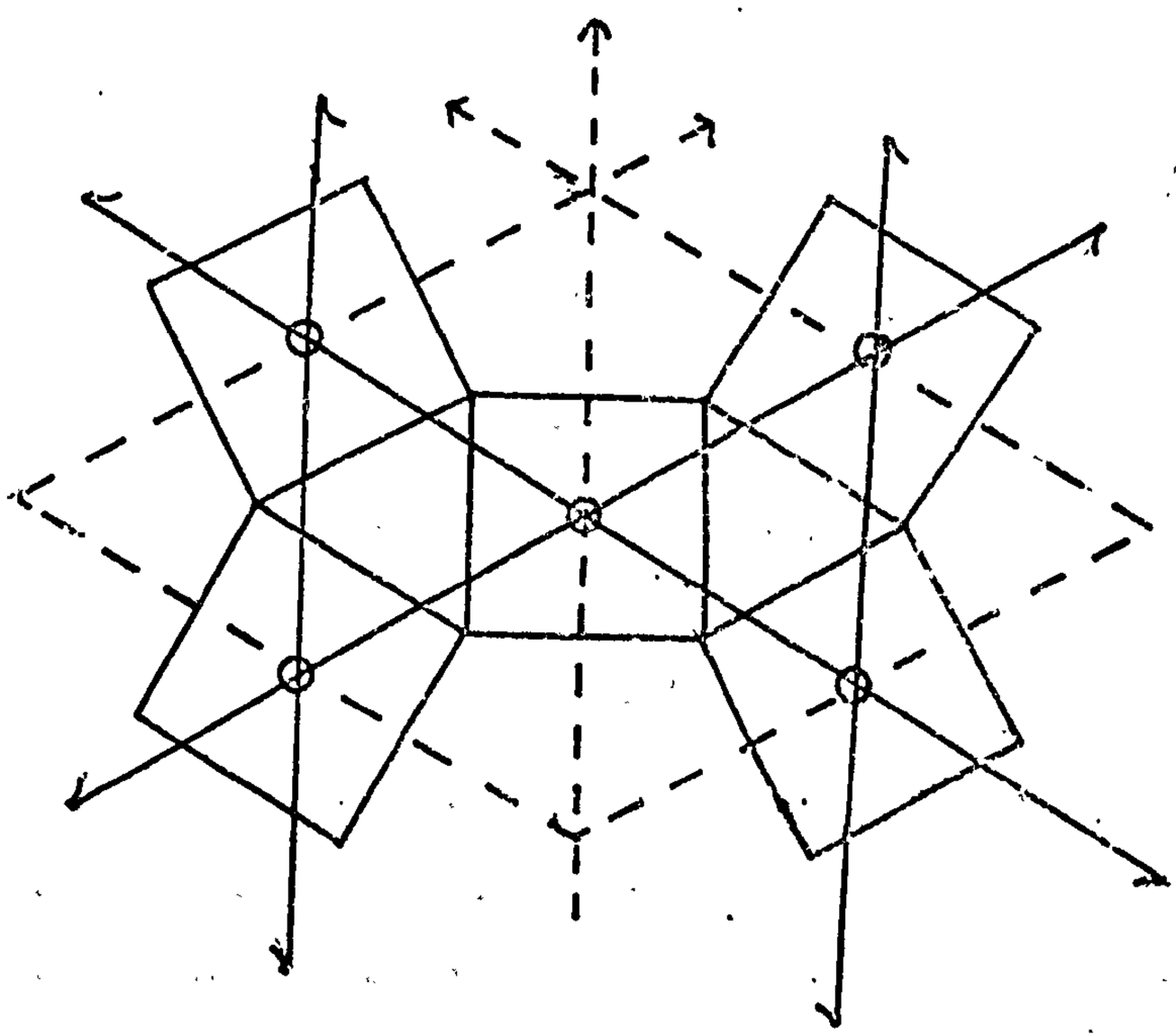

in Fig. 5.9(b) with ~~one~~ the calcium ionspositioned on the two-fold rotation axes.

5.6 Chemical Transformations in the Solid State

The washing of a type I salt form in 0.2N ethanolic hydrochloric acid produces a very definite change in the X-ray diagram, c.f. Chapter III, which could only be explained in terms of a reaction with the counterion involved. Similar experiments were tried with specimens which gave type III X-ray diagrams and in a few cases a distinct change in diffraction pattern was found. Fig. 5.10 shows the diffraction pattern from such an acid-washed specimen.

There has clearly been a conformational change in the molecule giving rise to a completely different packing scheme. The layer line spacing is now 19.6Å ± 0.3Å with meridionals on the 2nd and 6th layer lines. The transformation in some of the diagrams does not look complete and so far it has not been possible to index all the row lines on a single satisfactory unit cell. It is possible that there are two or more phases present which makes the indexing procedure difficult. Table 5.4 gives a list of the row line spacings as measured from Fig. 5.10 and a tentative orthorhombic unit cell which indexes many of the reflections is $a = 25.5Å \pm 0.4Å$, $b = 9Å \pm 0.2Å$, $c = 19.6Å \pm 0.4Å$ (where c is the fibre axis). The feature of the picture is the strong intensity of reflections on the equator compared with the almost complete absence of intensity until higher layer lines are reached. This suggests a strong 'sheet-like' bias to the packing which, in turn, suggests an extended ribbon-like conformation for the chains. This fits in well with the observed layer line repeat, where a two-fold backbone conformation, (c.f. Chapter II) would have an axial repeat somewhere between 9.5Å and 10.2Å. Fig. 5.11 is a diagram of two projections of such a two-fold conformation. It is like a rippled ribbon rather than a flat ribbon structure such as chitin or cellulose. No attempt has been made yet to assign a packing scheme to the chains owing to the uncertainty of the unit cell and the indexing of the equatorial reflections. An aspect

Fig. 5.10 Acid washed type III specimen showing a different backbone conformation

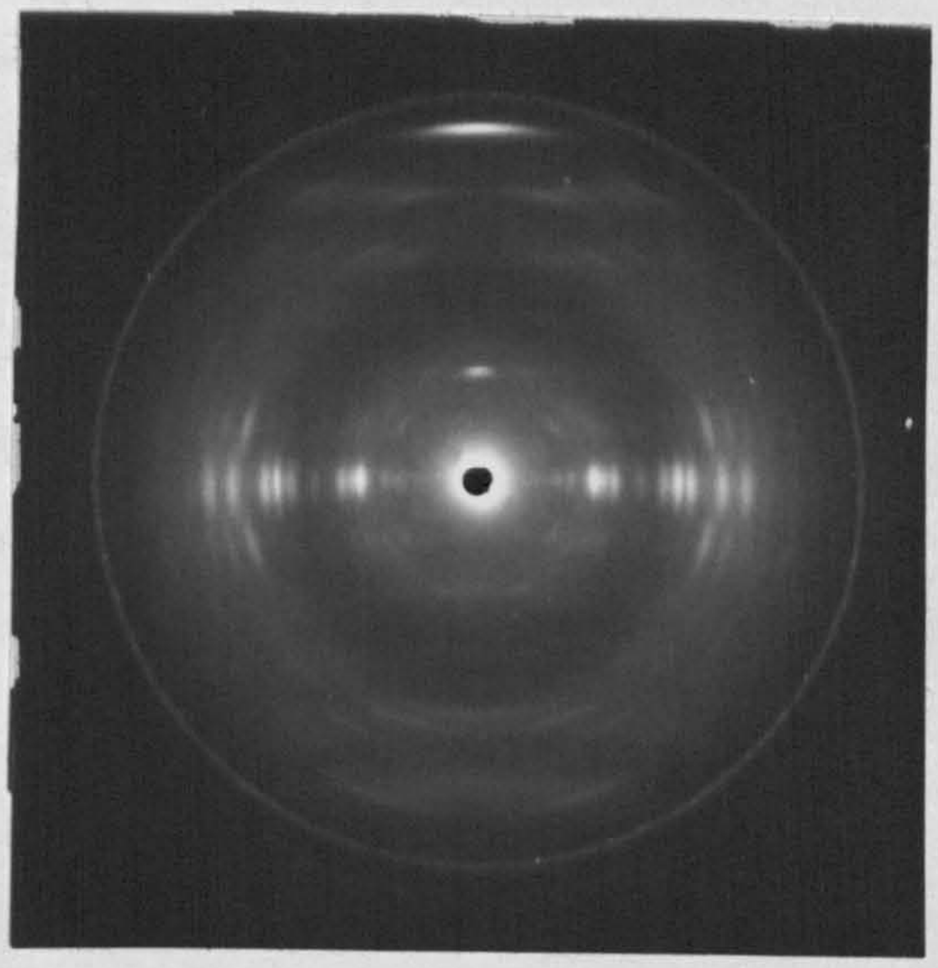

Table 5.4

Spacings from Diagram, Fig. 5.10, of Acid Washed Type III Specimen

Measured Spacings Å Row lines	Intensity	Index Type (Tentative)
13.4 ± 0.3	Weak	100
11.3 ± 0.3	Weak	*
9.05 ± 0.2	Strong	010
8.4 ± 0.2	Medium	*
7.7 ± 0.1	Medium Strong	110
6.5 ± 0.1	Medium Weak	200
5.8 ± 0.1	Medium	*
5.33 ± 0.1	Medium	210
5.05 ± 0.1	Medium	*
4.7 ± 0.1	Weak	*
4.4 ± 0.1	Strong	300, 120
4.0 ± 0.1	Strong	*
3.8 ± 0.1	Weak	220

The tentative lattice indexing some of the reflections above is rectangular with

$a = 13.4 \pm 0.3$Å and $b = 9.05 \pm 0.2$Å.

The layer line spacing is 19.6Å.

Meridionals are on the 2nd and 6th layer lines at

9.8Å ± 0.2 and 3.26 ± 0.1Å.

Fig. 5.11 Two projections of proposed model for 'acid washed' type III. (2 fold helix)

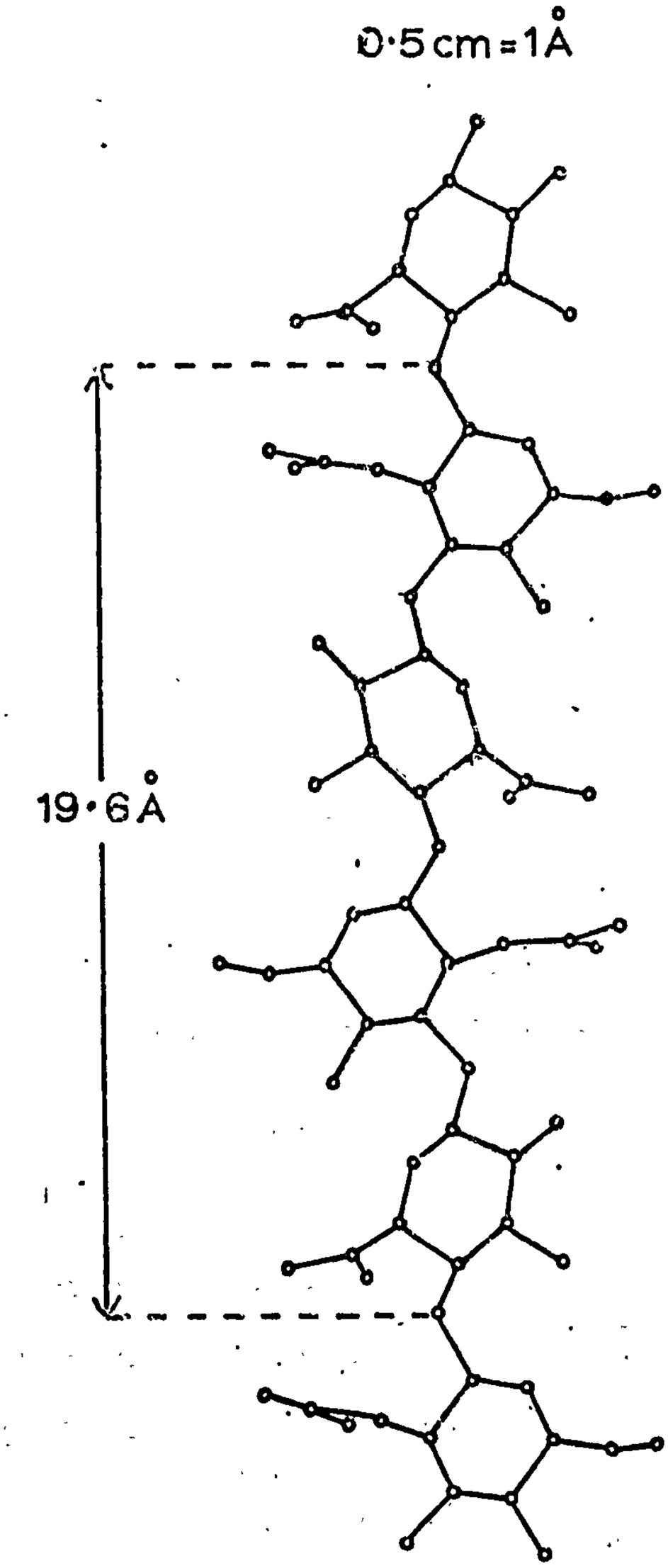

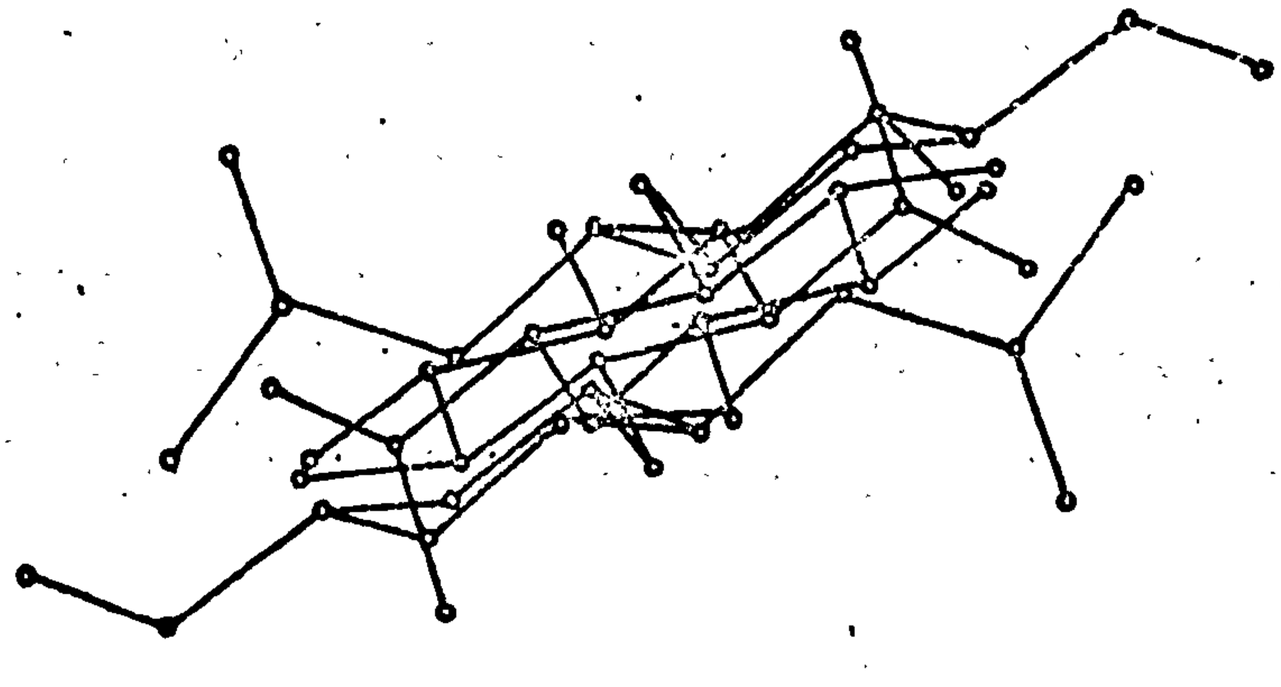

of this conformation is indicated in Fig. 5.12(a) and (b) which shows the possibility of parallel and antiparallel packing schemes that would utilise highly cooperative hydrogen bonding schemes. The parallel stacking of chains of this conformation would offer a particularly stable system with possibie hydrogen bonds between acetamido groups and between carboxyles.

Another aspect of some of the X-ray diagrams showing the above conformation is the presence of weak reflections on layer lines very close to the first layer line. Two possible explanations are offered for these reflections: (a) there is a small amount of another phase present, probably type III, or (b) that there are a very finely spaced set of layer lines possibly indicating a non integral helix i.e. if what appears to be the second layer line were really the eighth a possibility for an 8.3 helix exists which would be a halfway compromise between a full two-fold and three-fold helix. However this is not really supported by the general features of the diagram.

5.7 Experiments Demonstrating the Effect of Ionic Concentration

A brief summary is included here of some preliminary experiments demonstrating the effect of ionic concentration in solutions of hyaluronate. The experiments were of two types

(1) Immersing crystalline specimens of hyaluronate in ethanolic solutions of some salt.

(2) Adding various salt solutions to potassium hyaluronate solutions which under normal conditions would give a type I diagram.

Fig. 5.13(a) and (b) shows the change on washing a potassium specimen of hyaluronate giving 5.13(a) into a solution containing 80% ethanol and 20% calcium chloride solution. The specimen was humidified and X-rayed again c.f. 5.13(b) showing a type III conformation.

To get an idea of the effect of various excess salt concentrations in hyaluronate solutions the following simple experiment was carried out. A 1% solution of potassium hyaluronate from human umbilical cord was divided into six equal parts about 1c.c. in volume. A drop of five

Fig. 5.12 Models for parallel and antiparallel packing of 2 fold helices

Fig. 5.13 Change from type I conformation to type III in the solid state by washing specimen in salt solution of $CaCl_2$

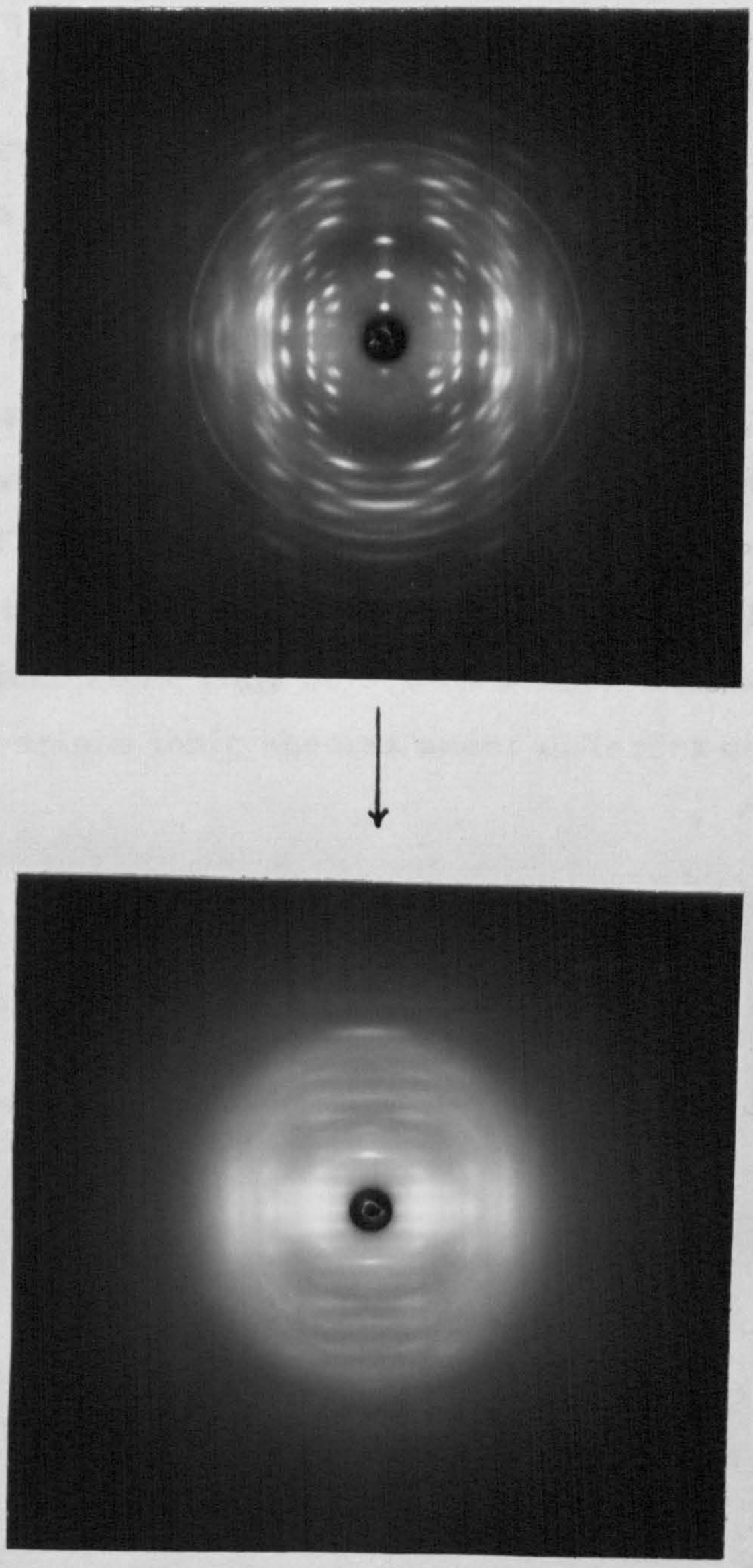

different concentrated salt solutions was put, one into each of the five solutions, leaving the sixth tube as a test solution. The salts used were

$$CsCl, \quad KCl, \quad NaCl, \quad CaCl_2, \quad Ba(OH)_2$$

The solutions were then cast as films in the normal way and it was found that, for the solutions containing excess salt, the salt crystals were the last to dry out from solution and therefore only covered the centre of the films. Specimens from the edge of the films were crystallised in the normal way. Fig. 5.14 shows the X-ray diagrams obtained from the films. There was a considerable conformational change. In the case of the solutions containing excess potassium and sodium the diagrams indicate features of conformations that have not been identified. This experiment is very crude but it shows clearly that the hyaluronate molecule has great versatility even in the solid state, and it will take some time before its transformations and interactions with various ionic species under different conditions are understood.

Fig. 5.14 Effect of excess counterion concentration on solutions of potassium hyaluronate

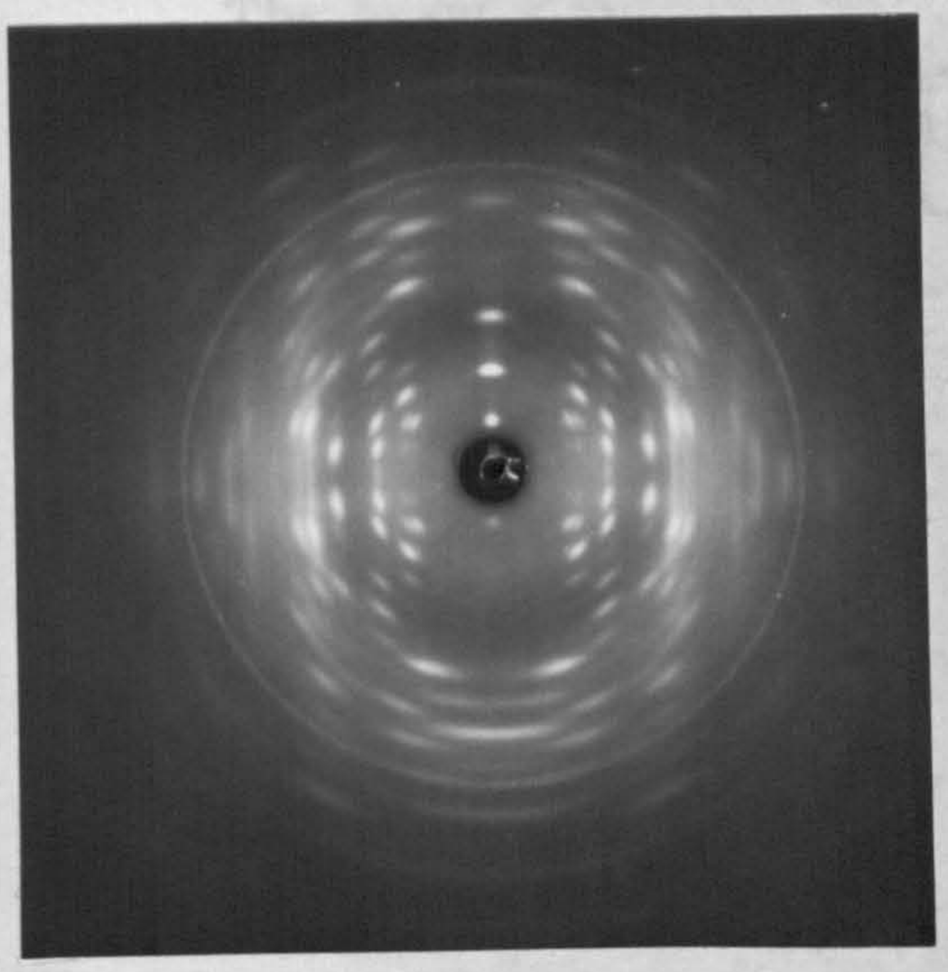

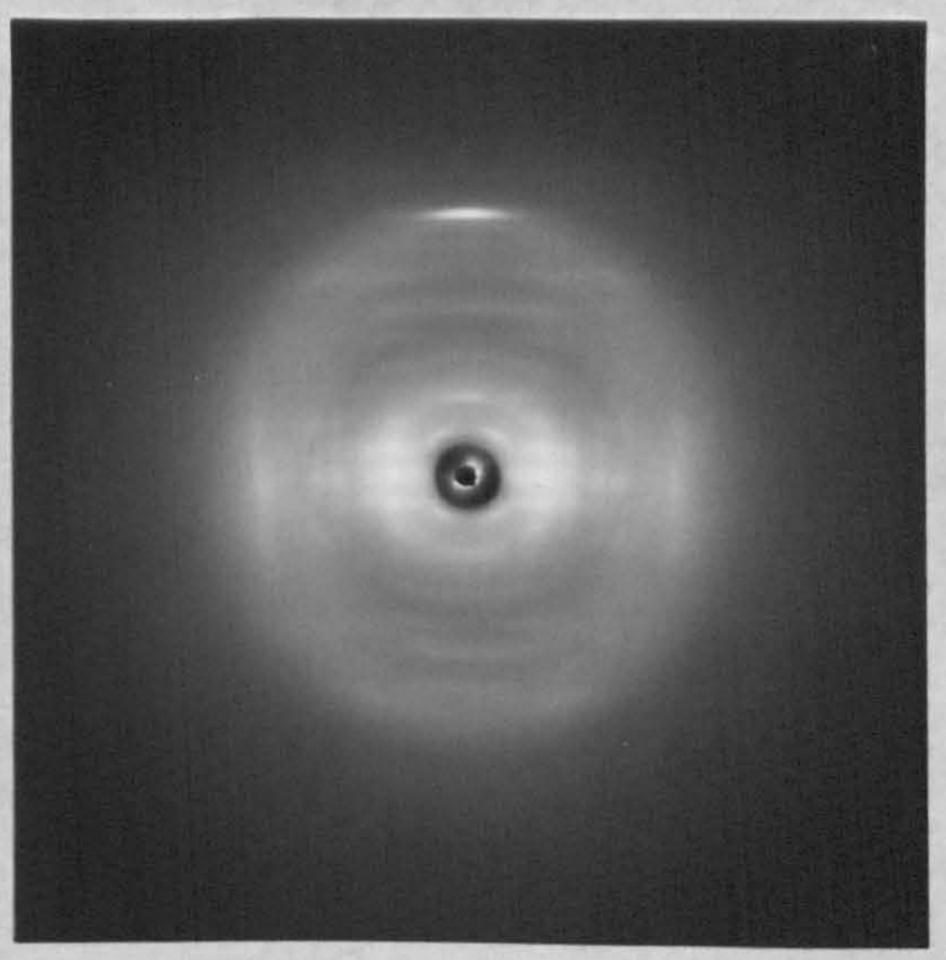

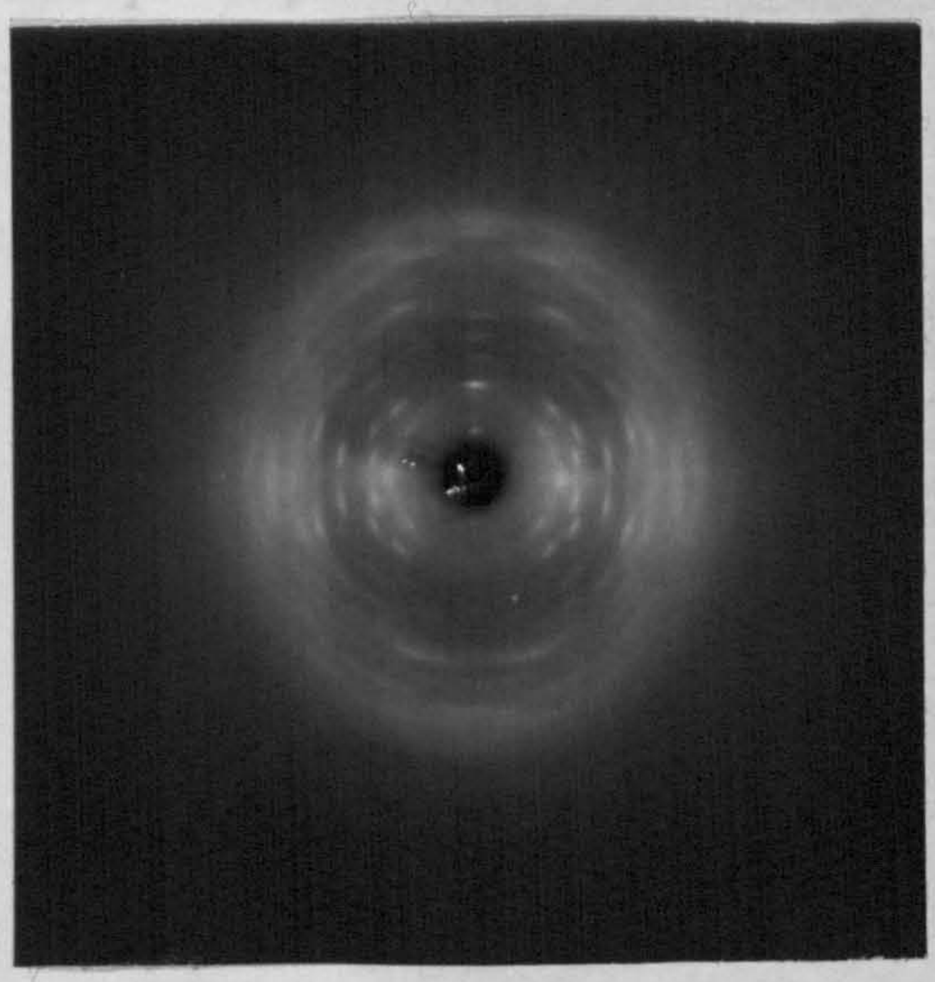

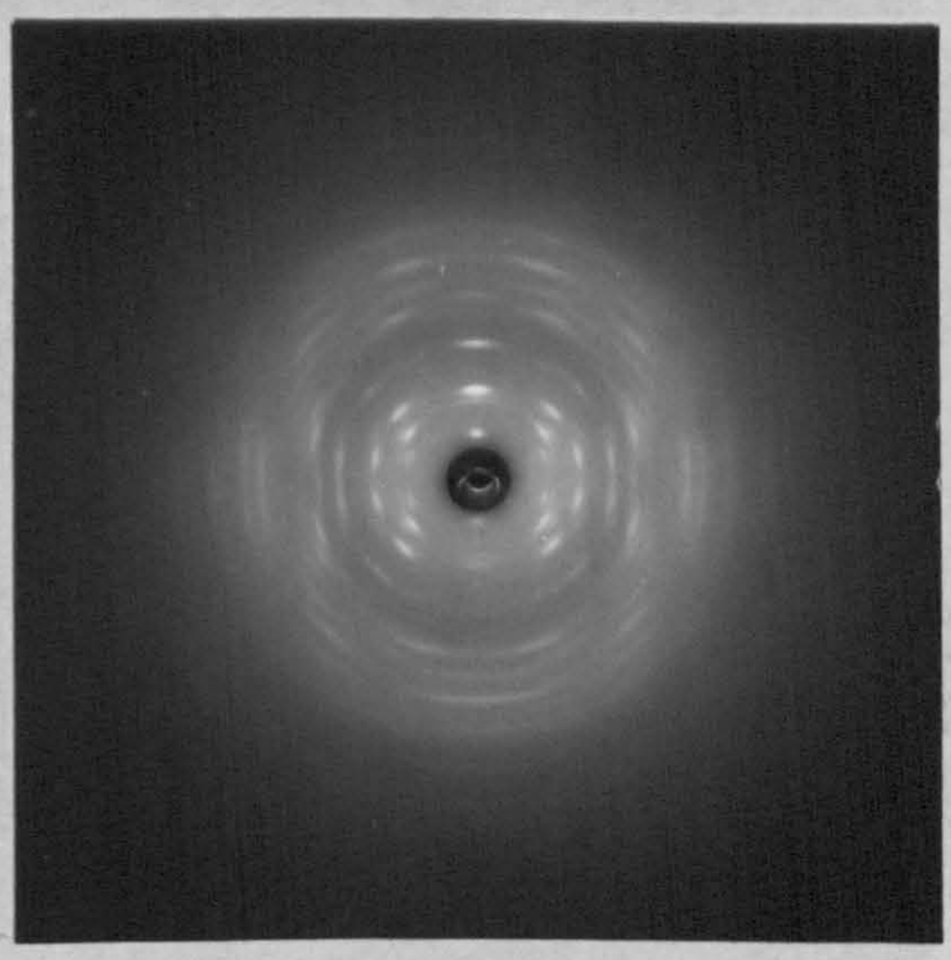

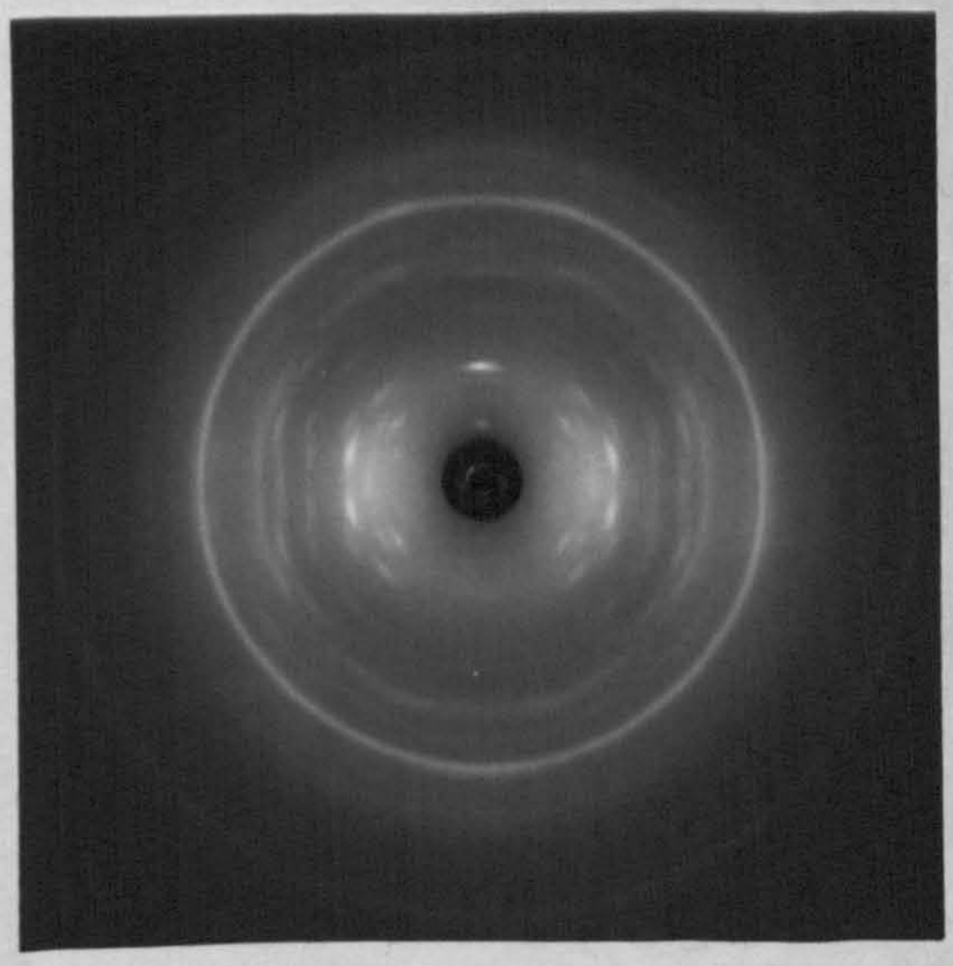

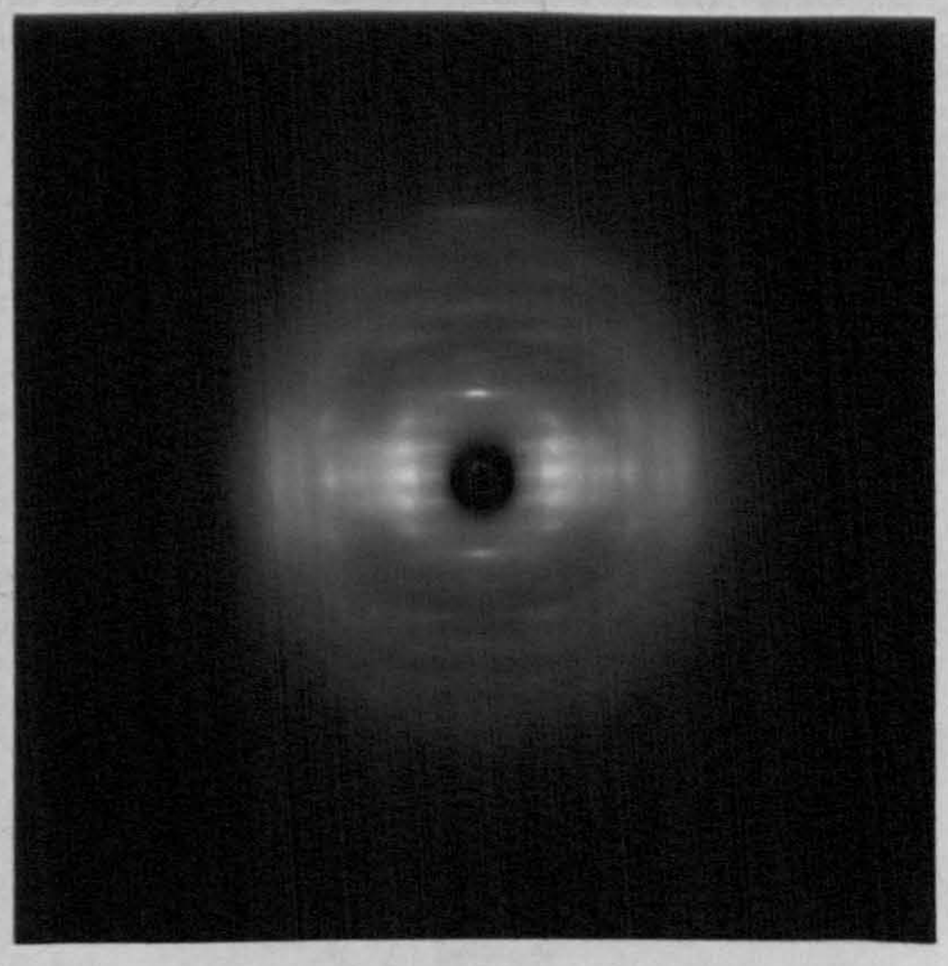

CHAPTER VI

6.1 Introduction

The hyaluronate molecule adopts a number of conformations and packing modes when observed in the solid state but the significance of this information and its relevance to solution studies is far from understood. Hyaluronates occur naturally in a dilute aqueous environment and it seems probable that their role is intimately connected with water and its structure. The importance of water in the crystallisation process has been touched upon but a more detailed review of the water present in the propcsed structures is undertaken in this chapter, and some ideas relating to this problem are discussed. In time, a detailed examination of some of these structures should not only tell more about the polymer-polymer interaction, but also about polymer-water effects and perhaps about water structure around these polymers.

6.2 Additivity of Volumes

To gain a useful estimate of the number of water molecules per asymmetric unit together with the total number in the unit cell a survey was made of the volume of the various components occurring in the polysaccharides, using published crystallographic data. Table 6.1 tabulates the volume of the asymmetric unit of some of the structures and also the number and volume of water molecules present. A number of hydrate structures was also considered in order to estimate volumes of substituent groups such as sulphate and to investigate the change in water molecule volume as a function of the degree of hydration. Table 6.2 lists some of these results.

Two observations may be made on the basis of the above data.

(1) There are two types of bound water.

(2) Addition of volumes for the various constituents of a connective tissue polysaccharide gives a reliable estimate of the volume of a molecule as a whole.

Considering (1) in more detail; the different type of water is a function

Table 6.1

Volume per Residue of some Polysaccharide Molecules and their Relationship with Water

Polymer	Vol/residue A^{o3}	No. of water/residue	Vol./water mol. A^{o3}
Cellulose I, II, III, IV	166 ± 2	0	-
Mannan I	163 ± 2	0	-
Mannan II	189 ± 2	1	26
α, β chitin	232 ± 2		
hydrate chitin	254 ± 2	1	21
Xylan 1e→4e			
Dry	166 ± 2		
Monohydrate	180 ± 2	1	14
Dihydrate	201 ± 2	2	18

Table 6.2

Volume per Molecule of some Salts and their Hydrates

Salt	Vol./molecule A^{o3}	Vol./water molecule A^{o3}
Li_2SO_4	82	
$Li_2SO_4.H_2O$	102	20
$CaSO_4$	76	
$CaSO_4.2H_2O$	124	24
(1) $MgSO_4.H_2O$	87	
(2) $MgSO_4.4H_2O$	159	(2) - (1) = 24
(3) $MgSO_4.6H_2O$	220	(3) - (1) = 26.6
(4) $MgSO_4.7H_2O$	244	(4) - (1) = 26.1

It is interesting to note for the case of $MgSO_4$ that

(2) - (3) gives 30.5 A^{o3} /water molecule added

(4) - (3) gives 24 A^{o3} /water molecule added.

i.e. In the high hydrates the overall volume per water molecule has a maximum of 27 A^{o3}.

of the number of water molecules present per asymmetric unit. When only one or two water molecules are present the volume per water molecule falls typically between 18-25$\mathring{A}^3$. However in heavily hydrated substances the volume per water molecule is more likely to be between 25-30$\mathring{A}^3$.

Applying (2), the volume of a disaccharide of hyaluronic acid is equal to the addition of one glucuronic acid residue and one N-acetyle-glucosamine residue. Using the values obtained from crystallographic data on mannuronic acid Ref. 1 and chitin Ref. 2 a value of 398$\mathring{A}$/disaccharide is obtained. Using this value and assigning the excess volume per disaccharide to water molecules, a listing of the hyaluronate conformations and the proposed number of water molecules present is given in Table 6.3.

6.3 Ice Structure

The large number of water molecules involved in some of the crystal structures raises the possibility that an interconnecting network is formed, and perhaps the polymer conformation stabilises, or is stabilised by, an ice-like structure. If this were so it might give important clues about the molecule's interaction in solution. Ice, has a density less than unity when crystallised at ordinary pressures. In the ice I structure shown in Fig. 6.1(a) each oxygen lies at the centre of a tetrahedron formed by four oxygen atoms 2.76$\mathring{A}$ away, and each molecule takes part in four hydrogen bonds stabilising the structure. The structure created by this tetrahedral environment of oxygens atoms has open shafts running through it as illustrated in Fig. 6.1(b), Ref. 3.

There are nine known polymorphs of ice and Table 6.4 lists these structures and their range of stability. Ice IC has no field of stability being formed only as a metastable phase. Kamb's drawings Ref. 4 of all the ice structures are shown in Fig. 6.2; an interesting feature is that in every case except ice VIII each water molecule has four near neighbours at distances between 2.75$\mathring{A}$ and 2.87$\mathring{A}$ followed by a variable number of more distant neighbours at 3.2$\mathring{A}$ or greater. Any increase in density for water structures is not achieved by an

Table 6.3

Volume per Disaccharide for the Conformations and Packings of Hyaluronates Found so far and the Proposed Number of Associated Water Molecules

Type	Foldedness of Helix	Description or Treatment	Vol/ disacch $\AA^3$	No. of water/ dis	Assumed Vol/water mol. $\AA^3$
I	4	Na. Dryed out (Ref. 16)	410	0	
I	4	Acid Washed	433	1	23
I	4	Na. or K. at 60% R.H.	455	2	22
II	4	K. after anneal at 60°C	444	1 - 2	22
III	3	Na. 11.7 hexagonal	573	6 - 7	25
III	3	Na. 18.7 hexagonal	479	3	23
III	3	Na. orthorhombic	475	3	23
III	3	Ca. 15.4Å hexagonal	650	8 - 10	27
III	3	Ca. 16.3Å "	730	11 - 13	27
III	3	Ca. 20.8Å "	595	6 - 8	26.5
IV*	2	Acid Washed 3 fold	408	0	

*This is a tentative guess based on 3 chains in the proposed unit cell.

N. B. The number of water molecules/disaccharide does not have to be an integral number.

Fig. 6.1 Structure of Ice I

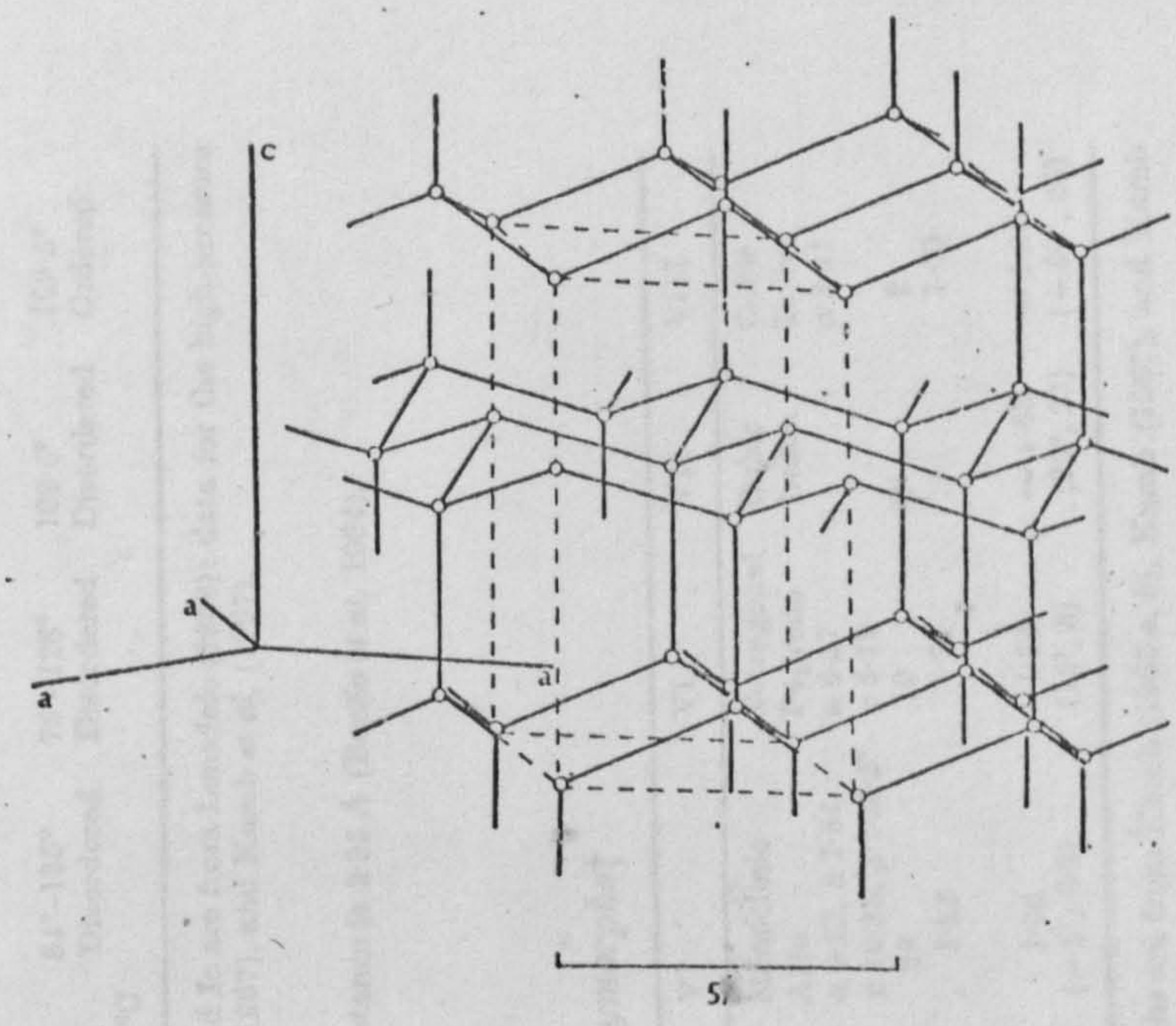

a) . The arrangement of the oxygen atoms in ice I. There are four molecules per unit cell, which is outlined in the figure by dashes. Redrawn from Owston (1958).

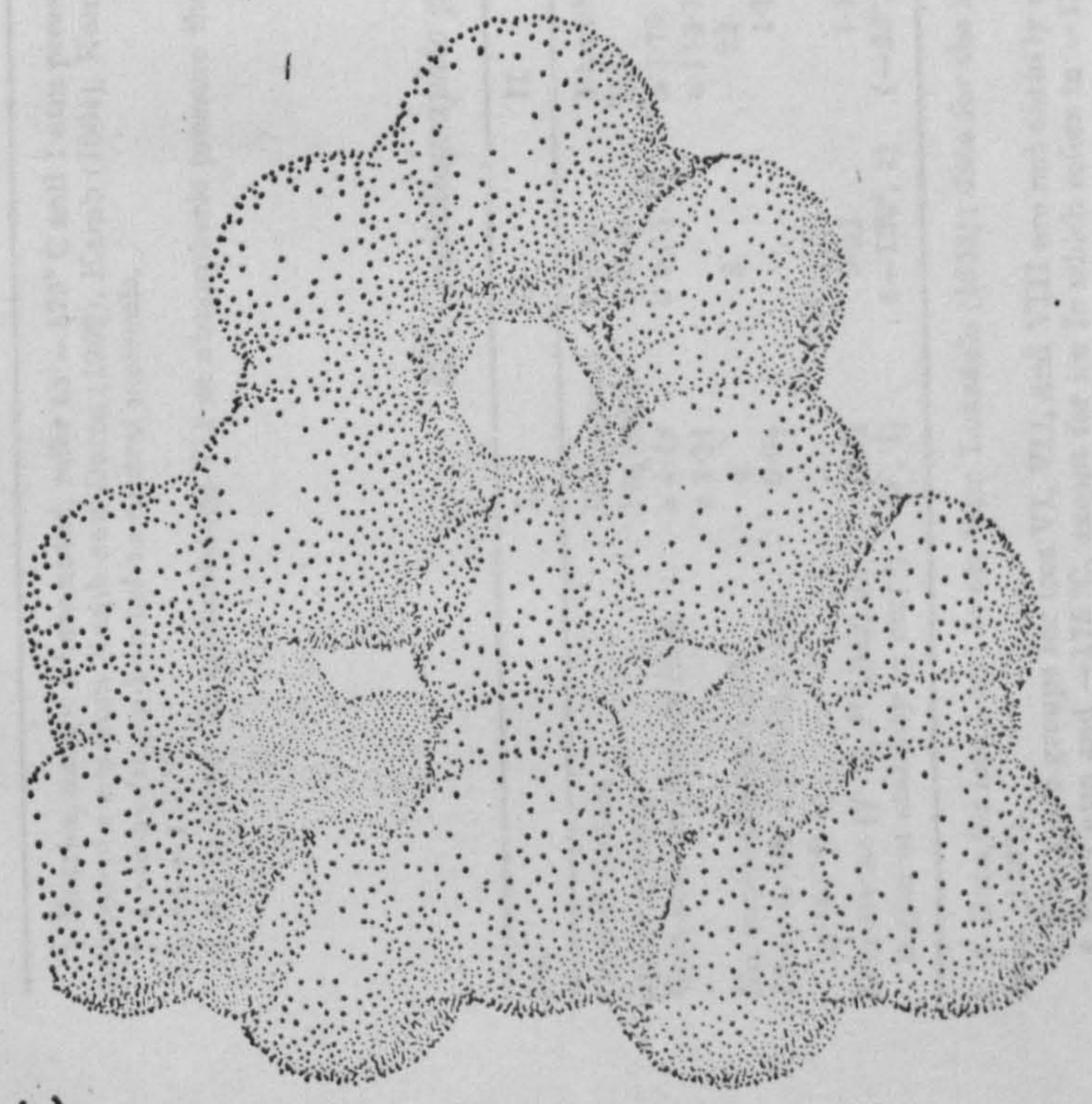

b) . A representation of an ice I crystal showing the van der Waals radii of the atoms. The view is down the c-axis, illustrating the open 'shafts'. Reproduced from Pimentel and McClellan (1960).

Table 6.4

a) *Structural characteristics of ice polymorphs*†

Ice	I	Ic	II	III	V	VI	VII	VIII
Number of nearest neighbours	4	4	4	4	4	4	8‡	8‡
Distances of nearest neighbours (Å)	2·74	2·75§	2·75–2·84	2·76–2·80	2·76–2·87	2·81	2·86‖	2·86‖
Distance of closest non-H-bonded neighbour (Å)	4·49	4·50§	3·24	3·47	3·28, 3·46	3·51	2·86‖	2·86‖
O—O—O angles (deg)	109·5°±0·2°	109·5°	80°–128°	87°–141?	84°–135°	76°–128°	109·5°	109·5°
Hydrogen positions	Disordered	Disordered	Ordered	Disordered above −40 °C	Disordered	Disordered	Disordered	Ordered

† Entries, except where noted, refer to −175° C and 1 atm pressure. Data for ices I and Ic are from Lonsdale (1958); data for the high-pressure polymorphs are from Kamb and Datta (1960), Kamb (1964), Kamb (1965 *a*, *b*), Kamb (1967), and Kamb *et al.* (1967).

‡ 4 are hydrogen-bonded to central molecule.

§ At −130 °C.

‖ At 25 kbar. In quenched ice VII at atmospheric pressure the nearest-neighbour distance is 2·95 Å (Bertie *et al.* 1964).

b) *Crystallographic properties of ice polymorphs*†

Ice	I	Ic	II	III	V	VI	VII	VIII
Crystal system	Hexagonal	Cubic	Rhombohedral	Tetragonal	Monoclinic	Tetragonal	Cubic	Cubic
Space group‡	$P6_3/mmc$	$F\bar{4}3m$	$R\bar{3}$	$P4_12_12$	$A2/a$	$P4_2/nmc$	$Im3m$	$Im3m$
Unit cell dimensions (Å)§	a 4·48 c 7·31	a 6·35	a 7·78 α 113·1°	a 6·73 c 6·83	a 9·22, b 7·54 c 10·35, β 109·2°	a 6·27 c 5·79		a 3·41
No. molecules/unit cell	4	8	12	12	28	10	2	2
Density at −175 °C, 1 atm (g cm^{-3})	0·94	..	1·17	1·14	1·23	1·31	..	1·50
Density at (T °C, P kbar) in region of stability (g cm^{-3})	0·92 (0°, 1)	0·93 (−130°, 1)	1·18 (−35°, 2·1)	1·15 (−22°, 2·0)	1·26 (−5°, 5·3)	1·34 (15°, 8)	~ 1·65 (25°, 25)	~ 1·66 (−50°, 25)

† Data for ices I and Ic are from Lonsdale (1958); data for the high-pressure polymorphs are from Kamb (1965 *a*, *b*), Kamb (1967), and Kamb *et al.* (1967).

‡ The space groups for ices VI, VII, and VIII are not entirely certain.

§ For 1 atm and −175 °C, except for ice Ic which refers to −130° C.

Fig. 6.2 Polymorphs of Ice

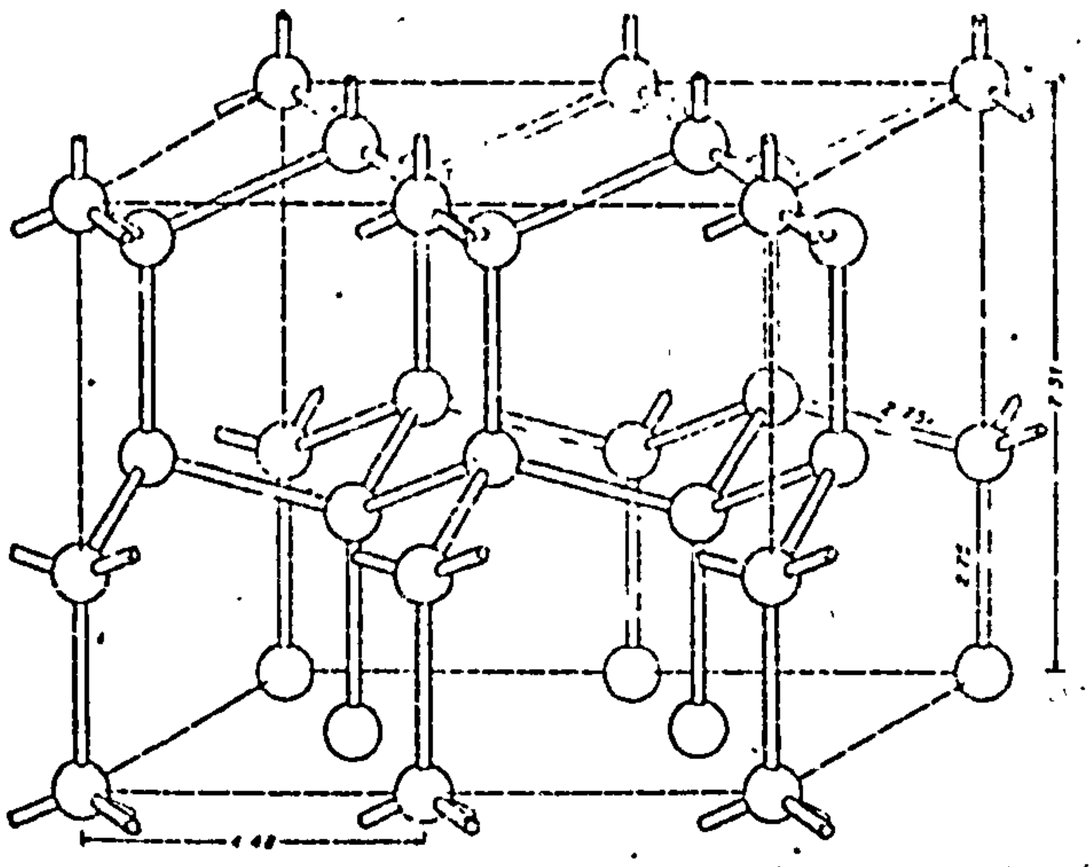

a) Ice I

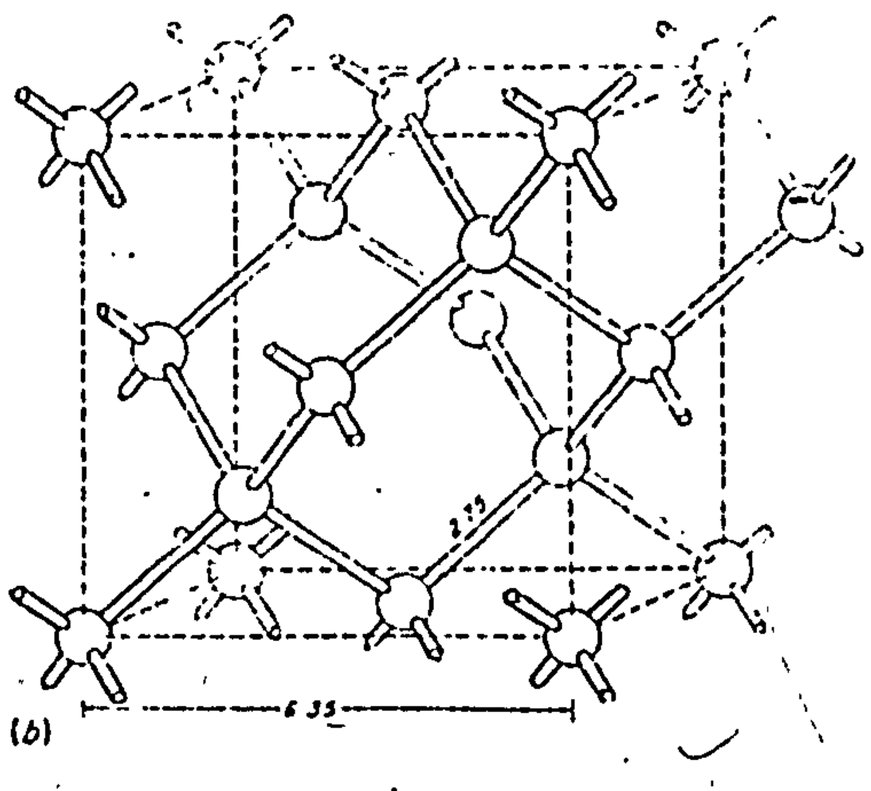

(b)

b) Ice Ic

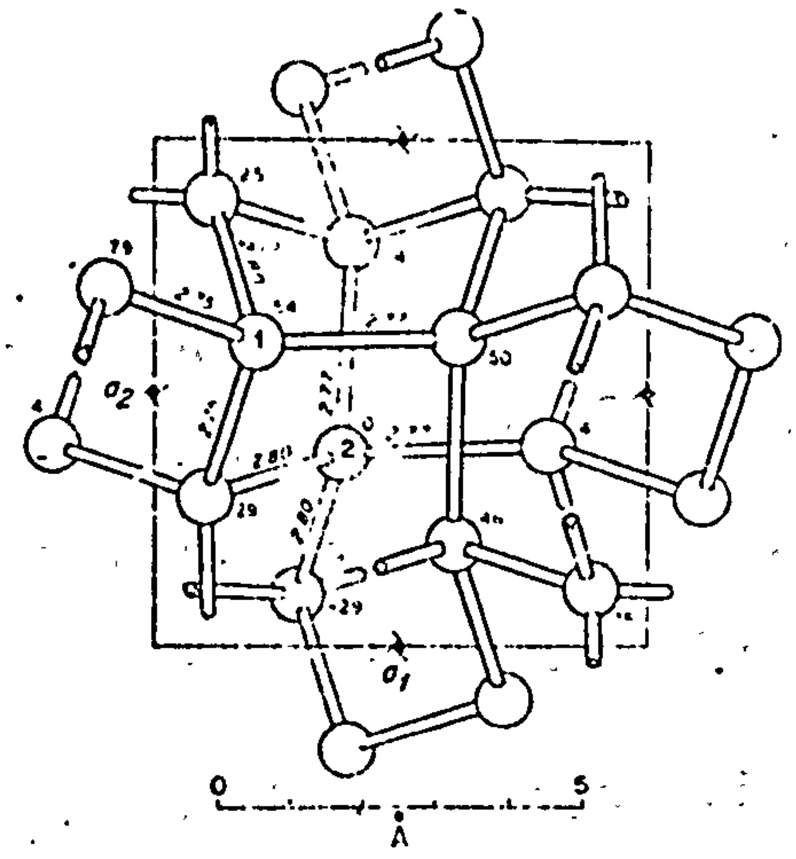

c) Ice III (along c axis)

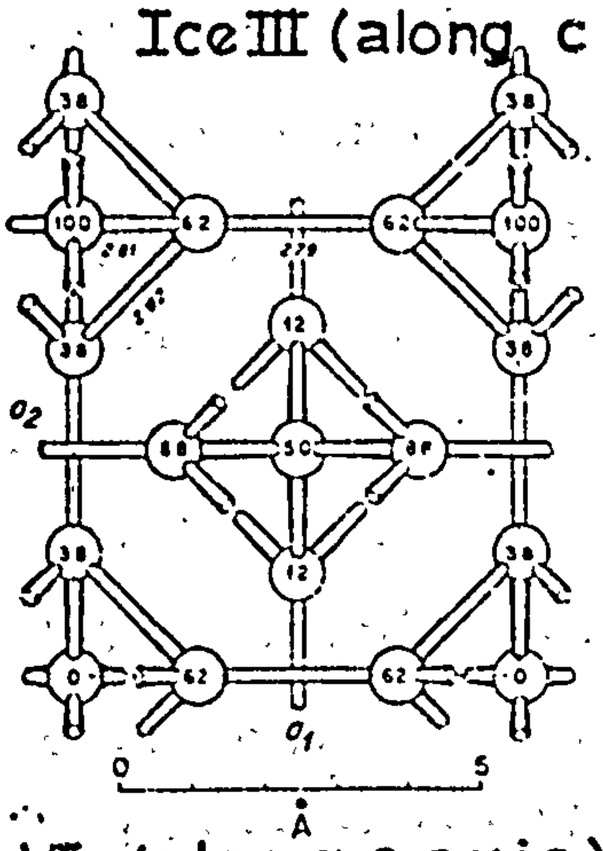

d) Ice V

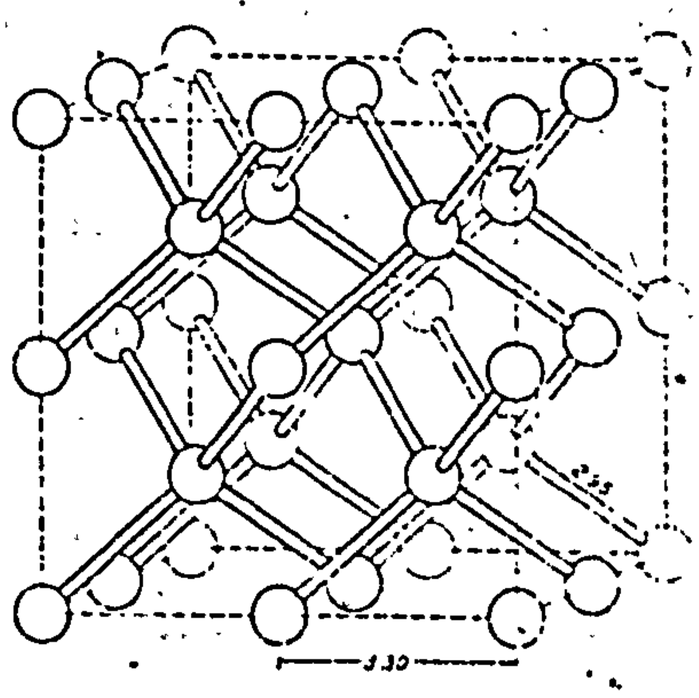

e) Ice VI (along c axis)

f) Ice VII

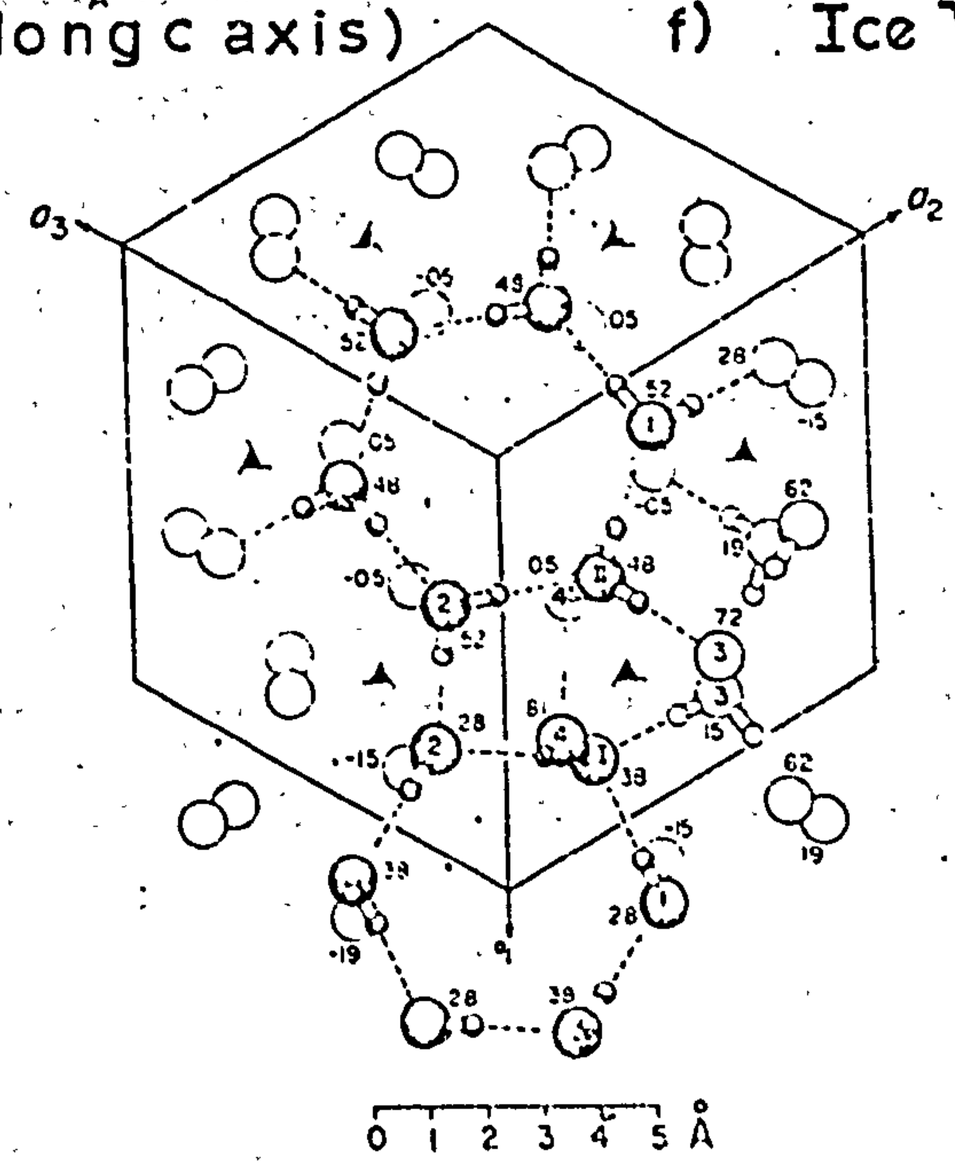

g) Ice III (along c axis)

increase in the number of near neighbours but rather through an increase in 'next near' neighbours.

Water occurring in crystalline structures of other materials has been extensively studied. It occurs as (a) single units, or in groups, in a number of crystalline hydrates e.g. pairs, in Rochelle salt, squares in NaOH $4H_2O$, hexagonal rings in dioptase, Refs. 5,6,7.

(b) Chain hydrates e.g. 1,3 dimethylxanthine, β 1-4 xylan Ref. 8,9.

(c) Layer hydrates as in some clays e.g. montmorillonite, and vermiculite Ref. 10,11. It has been estimated that effects of hydrated surfaces on these clays extend up to 30Å from the surface. Although evidence of water structure has been collected in the kinds of materials listed above, very little structure consideration has been given to water around biological molecules, thought there has been much interesting speculation.

6.4 Water Structure Around Biological Molecules

The introduction of order by solute molecules on the surrounding water has been discussed in terms of two concepts; the so-called hydrophobic and hydrophilic interactions. A hydrophobic interaction takes place where there is an unfavourable interaction between water and solute such that considerable entropic changes occur. The water near the surface of the solute favours a water-water interaction rather than a water-solute interaction, thereby forming an ordered water layer which lowers the entropy. To combat this decrease of entropy thermodynamic forces act to bring hydrophobic surfaces of the solute together thereby reducing unfavourable surface and giving rise to the term hydrophobic bonding Ref. 12. The other extreme case for water-solute interaction is hydrophilic bonding. A hydrophilic surface is one which forms or accepts hydrogen bonds to water. If a molecular surface forms arrays of hydrogen bonding sites to fit a regular water lattice, ice-like structures become stabilised in the liquid near that surface. Clearly, such a process could become a thermodynamic driving force for molecular interactions in biophysics, the conformations molecules

adopt and the way they 'see' each other being dependent on the structure of water. For the stabilisation of an ice I structure in the liquid the distances between two atoms that can form hydrogen bonds in a plane should correspond to the second nearest neighbour in ice I i.e. approximately 4.5Å. However, depending on the models for a water structure that one chooses, it is possible to envisage second nearest neighbour distances of up to 4.74Å.

Table 6.5(a) is taken from Berendsen Ref. 13 and shows an interesting correlation between a number of biological structures (mainly fibrous) and the second nearest neighbour distance in ice I. To this list may be added the conformations of hyaluronic acid found to date, Table 6.5(b). It should be emphasised, however, that the discussion so far is speculative. Examples of molecules or molecular structures that fit into hydrophilic hydrogen bonding schemes have been investigated by Warner and others Ref. 14, 15 and Fig. 6.3 shows some of these structures.

6.6 Hyaluronic Acid and Water Structure

Figure 2.6 shows photographs of ball and stick models, and space filling models of hyaluronic acid. The model may be regarded as having both hydrophobic and hydrophilic possibilities which can be varied by rotation about the tortional angles. This interaction between water and molecule holds the key to the understanding of mucopolysaccharide behaviour.

Consideration of Table 6.3 shows that the proposed three-fold conformation includes a considerable amount of water in the packing schemes adopted. Sodium hyaluronate has been found in three different packing modes in the three-fold conformation. Each of these modes exhibits the six-chain motif and this suggests that the environment within these six chains is the same for each packing scheme. Fig. 6.5 shows the three packing schemes for sodium hyaluronate and the proposed number of water molecules, based on volume calculations. It is seen that the data can be reconciled using the assumption that there are

Table 6.5

(a) Fit of Natural Water Molecules to Water Lattices around some Biological Molecules

Molecule (ref.)	Repeat in direction of best fit, A	Number of water repeats	Deviation from fit (%), based on 4.74 A	Deviation from fit (%), based on 4.52 A
Collagen (*214*)	28.6 axial	6	1	5
DNA (*215*)	34 axial	7	2	7
Feather keratin (*216*)	23.6 axial (quasi-repeat[a])	5	0	4
also observed by X-ray diffraction	18.9 axial	4	0	4
TMV (*217*)	23 axial (quasi-repeat[a])	5	−3	2
Cross-β-protein (*218*)	4.65 axial	1	−2	3
β-Protein parallel-chain pleated sheet (*219*)	4.73 perpendicular to fiber	1	0	5
β-Protein antiparallel-chain pleated sheet (*219*)	9.46 perpendicular to fiber	2	0	5
Chitin (*220*)	4.69	1	−1	4
Apatite (*221*)	9.43	2	0	5
Gramicidin S, etamycin, actinomycin, cirealin, staphylomycin (*227*, *228*)	4.8 (model)	1	~1 (fit in hexagonal pattern)	~6
Repeat in myelin (*222*)	4.7		~1	~4

[a] Not precisely in the axial direction.

(b) Fit of Water Molecules to Water Lattices around Hyaluronates

Molecule Type	Repeat in direction of best fit	No. of water repeats	Deviation of best fit % based on 4.74Å	Deviation of best fit % based on 4.52Å
Hyaluronate I	33.4	7	1	6
" II	37.2	8	2	3
" III	28.5	6	0	5
" IV*	19.6	4	3	8

* Acidified Type III.

Fig6.3 Some molecules fitting a water structure

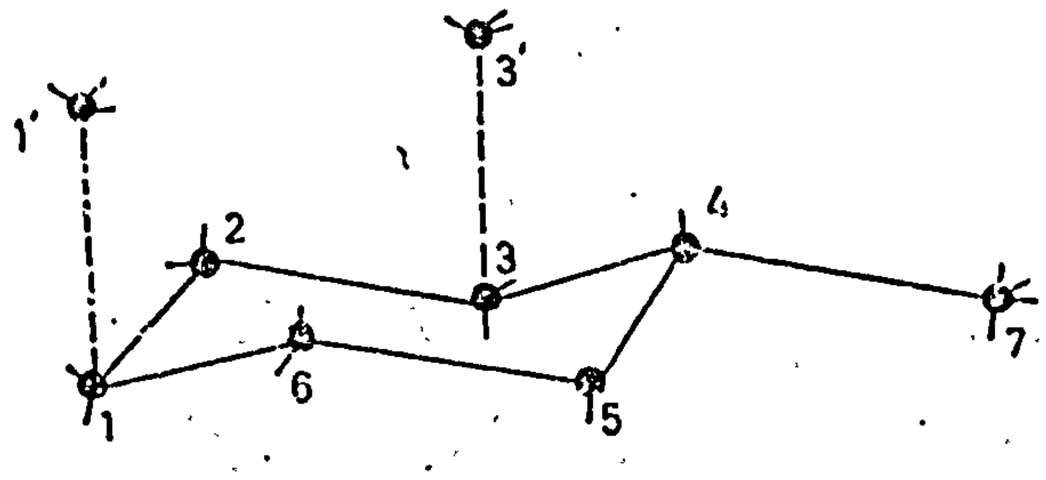

Model-Ice

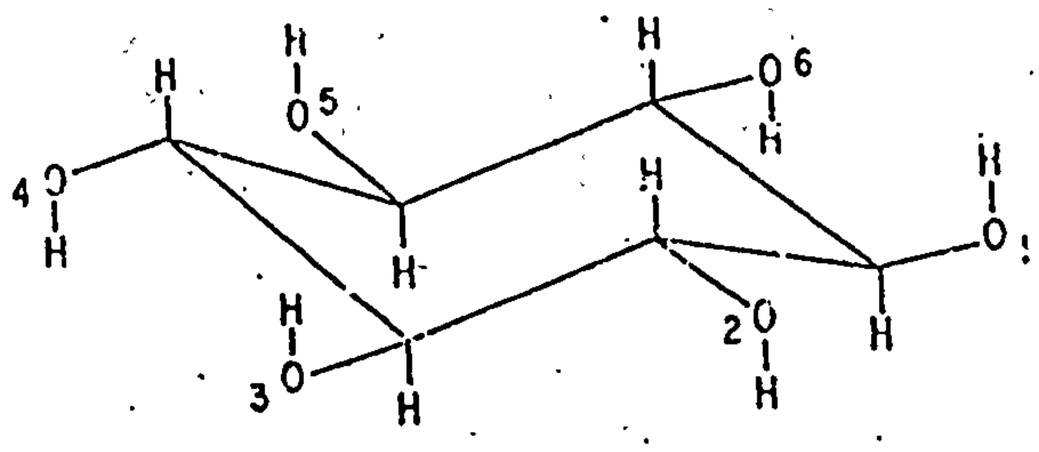

Scyllo-inositol

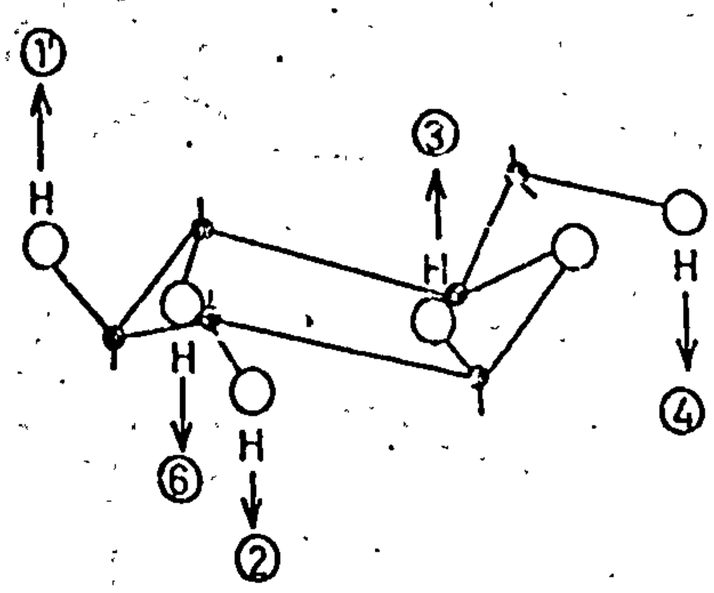

β-D-Glucose

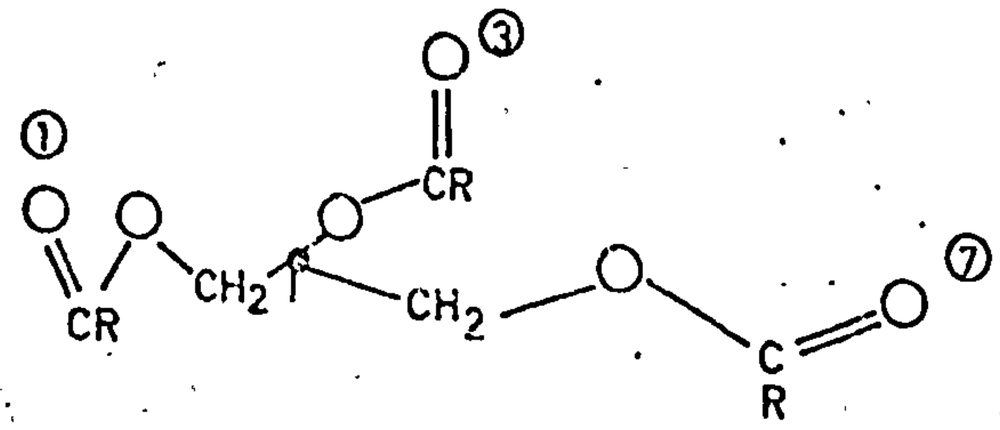

Triglyceride

Fig.6·5 Packing schemes for Sodium Hyaluronate with proposed number of water molecules.

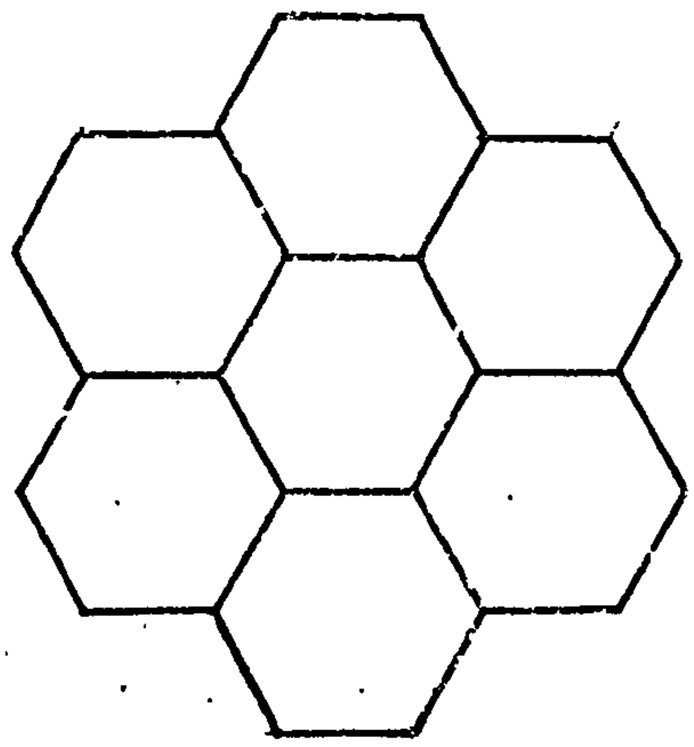

Environment	Proposed No. of waters
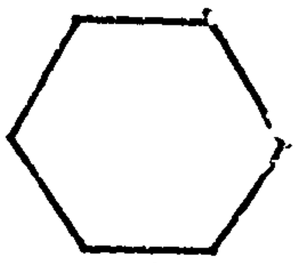	36
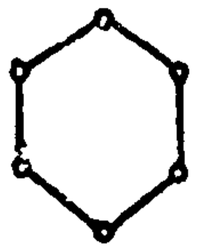	x 6 = 36

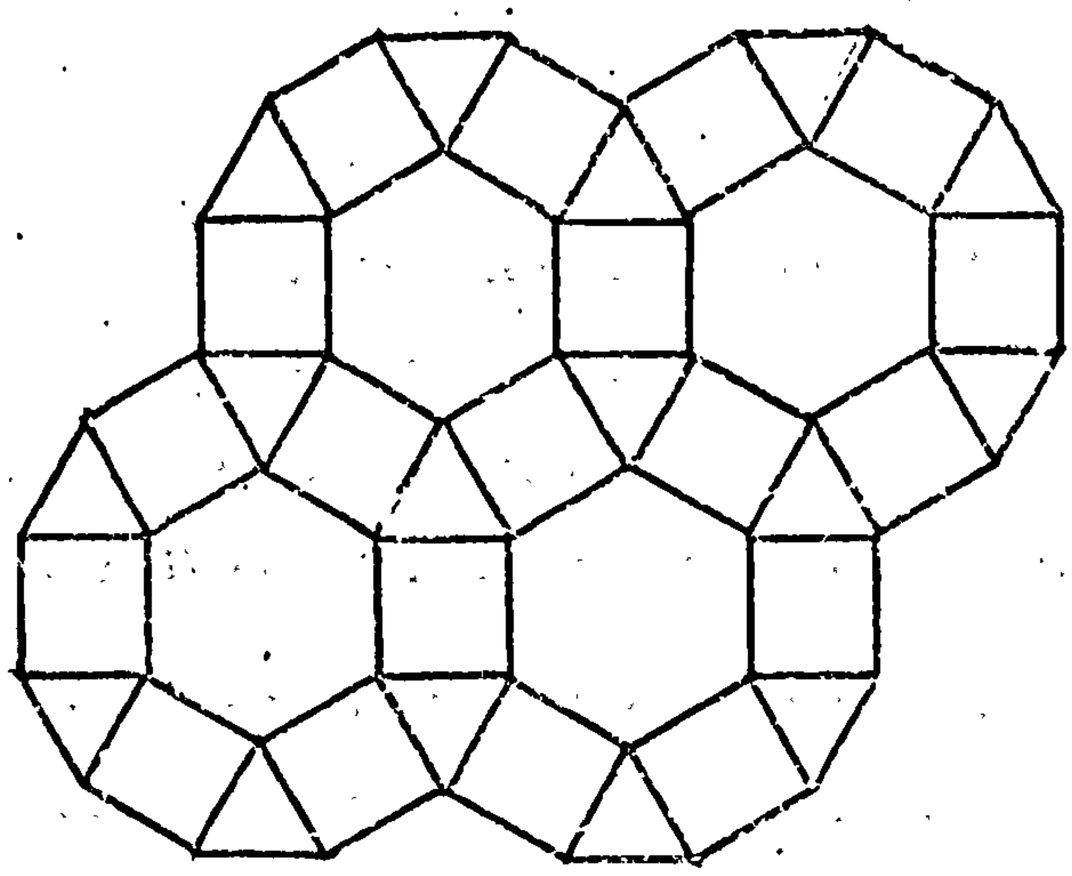

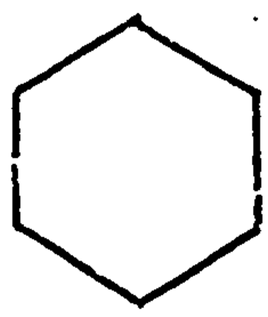	36
	12
	3

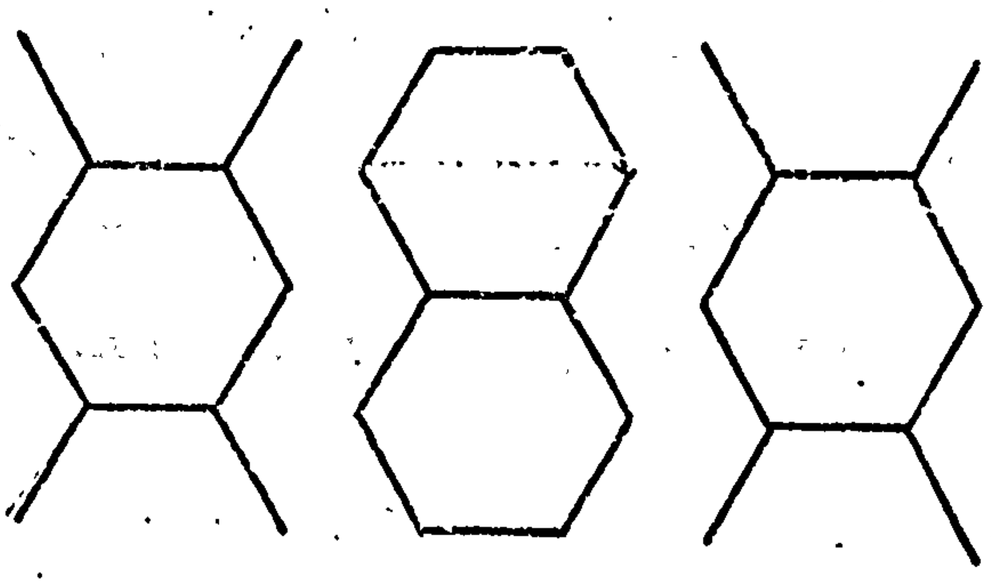

	x2 = 72

thirty six water molecules filling a 'vacant' site.

The packing of the water molecules within the 'vacant' site is a difficult problem and one which will require substantial computation. However there are a number of useful clues at hand which should simplify the task. The assumption of a three-fold screw symmetry around the 'vacant' site and the diameter of this site suggest that a puckered ring of six water molecules c.f. Fig. 6.1 might form the basis of the 'missing' lattice site. Hopefully, the problem will yield to a full packing analysis of all three structures plus a detailed structure factor calculation on the 18.7Å cell.

Fig. 6.6 shows the proposed packing schemes for the calcium hyaluronate specimens and the likely number of water molecules present in the unit cell. As indicated in Chapter V, the humidity dependence of the size of the unit cell parameters and the poor packing suggest that at least some of the chain-chain interaction has broken down, and that chains are linked via a water structure. Fig. 6.7 shows the kind of extension to the simple water structure that can be envisaged in going from six water molecules per asymmetric unit up to ten to thirteen water molecules per asymmetric unit. Why the presence of calcium should have the effect of increasing the water content is not clear but it might well be of some biological significance.

The proposed four-fold conformations of type I and II have fewer associated water molecules. The maximum number of water molecules per disaccharide for type I conformation according to the latest data is three and Arnott Ref. 16 has reported that, on drying down a type I specimen, a unit cell containing none or, at the most, one water molecule per disaccharide has been obtained. The possibility that the type I conformation is a double helix, as discussed in Chapter III, could have a considerable effect on the polymer network formed in solution, and so it will be considered separately.

Fig. 6.6 Calcium Hyaluronate packing schemes with proposed number of water molecules -

6.3.6.3 tesseliation

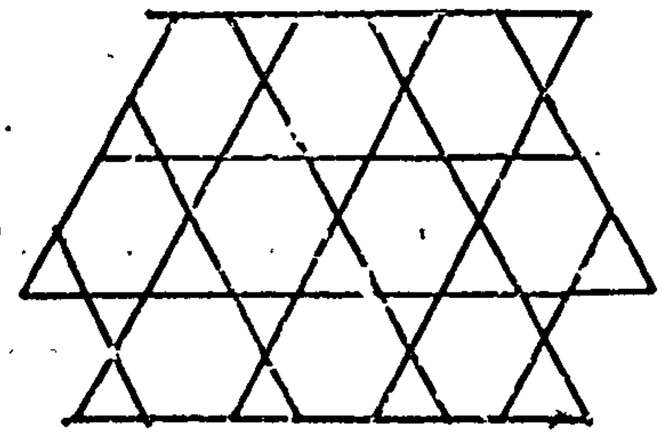

Environment	No. of water mols.	Possible water structure
(a) 15.4 Å Net 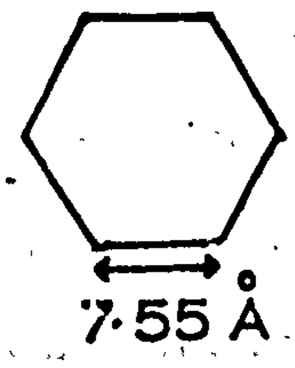 7.55 Å	76	6 x 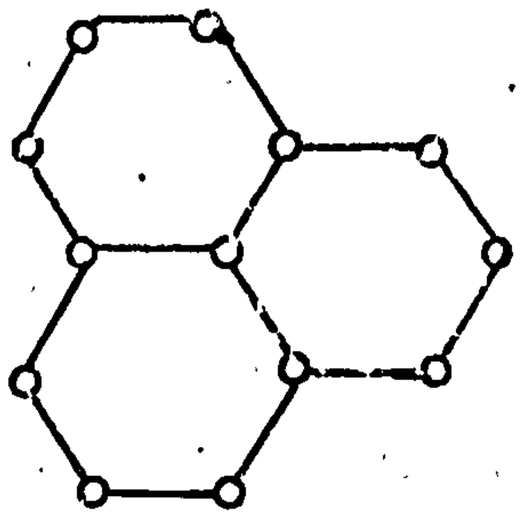
b) 16.2 Å Net 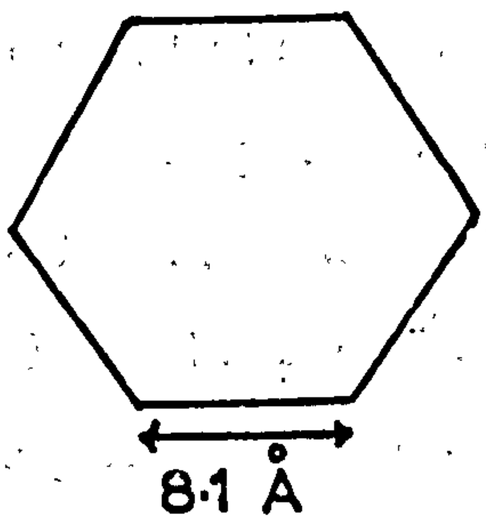 8.1 Å	108	6 x 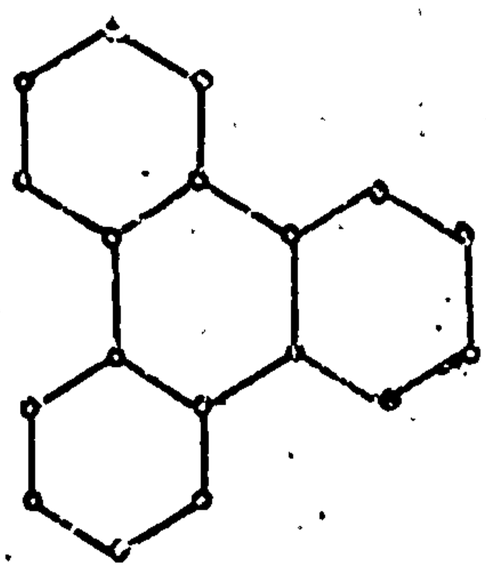

6.4.3.4 tessellation

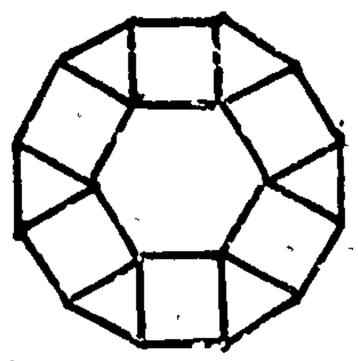

Environment	No. of water mols.
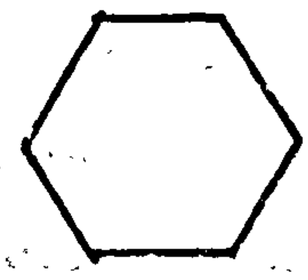	78
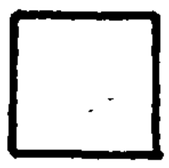	36
	3

6.7 Possible Significance of a Double Helix in Hyaluronates

Double helix formation can be regarded as a one dimensional crystallisation process and thus constitutes a reduction in entropy for the polymer system. However, the entropic effect is not limited to the process of turning a 'string-like' molecule into a rigid rod over a certain region, but also includes the possible formation of a network of chains by crosslinking.

Rees Ref. 17 has discussed this aspect of double helix formation of the related carrageenan polysaccharides and has proposed it as a mechanism of gell formation in some biological systems. Structural studies on two of the carrageenate forms, iota and kappa, showed them to form three-fold parallel, double helices with the charged sulphate groups on the outside, so as to make a fairly rigid polyelectrolyte Ref. 18. Rees proposed that the double helix segments of the molecules acted as crosslinks for a gell network c.f. Fig. 6.7 and that the melting behaviour of the gell could be explained by the thermal disruption of the double helix. On the basis of the carrageenan results Rees further proposed Ref. 17 that the same mechanism might be applicable to some animal polyurinides. On obtaining X-ray diagrams similar to those shown in Fig. 3.1 Dea et al. Ref. 18 proposed the double helical model similar to that shown in Fig. 3.7. The double helix gell formation was put forward as a mechanism to explain the rheological results of Balazs et al. as outlined in Chapter I; Ref. 20.

Though the explanations put forward appear plausible and offer a mechanism which is biologically interesting, the difference between the two systems, i.e. carrageenate and hyaluronate, indicate that perhaps it is only part of the story. The carrageenates have molecular weights typically of the order of 0.5×10^6 whereas the hyaluronate molecules often go up to $(10\text{-}20) \times 10^6$. There is also a considerable difference between the form of the double helices involved. As pointed out above, the carrageenan molecules form a parallel system with the charged groups on the outside, whilst the proposed hyaluronate double

Fig. 6.7 Gel Mechanism for parallel chains

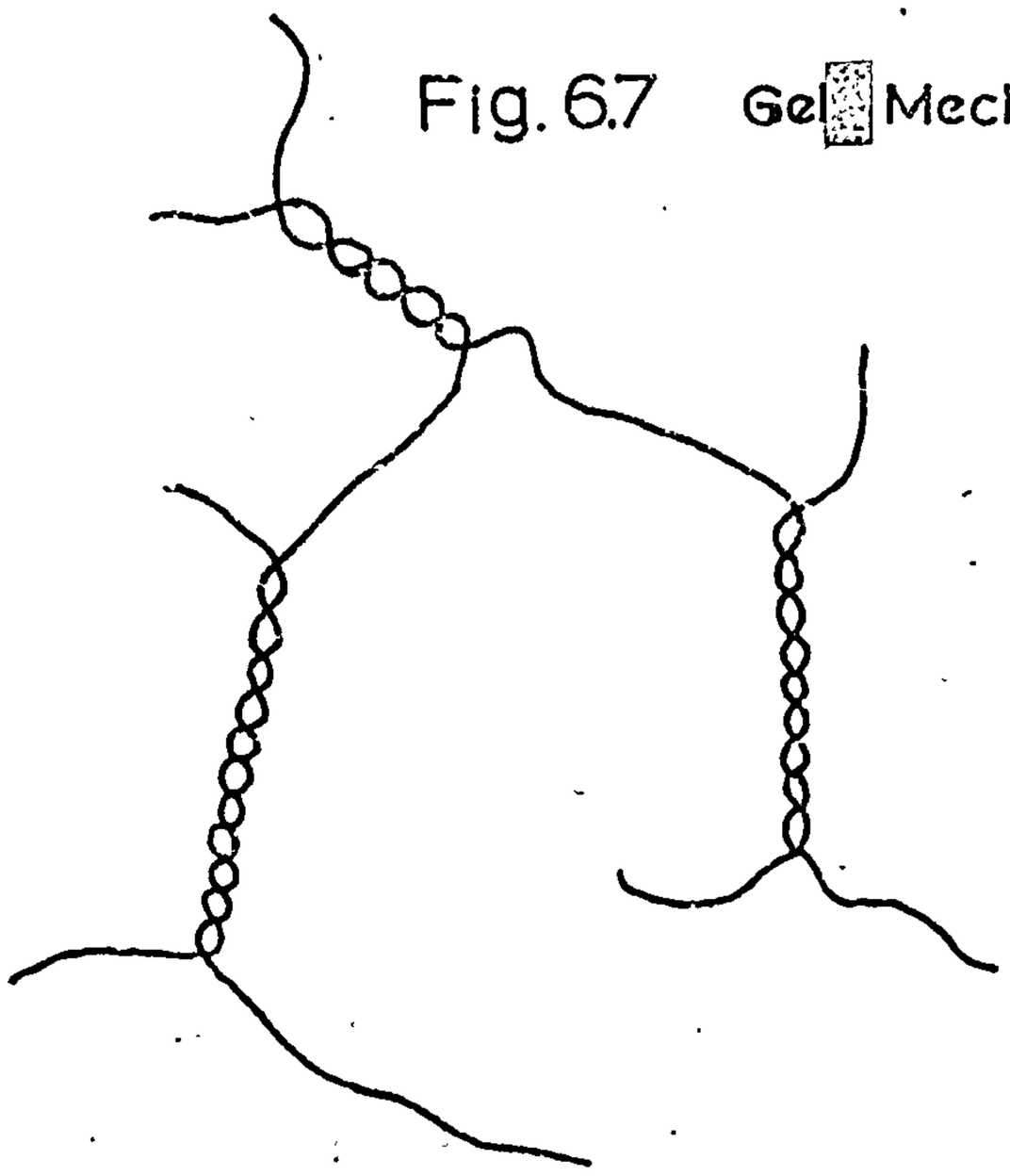

Fig. 6.8

a. Antiparallel Double Helix Chain folding

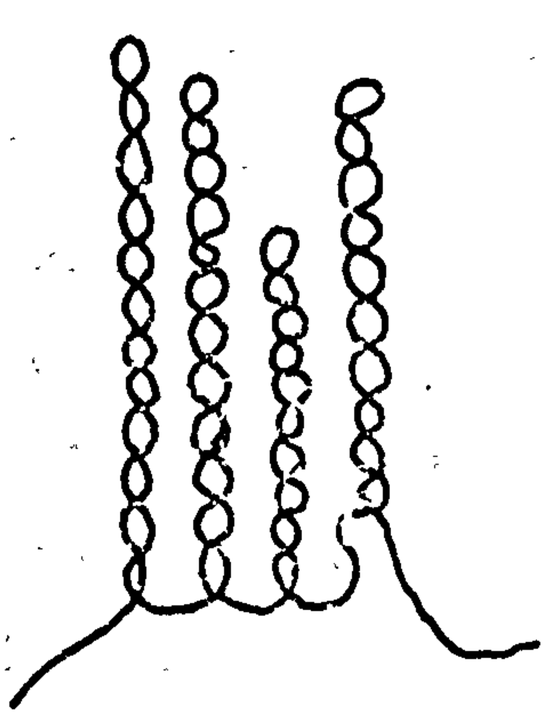

b. Antiparallel Double Helix Gel formation (taking up slack)

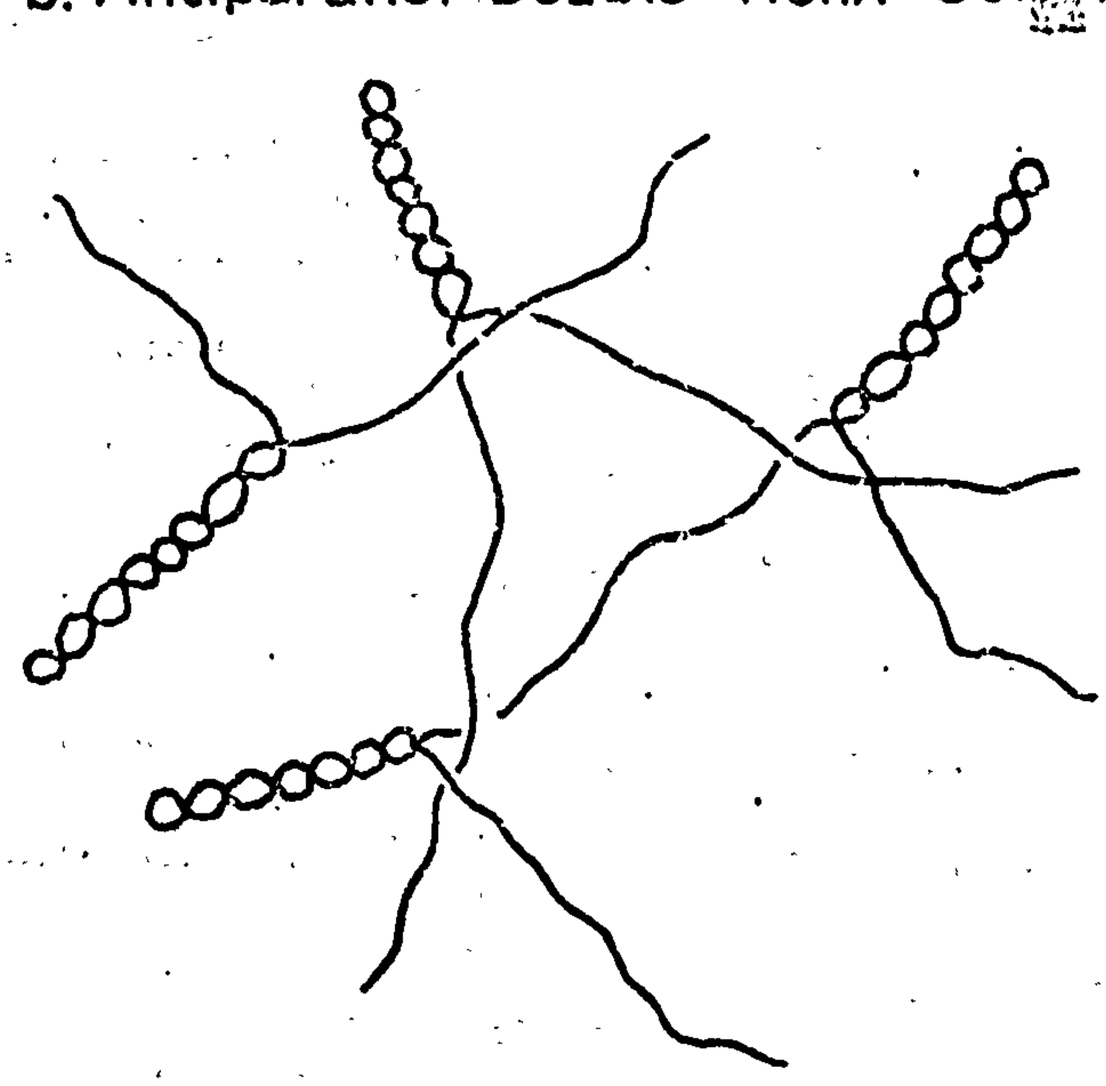

helix is antiparallel with the carboxyle groups at the centre of the helix: this positioning of the carboxyle groups could have important effects on the polyelectrolyte action of the complex and also make the stability of the complex sensitive to ionic species strength and p.H.

The high molecular weight of hyaluronate means that chain-ends become very rare and this presents a topological difficulty for the Rees mechanism. For the formation of double helical crosslinks between separate chains either there must be at least one free end for a chain or the chains involved must be able to store a considerable amount of tortional energy. Fig. 6.7. This aspect of the theory plus, in the case of hyaluronate, the antiparallel nature of the chains, has led to speculation about other possible mechanisms and functions for a hyaluronate double helix. An antiparallel double helix allows a chain to intertwine with itself and chain fold see Fig. 6.8(a). This mechanism would not necessarily present the same topological problems as it could act as a means of reducing stress in a long chain whose ends are fixed. Ref. 21 e.g. a twisted length of rubber band, when the ends are relaxed reduces stress by supercoiling. Fig. 6.8(b) is an attempt toproduce the same effect of crosslinking using the above mechanism. It acts simply by taking up the slack in the network, so producing a similar effect to the Rees mechanism. Fig. 6.8(b) also has the interesting possibility of forming microcrystallites in solution and a highly speculative suggestion is that such groupings of double helices could act as a way of immobilising counterions in a given region, thereby affecting the local ionic environment.

This raises the question of whether a double helix formation mechanism could be an important part of an intercellular transport system. As pointed out in Chapter I, Ogston's equation for the volume available to a sphere of radius R_S in a network of rigid rods is

$$K_{AV} = \exp(-\pi . L . (R_S + r_r)^2)$$

where L is the total length of rod per unit volume.
Clearly, the value of L in a given region of solution will be drastically

affected by a double helix formation and aggregation mechanism as outlined in Fig. 6.8(b).

If the hyaluronate double helix does exist the energetics of helix coil transformation will present interesting thermodynamic problems. The proposed model for the double helix appears to have no dominating, intermolecular, hydrogen bonding scheme that stabilises the system. This suggests that the balance between double helix and random coil is an entropic one. The simplest system that can be envisaged is a polymer/water/ionic salt complex. The interaction may be visualised as a triangle (e.g. below).

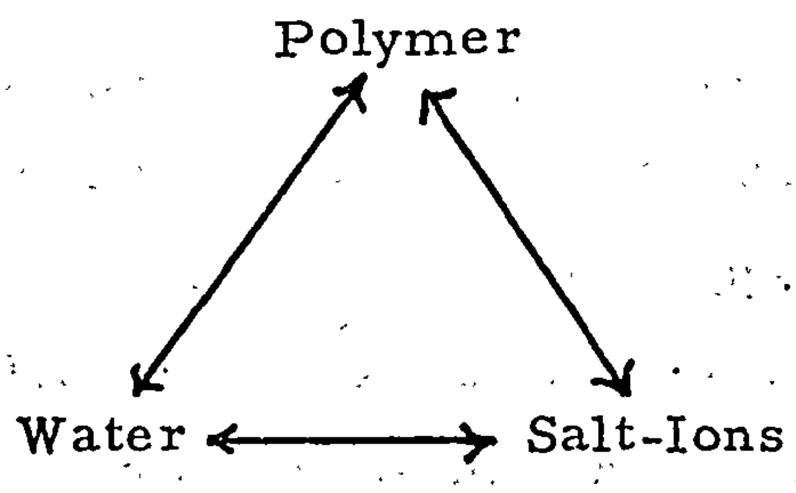

Each arrow implies entropy and enthalpy terms so that the total number of terms involved in a free energy change might be expressed as

$$\Delta S = \Delta(Sp.p + Sp.w + Sp.s + Sw.s + Ss.s)$$

$$\Delta E = \Delta(Ep.p + Ep.w + Ep.s + Ew.w + Ew.s)$$

Certains of these quantities could be evaluated or measured under special conditions but as yet the problem is too difficult to tackle. Possibly, the solid state studies now in progress will throw light on some of these interactions.

CHAPTER VII

7.1 Discussion of some Aspects of the Results

Until 1970 no high quality X-ray fibre diagrams of the connective tissue polyurinides existed but since June 1970 all these molecules have been crystallised using the techniques described here. Many of these molecules exhibit structural principles similar to hyaluronic acid and conformationally they all feature the versatility that has characterised the results on the hyaluronates.

In the X-ray studies carried out on many biological molecules to date, it is assumed (if it is not already obvious) that the knowledge of structure will give insight into the function and behaviour of the molecules. This idea of the molecule as a machine, the mechanism of which can be guessed once the shape is known, does not appear to be applicable to the connective tissue polyurinides for all these rather similar molecules occur, together with various proteins, in what is generally called the 'intercellular matrix', which is a complete system in itself. It is because the idea of a 'system' is so strong that the interpretation of results from fibre studies, in terms of biological significance, are particularly difficult. As our technique is to isolate one component of the system, taking it from its natural, aqueous environment into the solid state, we have to decide whether we are observing an artefact of the solid state or a realistic solution situation. If it is decided that the form being observed is an artefact of the solid state then what are the questions it poses and what clues does it give about the real situation?

Fig. 7.1 summarises the results obtained to date on the hyaluronate system. Clearly if the type I conformation is a double helix as proposed by Dea et al. (Ref. 1 Chapter III) and if, as is also proposed, it exists in solution, a detailed fibre diffraction study will be an important addition to our knowledge of hyaluronate in solution. The information embodied in the type II, type III and type IV conformations is more difficult to appreciate. Of these three, the type III conformation

Fig 7.1 Summary of Results

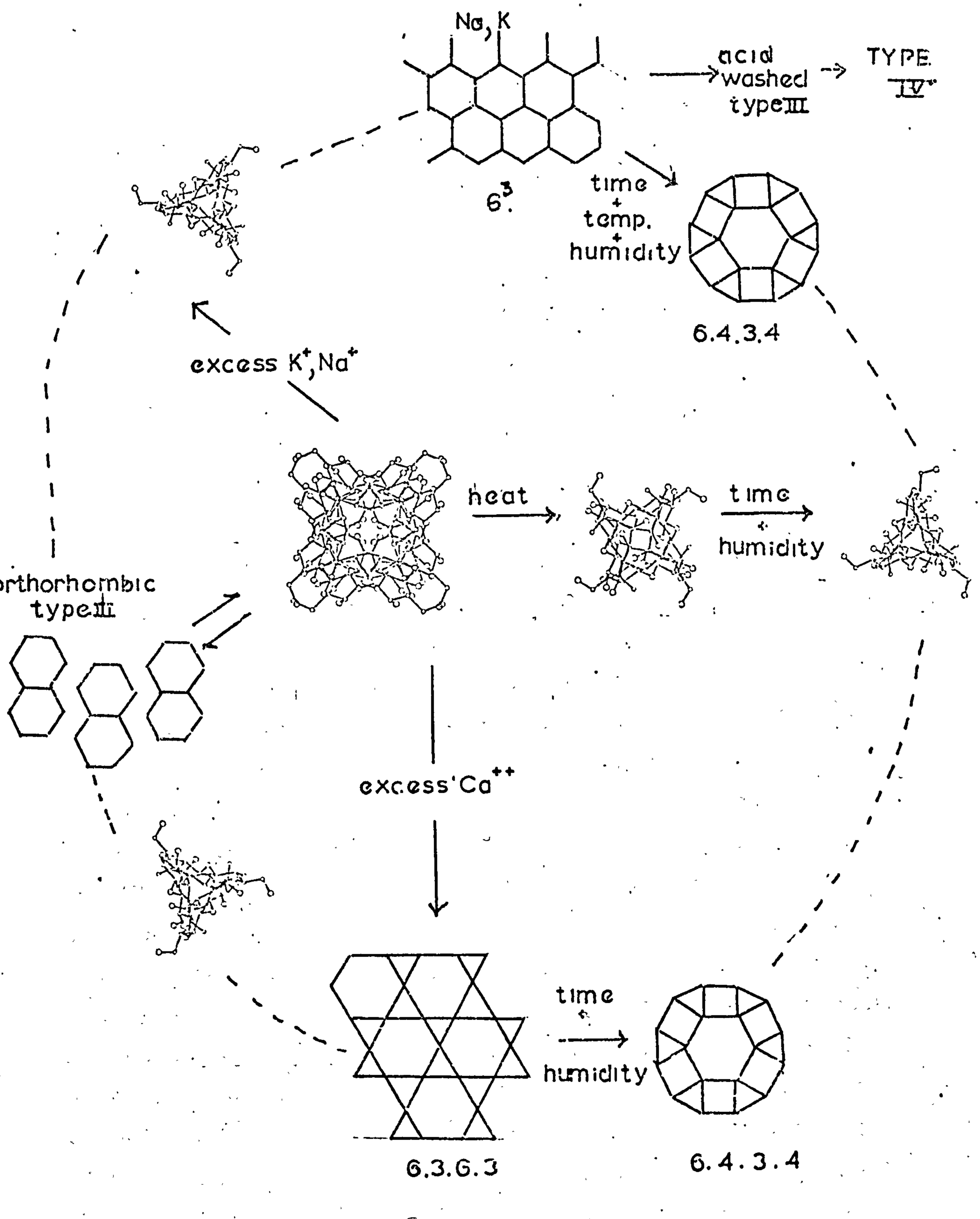

is the most interesting for three reasons

(1) The variety of packing modes and their mobility

(2) This conformation is also a feature of the chondroitin-4-sulphate, chondroitin-6-sulphate and dermatan sulphate molecules.

(3) There is a reversible transition between type I and type III conformations in the solid state.

The important question raised by (1), (2) and (3) is whether or not the type III conformation represents a possible situation in solution. Consideration of reason (1) in more detail shows that there are a number of aspects to it. The variety of the packing modes suggests that the system is not stabilised by strong chain-chain interaction which binds chains together at a specific distance with a specific environment. Fig. 7.2 shows all the packing modes of the type III conformations found to date. This lack of specific chain-chain interaction is emphasised by the increase of interchain distance in going from the sodium salt where it is 6.7Å to the calcium salt where at least some of the chain-chain distances have increased up to 7.7 - 8.2Å depending on the humidity. The general conclusion that I draw from (1) is that the environment i.e. water and ~~contributions~~ counterions are the determining influence on what packing mode should be adopted and thus also on the mobility between packing arrangements. This ties in with (2) where Isaacs and Atkins Ref. 1 have shown that the type III conformation exists for chondroitin-4-sulphate and that it is stabilised by water. Good crystalline fibre diagrams can only be obtained from this material at high relative humidities, in the region of 90-95%. These considerations suggest that the type III conformation is stabilised by a water-ion-structure as mentioned in Chapter VI.

Finally, the importance of (3) cannot be underestimated. The change of conformation in the solid state is one of the most fascinating aspects of the results. It has both topological and biological function implications. From a biological viewpoint it is interesting because the methods used to bring about these changes are comparatively gentle. Transitions

Fig 7.2 Packing of Type III Conformation

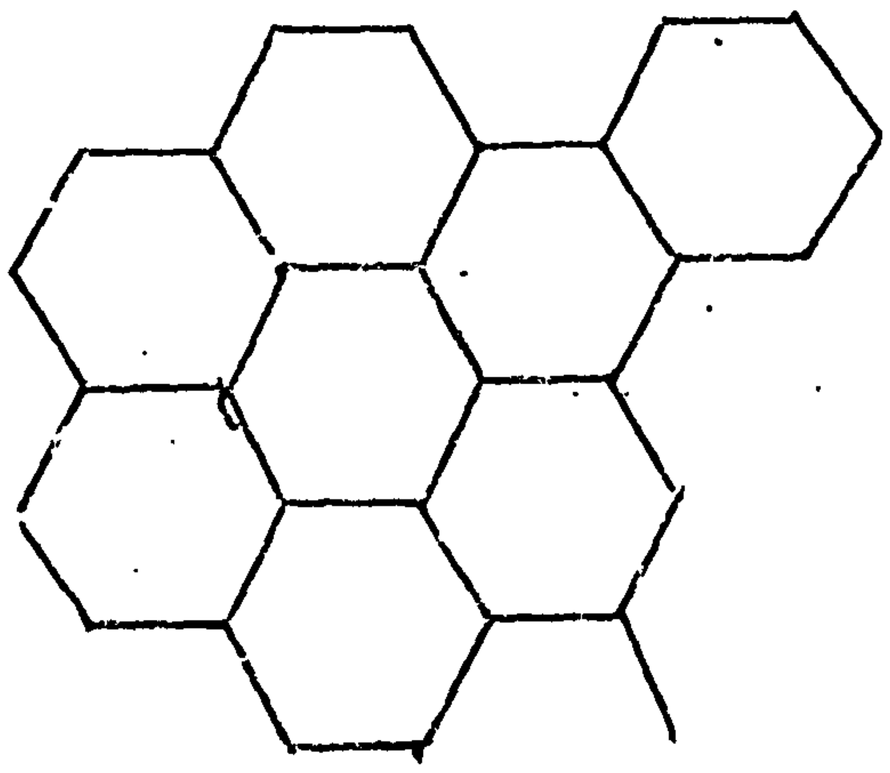

CHAIN ENVIRONMENT

3 chains 3 holes

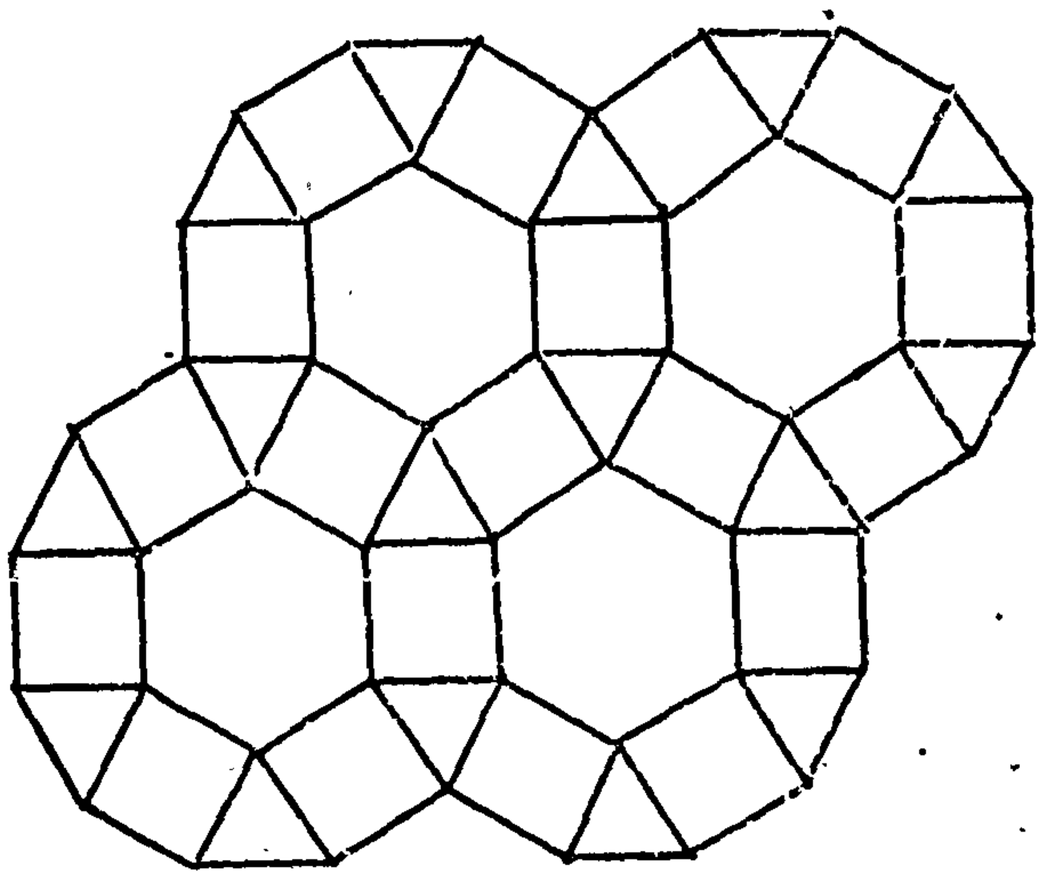

4 chains 1 hole

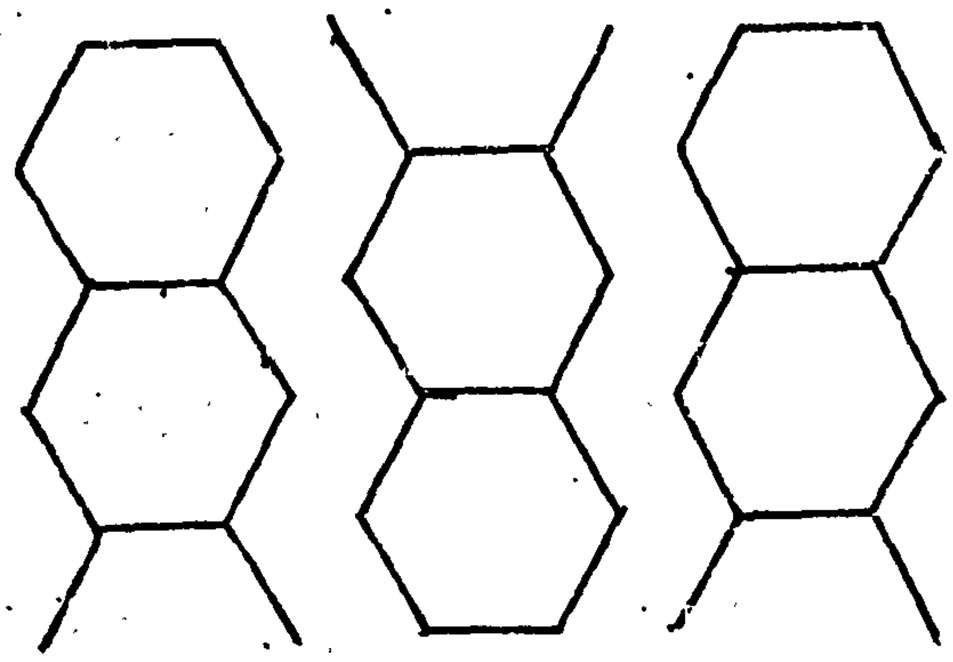

5 chains 1 hole

4 chains 2 hole

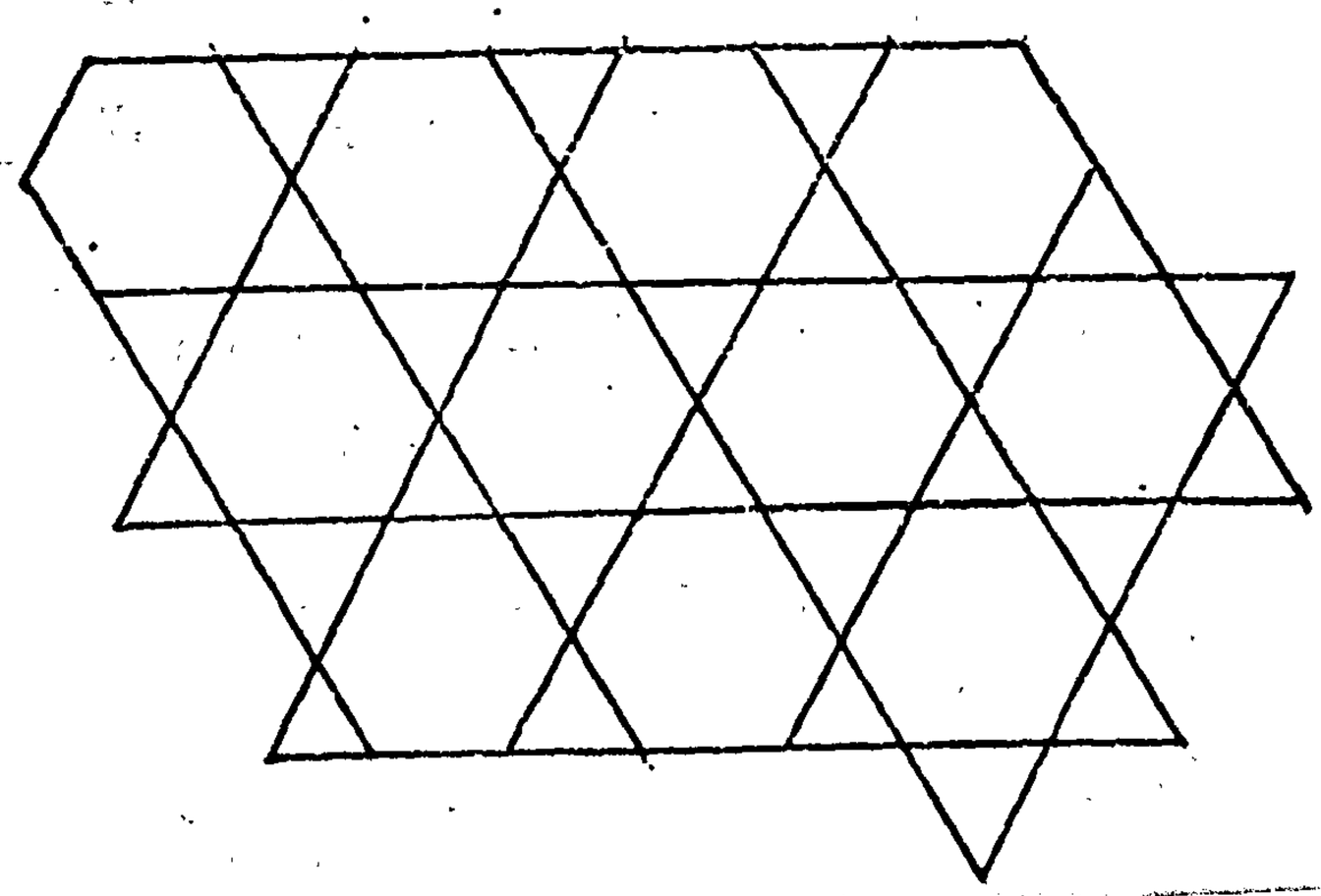

4 chains 2 holes

between type I and type III have been shown to occur reversibly.

Based on the above discussion it is my present opinion that type III represents a good average conformation over considerable stretches of hyaluronate chain in solution. Detailed fibre studies, especially in regard to the water-polymer water-ion situation, will possibly give a definite answer to this question.

The meaning of the type II conformation is much more dubious. It has only been attained at high temperatures and at present my view is that it represents a melted form of type I that would not occur under natural conditions. However, it is interesting for two reasons:

(1) The similarity of the backbone to the type I conformation should offer further study to clarify the tetrasaccharide nature of the type I helix and act as a useful companion to the type I.

(2) The possibility of type I being a two stranded system changing into a one stranded type II system, yet maintaining good crystalline order.

Finally, the type IV conformation attained on washing a type III specimen in ethanolic dilute acid presents some interesting possibilities. The rheological studies of Gibbs et al. (cf. Chapter I. 5) showed that there was a pronounced increase of elasticity in solutions of hyaluronate at p.H. 2. 5. At this p.H the polymer is largely unchanged and thus an extended, two-fold conformation is possible. As was pointed out in section 5. 5, the two-fold helix presents possibilities for a good cooperative hydrogen bonding system between chains, which would act as an efficient crosslinking mechanism, thereby increasing the elastic characteristics of the solution.

7.2 Conclusion

The research in this laboratory over the past three years has been summarised in a paper by Atkins, Isaacs, Nieduszynski,

Phelps and Sheehan Ref. 2, and in many ways this marks the crossroads of our research. The possibilities hereafter are too numerous to be followed in detail and a decision as to the most profitable road to follow will have to be made. For the hyaluronates, some of the questions raised are:

(1) Is the type I a double helix?
(2) Why has it a tetrasaccharide nature?
(3) Is there a water structure around the type III conformations and if so does it stabilise the chains or is it stabilised by the chains.
(4) What are the conditions of p.H and ionic strength that drive transitions?
(5) How do they occur in the solid state?
(6) Is the source of hyaluronate important to the conformation it adopts?
(7) Are there more conformations and packing schemes in the solid state?

The answers to most of these questions will only come after much more experimental and deep fibre work has been done on these systems. It is possible that in order to gain precise knowledge of water-ion interaction in these systems a direct crystallographic attack on oligomers of hyaluronates will have to be undertaken, as has recently been done for D.N.A. Ref. 3. However, fibre experiments involving mixtures of mucopolysaccharides, and the substitution and removal of various side groups have remained unexplored whilst the application of techniques such as electron microscopy has hardly commenced.

APPENDIX

The helical parameters for the various conformations were derived using a method due to Ramakrishnan (Ref. 11, Chapter II). However, there were some slight differences between the method as applied to planar pepticle units and that applied to sugar units so then method used will be outlined here.

A regular helix has a screw either integral or non integral. This implies that it is to bring any residue into coincidence with the adjacent residue by two operations

1) A unit twist Δ where $\Delta = \frac{2\pi}{n}$ and n is the number of residues/ turn of the helix.
2) A unit translation h where h is the projected residue length on the helix axis.

If a fixed coordinate system is set up in the residue then the problem in mathematic terms can be expressed as a rotation $\Delta = \frac{2\pi}{n}$ around a special axis (the helix axis) described by direction cosines L, M and N plus a translation h. The mathematical expression for the transformation is

$$X_{i+1} = h + MX_i$$

where X_i is a column vector describing a point in the i^{th} residue and X_{i+1} is a column vector describing a point in the (i+1)th residue. M is the general rotation matrix

$$(M) = \begin{pmatrix} a^2 + b^2 - c^2 - d^2 & 2(bc + ad) & 2(bd - ac) \\ 2(bc - ad) & a^2 - b^2 + c^2 - d^2 & 2(cd + ab) \\ 2(bd + ac) & 2(cd - ab) & a^2 - b^2 - c^2 + d^2 \end{pmatrix}$$

where $a = \cos \frac{\omega}{2}$ $\quad c = M \sin \frac{\omega}{2}$

$b = L \sin \frac{\omega}{2}$ $\quad d = N \sin \frac{\omega}{2}$

If the elements of the above matrix can be determined independently it is possible to determine the direction cosines of the helix axis

and thus the unit twist and unit translation. The problem is thus to determine the operations which take structural unit 1 (which in this case is a disaccharide) into unit 2, express them as a matrix and identify the elements of this matrix with the elements of matrix M.

For the case under consideration a coordinate system is set up in the 'pseudo monomer' c.f. Chapter II such that ON3 is the origin. Fig. A.1 shows a virtual bond description of the two residues. The Y axis is along direction ON3, OG1 and the X axis is then chosen to lie in the plane OG1-CG1-ON3, and the Z axis is such as to form a right handed system. It should be noted that CN3 is not in the XY plane.

To relate pseudo-monomer (1) to pseudo-monomer (2) a reference, or zero-zero position is defined such that the atoms ON3-CG1-OG1-C'N3-O'G1 all lie in the XY plane. Three operations are then required

1) Translation of ON3 to OG1 by h

2) An anticlockwise rotation of δ about the Y axis to bring CN3 into the XY plane

$$\text{where } \sin\delta = \frac{Z}{\ell' \sin\delta_2}$$

where δ is the deviation of CN3 atom from the XY plane i.e. the angle between the plane OG1-ON3-CN3 and the XY plane. ℓ' is the length of the CN3-ON3 bond and Z is the coordinate of the CN3 atom.

3) A rotation by θ around the Z axis where

$$\theta = \tau - 180 + \delta_1 + \delta_2$$

where these angles are defined in Fig. A.1.

* Therefore to bring pseudo-monomer (1) into coincidence with (2) from
* any general situation defined by tortional angles ψ and ϕ away from the zero-zero position, the order of operations are

Fig. A.1

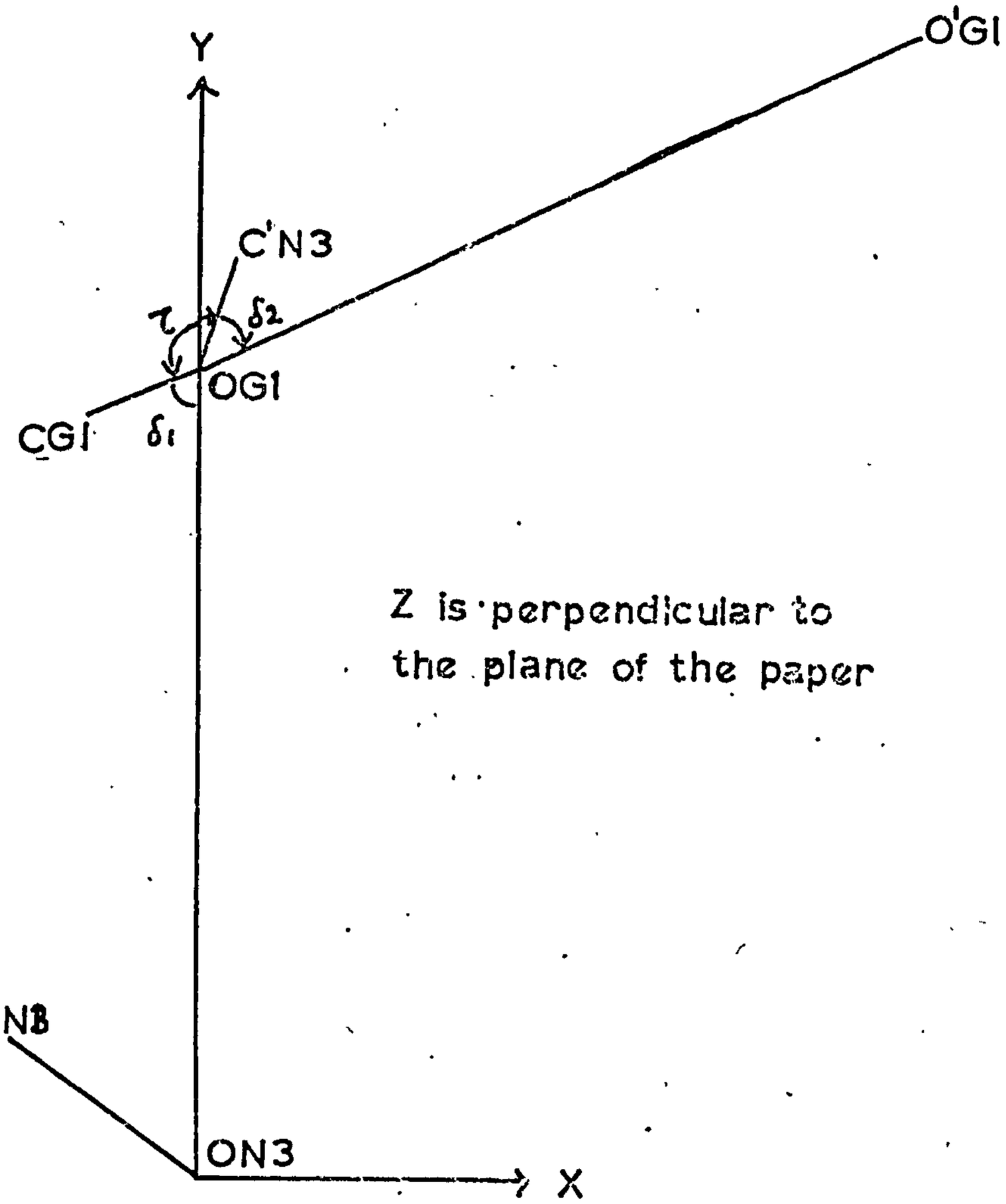
Y
O'G1
C'N3
τ
δ2
OG1
CG1
δ1
Z is perpendicular to
the plane of the paper
CNB
ON3
X

* 1) Rotation ψ^{-1} around OG1-CG1 to bring back pseudo monomer to zero

2) Rotation θ about the Z axis

3) Rotation δ about the Y axis

4) Rotation ϕ around ON3-CN3.

The general rotation matrix M is thus equal to

$$M = M(\phi)M(\theta)M(\delta)M(\psi)^{-1}$$

where $M(\phi)$, $M(\theta)$, $M(\delta)$, $M(\psi)^{-1}$ are the simple rotation matrices as defined above. By identifying the terms of the above matrix with that of the general rotation matrix M the rotation (ω) and axial rise h can be calculated as in Ref. 11, Chapter II.

ACKNOWLEDGEMENTS

My thanks are due to my supervisor, Dr. E.D.T. Atkins, for introducing me to the field of mucopolysaccharides and for his support, encouragement and advice during this research; to Dr. Charles Phelps for his generous provision of material and advice; also to all the technical staff who have provided assistance at various times, especially Miss Jean Robinson and Mr. Terry Owen. However, this work was was born of continuous discussion with my colleagues, especially Dr. Ian Nieduszynski on many walks around Brandon Hill. My appreciation is due to Sue Morgan for proof reading, Miss Juliet Blomfield for typing and to all the members of the Royal Fort for providing a conducive atmosphere.

Finally, I would like to thank the Science Research Council and the Arthritis and Rheumatism Research Council for financing me over the past three years.

REFERENCES TO CHAPTER I

1) D.A. Rees, "The Shapes of Molecules" Oliver and Boyd 1967.

2) Sundararajan, P.R. and Rao, V.S.R. Biopolymers Vol. 9 (1970).

3) Nicduszynski, I.A. and Marchessault, R.H. Biopolymers Vol. 11, No. 7 (1972)

4) Carlström, D. The Journal of Biophysical and Biochemical Cytology, Vol. 3, No. 5 (1957).

5) Atkins, E.D.T., Parker, K.D. and Preston, R.D. Proc. Roy. Soc. B. 173 (1969).

6) Atkins, E.D.T., Mackie, W., Parker, K.D., Smolko, E.E. Polymer Letters Vol. 9, (1971).

7) Hybl, A., Rundle, R.E. and Williams, D.E. J. Am. Chem. Soc. 87, (1965)

8) F.A. Bettelheim "Biological Polyelectrolytes" Ed. Veis, A. Marcel Dekker (1970).

9) R.W. Jeanioz "The Carbohydrates" Ed. Pigman, W.W. and Horton, Academic Press (1970).

10) T.C. Laurant "Chemical and Molecular Biology of the Intercellular Matrix" Ed. Balazs, E.A. Academic Press (1970).

11) Brimacombe and Webber "The Mucopolysaccharides" B.B.A. Library Vol. 6. Elsevier 1964.

12) Scott, J.E. Methods of Biochemical Analysis, 8, 145 (1960).

13) Silpanata, P. Dunstone, J.R. and Ogston, A.G. Biochem. J. 109, (1968).

14) Preston, B.N., Davies, M. and Ogston, A.G. Biochem. J. 96, (1965).

15) Cifonelli, J.A. and Mayeda, M. Biochem. Biophys. Acta 24, (1957).

16) Fessler, J.H. and Fessler, L.I. Proc. Nat. Acad. Sci. 56, (1966).

17) Ogston, A.G., Stanier, J.E. Disc. Faraday Soc. 50, 635, (1953).

18) Ogston, A.G., Stanier, J.E. Biochem. J. 49, 585, (1951).

19) Laurant, T.C. "Physical and Chemical Studies of Hyaluronic Acid" (1957).

20) B.I. Aldrich, Biochem. J. Vol. 70, No. 2, 236, (1958).

21) Fessler, J.H.F. and Ogston, A.G. Trans. Faraday Soc. 47, 667, (1951).

22) Laurant, T.C. and Pietruozkiewicz Biochem. Biophys. Acta 49, 258, (1961).

23) Ogston, A.G. Trans. Faraday Soc. 54, 1754, (1958)

24) Gibbs, D.A., Merril, E.W., Smith, K.A. and Balazs, E.A. Biopolymers 6, 777, (1968).

REFERENCES TO CHAPTER II

1) Laurant, T.C. Arkiv Kerni. 11, 513 (1957).

2) Bettelheim, F.A. J. Phys. Chem. 63, 2069 (1959).

3) Bettelheim, F.A. Nature

4) A. Keller and A. O'Connor, Disc. Faraday Soc., 25 (1958), 114.

5) E.W. Fischer, Zeit. Naturforsch., 12a (1957) 753, 25.

6) A Keller Reports on Progress in Physics (1968).

7) Atkins, E.D.T. and Mackie, W. Biopolymers (1972).

8) Atkins, E.D.T., Phelps, C.F. and Sheehan, J.K.P. Biochem. J. 128, 1255 (1972).

9) Arnott, S. and Wonacott, A. Polymer, 1966, 21, 371:

10) Ramachandran, G.N., Ramakrishnan, C. and Sasisikharan "Aspects of Protein Structure" Ed. Ramachandran, Academic Press (1963).

11) Ramakrishnan, C. Proc. India Acad. Sci., Sect. A, 12 (1964).

12) Rees, D.A., J. Chem. Soc. (B) (1969).

13) Sugeta, H. and Tatsuo Miuazawa, Biopolymers, Vol. 5, (1967).

14) Nieduszynski, I.A., Marchessault, R.H., Canadian Journal of Chemistry, Vol. 50, No. 13 (1972) p.2130.

15) * Same as Ref. 10 Chapter II.

16) Round Table Discussion 161st Meeting of Am. Chem. Soc.

17) Sathyanarayana, B.K. and Rao, V.S.R. Biopolymers Vol. 10, (1972).

CHAPTER III

1) Dea, I.C.M., Moorhouse, R., and Rees, D.A. with Arnott, S. Guss, J.M. and Balazs, E.A. Science; Vol. 179, 560, (1973).

2) Anderson, N.S., Campbell, J.W., Harding, M.M., Rees, D.A. and Samuel, J.W.B. J. Mol. Biol. (1969) 45, 85-99.

CHAPTER IV

1) Nieduszynski, I.A. and Marchessault, R.H. Nature, Vol. 232, No. 5305, p.46 (1971).

2) Nieduszynski, I.A. and Marchessault, R.H. Biopolymers, Vol. 11, No. 7, 1335 (1972).

3) Arnott, S. and Wonacott, J., Polymer, 7(1966) 157.

REFERENCES TO CHAPTER V

1) Same as Ref. 1 Chapter III.

2) Cundy, H.M. and Rollett, A.P. "Mathematical Models" Oxford, Clarendon Press 1962.

CHAPTER VI

1) Atkins, E.D.T., Mackie, W., Parker, K.D., Smolko, E.E. Polymer Letters, Vol. 9, p.311 (1971).

2) Blackwell, J. Biopolymers, Vol. 7, p.281 (1969).

3) Pimentel, G.C. and McCellan , A.L. (1960) "The Hydrogen Bond", Freeman, San Francisco.

4) Kamb, B. in "Structural Chemistry and Molecular Biology" Ed. Rich, A. and Davidson, N. Freeman, San Francisco.

5)

6) Hemily, P.W. Mem. Serv. Chim. Etat, Paris 38, No.1,7

7) Heide, H.G. Naturwissinschaften, 41, 402.

8)

9) See Ref. 2, Chapter IV.

10) Norrish, K. Disc. of Faraday Soc., 42B, 187 (1946).

11) Low, P.F. Advan. Agronomy., 13 269, (1961).

12) Nemethy and Scheraga, J. Chem. Phys., 36, 3401, (1962).

13) Berendson, G.W. in "Theoretical and Experimental Biophysics" Ed. Cole, A. Marcell Dekker 1967.

14) Warner, D.T., Nature, 196, 1055 (1962).

15) Warner, D.T., Nature, 190, 120 (1961).

16) Arnott, S., Guss, J.M., Huskins, D.W.L. and Matthews, M.B. Science, June 1973.

17) Rees, D.A. Advan. Carbohyd. Chem. Biochem. 24 (1969) p.267-332.

18) Anderson, N.S., Campbell, J.W., Harding, M.M., Rees, D.A. and Samuel, J.W.B. J. Mol. Biol. 45, 85-99 (1969).

19) Dea et al. see Ref. 1, Chapter III.

20) See Ref. 42. Chapter I.

21) Discussion with D. Isaacs.

CHAPTER VII

1) Isaac , D. and Atkins, E.D.T. in press.

2) Atkins, E.D.T., Isaac, D., Nieduszynski, I.A., Phelps, C.F. and Sheehan, J.K.P. in press.

3) Rosenberg, J.M., Seeman, N.C., Kim, J.J.P., Suddath, F.L., Nicholas, H.B. and Rich, A. Nature, Vol. 243 (1973) p.150.